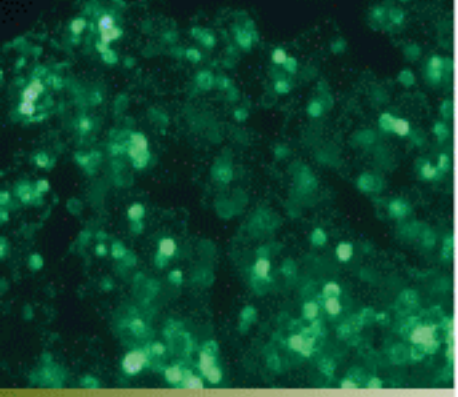

Vol.2 ,No.2, October 2014

Transactions on GIGAKU

Special issue of
The 1st International Conference on Energy, Environment and Human Engineering(ICEEHE), 2013

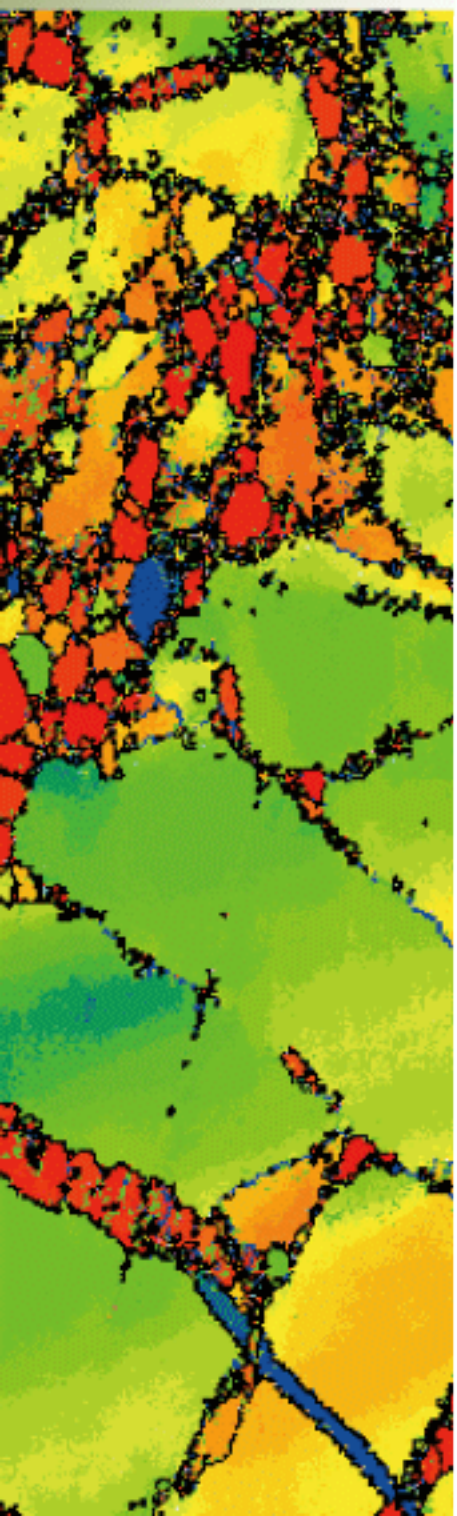

GIGAKU Press
Nagaoka University of Technology

Transactions on GIGAKU: Scope and Policy

Nagaoka University of Technology publishes an online, open access journal titled “Transactions on GIGAKU”, which is focused on the science and technology related to GIGAKU*. The mission of this journal is to spread out the concept of GIGAKU and the fruits of GIGAKU to the global world and to be a strong network for innovations in science and technology and for development of next generations of high-level human resources. This journal, therefore, covers research and education activities related to GIGAKU in broad areas.

* See ‘What is GIGAKU?’ below.

‘What is GIGAKU?’

GIGAKU is a term composed of two Japanese word-roots; GI and GAKU. The word GI〔技〕 literally stands for all kinds of arts and technology, and GAKU〔学〕stands for scientific disciplines in general when used as a suffix.

The term was originally coined to describe the fundamental philosophy of education and research of Nagaoka University of Technology (NUT) when it was established in 1976. Through this term the founders of NUT intended to express their recognition that all technical challenges in the real world require a scientific approach. And NUT has a relentlessly pursued GIGAKU since then.

Thirty-five years have passed and all surrounding conditions have changed dramatically during those years. We are witnessing rapidly globalizing economics and huge scale changes in demographic, industrial and employment structures. All those changes seem to necessitate the further evolution of GIGAKU. In response to this, NUT recently announced its new “Growth Plan” and a renewed definition of the term is given;

GIGAKU is a science of technologies, which gives us an angle to analyze and reinterpret diverse technical processes and objects and thus helps us to advance technologies forward. By employing a broad range of knowledge about science and engineering, management, safety, information technology and life sciences, GIGAKU provides us with workable solution and induces future innovations.

July 2012
Koichi Niihara, President of Nagaoka Univesrsity of Technology

Submission and Publishing

"Transactions on GIGAKU" publishes original papers focusing on education, science, and technology related to GIGAKU. Proposals for special issues aligned with conferences are strongly encouraged*, and guest editors are welcomed. Papers submitted are peer-reviewed before publication. Publication charge is free for all submitted papers.

* Please contact to Editor-in chief, itoy@mech.nagaokaut.ac.jp

Copyright

Contact

joho-kiban@jcom.nagaokaut.ac.jp

(Revised January 2014)

Editorial board of special issue of 1st International Conference on Energy, Environment and Human Engineering (ICEEHE), in Transactions on GIGAKU

Guest Editor

Guest Co-Editors

Preface of the special issue for the 1st ICEEHE

The 1st International Conference on Energy, Environment and Human Engineering (ICEEHE) was held at Kandawgyi Palace Hotel, Yangon, Myanmar on 22nd and 23rd December 2013. This international conference was co-organized by Myanmar Maritime University, Nagaoka University of Technology, Nihon University, Saitama University and AJMMC (Association of Japan Myanmar Mutual Cooperation). This conference was supported by Ministry of Transport, Ministry of Environmental Conservation and Forestry, Myanmar Embassy in Japan, Embassy of Japan in Myanmar, Japan International Cooperation Agency, Japan External Trade Organization (Yangon Office), The Overseas Human Resources and Industry Development Association. The Governor of Yangon and other prominent guests gave warm welcome speeches in the opening ceremony.

More than 250 participants were attended from Myanmar, Japan, Malaysia, Thailand, India and other countries including Australia, China, USA, etc. There were 135 oral presentations and 84 poster presentations in various sessions: Renewable Energy and Energy Management, Information and Communication Technology, Manufacturing and Design, Environmental Technology and Management, Human Engineering, Transportation and Logistics, Agricultural and Bio Engineering, Materials Engineering for Sustainable Society, Sensing and Control Engineering. Among a large number of the presented papers, the selected and peer-reviewed 18 papers are included in this special issue. Hope you enjoy these interesting papers.

The 2nd ICEEHE will be held in August 2015 in Yangon. I would like to encourage you to join the next conference and also enjoy Yangon city with beautiful Pagodas.

Yoshiharu MUTOH
Chairman of the 1st ICEEHE
Director / Vice President
Nagaoka University of Technology

Transactions on GIGAKU

Volume 2, No. 2, October 2014

pecial Issue of 1st ICEEHE

The 1st International Conference on Energy, Environment and Human Engineering.(December 22-23, 2013Kandawgyi Palace Hotel, Yangon, Myanmar)

The 1st International Conference on Energy, Environment and Human Engineering (1st ICEEHE) aims to serve as a platform for international exchange on the latest engineering development in the fields of energy, environment and human for sustainable society. Engineering is not for the engineering profession but it should contribute to social, economic and environmental development. In the recent globalized world, the local or regional problems are immediately corresponding to the global problems and vice versa. Therefore, it is increasingly of importance to discuss the role of engineering for sustainable society. Total 72 manuscripts have been submitted and 18 peer-reviewed papers are published in special issue of Transactions on GIGAKU.

Table of contents

Surface Roughness Measurements of a Narrow Borehole --- Development of a carriage ---

Eiki OKUYAMA[1*], Yuichi SUZUKI[1] and Ichiro YOSHIDA[2]
[1)]Department of Mechanical Engineering, Akita University,
Akita, 010-8502, Japan
[2)] Kosaka Laboratory,
Mitaka, Saitama,341-0035, Japan
**E-mail: okuyama@ipc.akita-u.ac.jp*

In various industrial fields, it is frequently necessary to measure surface roughness in confined spaces such as boreholes and grooves. However, using a small stylus, the surface roughness of a narrow borehole can be directly measured only a few millimeters from its end; alternatively, destructive measurements must be performed. This major disadvantage of conventional stylus-based surface profilometers is mainly due to an inductive pick-up that is connected to the stylus used to detect the surface roughness. We already proposed a novel surface roughness measurement sensor. To make the surface roughness sensor small, we used a stylus with a cylindrical mirror and a lensed fiber instead of a conventional inductive pick-up. The proposed sensor converts the signal obtained by measuring the surface roughness of a borehole into an optical signal, which is transferred outside the borehole by an optical fiber. Experimental results demonstrate that this system has a measurement range of 8 μm and a sensitivity of 19 nm. In this paper, a carriage to measure the surface roughness in a small borehole is designed. The proposed carriage has two degree of freedom, displacement along the borehole axis and rotation around the borehole axis.

1. Introduction

In various industrial fields, it is frequently necessary to measure surface roughness in confined spaces such as boreholes and grooves. However, using a small stylus, the surface roughness of a narrow borehole can be directly measured only a few millimeters from its end. For example, a type I5B stylus designed from measuring the surface roughness of small boreholes[1] (Kosaka Laboratory Ltd.) has a height of 0.5 mm and a reach of 4 mm. Therefore, this stylus can measure surface roughness up to 4 mm from the end of the borehole. When it is necessary to measure the surface roughness of an area far from the end of the borehole, the borehole must be cut in the axial direction and destructive measurements performed. This major disadvantage of conventional stylus-based surface profilometers is mainly due to the inductive pick-up that is connected to the stylus. The minimum size of an inductive pick-up is approximately 20 mm. When the stylus and inductive pick-up scan inside a borehole, the smallest measureable borehole is approximately 20 mm in diameter. When only a stylus scans inside a borehole and the inductive pick-up remains outside the borehole, the measureable area is restricted to near the end of the borehole.

We have been seeking to measure the profiles of boreholes with a diameter of less than 2 mm and a length of over 100 mm. We already proposed a novel surface roughness measurement sensor[2]. To make the surface roughness sensor small, we employed a stylus with a cylindrical mirror and a lensed fiber, instead of a conventional inductive pick-up. The proposed sensor converts the signal obtained by measuring the surface roughness of a borehole into an optical signal, which is transferred outside the borehole by an optical fiber.

In this paper, a carriage to measure the surface roughness in a small borehole is proposed.The proposed carriage has two degree of freedom, displacement along borehole axis and rotation around

the borehole axis.

2. Sensing principle

Fig. 1(a) shows a schematic diagram of the surface roughness measurement system, which has a stylus with a cylindrical mirror and a lensed fiber. The stylus is connected to a carriage by an elastic hinge and it is used to measure the surface roughness of a narrow borehole. The cylindrical mirror is fixed on the stylus and the lensed fiber is fixed on the carriage. A laser beam from a laser diode (LD) passes through an optical coupler and the lensed fiber. The laser beam from the lensed fiber is focused on a cylindrical mirror. A portion of the beam reflected from the cylindrical mirror enters the lensed fiber and is detected by a photodiode (PD). The PD output is transformed into a voltage and digitized by an A/D converter. As the cylindrical mirror moves in response to the surface roughness in the borehole, the surface roughness can be converted into an electrical signal.

Fig. 1(b) shows the force and measurement loops[3] of the proposed system. The dashed curve in this figure indicates the force loop, which passes through the stylus, the carriage, the skids, and the measured borehole. The dash-dotted curve indicates the measurement loop, which passes through the cylindrical mirror, the lensed fiber, the carriage, and the stylus.

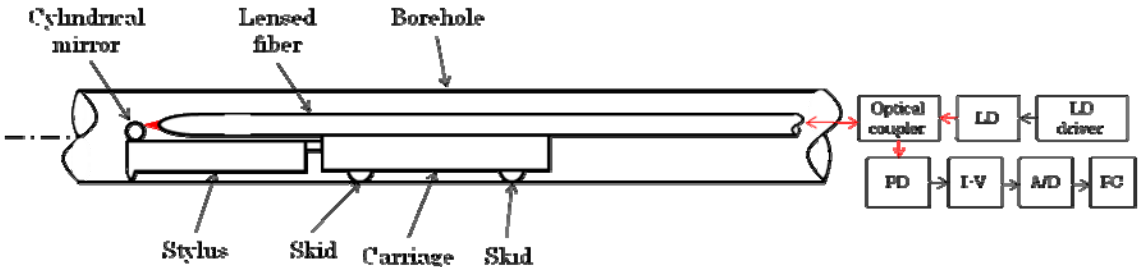

(a) Schematic diagram of surface roughness measurement system in a small borehole

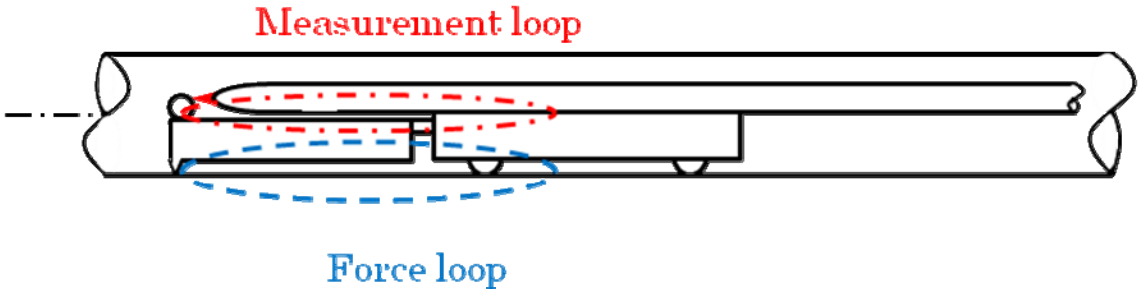

(b) Force and measurement loops

Fig. 1 Surface roughness measurement system in a small borehole

3. Fundamental characteristics

Figs. 2(a) and (b) respectively show a schematic diagram and a photograph of the experimental system of the surface roughness sensor with the stylus having a cylindrical mirror and a lensed fiber. A stylus (Mitsutoyo, 12AAB406) is used to trace the surface roughness. The V-groove of the stylus is placed on the knife edge of the carriage. The cylindrical surface of an optical fiber (diameter: 125 μm; length: 2 mm) coated with Cr is used as the mirror. The cylindrical mirror is fixed on the stylus. A lensed fiber (Moritex Co., Circletran MST-CT1310G11W320/BS10FAd; focal length: 320 μm; spot diameter: 11 μm) is fixed on the carriage using a shallow V-groove formed by a scriber.

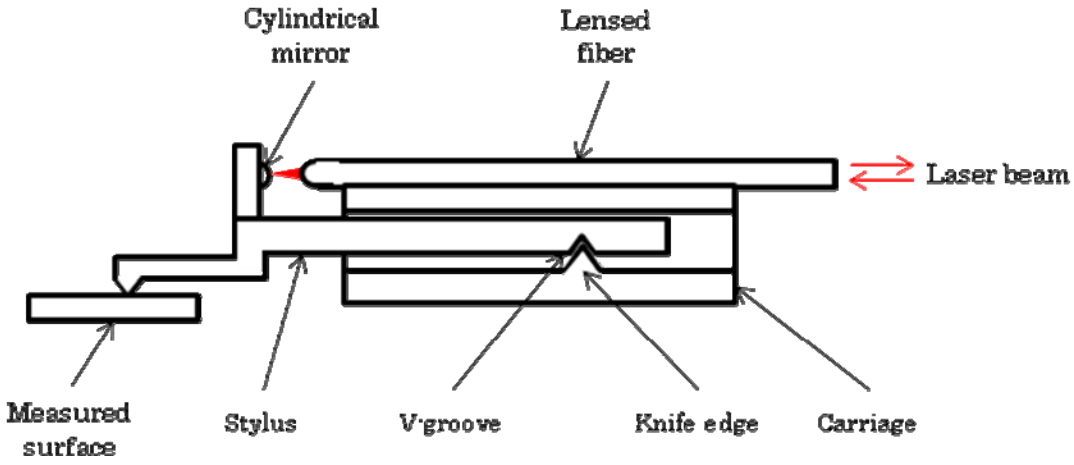

(a) Schematic diagram

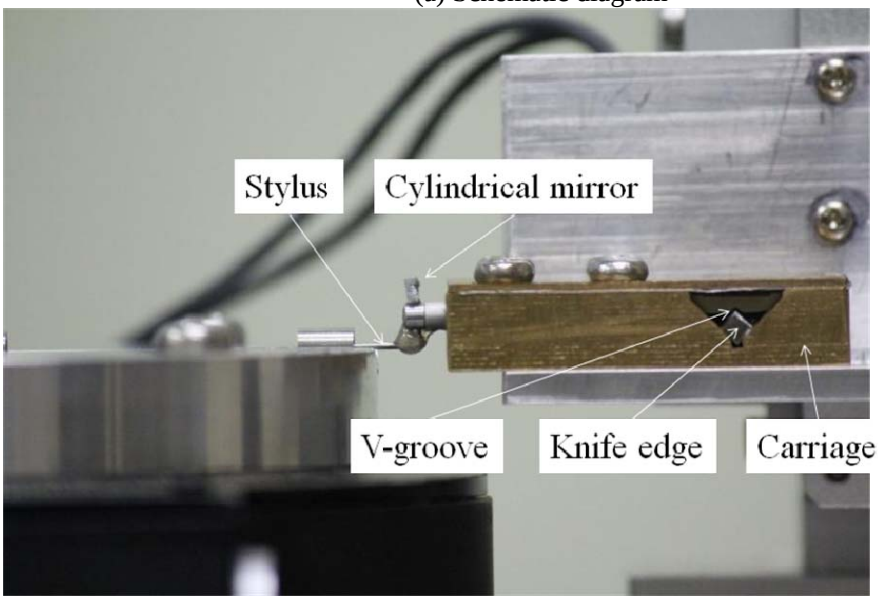

(b) Photograph

Fig. 2 Experimental system

Fig. 3 shows a block diagram of the process used to calibrate the proposed surface roughness sensor. The sensor is set on a Z-stage (Chuo Precision Industrial Co. Ltd., NPZ-347-S1). The Z-stage can be finely translated in a 10 μm range and it is driven by a PZT actuator. It can be roughly translated by a micrometer. The tip of the stylus is placed on the surface to be measured. The Z-stage is driven by a triangular wave (period: 2 s; peak-to-valley amplitude: 8.5 μm) (see Fig. 4) generated by a function generator (Agilent, 33120A) and the output of the stage driver, the displacement of the Z-stage (measured by a strain gauge), and the output of the surface roughness sensor are acquired by A/D converters (Agilent, 34410A). These A/D converters are double integration type and integration times are set to 0.02 s to eliminate noise from the power line cycle that has a frequency of 50 Hz.

As the Z-stage has a short fine motion range, it was roughly translated by approximately 5 μm by the micrometer and calibration was performed. This process was repeated five times. Fig. 5 shows the calibration results, where the abscissa is the displacement in the Z direction and the ordinate is the output of the surface roughness sensor. It shows that the sensor output changes when the displacement is changed. A small amount of hysteresis was observed. The sensor output was small (–5 V) when the laser beam was focused lower side of the cylindrical mirror, whereas when the laser beam was focused near the center of the cylindrical mirror, the sensor output was large (–7 V).

Furthermore, when the laser beam was focused upper side of the cylindrical mirror, the sensor output was small (–5 V). The two areas indicated by the dashed ellipses in Fig. 5 are suitable for surface roughness measurements. Since it is nonlinear, a least-squares by a third-order polynomial is used as the calibration curve. The measurement range was 8 μm. Since the noise was 5.2 mV(±2σ), the sensitivity was 19 nm.

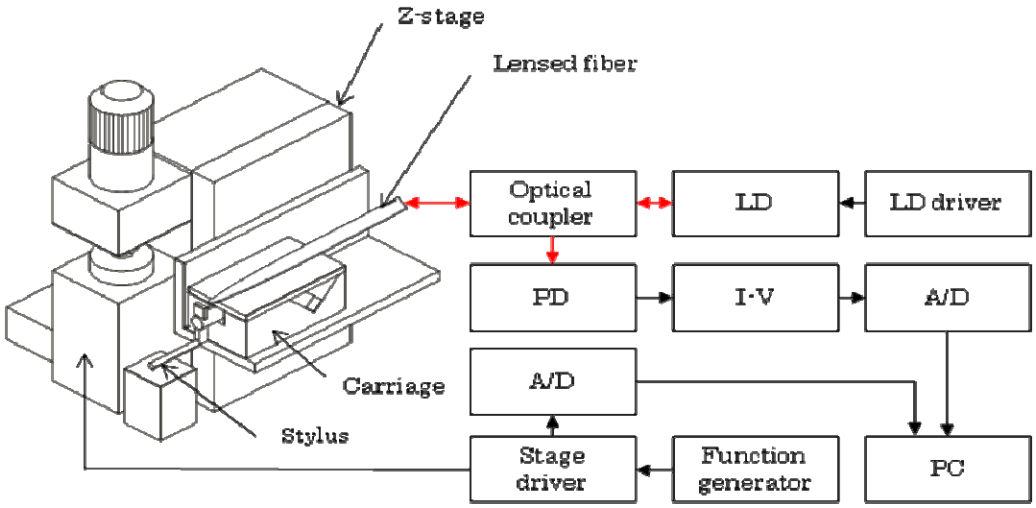

Fig. 3 Block diagram of proposed system

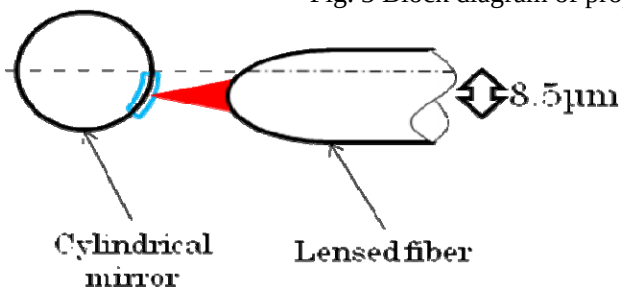

Fig. 4 Schematic diagram of calibration

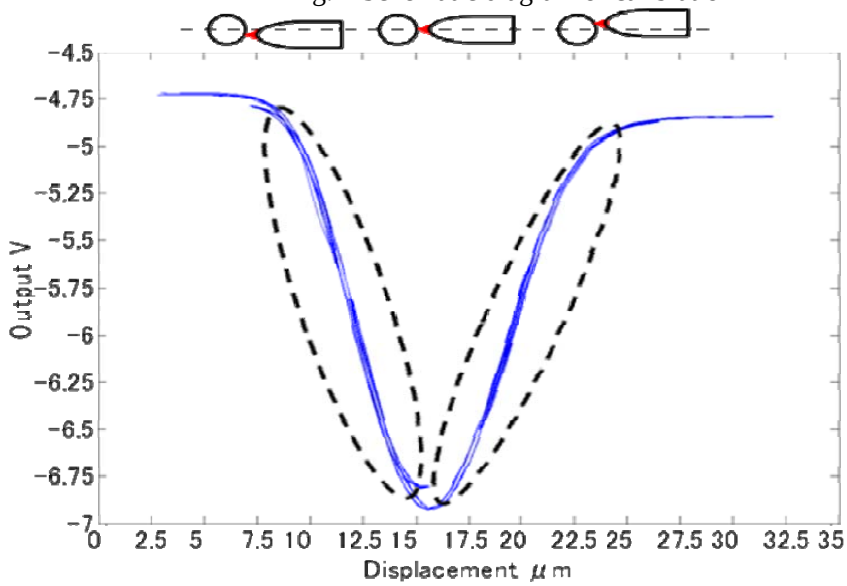

Fig. 5 Calibration results (wide area)

4. Design of carriage

In case of surface roughness measurement system, a skid is used to eliminate lower spatial frequency component, i.e., surface waviness. In the proposed system, two skids are set to the carriage and the carriage scans along the borehole axis. Therefore, degree of freedom of the carriage should be constrained properly. Fig.6 shows the outline of the constraint of the carriage in the borehole. The borehole axis is X-axis. Required motions of the carriage are scanning along X-axis and rotation around X-axis. Originally, the carriage has six degree of freedom. Then, four degree of freedom should be constrained. Consequently, number of contact point between the carriage and the borehole is four. Two skids are set at both ends of the carriage and they make two contact points. Furthermore, two springs are set at upper position of the carriage to make two contact points.

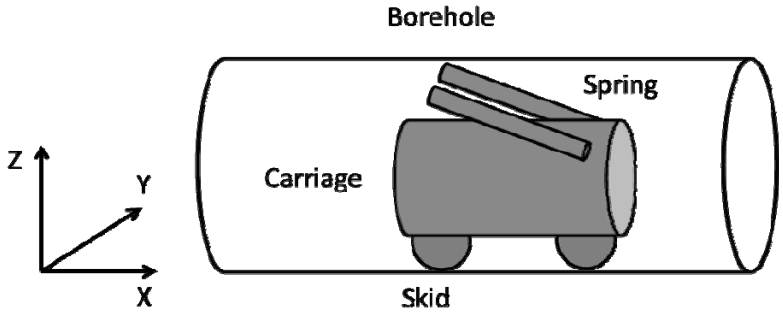

Fig.6 Constraint of the carriage in the borehole

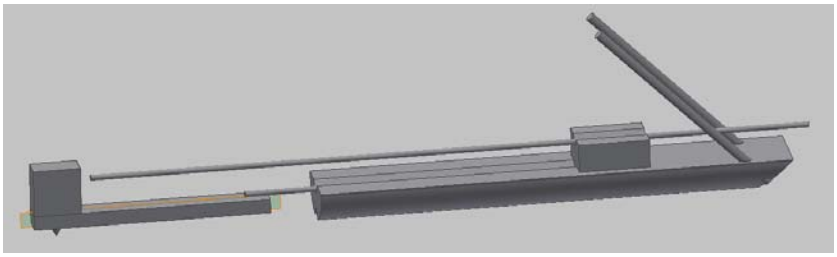

a) single view

b) Front view

Fig.7 Draught of the carriage with the stylus

Fig.7 shows a draught of the carriage with the stylus and the lensed fiber. Fig.7 a) is a single view drawing and Fig.7 b) is the front view drawing. Length of the carriage along X-axis is 10mm. Height is 1.3mm and width is 1.5mm. V-groove is made at the lower part of the carriage and two steel balls with 0.15mm diameter are set in the V-groove as the skid. The end face of the carriage is cut as an inclined plane and two small through holes with 0.18mm diameter are made. Furthermore, two springs are set to the carriage using these through holes. Upper part of the carriage is two stage. Each stage has a V-groove. A spring is set in the lower V-groove and the stylus is set to the spring. The lensed fiber is set at the higher V-groove.

5. Trial manufacture of the carriage

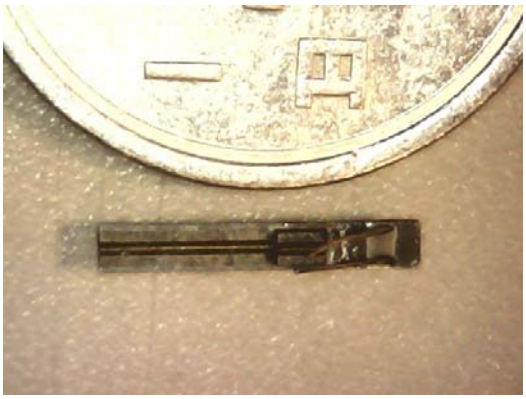

Fig.8 Trial manufacture of the carriage

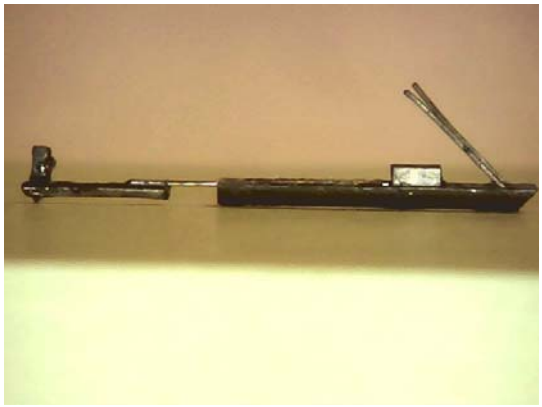

Fig.9 Trial manufacture of the carriage with the stylus

Fig.8 shows photograph of the trial manufacture of the carriage. Fig.8 is the top view photograph. A string of an electric guitar, D'Addario 0.07(0.178mm diameter), is used as the spring.

Fig.9 shows the carriage with the stylus. The stylus, Kosaka Laboratory I5B, with cylindrical mirror is connected to the carriage using a guitar string. In the near future, we will try to measure the surface roughness in a borehole using this carriage system.

6. Conclusions

The carriage to measure the surface roughness in a small borehole is designed. The proposed carriage has two degree of freedom, displacement along the borehole axis and rotation around the borehole axis.

Acknowledgments

The authors would like to thank Masahiro Morikawa and Yuki Toku of Akita University for their help. Further, the authors would like to acknowledge Prof. Kazuhisa Yanagi of Nagaoka of University of Technology for his advice. A part of this work was supported by a Grant-in-Aid for Scientific Research (C) (23560112), Japan.

References

[1]Suefcorder Formcorder, Accessories & Options Catalogue, Kosaka Laboratory LTD., (2006)
[2] Eiki OKUYAMA et.al., Surface Roughness Measurements of a Narrow Borehole
--- Development of Stylus with Cylindrical Mirror and Lensed Fiber ---, AMPT(2013)
[3]S.T.Smith and D.G.Chetwynd, Foundations of Ultraprecision Mechanism Design, Gordon and Breach Science Publishers(1992)

(Received; 23rd December ,2013, Accepted; 5th May, 2014)

Introducing and Identifying the Role of Eye Blinking in the Virtual e-Learning Environment

Asanka D. Dharmawansa*, Katsuko T. Nakahira, Yoshimi Fukumura, Marasinghe A.
Department of Management and Information Systems Engineering,
Nagaoka University of Technology
1603-1 Kamitomioka, Nagaoka 940-2188, Japan
**E-mail: addharmawansa@yahoo.com*

With the improvement of ICT (Information and Communication Technology), the synchronous e-Learning becomes an attractive method for delivering learning. The virtual environment is the one way of provideing synchronous e-Learning and avatars are active on behalf of the human users in that environment. The non-verbal communication, which is very essential in the learning process is covered 82% of all classroom communication process and it is lack in the virtual class due to poor connection between the avatar and the real user. The ultimate objective of this research is establishing non-verbal communication in the Virtual e-Learning Environment (VeLE) and identifing the behaviuor of non-verbal features during the e-Learning activities. The eye blinking which is a major portion of the non-verbal communication is designated to introduce to the virtual environment. Initially a system of eye blink detection for the real user is constructed using geometric feature based method. A human head model is also prepared and exported to the virtual world to create the avatar with eye blinking. The connection is established between the real world and the virtual world through a http protocol. When the real user is blinking his eyes, it is appeared in the VeLE through the avatar. An experiment was conducted with the eye blink visualization system to identify the behavior of eye blinking in the VeLE. Student tried to control the eye blink to avoid the loss of critical information and tried to keep the eyes open when they demanded the visual attraction during the experiment. The results of the experiment convey that the eye blink rate depends on the visual attraction and most of the eye blink happened at the speaking time but at the break points of the speaking. The result conclude that the behavior of eye blinking changes based on the activities that students engage in the learning process of the virtual e-Learning.

1. Introduction

The advancement of technology is affected to the each and every field including education. Simultaneously, internet makes the immense effect to the education with the increment of online users day by day [1]. As a result of that knowledge can be delivered through the electronic media and that is called e-Learning [2]. Currently most of universities conduct both e-Learning and traditional class room system concurrently. Defense Acquisition University in UK is one of the university provides both web and resident based learning. The number of graduated students who are following web based method is growing rapidly in recent years and it is shown that the significant increment in e-Learning students than the students in traditional class [3].

There are several ways to deliver the knowledge through e-Learning and synchronous virtual e-Learning method is considered in this research. To conduct the synchronous virtual e-Learning, Second Life is chosen as our virtual world since the Second Life is the leader of compelling, cost-effective virtual education solutions to amplify an existing curriculum or create a new model to engage for collaborative learning [4]. The three dimensional VeLE which is an online area where students and staff can interact synchronously is very attractive and different types of class rooms were built in that environment. Office package, white board, online-resources can be employed to deliver the knowledge and chat, voice are utilized for the communication in the VeLE. Avatar is an online manifestation of self in the virtual world and it is designed to enhance the interaction of the virtual space [5]. While using avatars for social networking (Ex: MogiMe, MOOLTO) and entertainment purposes is now well established, they are used in educational contexts is still in its early stage of development [6]. Even though, the avatar represents the real user in VeLE, the avatar cannot make the

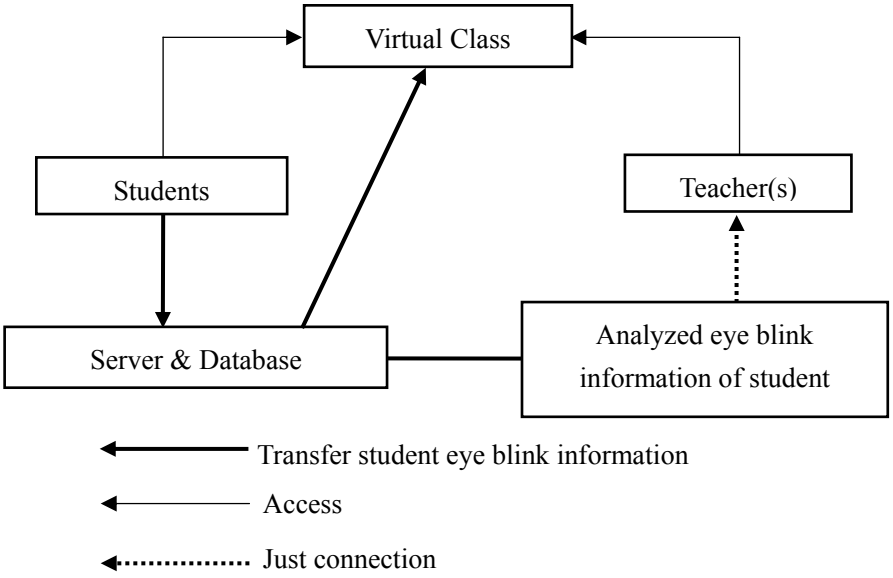

Fig. 1 Architecture of the Eye Blinks Visualization System

reasonable representative of the real user because the relationship between the avatar and the real user is only depending on the control of arrow keys of the keyboard. If there is rich connection between the real users and the avatar, it will be very useful for the teacher to maintain the class effectively because teacher can obtain the feedback or the student response via the avatar will contribute for the better learning environment.

Even though teacher and students can sight their avatars in the virtual classroom, their physical bodies are located in different places and they don't know real conditions of the participants. All avatars are like artificial icon and they couldn't make a reasonable representation of the human. Therefore the usefulness of the face to face layout cannot be obtained due to the poor connection between the real user and the avatar. Non-verbal communication which is essential component of the education [7] should be established to enable the effective face to face layout to view their real condition in the virtual environment.

Facial expressions, eye blinking, gestures including head direction and hand positions are majority of the non-verbal features that can be established in the VeLE. In this research, the establishment of the eye blinking is discussed because eye is the most expressive part on the face. It is called the window of the soul [8].

The ultimate objectives of this research are establishing non-verbal communication in the VeLE to raise the connection between the real user and the avatar and identify the behavior of non-verbal features in the virtual classroom. As an initial step of this target, eye blinking which is an element of most expressive part in the face is introducing to the virtual learning environment and analyzing the behavior of eye blink in the virtual class.

2. Proposed System

2.1. Architecture of the System

The layout of the eye blink visualization system and the way of identifying the role of eye blinking in the virtual learning environment is shown in Fig. 1. Students are directly access the virtual class and they can engage with the learning activities. The eye blink information of the real user is obtained at the same time through a web-camera. The extracted data is transferred to the virtual environment through a server and it is stored in that server. Then the real user eye blink can be visualized in the VeLE. When the real user eye blink happens in the real world it is appeared in the virtual world. The teacher or the instructor can observe the student non-verbal behavior using direct and indirect methods. The behavior of the student is feasible to obtain directly through interacting with the virtual class because it is conducted as a face to face layout. Non-verbal behavior information could be extracted from the server for the indirect observation as a post analyze. The next sections provide more details regarding the way of fulfilling this design.

2.2. Methodology

Mainly there are three steps that should be completed to establish the eye blink visualization in the virtual class. The eye blink of the real student needs to be captured in a real time is considered as the initial step. The avatar should be modified to represent the real user eye blinking is the second activity of this process because the avatar in the virtual environment hasn't any way to represent the human non-verbal features. Establishment of a link between the real world and the virtual world is the last step of the eye blink visualization system. The development of eye blink visualization system and the method, which are helps to construct the system, is discussed in the next sections.

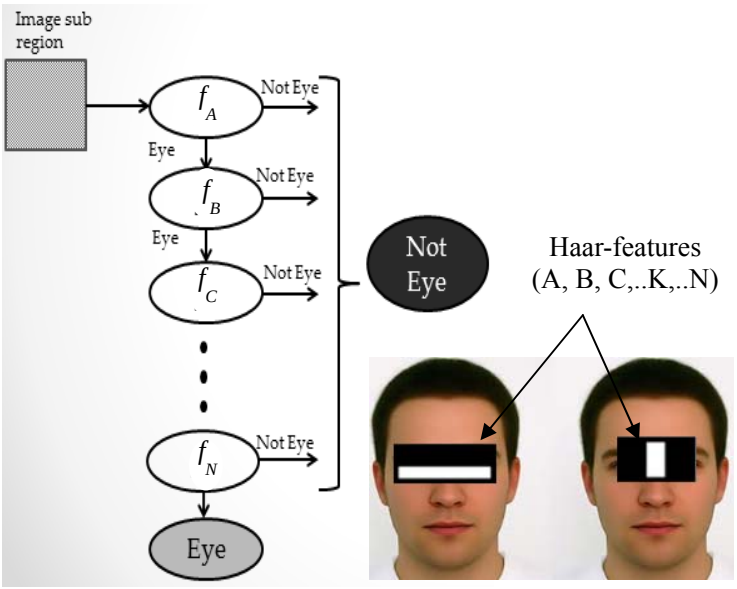

Fig.2 Apply Haar-like Classifier Features

2.2.1. Algorithm development: Haar like feature

The detection methods of face and eyes of the user are needed to identify the eye blink. In this research, Haar feature-based cascade classifier for object detection is used to detect the face and eyes because of following factors.

- Detection at any scale
- 90% of objects detected
- Face detection at 15 frames per second for 384 × 288 pixel images

The Classification need to be developed based on the Haar-features to detect the face and eye. The procedure to detect the eye is explained here and the same procedure can be used to detect the face. The appropriate Haar-features need to apply for the positive images which consist of specific eye component and notify range of filter and threshold value as shown in Table 1. The threshold value (f_i) is determined by subtracting the summation of white-region pixel value from the summation of dark-region pixel value.

$$f_i = \sum X_i(w) - \sum X_i(b) \quad \text{..... (1)}$$

Where $X_i(w)$ means white pixel values and $X_i(b)$ means black pixel values.

The same procedure needs to be applied for many positive images and obtained average value for threshold and filtering range to develop the classification. The classification can be applied to real time image as shown in Fig.2. To detect the eye area, the relevant features have to be gone through the all area of image. After apply the relevant Haar-feature in real world application f_i value is able to determined. If the real image f_i value is greater than the f_i value of classifier, then the relevant eye feature is available for one Haar-feature. All the selected Haar-features are needed to satisfy to confirm the availability of eye components as indicated in Fig.2. This is the way for detecting the face and eye of the image.

Table 1 Train Haar-like Classifier Features

Correspond facial part	Haar-features	Range of Filtering	Threshold value
Eye	A:	J_A	f_A
	B:	J_B	f_B
	C:	J_C	f_C
	K:	J_K	f_K
	N:	J_N	f_N

2.2.2. Eye blink Detection

When the e-Learner engages with the learning activities in front of the computer, the web-camera is located to capture the frontal view of the user to obtain the real-time video. The video consists with set of frames. We have to analyze the frame by frame to catch the user eye information continually and constantly. Haar-feature cascade

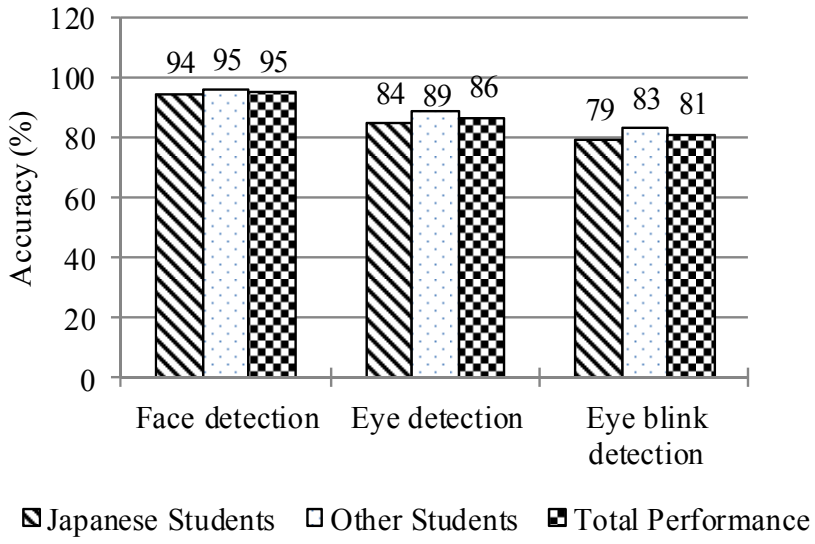

Fig. 3 Accuracy of the Eye Blink Detection

classification is used to detect the face area of an image. When the face detection is successful, we can proceed to the next step to detect the eyes. Otherwise procedure should be started from the beginning. When the face is detected, location of the eyes can be roughly determined based on the human face layout and possible to define the region of interest to detect the eyes. Then Haar-feature cascade classification can be applied to the location, which is defined as a region of interest. The result is categorized as eyes are detected or not detected. When the eyes are not detected, then it is classified as a blink due to the close eyes when the blink is occurring and at that time face is also detected. When the eyes are detected, further analysis is carried on to identify whether the eyes open or close. There are two measurements that are available to determine whether the eyes open or close. The white and black pixels of the eye region and the width and height ratio of the eyes are considered. Threshold values for the both measurements are obtained through previously trained images. When these both measurements are satisfied, the eyes of the candidate are classified as open and that is indicated as not a blink. Otherwise it is identified as eyes close and that is indicated as a blink. Then the procedure is started from the beginning and continuously updated till the stop command of the user. The eye blink detection procedure is conducted with the software of Visual C++ with OpenCV library.

Accuracy of the detection is evaluated by considering the detection of the face, eyes and blink for the Japanese and international students as shown in Fig. 3. The last bars of the each section of that graph indicate the total performance of the system. Although it is shown that the detection was less in Japanese students than the other students, total performance for the blink detection is more than 80%.

2.2.3. Avatar modification

The avatar who represents the real student in the virtual world is not allowed to the dynamic changes during the learning activity automatically due to the restrictions of the Second Life software which is provided an avatar and the three dimensional environment. The mechanism needs to be prepared to change the eye blinking of the avatar based on the real user requirement. The head model was prepared in the real world using graphics software (Maya) and exported to the virtual world as an initial step of introducing eye blink to the avatar. Eyes and eyelids were prepared using objects in the virtual world and attached to the head. The head model was coupled to the avatar and modified to represent the eye blink.

2.2.4. Visualize eye blink in the virtual learning world

When the avatar eye blink model and the real user eye blink detection are constructed, the union between these two places needs to be initiated. PHP, JavaScript and the http request are used to establish a link between the real world and the virtual world. When the real user eye blink information is obtained, it is transferred to the server which is located in our university and it is conveyed to the virtual world through the http request. The eye blink visualization system is originated and eye blink is appeared on the avatar face after few seconds when the real user blink happens. We need only a web-camera (3 or higher mega pixel for better accuracy), a personal computer (Processor: core i5 or higher) with better performance because Second Life and the image processing software for the eye blink

Fig. 4 Work with Eye Blink Visualization System

detection are graphical software and a person who works with the eye blink visualization system in the virtual world as shown in Fig. 4.

3. Experiment

3.1. Aim

This experiment was conducted to identify the behavior of the eye blinking during an e-Learning session of the VeLE and the possibility of conducting the experiment with implemented eye blink visualization system. The behavior of the eye blinking during the activities in the VeLE can be recognized with the frequency of the eye blinking based on the learning activity and measuring the occasion of the eye blink.

3.2. Hypothesis

The three hypotheses are derived from the previous studies regarding the eye blink of the real world activities. Eye blinks is controlled to minimizing the loss of important visual information [9]. This leads us to hypothesize that we try to control the eye to avoid temporal loss of critical visual information.

The second hypothesis is eye blinks occur immediately before or after the task when we are explicitly give the break time. Eye blinks may occur at the explicit attentional breaks. It does not occur during the middle of the task due to the demand of the visual attention [10].

The third hypothesis is valid only for the conversation. The higher eye blink rate is appeared during the speaking in the conversation which is happened in the real world [11]. Therefore we hypothesize that the higher eye blink rate appears while speaking than the silence during the conversation in the virtual world. We are going to identify the behavior of eye blinking via the measuring frequency of eye blink and occasion of eye blink during the e-Learning activities in virtual world.

3.3. Subjects

There were six students that aged from 25 to 35 years voluntaries participated to this study. The students belong to different nations namely Sri Lanka, India and Nepal. They are following the postgraduate course and majoring in management and information science engineering.

3.4. Experiment Procedure

The subjects were instructed to attend three e-Learning sessions; 1) a lecture related to operational research, 2) an individual exercise based on the previously mentioned lecture about operational research and 3) a group exercise based on the operational research that was taught in the 1st session and all the sessions were utilized the eye blink visualization system. Each student had a web-camera to detect the eye blink and a personal computer to engage the learning activities in Second Life. The course materials were provided by the Department of Industrial Management of Wayamba University of Sri Lanka. The lecture on operational research was delivered as face-to-face lecture and the power point slides were used to explain the content in the virtual environment as shown in Fig 5(a). The second session of the individual exercise was carried on using an excel sheet appears in front of their table and the zoomed view of the exercise sheet appear as shown in Fig. 5(b). The discussion were carried to solve the group exercise and there was only one large excel sheet to enter the answer which was possible to edit by any student as shown in Fig. 5(c). All subjects experienced all three conditions (within-subjects experiment). Each session was taken roughly about 15-20 minutes to complete. The voices of the all participants were recorded and the eye blink was already stored with the time via the eye blink visualization system.

4. Result and Discussion

The mean eye blink rate was obtained during the three sessions and the relax time. The minimal values are appears during the lecture and the group discussion while higher rate was appeared during

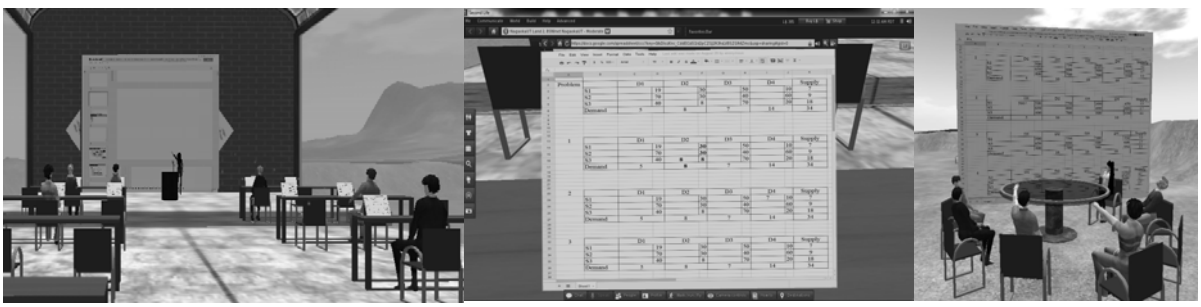

Fig. 5 Students View During the (a) Lecture Session (b) Individual Exercise (c) Group Exercise

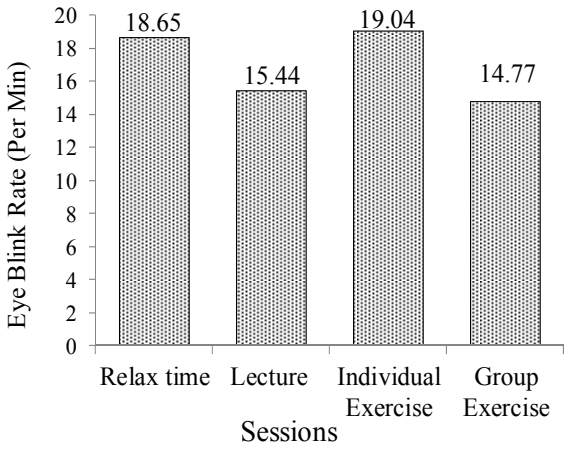

Fig. 6 Average Eye Blink Rate of Whole Students

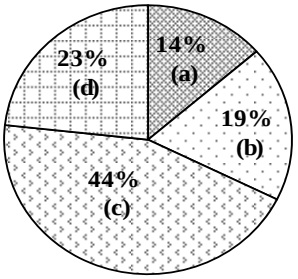

(a)Just before the speaking
(b)During the speaking
(c)During the breaks of the speaking
(d)Just after the speaking

Fig. 7 Occurrences of the Eye Blink

the individual exercise as shown in Fig.6. The student views during the three sessions were indicated in Fig. 5 respectively. Each and every student can view others in the virtual class and they have to cover the whole area of the class room including teacher as well as a power point slides through their eyes during the lecture. Same as the group exercise, they have to cover whole area of the discussion place including an excel sheet and especially the excel sheet can be edited by any other students. Therefore they try to keep eyes open and minimize the blink. The result is confirmed that the student had a minimum eye blink rate during lecture and the group exercise sessions. They viewed only the excel sheet completely throughout the computer monitor during the individual exercise and the excel sheet cannot be edited by any other user except the owner. The result is indicated that the eye blink rate went high due to the less demand of the visual attraction as shown in Fig. 5(b). The average rate of the eye blink confirms the first hypothesis that is the student try to control the eye blink to minimize the loss of visual information.

Then the occurrence of eye blinks during the speaking is needed to investigate to identify the occasion of the eye blink. There are mainly four occasions where the eye blink happens during the conversation. Just before or after the speaking, during the speaking and the break point during the speaking are the occasions that an eye blink can be happened during the conversation. Fig. 7 shows the allocations of students' eye blink timing under the major four occasions.

Highest portion (44%) of eye blinking happened during the breakpoints of the speaking time. "Just after the speaking" obtained the second highest value (23%). During the speaking time, eye blink rate was very less and it is obtained only 19%.

The eye blink rarely occurred at the speaking time and most of the eye blink occurred at the break

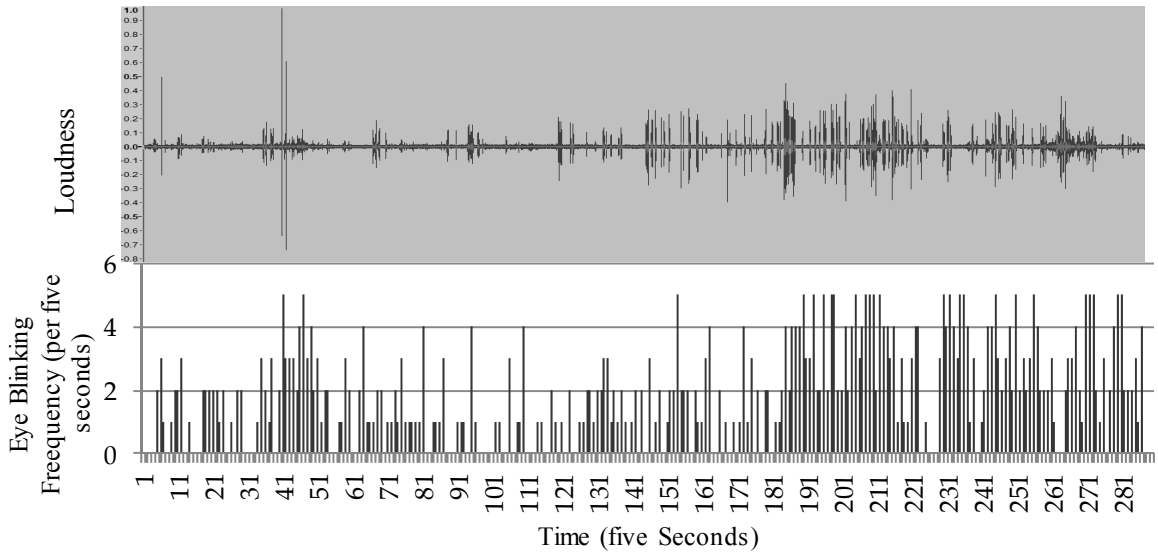

Fig. 8 Voice and Eye Blinking of a Student

points of the speaking. Therefore the second hypothesis also confirmed that the eye blink does not occur at the middle of the task and it occurs at the break points of speak.

Eye blink and the voice of the students during the group exercise were analyzed to identify the variation of eye blinking in the conversation process and the result is appeared in Fig. 8. For this analysis, the student information during the group exercise was only considered because the active conversation among the students was appeared only during the group exercise.

The below chart of that figure indicates that the eye blink rate of a student per five seconds and the voice loudness of that particular student appears in the above chart. One of the students' voice and eye blinking information are included in Fig.8 and other students also showed the same behavior. We can identify that a higher rate was appeared during the speaking time and a less blink rate was illuminated during the listening time. Therefore the last hypothesis is verified that the higher eye blink rate is appeared during the speaking and it is reduced with the silence.

5. Conclusion

The eye blink which is one of the main non-verbal components [8] has been visualized in the virtual e-Learning environment and an experiment was conducted to identify the behavior of eye blinking in the virtual e-Learning environment. The result of the experiment showed that the student tried to control the eye blink to avoid the loss of critical information because the highest eye blink rate appears during the session of individual exercise which has only an excel sheet to view. Lecture and the group exercise showed the higher rate of eye blink with broad area to view that leads us to conclude that the student try to keep the eyes open when they demand the visual attraction.

Further analysis was conducted to identify the occasions of the eye blinks during the speaking time and it is confirmed that a highest rate of eye blink happens during the break point of the speaking. Most of the eye blink does not occur during a speak time. In addition, the rate of the eye blink is higher during the speaking than the silence time of the conversation. We have identified that the eye blink rate depends on the visual attraction and most of eye blink happens at the speaking time but at the break points of the speaking leads us to conclude that the behavior of eye blinking changes based on the activities that students engage in the learning process of the virtual e-Learning.

References

[1]. Internet World Stats, History and Growth of the Internet from 1995 till Today, available on http://www.internetworldstats.com/emarketing.htm, last visited on Nov. 2013.
[2]. I Ketut Trika Adi Ana, Putu Kerti Nitiasih, Teaching Reading through E-learning Website, 3rd International Conference on Foreign Language Learning and Teaching, 554-563, (2013).
[3]. Annual Report of the Defence Acquisition University, (2012), page 7.
[4]. Second Life: Ready for Learning, Spotlight on Education, available at http://wiki.secondlife.com/wiki/Second_Life_Education, last visited on March 2014.
[5]. Peterson, M., Learning interaction in an avatar-based virtual environment: a preliminary study. PacCALL Journal, 1, 29–40, (2005).
[6]. de Freitas, S., Learning in immersive worlds: a review of game-based learning. a report prepared for the JISC e-Learning Programme, (2006).
[7]. G. Theonas, D. Employing Virtual Lecturers' Facial Expressions in Virtual Educational Environments, The International Journal of Virtual Reality, 7(1), 31-44, (2008).
[8]. Priya Irabatti, Study on Increasing Importance of Nonverbal Communication in Retail Industry, Abhinav Publication, volume no.1, issue no.4, (2012).
[9]. Stern J. A., Walrath L.., Goldstein The endogenous eyeblink. Psychophysiology 21, 22–33, (1984).
[10]. Hall A., The origin and purposes of blinking. Br. J. Opthalmol. 29, 445–467, (1945).
[11]. Perelman, Detecting deception via eyeblink frequency modulation, PeerJ, (2014).

(Received; 23rd December, 2013, Accepted; 30th July, 2014)

Light Trapping Effect of SnO_2Nanoparticles for Solar Cell Application

Cho Cho Thet[1,*], Hla Toe[2], Cho Cho[1], Aye Aye Myint[1]
[1)] Universities' Research Centre, University of Yangon
[2)] Department of Physics, University of Yangon
University Avenue Road, Yangon, Myanmar
**E-mail: chochot@gmail.com*

Chemical synthesis of SnO_2 nanoparticles (NPs) were prepared by co-precipitation method using the stannous chloride ($SnCl_2.2H_2O$) as a precursor and ammonia solution as a precipitating agent. The as-synthesized SnO_2 colloids were centrifuged and dried at 60 °C for 24 h. The crystal structure of the prepared samples was examined by X-ray diffraction (XRD) which reveals the structure of SnO_2 NPs was tetragonal structure. The average crystallite size of SnO_2 was about 25 nm. The surface morphology of the agglomerated SnO_2 was almost spherical shape by scanning electron microscope (SEM). The effect of annealing temperature of the sample was confirmed by Fourier transform infrared spectrophotometer (FTIR). The as-synthesized SnO_2 layers were deposited onto a polycrystalline p-Si (100) wafer by screen printing method and SnO_2/Si thin films were carried out by thermal diffusion method at different deposition temperatures 400, 500, 600, 700 and 800 °C for 1 hour (h). The structural characterization of SnO_2/Si junction was observed by XRD. The photovoltaic properties of SnO_2/Si were measured by LUX meter and FLUKE 45 dual display multimeter respectively. The photovoltaic parameters including resistance, voltage and current of SnO_2/Si thin film were measured depending on the light intensities. It was found out that the annealing temperature 500 °C was the optimum temperature for the better trapping properties for light intensities of SnO_2 thin film.

1. Introduction

A light trapping of a semiconductor is the absorption of light by the active layer of semiconductor using the incoming photon energy which is less than or equal to the band gap energy of semiconductor. Light trapping can enhance the solar cell efficiency due to creation of electron hole pairs which generates a better collection of photogenerated current and a higher open circuit voltage of thin film solar cells. Therefore, the role of semiconductor material using as the active layer is the important consideration for the better light trapping. The material for light trapping has been used the transparent conductive oxide (TCO) such as tin-doped indium oxide (ITO), fluorine- and antimony-doped tin oxide (FTO, ATO) layers since they are high optical transparency in the visible region of electromagnetic spectrum, low electrical resistance, high electrical conductivity and high reflectivity in infrared range [1]. TCO are applied in numerous applications including light emitting diodes [2], dye sensitized solar cells [3], electrodes in solar cells and batteries [4, 5], sensors [6], flat panel displays [7]. SnO_2 is an n-type semiconductor with a bulk energy band gap (3.7 eV) at the room temperature and pressure. Various methods have been developed for preparing the transparent conducting oxide thin films. Some of them are sol gel [8], screen printing [9], thermal evaporation [10], chemical bath deposition [11], dc and rf sputtering [12, 13], spray pyrolysis [14], pulse laser ablation [15], electrodeposition [16] and spin coating [17].

Since the knowing the absorption coefficients of materials aids engineers in determining which material to use in their solar cell designs, the synthesized SnO_2 NPs has been deposited onto p-Si wafers to investigate the potential for light harvesting in this paper. Valuable understanding of the optical properties of NPs has been measured by meters under different illuminations for the insightful information on how the optical absorption of NPs reflects the properties of the dispersed

nanoparticles. The aim of this contribution is the use of SnO_2 NPs as the absorption layers of thin film and study on their fundamental physical and electrical properties on photovoltaic effect.

2. Experiment

0.1 M of stannous chloride dihydrate ($SnCl_2.2H_2O$) was dissolved in 100 mL of deionized water. After complete dissolution, 11 mL of ammonia was added by drop wise method at the room temperature. The white solution was suddenly changed into milky as soon as the ammonia was added. The solution then was vigorously stirred for a certain period until the white precipitates were obtained. During the stirring, the pH of solution was adjusted until greater than 10. When the precipitates were clearly separated from the solution, the stirring was stopped and stayed at overnight. The precipitates were centrifuged for 15 minutes at rpm 1500 and washed them by deionized water three times to remove excess ions and they were dried at 60 °C in air for 24 h. After that, dried SnO_2 were grinded by agate motor in order to get the fine powders. Then, the as-synthesized SnO_2 NPs were printed on Si wafer by screen printing method followed by the SnO_2/Si thin film by thermal diffusion method at the different annealing temperatures 400 - 800 °C for 1 h respectively. While the characterizations of SnO_2 films were investigated by XRD, FTIR, SEM and the electrical properties are measured by LUX meter and dual multimeter respectively. The crystal structure and crystallite size of the samples were confirmed by XRD (model Rigaku Multi Flux) using CuK_α radiation (40 kV, 40 mA) over a 2θ range from 10º to 70º on a powder type X-ray diffractometer equipped with a diffracted-beam graphite monochromator. The structural changes of the as-synthesized and calcinated SnO_2 samples were analyzed by FTIR. The spectra formation of SnO_2 structure were obtained by FTIR 8400 Shimadzu spectrophotometer by using a KBr pallet method in the Mid Infrared (MIR) radiation with the wavelength ranges from 4000 cm^{-1} to 400 cm^{-1} range with a resolution of 4.0 cm^{-1}. Surface morphology of the samples was investigated by SEM (JEOL 15 kV). Centrifuge machine (Kokusan H-200 series) with maximum 6000 rpm was used to separate the SnO_2 from the colloidal solution.

3. Results and Discussion

The crystal structures of the SnO_2 NPs were examined by XRD. The XRD spectra of the SnO_2 NPs (Fig. 1a) and SnO_2 thin film (Fig. 1b) at the annealing temperatures 600 °C for 1 h each were shown in Fig 1. The diffraction peaks from SnO_2 NPs (110), (101), (111), (211), (220), (002), (310) and (301) were observed in both Figs. They were broaden due to the crystallite sizes of SnO_2 particles in the samples were very small. All diffraction peaks were matched with the tetragonal structure of SnO_2 with the standard library file (ICDD-PDF #88-0287). The average lattice constant of a=4.7365 and c=3.1727. It was noted that the two prominent peaks (311) and (400) were found only in Fig. 1b which were attributed to diffraction peaks from Si wafer. Apart from these peaks, no other additional peaks were observed in XRD spectra. This showed that the samples have no more impurity after annealing. The predicted crystallite size of NPs was 25 nm by using Sherrer's formula.

$$D = \frac{K\lambda}{\beta \cos\theta} \tag{1}$$

Where λ is the wavelength of the incident X-ray beam (1.5405 Å for $CuK_{\alpha 1}$), K is a constant equal to 0.89 for spherical shape of particle, β is the FWHM (full width at half maximum), θ is the diffraction angle and D is the crystallite size.

FTIR spectra of as-synthesized and calcinated SnO_2 NPs were shown in Fig. 2a to study the effect of annealing temperature on the chemical bonding of SnO_2 NPs. The peaks were similar for all samples. The well configured band at 3400 cm^{-1} could be seen before the heat treatment on as-synthesized SnO_2 NPs. This was due to absorption of water. After the heat treatment at 600 °C and 800 °C, this band was not very strong as before because of dehydration / condensation [18]. Figure 2b showed the comparison of the IR spectra of the as-synthesized SnO_2 NPs after annealing at 600 °C and SnO_2/Si film at the deposition temperature 600 °C. In the spectrum (a), the observed two intense bands 663.53 cm^{-1} and 547.80 cm^{-1} were attributed to the vibrations of Sn-O [18-20]. In the spectrum (b), the band at 1107.18 cm^{-1} was assigned to the vibration mode of Si-O-Si/ O-Si-O group [21]. These were well known absorption bands of the SiO_2 network formed by the surface

oxidation of Si substrate. Another well absorption band appeared at 620 cm^{-1} was associated at Sn-O-Sn covalent bonds vibration [22].

To investigate the surface morphology and film thickness of the SnO_2 NPs, the sample was examined by SEM. Figure 3a shows the SEM micrographs of SnO_2 NPs at 600 °C. The size of observed particles shows the agglomeration of many single crystallites due to the inhomogeneous size distribution. This micrograph shows that the agglomeration of NPs has almost spherical shape. The film thickness of this sample was about 12.6 μm (Fig. 3b) which were measured by cross section position of film by SEM. For all samples, the measured film thicknesses were more than 10 μm.

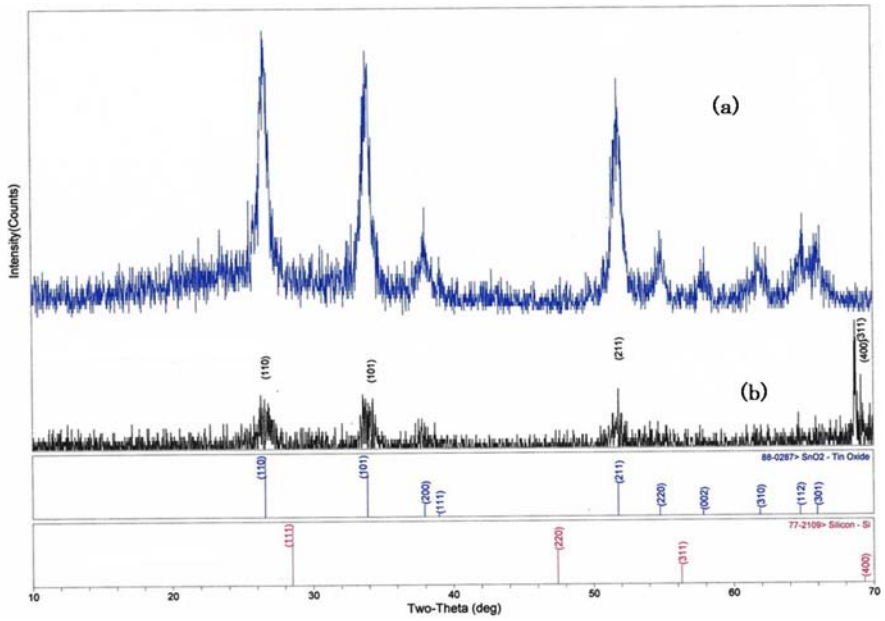

Fig. 1 XRD diffractograms of (a) SnO_2 NPs (b) SnO_2 thin film

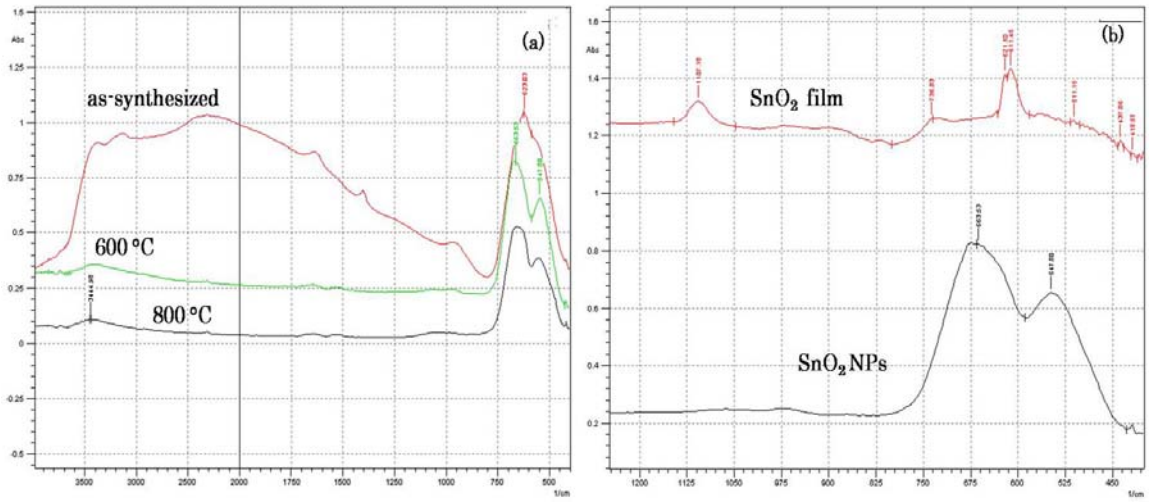

Fig. 2 FTIR spectra of SnO_2

I-V characteristic of each SnO_2/Si thin films were measured by using the LUX meter for illumination and FLUKE 45 dual display multimeter for measuring resistance, voltage and current.

The graphs measuring values of resistance, voltage and current depending on different illuminations were shown in Fig. 4. The graph revealed that the greater the illuminations, the lower the resistance values in all samples. Besides, the more increased the illuminations, the gradually higher values of voltage were resulted only for the film annealing at the deposition temperature 500 °C. As a result, the current values were also increased for that sample. In contrast, the voltage and current values were not sharply increased for other samples although the light intensities were increased. It can be concluded that the resistance and voltage values were depended on the light intensities which in turn depended on the deposition temperatures during the preparing of SnO_2 NPs deposited on Si substrate. It was observed that SnO_2 thin film showed photovoltaic characteristics since the resistance values were inversely proportional and the voltage values were directly proportional to the light intensities.

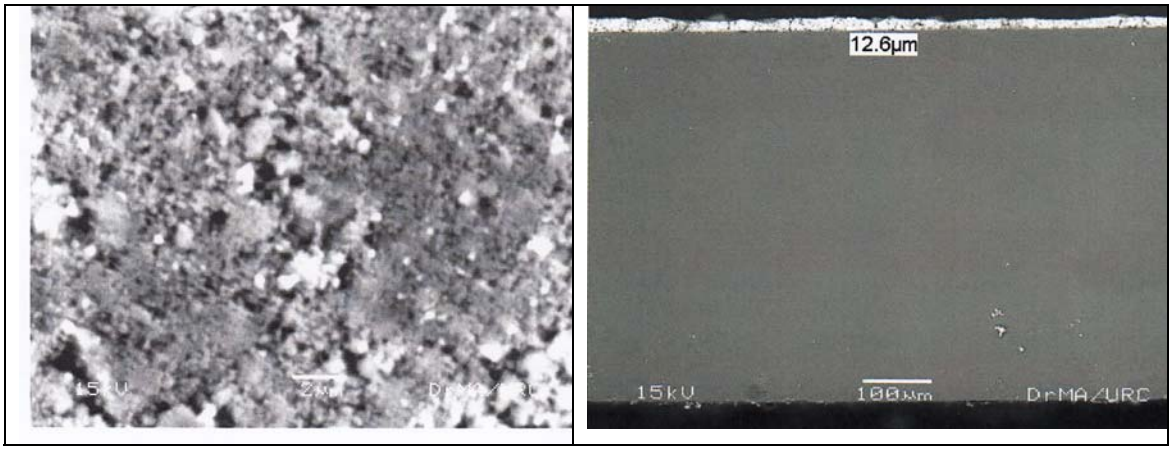

Fig. 3 SEM image of (a) surface morphology of SnO_2 NPs (b) cross-section of SnO_2 film

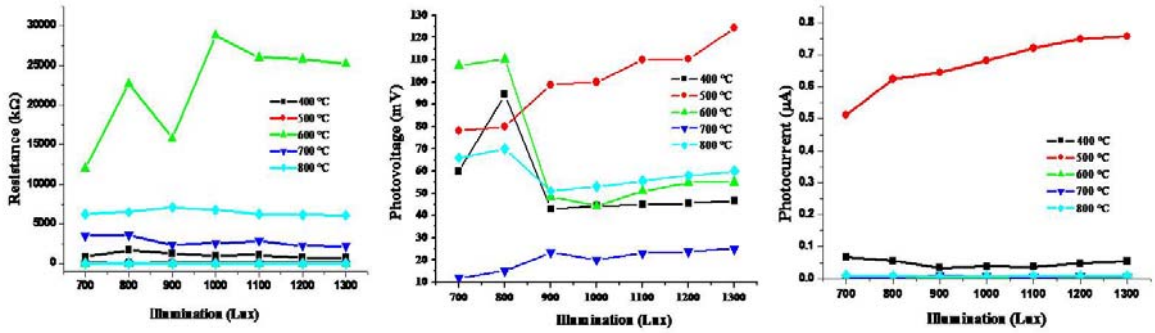

Fig. 4 The graph of SnO_2 /Si films showing (a) resistance, (b) photovoltage and (c) photocurrent depending on different illuminations

4. Conclusion

SnO_2 NPs were successfully synthesized by co-precipitation method. The crystal structure of SnO_2 NPs was tetragonal and the crystallite size was 25 nm by XRD. As-synthesized SnO_2 was deposited onto Si substrate at various diffusion temperatures from 400 °C to 800 °C by thermal diffusion method. The characterizations of the films were also investigated by XRD, SEM, FTIR and optical parameters depending on light intensities were measured by meters. According to measurements, SnO_2/Si junction resistance decreased with increasing illumination for all samples. However, the photovoltage values for the film at the diffusion temperature 500 °C were increased while the other films at the diffusion temperatures 400, 600, 700 and 800 °C were almost constants when the light intensities were increased. As a result, diffusion temperature 500 ˚C is the optimum temperature for the highest photovoltaic performances in this work.

Since the resistance values were inversely proportional and the photovoltage and photocurrent were directly proportional to the light intensities, the SnO_2/Si thin film behaved as a solar cell. This could be attributed to the absorption of light energy by SnO_2 NPs which converted then into the electrical energy. Therefore, SnO_2 NPs has the light trapping effect which can be applied in photovoltaic cells.

Acknowledgments

The authors acknowledge Prof Dr Tin Tun, Rector of University of Yangon and Prof Dr Pho Kaung, Pro-Rector of University of Yangon and Head of Universities' Research Centre (URC) for their encourages in carrying out the research. We also do thank to Dr Nay Myo Khaing (Associate Professor), Dr. Myo Aung (Assistant Lecturer) and Dr. San Htoo (Assistant Lecturer) for their help in the sample characterizations.

References

[1] A. V. Moholkar, S. M. Pawar, K. Y. Rajpure, C. H. Bhosale and J. H. Kim, Applied Surface Science, **255** (2009) 9358.
[2] H. Lee, C. M. Kang, M. Park, J. Kwak and C. Lee, ACS Appl Mater Interfaces, **5** (2013)1977.
[3] T-T. Duong, H-J. Choi, Q-J. He, A.-T. Le and S-G.Yoon, Journal of Alloys and Compounds, **561** (2013) 206.
[4] S. Chappel, S-G Chen and A. Zaban, Langmuir, **18** (2002) 3336.
[5] H. Köse, A.O. Aydin and H. Akbulut, Acta Physic Polonica A , **121** (2012).
[6] S. Chaisitsak, Sensors, **11** (2011) 7127.
[7] T. Isono, T.Fukuda, K. Nakagawa, R. Usui, R. Satoh, E. Morinaga and Y. Mihara, Journal of the Information Display, **15** (2007) 161.
[8] S. Gnanam and V. Rajendran, Digest Journal of Nanomaterials and Biostructures, **5** (2010) 925.
[9] M. H. S. Abadi, M.N.Hamidon, A. H. Shaari, N. Abdullah and R. Wagiran, Sensors, **11** (2011) 7724.
[10] S. J. Ikhmayies, International Journal of Materials and Chemistry, **2** (2012) 173.
[11] H. U. Igwe and E- I. Ugwu, Advances in Applied Science Research, **1** (2010) 240.
[12] S.-W. Ryu, J.-S. Hong, S.-T. Kim, J.-Y. Yang, B.-C. Ahn, W.-P. Hong, S.-H. Park, H.-M. Kim and J.-J. Kim, Journal of the Korean Physical Society, 50 (2007) 1833.
[13] A. F. Khan, M. Mehmooda, A.M. Rana and M.T. Bhatti, Applied Surface Science, **255** (2009) 8562.
[14] D. Tatar and B. Duzgun, Journal of Physics, **79** (2012) 137.
[15] C. Ristoscu, L. Cultrera, A. Dima, A. Perrone, R. Cutting d, H.L. Du, A. Busiakiewicz, Z. Klusek, P.K. Datta and S.R. Rose, Applied Surface Science, **247** (2005) 95.
[16] J. Jhon M, Vequizo, Jun and M. I. Wang, JJAP, **49**(2010) 125502.
[17] F. Gu, S. F. Wang, M. K. Lu, X. F. Cheng, S. W. Liu, G. J. Zhou and D. Xu, D. R. Yuan, Journal of Crystal Growth, **262** (2004) 182.
[18] A. S. Lanje1, S. J. Sharma , R. B. Pode and R. S. Ningthoujam, Archives of Applied Science Research, **2** (2010)127.
[19] C. M. Liu, X.T. Zu and W.L .Zhou, J. Phys, Condens. Matter, **18** (2006) 6001.
[20] A. Punnoose, J Hays, A. Thuber, M.H. Engelhard; R.K. Kukkadapu, C. Wang, V. Shutthanandan and S. Thevuthasan, Phys. Rev.B, **72** (2005) 54402.
[21] A. Sharma, D. Prakaha and K.D.Verma, Optoelectronics and Advanced Materials, **1** (2007) 683.
[22] C. Cobianu, C. Savaniu, O. Buiu, D. Dascalu , M. Zaharescu, C. Parlog , A. van den Berg and B. Pecz , Sensors and Actuators B, **43** (1997) 114.

(Received; 23rd December, 2013, Accepted; 15th July, 2014)

Flywheel Motor Powered by Road User

Aung Naing Win[1,2,*], Khin Khin Moe[1,*], Prof. Ying Jie Xiao[3,*,]
[1)] *Lecturer, Myanmar Maritime University, Yangon, Myanmar*
[2)] *Ph.D Student, Shanghai Maritime University, Shanghai, China*
[3)] *Dean, Merchant Marine College, Shanghai Maritime University, Shanghai, China*
**E-mail: aungnaingwin29@hotmail.com, khinkhinmoe1@gmail.com*

Extracting energy from several sources such as solar, wind, hydro and all available sources ,which does not impact the environment so much and is sustainable, is the most popular and thirsty technology of the world. Several of experts all over the world have been trying to get the more and more superior technologies of the production of energy which is environmentally friendly and sustainable. The paper presents the conceptual idea to recover energy from the downward acting forces of the vehicles moving on the road.
Flywheel is a kind of energy storage unit that has been used for a long time. It is a rotating mechanical device where energy is stored mechanically and transferred to and from the flywheel by an integrated motor/generator. The paper proposes a flywheel motor powered by moving truck (road user) on the road. Energy source places considered in this paper are the places where speed bumps are installed on the road for speed reduction purpose such as the places in front the toll gate where vehicles are needed to stop. Flywheel energy storage system is used because of the intermittent nature of energy formation process. Energy will collect from the downward acting force of the vehicle when it passes over the speed bump and the collected energy will be stored in the flywheel to drive the integrated motor. In this paper, the basic concept of the proposed machine is presented with a simple schematic diagram and the required materials are also listed. Feasibility of the installation of this kind of machine is also discussed in all aspects.
The proposed machine will give comfort of driving to the road user in spite of giving them discomfort because of installing the machine. Although the proposed idea mainly based on intuition without any design data, the machine would be functionally feasible and economically viable. The idea discussed in this paper is only the simple way but it is believed to be one of the ways that can contribute some amount to the future green energy production process.

Keywords: *Flywheel, Motor/Generator, Speed bump, Sustainable energy, Energy storage system.*

1. Introduction

Whenever a car pass over a speed bump, it must use some energy to climb up the bump because it is designed as a fixed bar and is protruding on the road bed (3 to 4 inches). Off course it is need to protrude on the road bed to make driver getting scene to slowdown his car but making as a fixed bar make vehicle to use more energy and let driver lost comfort of driving. In spite of installing as a fixed bump, if it is installed as an up and down movable bump, it will give not only comfort of driving and lesser use of energy but also can collect some energy from up and down moving force of the bump.

Actually to collect this kind of energy, no more high technology is needed. It can be done only with basic mechanical knowledge. The problem is the absent of initiator. With the aim of initiating to

recovery energy from this kind of source, the simple flywheel motor powered by moving truck on the road is presented in this paper. It is hoped that from this conceptual idea, more and more deeper research will be carried out in future in regard of energy recovery contribution.

2. Basic Concept of Machine

Schematic arrangement of the proposed flywheel motor is shown in figure .1. In this proposed machine system, there include three sub-unit: (1) the energy unit, (2) the transmission unit, and (3) the process unit.

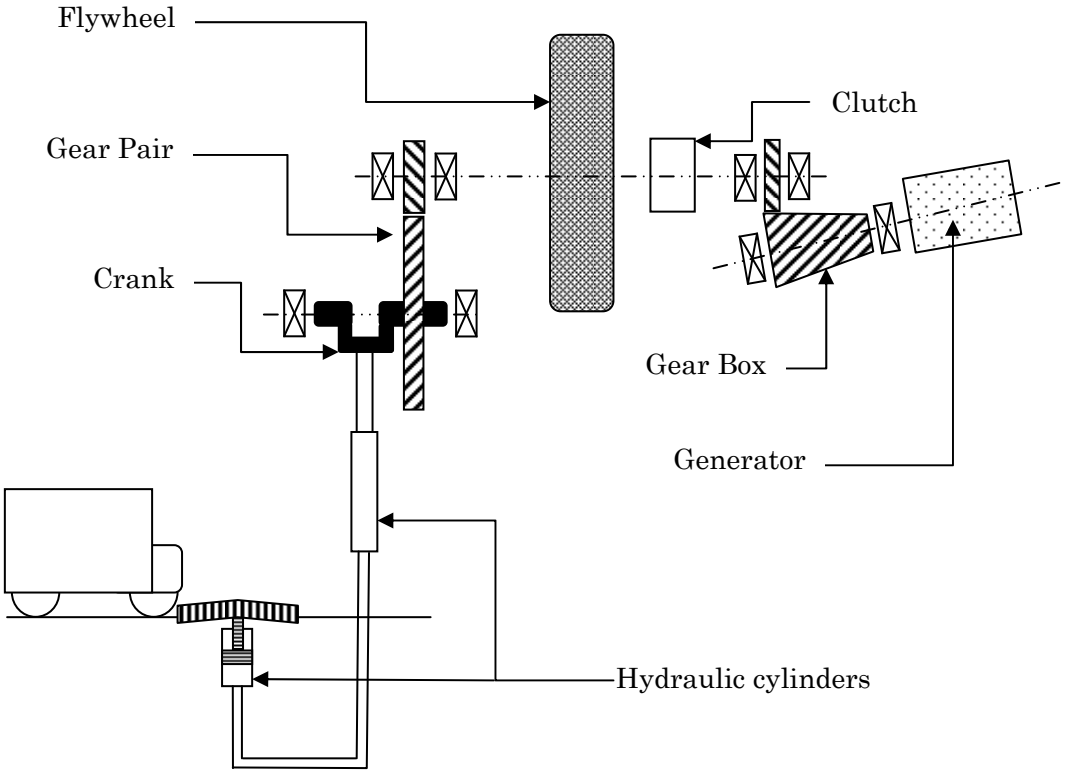

Fig. 1 Schematic Arrangement of the Proposed Machine

Energy unit consists of a hydraulic force collecting mechanism, a speed rise gears pair with appropriate gears ratio and a flywheel. Force collecting mechanism contains two hydraulic cylinders. One cylinder is to accept the downward acting force of the speed bump exerted by the over passing truck. The other cylinder is to drive the crank with this collected force. The speed rise gears pair is to transfer the torque on the crank to flywheel, a rotating mechanical device where energy is stored mechanically. The transmission unit consists of appropriate clutch and gear transmission. Because RPM of the flywheel will vary with the amount of energy stored in it, appropriate gear transmission is needed to regulate constant output. The process unit is just an electric generator.

Whenever a vehicle passes over the speed bump, it will give a driving force to the crank via hydraulic assembly. This driving force will give torque to flywheel via the gears where energy will stored mechanically. When the flywheel has stored the required amount of energy, that energy would be available for actuation of the generator through a suitable clutch and gear transmission.

3. Required Materials for the Proposed Machine

According to the schematic arrange of the proposed machine, the basic required materials are listed below;

- One adjustable up and down moveable speed bump with spring loaded lift

The purpose of this item is not only to serve as a speed bump, but also to accept the downward acting force of the passed over vehicle by moving up and down according to the force exerted.

- Two hydraulic cylinders,

The purpose of one cylinder is to accept force from up and down movement of speed bump and the other one is to drive the crank with that accepted force (i.e. giving torque to flywheel). The sizes of the pistons will be chosen based on the crank throw and high of speed bump.

- One crank shaft

The purpose of this item is to change reciprocating motion to rotary motion.

- One speed rise gears pair

The purpose of this gears pair is to increase the RPM.

- One flywheel

This one purposes to store energy.

- One set of clutch and gear transmission box

The purpose of this set is to transmit the stored energy with stable output to the generator

- One generator

This is for electricity generation

- 4 pairs of bearing and support frame

These will used in the installation of crank, gears, flywheel and generator.

Example of specifications of major machine parts intended to use in proposed machine prototype are listed in the following table 1.

Table 1 Specification of Major Machine Parts

No.	Name of Component	Major Dimensions	Material
1	High adjustable spring lifted speed bump	Length 72” x Width 12” x Height 2.25”	RUBBER
2	hydraulic cylinder 1	70 ton capacity, Single Acting	-
3	hydraulic cylinder 2	70 ton capacity, Single Acting	-
4	Crank shaft	CPO = 0.225 Crank stoke = 107.95 mm Rod journals = 53.34 mm Main journals = 66.04 mm	SAE 4340 steel alloy
5	Gear (Crank)	PCD = 450 mm, face width = 50 mm No. of teeth = 91	Cast Iron
6	Pinion (Flywheel shaft)	PCD = 190 mm, face width = 50 mm No. of teeth = 24	Cast Iron
7	Flywheel	Outer diam = 1000 mm, rim Width = 1000 mm, no. of arms = 6 Hub diam = 100 Wgt = 50 kg	Cast Iron
8	Flywheel shaft	Length 1050 mm, max. diam = 72 mm	SAE 1030 mild steel
9	Clutch	Length of one half = 118 mm Mean diam = 67 mm	Cast Steel
10	Drive Shaft	Length 740 mm, max. diam = 72 mm	SAE 1030 mild steel
11	Driven Shaft	Length 740 mm, max. diam = 72 mm	SAE 1030 mild steel
12	Pinion (Drive shaft)	PCD = 130 mm, face width = 55 mm No. of teeth = 24	Cast Iron
13	Gear (Driven shaft)	PCD = 530 mm, face width = 55 mm No. of teeth = 97	Cast Iron
14	Bearing	Crank Shaft Flywheel Shaft Drive Shaft Driven Shaft	-
15	Dynamo	5 Kw	-

4. Feasibility of the Proposed Machine

The proposed machine is very simple and only need to have basic mechanical knowledge to evolve this kind of machine. The only idea is to convert the reciprocating motion that generated from downward acting force of the truck exerted on speed bump to rotary motion so as to power the generator. According to the schematic diagram, if the developer has basic knowledge of hydraulic, crank, gear train, flywheel and motor/generator, it is enough to develop the machine. So it can say that the proposed machine is technically feasible. Moreover, the parts include in the proposed machine are very conventional and can easily get from the market with reasonable price. This fact also pointed out the economic feasibility of the machine.

In environmental point of view, the machine uses no fuel and it is like an energy compensating machine. It recovers the energy that truck will used in passing over the speed bump. The energy generated from this kind of machine can be called free, green and waste compensating energy. The machine will contribute in saving environment in spite of giving any impact to environment. Moreover, in driver point of view, they will welcome this kind of machine because of giving them driving comfort in passing the toll collection.

But a flywheel stores energy in a rotating mass. Depending on the inertia and speed of the rotating mass, a given amount of kinetic energy is stored as rotational energy. The kinetic energy stored in a flywheel is proportional to the mass and to the square of its rotational speed according to the following equation.

$$E_k = \frac{1}{2} I\omega^2$$

Where Ek is kinetic energy stored in the flywheel, I is moment of inertia and ω is the angular velocity of the flywheel. The moment of inertia for a circular object is a function of its shape and mass.

$$I = \frac{1}{2} Mr^2$$

To optimize the energy to mass ratio the flywheel needs to spin at the maximum possible speed. Kinetic energy only increases linearly with mass but increases at the square of the rotational speed. On the other hand, for effective storage of energy, long rundown times are also required.

The literature search made did not produce data regarding what should be the optimal gear ratio and the moment of inertia of the flywheel so that this proposed machine system could store maximum energy in the flywheel for the shortest possible running time. Obviously the most compatible system with the minimum possible energy loss is wanted. Thus the most obvious drawback or weak point of the proposed system is no design data were available for the energy unit.

5. Conclusion

Although the proposed machine is a simple one, it is sure that more or less energy could be generated. Several of experts all over the world have been trying to get the more and more superior technologies of the production of energy which is environmentally friendly and sustainable. Every day there has millions of several heavy weight trucks and vehicles operating all over the world for transportation purpose. If a reasonable amount of energy used by these vehicles in speed bump can be recovered by the proposed system, it would be a contribution to the future green energy production process. So it is recommend that, this kind of simple and low tech arrangement should not be underestimated and a deeper research should be carried out. Therefore, future work would be the development of a prototype and making research for the best arrangement and analysis of how much energy that this kind machine can generate on an average.

Acknowledgments

Special appreciation goes deeply to supervisor, Prof. Ying Jie Xiao, Dean, Merchant Marine College, Shanghai Maritime University, Shanghai, China for his kindness to me. And special thanks to my wife Khin Khin Moe, who gives me encouragement, motivation and advice, moreover gives me present for poster presentation at 1st ICEEHE.

References

[1] J. P. Modak, Design and Development of Manually Energised Process Machines having relevance to Village/ Agriculture and other Productive Operations, HUMAN POWER, International Journal of Human Powered Vehicle Association USA, April 2006, No. 57.
[2] J. P. Modak, Human Powered Flywheel Motor Concept, Design, Dynamics and Applications
[3] Luís de Sousa, Energy storage – flywheel, The Oil Drum, OCT 5, 2011, http://www.resilience.org/stories/2011-10-05/energy-storage-flywheel
[4] Pedal powered farms and factories: the forgotten future of the stationary bicycle, Low-tech Magazine, May 25, 201 1, http://www.lowtechmagazine.com/
[5] United Nations Environment Programme(UNEP), Energy Efficiency Guide for Industry in Asia, 2006, www.energyefficiencyasia.org
[6] B. Bolund et al., Flywheel energy and power storage systems, Renewable and Sustainable Energy Reviews, November 2007, Pg. 235–258
[7] Gabrys CW. High Performance Composite Flywheel, US patent Pub. No.: US 2001/0054856 A1; 27 Dec 2001.
[8] Ojo O. Multiobjective optimum design of electrical machines for variable speed motor drives. IEEE Conferrence Record 1991 p. 163–168.
[9] Kim WH, Kim JS, Baek JW, Ryoo HJ, Rim GH, Choi SK. Improving efficiency of flywheel energy storage system with a new system configuration PESC 98 Record. 29th Annual IEEE Power Electronics Specialists Conference; 1998, p. 24–28.
[10] A. R. Bapat, "Formulation of Generalised Experimental Models for various Dynamic Responses of a Manually Energised Flywheel Motor". Ph. D. Thesis of Nagpur University, 1996 under the supervision of Dr. J. P. Modak.
[11] Bitterly JG. Flywheel technology: past, present, and 21st century projections. IEEE Aerospace Electron Syst Mag 1998;13:13–6.
[12] Taylor P, Johnsson L, Reichert K, DiPietro P, Philip J, Butler P. A summary of the state of the art of superconducting magnetic energy storage systems, flywheel energy storage systems and compressed air energy storage systems SAND99-1854, unlimited release. Albuquerque, New Mexico 87185 and Livermore, California 94550: Sandia National Laboratory; 1999.
[13] Aanstoos TA, Kajs JP, Brinkman WG, Liu HP, Ouroua A, Hayes RJ, et al. High voltage stator for a flywheel energy storage system. IEEE Trans Magn 2001;37:242–7.
[14] Hofmann H, Sanders SR. Synchronous reluctance motor/alternator for flywheel energy storage systems. IEEE Power Electron Transport 1996;199–206.
[15] Cengelci E, Enjeti P. Modular PM generator/converter topologies, suitable for utility interface of wind/micro turbine and flywheel type electromechanical energy conversion systems. Conference Record of the 2000 IEEE Industry Applications Conference, vol. 4, p. 2269–2276.
[16] Mellor PH, Schofield N, Howe D. Flywheel and supercapacitor peak power buffer technologies, IEE seminar electric hybrid fuel cell vehicles, p. 8/1–5.
[17] Kan HP, Chau KT, Cheng M. Development of a doubly salient permanent magnet motor flywheel energy storage for building integrated photovoltaic system APEC 2001, Proceedings of the 16th IEEE conference, p. 314–320.
[18] Yoon-Ho K, Kyoung-Hun L, Young-Hyun C, Young-Keun H. Comparison of harmonic compensation based on wound/squirrel-cage rotor type induction motors with flywheel. Proceedings of third international conference on power electronics and motion control; 2000, p. 531–536.
[19] Jiancheng Z, Zhiye C, Lijun C, Yuhua Z. Flywheel energy storage system design for distribution network. IEEE Conf Proc 2000;4:2619–23.
[20] Truong LV, Wolff FJ, Dravid NV. Simulation of flywheel electrical system for aerospace applications. Collection of Technical Papers. 35th Intersociety Energy Conversion Engineering Conference and Exhibit (IECEC) (Cat. No. 00CH37022). vol. 1, pt. 1 2000 p. 601–68.
[21] Bakholdin D, Bosley RW, Rosen HA, Pearson CC, Pano SB. Hub and cylinder design for flywheel for mobile energy storage US Patent No: 6,175,172 B1; 16 Jan 2001.

(Received; 23rd December, 2013, Accepted; 8th May, 2014)

Demonstration of Text Similarity Metric for Plagiarism Detection

Ohnmar Htun[1], Yoshiki Mikami[2,*]
[1)]*Department of Management & Information System Science, Nagaoka University of Technology,*
[2)]*Department of System Safety, Nagaoka University of Technology,*
1603-1 Kamitomioka-cho, Nagaoka 940-2188, Japan
**E-mail: mikami@kjs.nagaokaut.ac.jp*

This paper proposes an enhanced text similarity metric, and presents a detailed study of its application to plagiarism detection. Text can be plagiarized in many ways; typically text is reused material (copy & paste) and in addition some parts of the reused text may be changed. Our method combines tree based indexing and string edit-distance measure algorithms: suffix tree and longest common subsequence, as well as introducing a text chunking approach to break a given document into segments that provides a way to efficiently identify the level of plagiarism. The proposed algorithm consists of three phases: pre-processing, the processing, and post processing. The pre-processing phase executes two tasks: text-chunking and indexing the documents. Then the processing phase performs string matching task by calculating the longest common subsequence. Finally the post-processing step carries out a two level local and global analysis, which identifies the similar text passages that may have been plagiarized. The proposed algorithm is evaluated by using four artifical plagrized suspicious documents (i.e., 100%, 50%, 25%, and 0% plagiarized dataset) made from academic papers and science & technology review works as source. The results were 99.64% accuracy, 94.22% recall, and 99.32% precision, on average. We also found that if 5% of text in sentences were replaced with synonyms, the precision was adversely affected. Synonym replacement cannot be detected easily and this can make plagiarism detection considerably more difficult. The proposed algorithm takes time $O(m^2n^2\omega)$ to compute *LCS*, it is required to optimize in future work.

1. Introduction

Text can be plagiarized in many ways; typically text is reused material (copy & paste) and in addition some parts of the reused text may be changed. The problems of plagiarism are often dealt with in several domains (e.g., the software and entertainment industries), but it probably occurs most frequently in academic institutions [1]. Today, the Internet is a vast information resource for everyone. Students can easily reproduce one another's work without acknowledging the source. These dishonorable activities are not acceptable in the academic community. Research and development of plagiarism detection methodology is active in the fields of both Natural Language Processing (NLP) and Information Retrieval (IR). There are many tools available, both commercial and free GNU (General Public License). These systems use many different sorts of retrieval techniques: vector space models (VSM), fingerprint, sliding window techniques, etc. The application of techniques involving the longest common subsequence (LCS) (i.e., approximate string matching approaches) are limited. Each method of plagiarism detection has a basic problem with large amounts of data, because every usable method is capable of processing only a limited amount of data within an appropriate time limit [2]. Furthermore, most applications support a particular language only, so that methods for multi-source and multi-lingual plagiarism detection are currently a challenging issue in information retrieval area. Therefore, our research objective is to develop an efficient text similarity metric that can be applicable detecting reused/plagiarized texts and finding source/reference documents of the manuscripts in the academic domain. In addition, using an approximate string matching approach that can be easily scaled up to linear data processing. In order to demonstrate this proposed methodology, we applied a powerful dynamic programming technique that combines a number of methods: suffix tree, suffix arrays, longest repeated substring (LRS), longest common subsequence (LCS), and a new improvement of LCS that yields the common string matching. Experiment is conducted with the four different proportions of text reuse (i.e., 100%, 50%, 25%, and non-plagiarized) in the suspicious documents and the collection of nine source documents (i.e., size 280,180 bytes in total). This paper is organized as follows: the next section gives an

overview of related research and technologies. The proposed methodology is presented in Section 3. The detail of experiment: data, results, and evaluations are reported in Section 4. Finally, a conclusion and avenues for future work are presented in Section 5.

2. Related Research

Narayanan et al. (2008) proposes the architecture and design of a copy-paste checking system [3]. Their approach begins with building an index of documents. Text in a source document is broken down into snippets of 20 words. Then, document similarity is computed based on the extent of the matching fingerprints in a target document. The scope of the system is that it is only to serve as a function in this particular e-learning system. Kasprzak et al. (2009) presents an external plagiarism detection system that is a modified version of an existing anti-plagiarism system used in the Czech National Archive of Graduate Theses [4]. The detection approach of the retrieval method is based on tokenization, a word-5-gram vector space model (VSM) using Boolean weights, and Jaccard similarity. If a suspicious document shares at least 20 n-grams with the reference collection documents, it is taken to have plagiarized sections. Their overall performance result achieved 2nd place in the PAN Workshop-2009 competition. In pre-processing, a language-dependent step to translate and stem words is required. Kong et al. (2013) presents plagiarism detection for source retrieval and text alignment in previous contest at the PAN Workshop-2013 [5]. Source retrieval method combined TF-IDF (i.e., Term Frequency - Inverse Document Frequency) PatTree, and Weighted TF-IDF to retrieve the keywords to search in suspicious documents. Their text alignment method is based on sentence similarity: text alignment algorithm and similar sentences merging algorithm, which is called Bilateral Alternating Merging algorithm. Their results did not perform well in all detection tasks. Osama et al. (2013) presents an implementation of a plagiarism source retrieval system in English at the PAN Workshop-2013 [6]. In their approach, the TextTiling algorithm is used to break a given document into segments, and the KPMiner key phrase extraction system generates the key phrases from segments. And then these key phrases and segments are used in generating queries to ChatNoir search engine for finding plagiarism sources in the ClueWeb09 corpus. The proposed system reached the highest number of top performance indicators (recall and F1 score).

In general, plagiarism detection algorithms specifically depend on the knowledge of natural languages processing (NLP) such as grammatical rules, parsing words, dictionaries, translation, etc. The performance of plagiarism detection is as important as their underlying algorithms implementing in dynamic programming. Many string-matching algorithms feature have both merits and demerits based upon the length of the strings and the technique used. The PAN2013 [7] developed a baseline algorithm using n-gram tokenizer with a filter that breaks tokens into N-grams (50-grams) to identify the length passages of reused text between source and suspicious documents. Using this tokenizer leads to spaces in the tokens. In the previous literatures, most of the methods were based on n-gram matching and vector space models. Our approach is based on the approximate string matching by applying two particular techniques: document level text chunking and suffix array that is able to reduce the memory problems found in suffix tree construction. In addition, calculating enhanced common string affirms the reused text passages between source and suspicious documents accurately.

3. Methodology

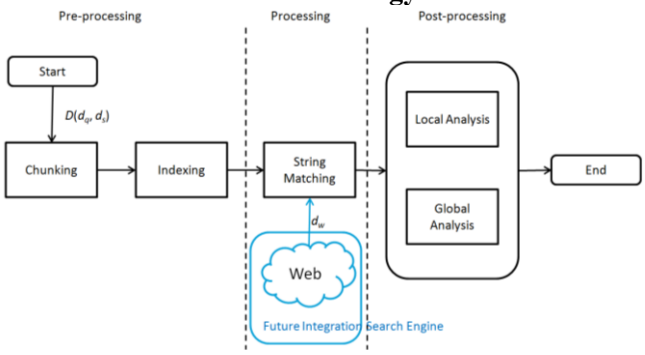

Fig. 1 Overview of proposed system: Text Similarity Metrics

The proposed algorithm, enhanced Text Similarity Metric (eTSM) is composed of three phases: pre-processing, the processing, and post processing. The pre-processing phase executes two tasks:

chunking and indexing the documents. Mid-processing phase performs the string-matching task. Finally, post-processing determines the similar text passages that may have been plagiarized. Figure 1 depicts an overview of methodology, in this figure, D is a collection of documents in general, d_q is a suspicious document (i.e., possibly plagiarized document), d_s is the source documents (i.e., documents are possible to plagiarize by d_q), and d_w is the source documents from the Web (i.e., apply to the future search engine implementation). We will use these notations in the following sections.

3.1 Text chunking

Typically text chunking is the task of dividing sentences/phrases into non-overlapping segments/chunks [8]. The length of a document can be an arbitrarily large string that must be split into groups of bytes called chunks. In this case, we chose appropriately the maximum size of a chunk to be 1,024 bytes of content-length. This size is chosen an optimal value because the limit of a query string in Google advanced search is 1,024 bytes[1], which is intended to be used in the processing phase (i.e., search engine). The chunk of the candidate suspicious document d_q is denoted by c_q, and the source document d_s of chunks is denoted by c_s. Generally, the document d_q and d_s with nonempty strings can be split into m and n number of chunks as shown below:

$$d_q = \{c_{q1}, c_{q2}, c_{q3}, \ldots, c_{qn}\}$$
$$d_s = \{c_{s1}, c_{s2}, c_{s3}, \ldots, c_{sm}\}$$

Where the length of chunk c_q and c_s can be 1,024 bytes in maximum.

3.2 Indexing

Then each set of chunks (c_q,c_s) is built into an index. We applied linearithmic algorithm [9, 10] to construct a suffix tree index and convert it into a suffix array index for each chunk. Let the suffix tree of a candidate suspicious chunk be T_q and a source chunk be T_s, which can be split into a set of substrings as shown below:

$$c_q = T_q = \{s_{q1}, s_{q2}, s_{q3}, \ldots, s_{qi}\}$$
$$c_s = T_s = \{s_{s1}, s_{s2}, s_{s3}, \ldots, s_{si}\}$$

Then the substrings of T_q and T_s are merged and sorted in a suffix array T_w, as shown below:

$$T_w = T_q + T_s$$

Building suffix array is able to reduce the memory problems found in suffix tree construction.

3.3 String matching

In the processing phase, we find all possible longest common strings in each suspicious chunk by applying the *LCS* algorithm [11, 12], and define M_i to be the longest length of a longest common subsequence that is found in the suffix array T_w of a suspicious chunk. M_i is given by the following:

$$M_i = longest(LCS(T_q, T_s)) \quad (1)$$

Then the filtering process begins to extract the common strings, comparing each $|M_i|$ against a threshold t. According to our observations, we set a parameter of t to a minimum string length of 28 bytes for the length of each common string, $|M_i|$. If the score of $|M_i|$ is equal to or lower than t, the value of the similarity chunk will be disregarded. Alternatively, if $|M_i|$ is greater than t, we assume that there may be a similar/plagiarized passage in a chunk. In addition, this process reduces mismatching and the unnecessary performance of calculation tasks. After the filtering process, the longest common string M_i is matched in a chunk of c_q. Then again, the scalar value of enhanced common string *eCS* of each matching substrings is calculates as follows:

$$eCS = \frac{2|M_i|}{L_q + L_s}$$

where L_q and L_s are the lengths of suspicious and source chunk.

3.4 Local analysis

Then the degree of similarity (θ_i) between all i chunks in a suspicious document (i.e., $\forall c_i$ in d_q) and all j chunks in a source document (i.e., $\forall c_j$ in d_s) is calculated based on the enhanced common string value $|eCS_{ij}|$ as follows:

$$\theta_i = \sum_{j=1}^{m} (eCS_{ij})$$

This level determines the degree of similarity (i.e., the amount of plagiarized data) between a suspicious document d_q and a source document d_s (i.e., one-to-one document).

---

[1] http://www.googleguide.com/search_forms.html

3.4 Global analysis

Finally, the evaluation of total similarity/reused text (Sim_{dq}) between a candidate suspicious document d_q (i.e., for all c_i) and all candidate source documents (k) for all d_s (one-to-many document) is calculated as follows:

$$Sim_{dq} = \sum_{k=1}^{n} \theta_{ik}$$

This level gives a final similarity/detection score of a suspicious document (i.e., d_q-to-$\forall d_s$).

4. Experiments

4.1 Data

We developed a simulation dataset, which contains a collection of nine source documents (i.e., size 280,180 bytes in total) from academic papers (i.e., conference proceedings, journals, and white papers) and four suspicious documents (i.e., formed as 100%, 50%, 25%, and 0% non-plagiarized). The sizes of reused text passages in a suspicious document ranged from 142~722 bytes and were taken from the collection of source documents. The size of each suspicious document is shown in Table 1.

Table 1 The size of candidate suspicious documents

Suspicious Document	% of Text Reuse	Size (byte)
Test-1 (d_s1)	100%	7,356
Test-2 (d_s2)	50%	6,431
Test-3 (d_s3)	25%	6,864
Test-4 (d_s4)	0%	16,631

In addition, the degree of text reuse amount can be changed using synonyms in the sentences. Therefore, Test-3 data is modified by replacing synonyms in a part of d_s4 (229 bytes), then we evaluate the results between Test-3 and synonyms replacing Test-3/1. Both suspicious and source text files are encoded in UTF-8 without BOM format. Our proposed method is expected to cover detection for a group of UTF-8 encoded languages, but the current experimental test data was only in English.

4.2 Experimental results

In this experiment, we applied seven variable character-level thresholds (i.e., 0, 8, 16, 24, 32, 48, 64, and 128) to evaluate the detection results. Based on these threshold values, the results are listed in below Figures 5~12. The results for 0 byte (without filtering), 8 byte, and 16 byte thresholds found more than the actual number of characters of text reuse in each suspicious document. The results for threshold 24 byte and 32 byte are close to the number of actual reused characters in each suspicious document.

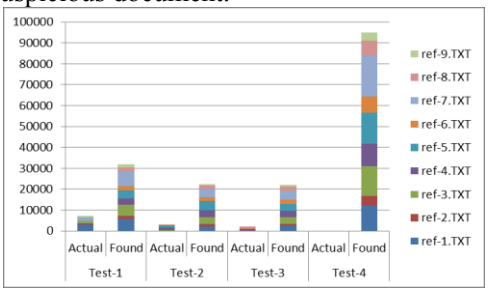

Fig. 2 Characters in actual plagiarized and detected by eTSM with a 0-byte threshold

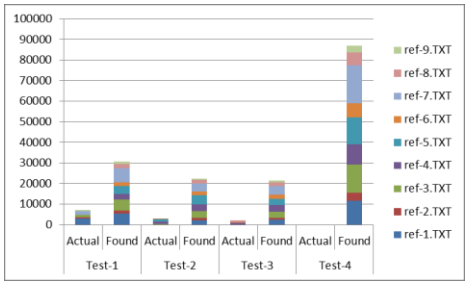

Fig. 3 Characters in actual plagiarized and detected by eTSM with a 8-byte threshold

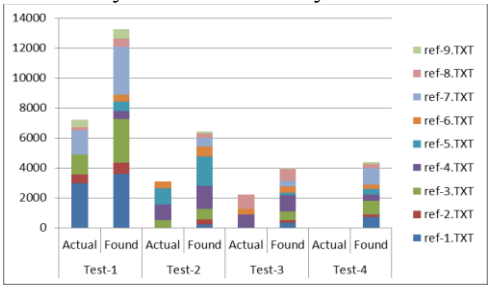

Fig. 4 Characters in actual plagiarized and detected by eTSM with a 16-byte threshold

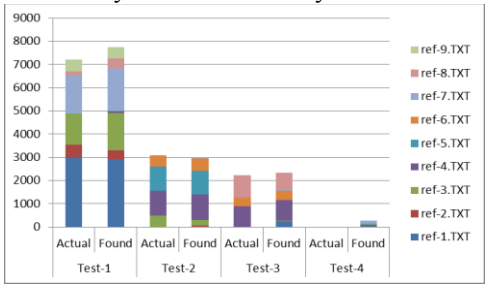

Fig. 5 Characters in actual plagiarized and detected by eTSM with a 24-byte threshold

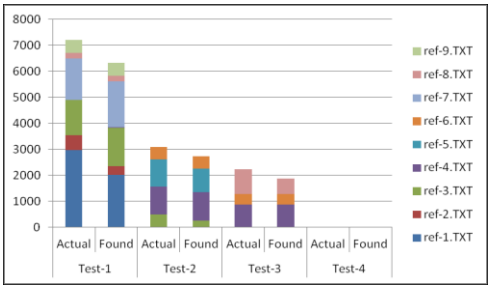

Fig. 6 Characters in actual plagiarized and detected by eTSM with a 32-byte threshold

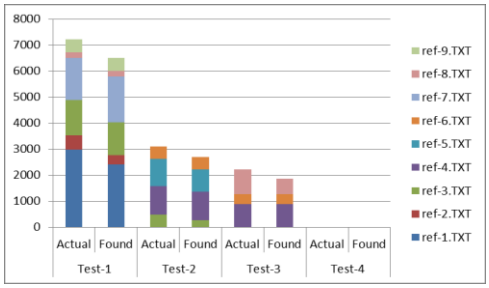

Fig. 7 Characters in actual plagiarized and detected by eTSM with a 48-byte threshold

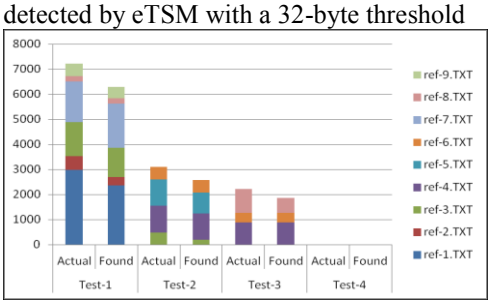

Fig. 8 Characters in actual plagiarized and detected by eTSM with a 64-byte threshold

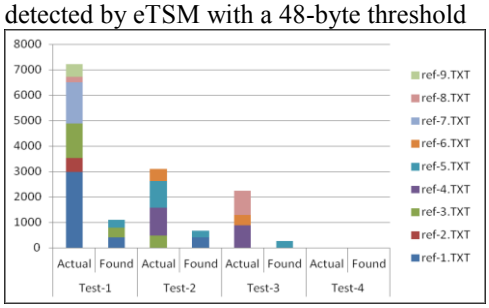

Fig. 9 Characters in actual plagiarized and detected by eTSM with a 128-byte threshold

However the results for thresholds of 48 bytes and 64 bytes are lower, and the result for a 128 threshold byte is much less than the actual size. In order to setup an optimal threshold at the filter process, we selected to calculate a mean value between 24 and 32 byte thresholds.

Searching a large document or long text queries in documents containing hundreds or even thousands of lines is challenged work. In this case, there is usually a trade-off between performance and accuracy. Utilizing the advantages of dynamic programming, for two sequences of length m and n ($m \geq n$), a basic *LCS* problem can be solved in $O(mn)$ time and space complexity [13]. Our approach in dynamic programming, *LCS* for two strings T_s and T_q such that M_i is a subsequence of the solution *LCS*, then since there are $O(m^2n^2\omega)$ time, where m, n, and ω are length of T_s, T_q, and M_i, respectively. This prototype implementation has a problem to optimize the time.

4.3 Evaluation

Precision states the degree of detection in text reuse passages between a suspicious document and source documents. Recall states the percentage of the reused text passages in a suspicious document that is detected correctly by algorithm. In addition, the harmonic mean between the precision and recall (F-measure) and the overall percentage of correctness of detection result (Accuracy) are also evaluated. Table 2 shows the results in precision, recall, F-measure, and accuracy for each suspicious document using an optimal threshold at 28-bytes. Our algorithm achieves an average of 99.32% precision, 94.22% recall, 96.42% F-measure, and 99.64% accuracy.

Table 2 Results in precision, recall, F-measure, and accuracy for each suspicious document using a 28-byte threshold

	Test -1	Test-2	Test -3	Test-4	Averages
Precision	98.22	99.05	100.00	100.00	99.32
Recall	95.97	96.08	84.81	100.00	94.22
F-measure	97.07	97.52	91.08	100.00	96.42
Accuracy	99.18	99.76	99.63	100.00	99.64

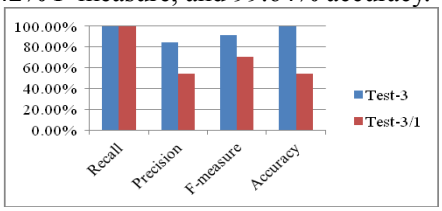

Fig. 10 Performance comparison between Test-3 and Test-3/1

Moreover, in the real word, the most cases of plagiarism occur by copying from a source changing synonyms (substitution of equivalent words) and noun phrase modifiers. After replacing 5% of the content words in sentences from Test-3 with synonyms, we found that the result in recall was still maintained, but the precision decreased by 30.67%. Figure 10 depicts the comparison of recall, precision, F-measure, and accuracy between Test-3 (text reuse only) and Test-3/1 (replacing synonyms). In addition, we implemented a n-gram baseline matching algorithm from PAN2013 [7] to compare the performance of our algorithm. In this attempt, the baseline algorithm detected a less number of reused texts in each suspicious document while eTSM retrieved the reused text passages

from the source document correctly. Table 3 depicts the precision of retrieval comparison between eTSM (at 28 byte threshold) and the baseline algorithm.

Table 3 The Precision of Retrieval Comparison

	Test -1	Test-2	Test -3	Test-4
Baseline	37.91%	19.35%	23.24%	0%
eTSM	98.22%	99.05%	100%	100%

We setup this baseline algorithm with a filter that breaks tokens into 20-grams to identify the reused texts between source and suspicious documents.

5. Conclusion

In this paper, we demonstrate a technique for plagiarism detection called the enhanced text similarity metric (eTSM) based on approximate string edit distance measures. We combines tree based indexing and string edit distance measure algorithms, as well as introducing a text chunking approach to break a given document into segments that provides a way to efficiently identify the level of text reuse plagiarism. The initial results (text reuse) were 99.64% accuracy, 94.22% recall, and 99.32% precision, on average. We also found that if 5% of words in sentences were replaced with synonyms, the precision was adversely affected. Synonym replacement cannot be detected easily and this can make plagiarism detection considerably more difficult. Our approach is computationally efficient by using text chunking, an building suffix array index, and threshold filtering. We expect that it would readily scale up to large data collections and potentially to the plagiarism detection for source retrieval and text alignment tasks. In future work, eTSM has room for improvement in detecting sentences with replaced synonyms and to optimize the time and space for the source retrieval and text alignment tasks in the next PAN2015 contest.

References

[1] Paul Clough: Plagiarism in natural and programming languages: an overview of current tools and technologies, Journal of Finance, July issue, pp.1-31, doi:10.1.1.65.774, (2000).

[2] Jan Grman and Rudolf Ravas: Improved implementation for finding text similarity in large collections of data, CLEF 2011 Labs and Workshop Proceedings, Notebook Papers, Amsterdam, The Netherlands, (2011).

[3] Narayanan Kulathuramaiyer, Bilal Zaka, Denis Helic: Integrated Copy-Paste Checking: Design and Services, Proc.Intl.Conf. the Eighth IEEE International Conference on Advanced Learning Technologies, ICALT '08, pp. 519 - 523, (2008).

[4] Jan Kasprzak, Michal Brandejs, Miroslav Kripac: Finding Plagiarism by Evaluation Document Similarities, 3rd PAN Workshop & 1st Competition on Plagiarism Detection Proceedings, pp. 24-28, (2009).

[5] Kong Leilei, Qi Haoliang, Du Cuixia, Wang Mingxing, Han Zhongyuan: Approaches for Source Retrieval and Text Alignment of Plagiarism Detection, Notebook for PAN at CLIF Evaluation Labs and Workshop Proceedings, (2013).

[6] Osama Haggag and Samhaa EI-Beltagy: Plagiarism Candidate Retrieval Using Selective Query Formulation and Discriminative Query Scoring, Notebook for PAN at CLIF Evaluation Labs and Workshop Proceedings, (2013).

[7] Martin Potthast, Benno Stein, Alberto Barrón-Cedeño, Paolo Rosso: An Evaluation Framework for Plagiarism Detection, Proceedings of the 23rd International Conference on Computational Linguistics, COLING (2010).

[8] Baker, Paul, Andrew Hardie & Tony McEnery: A Glossary of Corpus Linguistics. Edinburgh: Edinburgh University Press, (2006).

[9] U. Manber and E. Myers: Suffix Arrays: A New Method for On-Line String Searches, SIAM Journal on Computing 22, 5 (1993), 935-948. (Also appeared in: Proceedings of the First ACM-SIAM Symposium on Discrete Algorithms (1990), 319-327.)

[10] Robert Sedgewick and Kevin Wayne: Algorithms Fourth Edition, Addison Wesley, USA, (2011).

[11] Brian Martin, Plagiarism: a misplaced emphasis, Journal of Information Ethics, vol. 3(2), 36-47, (1994).

[12] Dan Gusfield: Algorithms on strings, trees, and sequences: Computer Science and Computational Biology, Cambridge University Press, (2007).

[13] Robert A. Wagner and Michael J. Fischer, The string-to-string correction problem, J. ACM 21 (1974), no. 1, 168–173.

Identifying the Associations between Music and Emotion in Developing an Emotion Based Music Recommendation System

Sugeeswari Lekamge, Ashu Marasinghe
Department of Management and Information Systems Engineering,
Nagaoka University of Technology,
1603-1 Kamitomioka-cho, Nagaoka 940-2188, Japan
E-mail: sugeeswarilekamge@gmail.com, ashu@kjs.nagaokaut.ac.jp

Emotion based music retrieval has a great potential in catering today's digital music archives rapidly expanding in the growing mobile and ubiquitous environments. Existing literature provides evidence for various efforts made in music classification based on genre, artist and emotion which utilize Signal Processing, Machine Learning and Data Mining techniques. This research aims at identifying the associations between the acoustic features of music and the perceived emotions as an initiating step in developing an emotion based music recommendation system. The above discoveries will also be assisting in a number of areas including music therapy and emotion based music composition. As the source for identifying the above relationships Sri Lankan folk melodies have been selected considering their potential in emotional expression. An emotion annotated corpus is being built storing the above melodies in the digital form allowing them to be analyzed, enabling them to be utilized in a constructive manner. Annotating the music clips with emotions which are highly subjective in nature and heavily affected by human Kansei, is viewed as a critical step. A new music emotion model which will allow to better describe the emotional expression inherent in Sri Lankan folk melodies is being built followed by a review of the existing general and music-specific emotion models. In identifying the potential of Sri Lankan folk melodies in emotional arousal, a pilot survey was conducted using folk music excerpts which are demonstrative of the basic emotions discussed in the Sri Lankan traditional arts, as the stimuli. Orchestral music was used considering the possible impact by the lyrical content on the perceived emotion as the research is focused on the audio content of music.

1. Introduction

Emotion based music classification is currently gaining high popularity among the Music Information Retrieval research. Along with the growth of digital music archives accelerated by the internet and mobile phone penetration a higher demand is anticipated for emotion based music retrieval. Music retrieval based on searches given a particular emotion as the query is believed to be highly preferred over the searches simply based on the title, artist or genre. Though there are various attempts made in developing music recommendation systems, most of them are trying to make accurate predictions about what people demand to listen to, or buy next, independently of how useful to the user could be the provided recommendations. Quite often these algorithms tend to recommend popular or well known to the user-music decreasing the effectiveness of the recommendations [1]. In contrast, emotion based music recommendation focuses on the perceived quality of music. On the other hand this will help discover the creative musical content having a huge potential in emotional arousal which are still hidden in the long tail of the popularity distribution. Music is successfully used for mental healing in a number of specific applications including music therapy, selection of background music played in shopping malls to stimulate sales and in context-aware homes to match with the emotional states of the inhabitants. Identifying the associations between musical features and emotions is also assisting in automatic composition of emotion-based music.

In discovering the above associations between music and emotion the study utilizes Sri Lankan folk melodies which can be regarded the transformations of true and innate feelings of the native community in the form of music. Emotional expression is inherent in these melodies as they have been emerged as a means of expressing or overcoming certain emotional states. This emotional expression is accompanied by unique ensembles of musical features that are within the human perception. Though Sri Lanka possesses such a folk song repository enriched with a wide variety of folk songs that can be explored in both the mathematical and psychological perspectives, storing the above melodies in the digital form which will allow them to be analyzed, enabling them to be utilized in a constructive manner remains as a need yet to be served. Catering the above need, this study will contribute in preserving the Sri Lankan identity of folk music while promoting it globally.

The emotional experience one gains through listening to a music piece is heavily associated with human Kansei. Music induced emotions are always affected by a number of factors including the listener's previous experiences, contextual knowledge and understanding and the cultural or religious background he has grown up. Due to the subjective nature inherent in emotions and the vagueness in expressing the perceived emotion, music emotion annotation has become a critical task. At the same time a single music clip may convey different emotions in various degrees while representing a single predominant emotion. Therefore assigning a music clip with one discrete emotion label is viewed to be unrealistic and for this reason the dimensional approach of emotion assignment has been utilized in this study.

Many of the research which tries to address the emotional aspect of music have utilized the two dimensional circumplex model comprising the dimensions valence and arousal, proposed by Russel. (Fig. 1) However, it is still unclear whether models and theories designed for ‘everyday’ emotions can also be applied to an aesthetic context such as music, and there have been doubts whether a few primary basic emotions – or the two dimensions of valence and arousal – are adequate to describe the richness of emotional experiences induced by music (Zentner, Grandjean, & Scherer, 2008).

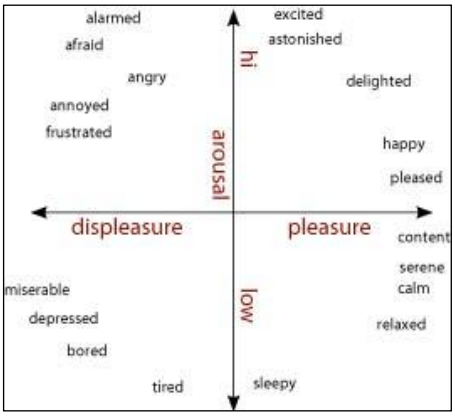

Fig. 1 Two Dimensional Circumplex Model proposed by Russel
Source: http://www.ieee-tcdl.org/Bulletin/v5n3/Hu/hu.htm

Another emotion scale which is largely used in music emotion research is the Geneva Emotion Music Scale (GEMS) - the first instrument that has been specifically devised to measure musically evoked emotions [3]. The GEMS is composed of nine emotional scales namely wonder, transcendence, power, tenderness, nostalgia, peacefulness, joyful activation, sadness, and tension each represented by two or three adjectives (Zentner et al., 2008). Though the application of a music -specific scale in measuring the music induced emotion is viewed to be more effective rather than applying a general emotion model, the study tries to better capture the emotions expressed by Sri Lankan folk melodies through introducing a new music-emotion scale based on the nine basic emotions discussed in the Sri Lankan traditional arts while trying to be compatible with the established models of emotion currently employed in related research.

2. The Proposed System

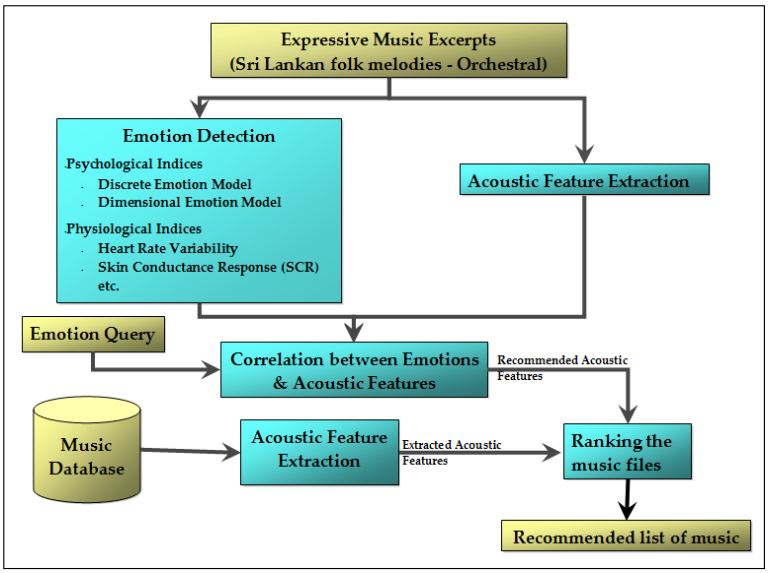

Fig. 2 Major phases of the study

The audio content is to be analyzed by reducing the sheer quantity of data down to a manageable set of features including the Mel-frequency Cepstral Coefficient (MFCC) and other acoustic features representing the pitch, timbre and rhythm of the music excerpts. In emotion detection previous researchers have utilized physiological indices as well as psychological indices whereas some researchers have employed both types collaboratively with the aim of achieving an enhanced performance. Heart rate variability and the Skin Conductance Response (SCR) can be regarded as two commonly used physiological indices used in measuring the induced emotion. Discrete and dimensional emotion models have been used in measuring the music induced emotion in a conscious manner whereas the study focuses on the dimensional approach. It is aimed at developing an emotion annotated corpus of Sri Lankan folk melodies allowing the future researchers to further explore the above melodies in the emotional perspective. Once the acoustic features are extracted and the emotions are detected, the associations between them could be discovered with the use of data mining techniques. Based on the discovered associations, the system will be able to recommend acoustic features that need to be present in a music clip so as to induce the queried emotion. Each unlabeled music clip in the music database will be indexed with a predicted emotion distribution and once a preferred emotion is passed as a query, the system will return a ranked list of recommended music clips which are capable of inducing the queried emotion.

3. Listening Experiment

A listening experiment was conducted as a pilot survey in identifying the potential of Sri Lankan folk melodies in emotional expression. For the experiment 13 Sri Lankan folk music excerpts belonging to diverse emotional categories were selected as the stimuli. Since the research aims at identifying the associations between acoustic features of music and perceived emotions, orchestral music was used in the experiment considering the potential effect by the lyrical content on the subjects' emotional experience. The clips were in the .wav format and the duration of each clip was on average 40s. 12 subjects were asked to rate the above music clips in a 5 point Semantic Differential scale. In selecting the bipolar adjective pairs the nine basic emotions associated with Sri Lankan traditional arts were considered to serve as the base considering their capability in capturing the emotions associated with Sri Lankan folk music. The scale is to be refined followed by a comprehensive review of the existing music-emotion thesauri. The experiment was conducted for two populations representing Sri Lankans having moderate knowledge in Sri Lankan folk music and professionals having expertise domain knowledge.

4. Results and Discussion

For each stimulus, the targeted predominant emotion was determined with the use of the folk song type the excerpt is associated with. The mean values of the ratings given by the subjects for each stimulus denoting the degree of emotional experience pertaining to each of the bipolar adjective pairs were obtained. The semantic differential chart (Fig. 3) shows the mean rating for two of the stimuli of which the predominant emotions were determined as Happy and Sad.

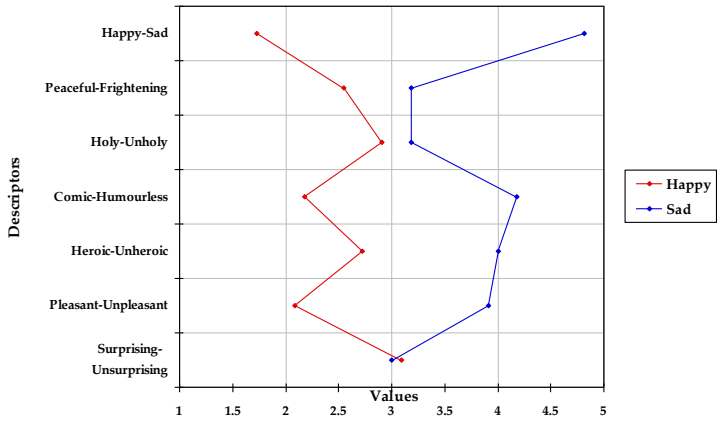

Fig. 3 Semantic Differential Chart

A Principal Component Analysis was run and Fig. 4 shows how the music excerpts were clustered together based on the ratings given by the subjects who were having an average understanding of Sri Lankan folk music whereas Fig. 5 shows the result of the PCA for the music stimuli rated by domain experts.

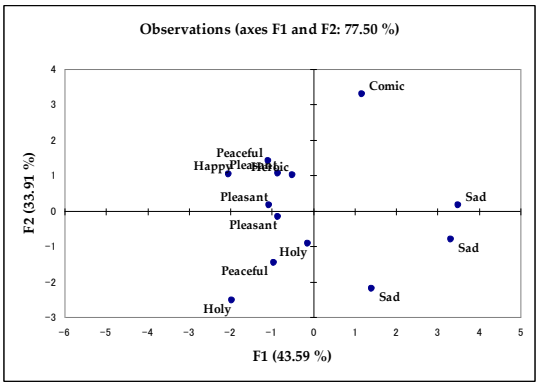

Fig. 4 Excerpts rated by the subjects having moderate knowledge in SL folk music

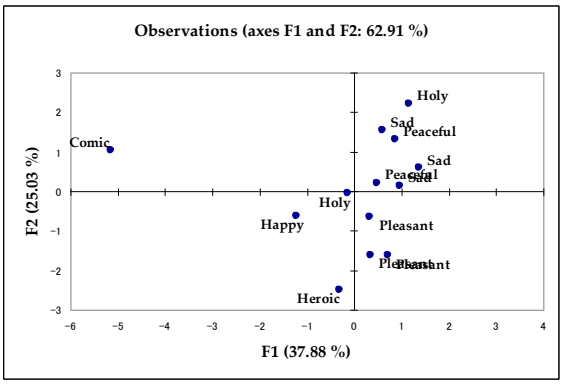

Fig. 5 Excerpts rated by subjects having expertise knowledge in SL folk music

The emotional experience of music arises as a result of the interaction between a given music piece and a particular listener. During this interaction the listener will apply his knowledge in music and the contextual understanding in arriving at various aesthetic judgments. The individual differences in terms of personality and emotional intelligence are also among the factors that influence the perception of emotion in music. Accordingly, remarkable differences are anticipated between domain experts and the general community in the way the music is understood and interpreted. A rating done by an expert is usually followed by an analysis of the music clip taking into consideration the rules in music associated with emotional expression, present in the composition, instrumentation and performance of the musical work. Therefore it is believed that the level of emotional perception of music of an expert usually lies beyond that of a general listener. In

this regard it should be clearly understood that the emotion perception is all instances where a listener perceives or recognizes expressed emotions in music (e.g., a sad expression), without necessarily feeling an emotion [4].

While serving as a pilot study, the initial experiment conducted among the two groups provides evidence for the expected difference in perception of emotion in music, between a common listener and a domain expert. Using the correlation circle, the axes F1 and F2 can be interpreted and based on the squared cosines of the variables, the linkage of each variable with the axes can be identified. The above findings of running a PCA on the experimental results obtained from the two populations will give important insights on differences in emotional perception of music and serve as an important consideration in developing an emotion based music recommendation system.

In realizing the complicated task of meeting the listener expectations, various approaches are currently being utilized by today's commercial applications for personalized music recommendation. Content-Based Filtering, Collaborative Filtering, Demographic Filtering and Context-Based Filtering are among such algorithms which are being used independently as well as in combination with others. Although the Nearest-neighbour Collaborative Filtering which is the current mainstream approach used in web-based recommender systems is believed to provide a successful means of generating recommendations for web users, it suffers from several short comings, including data sparsity and noise, the cold-start problem, and scalability [5]. Addressing the above issue, Amatriain etal. [5] have attempted to explore how the professional raters in a given domain (i.e. *experts*) can predict the behaviour of the general population, by introducing a collaborative filtering approach based on expert opinions from the web. In this study, the experiment conducted using the domain experts serves as a controlled experiment in identifying the potential for fusing *the wisdom of the few* [5] in enhancing the effectiveness of emotion based music recommendation.

5. Future Developments

Through the pilot survey, several limitations could be identified which need to be addressed in the future in order to achieve an effective performance. Ambiguities in emotional expression were noticed in several music clips used. The stimuli used in this survey were derived from existing compositions in which the primary objective was not the emotional expression. The gap between the expressed emotion and the perceived emotion can be reduced to a greater extent by purposely composing emotion based music, appropriately orchestrating and adjusting the mood of the performer. Therefore such kinds of music excerpts are to be employed in the future research. Similarly the emotion scale used needs to be revised by introducing more precise adjective pairs which will eliminate the existing ambiguities.

Though the music analysis is usually performed using audio files, notated scores and can be enhanced by lyrical analysis, the initial study focuses only on the audio content disregarding the linguistic approaches. But the emotions evoked within a person through listening to a music piece are always affected by the lyrical content as well as by human Kansei. Therefore the potential of Sri Lankan folk melodies in emotional arousal in the universal context, overcoming the above mentioned language and cultural barriers are to be further explored incorporating Kansei Engineering approaches.

As a means of promoting emotion based music retrieval, interactions with the interface for querying can be enhanced by enabling the users to pass the emotion query as a point or a trajectory on the emotion space displayed on a touch sensitive mobile device.

Acknowledgments

Foremost, I would like to express my sincere gratitude to my academic advisor Prof. Ashu Marasinghe for the continuous guidance provided in this study from the initiation of the concept to writing of this paper. Besides, I would like to thank the rest of the academic staff members of Nagaoka University of Technology for their valuable advices and guidance. I am very much grateful to the veteran artists in the field of Sri Lankan folk music for the shared knowledge and views which immensely helped me in identifying and shaping the way to proceed in this research. I am thankful to everyone who supported me in all the means in gathering the audio resources required. I am also thankful to all the lab mates in the Kansei Informatics Laboratory, Nagaoka University of Technology for the stimulating discussions, shared views, motivations and the support provided in successfully completing this task. Last but not the least I would like to thank my family; my parents

for making me the person I am.

References

[1] C. Herrada, "Music recommendation and discovery in the long tail," PhD Thesis, Internet: http://mtg.upf.edu/static/media/PhD_ocelma.pdf

[2] J. K. Vuoskoski and T. Eerola, "Measuring music-induced emotion: A comparison of emotion models, personality biases and intensity of experiences," Proc. Musicae Scientae, 2011 15: 159, Internet: http://msx.sagepub.com/content/15/2/159

[3] Zentnerlab, "The Geneva Emotional Music Scale (GEMS)," Internet: http://www.zentnerlab.com/psychological-tests/geneva-emotional-music-scales

[4] P. N. Juslin and D. Vastfjall, "Emotional responses to music: The need to consider underlying mechanisms," *Behavioral and Brain Sciences*, vol. 31, pp. 559 –621, 2008. doi:10.1017/S0140525X08005293

[5] X. Amatriain, N. Lathia, J. M. Pujol, H. Kwak and N. Oliver, "The wisdom of the few: A collaborative filtering approach based on expert opinions from the Web," Internet: http://www.nuriaoliver.com/RecSys/wisdomFew_sigir09.pdf

[6] A. Mattek, "Computational methods for portraying emotion in generative music composition," Internet: http://alisonmattek.files.wordpress.com/2010/08/mattek_thesisd2.pdf

[7] A. Mattek, "Emotional communication in computer-generated music: Experimenting with affective algorithms," Proc. 26th Annu. Conf. of the Society for Electro-Acoustic Music in the U.S, 2011

[8] A. Manaris, P. Roos, P. Machado, D. Krehbiel, L. Pellicoro and J. Romero, "A corpus-based hybrid approach to music analysis and composition," Proc. 22nd Conf. on Artificial Intelligence (AAAI-07), Vancouver, BC, Jul. 2007

[9] H.Y. Lo, S.D. Lin and H.M. Wang, "Audio tag annotation and retrieval using tag count information," Internet: http://www.iis.sinica.edu.tw/papers/whm/11116-F.pdf

[10] J. Taminau, R. Hillewaere, S. Meganck, D. Conklin, A. Now´e and B. Manderick, "Descriptive subgroup mining of folk music," Internet: http://www.ehu.es/cs-ikerbasque/conklin/papers/mml09taminau.pdf

[11] K. Trochidis, D. Sears, D.L. Tran and S. McAdams, "Psychophysiological measures of emotional response to romantic orchestral music and their musical and acoustic correlates," Internet:http://www.cmmr2012.eecs.qmul.ac.uk/sites/cmmr2012.eecs.qmul.ac.uk/files/pdf/papers/cmmr2012_submission_49.pdf

[12] M. Lesaffre, "Music Information Retrieval," 2005-2006

[13] M. M. Wanderley, "Report – Kansei the technology of emotion workshop rapport de mission," Proc. Int'l Report-Kansei- The Technology of Emotion Workshop – Genoa, Italy, Oct. 1997

[14] P. M. Brossier, "Automatic annotation of musical audio for interactive application," Internet: https://qmro.qmul.ac.uk/jspui/bitstream/123456789/3809/1/BROSSIERAutomaticAnnotation2006.pdf

[15] S. Brown, " From mode to emotion in musical communication," Internet: http://www.unige.ch/emotionalpowerofmusic/conference/brown.pdf

[16] S. Koga and T. Inoue, "A proposal for intervention by user in interactive genetic algorithm for creation of music melody," Internet: http://ieeexplore.ieee.org/xpl/freeabs_all.jsp?arnumber=6603488&abstractAccess=no&userType=inst

[17] S.R. Livingstone, R. Muhlberger, A.R. Brown and W. F. Thompson, "Changing musical emotion: A computational rule system for modifying score and performance," Internet: http://www.mcgill.ca/files/spl/LivingstoneCMJ2010.pdf

[18] T. Inoue, M. Fukumoto, "Creation of sound contents by extended interactive evolutionary computation using heart rate variability," Proc. Int'l Conf. on Biometrics and Kansei Engineering, 2013

[19] W. Chai and B. Vercoe, "Folk music classification using Hidden Markov Models," Internet: http://citeseerx.ist.psu.edu/viewdoc/download?doi=10.1.1.68.206&rep=rep1&type=pdf

Application of Unscented Kalman Filter with Non-symmetric Sigma Point Sampling on the Integrated Navigation System

Ye Chan[1], Chan Gook Park[2], Pho Kaung[1]
[1)]*Universities' Research Centre, Yangon University, Yangon, Myanmar, 11041.*
[2)]*School of Mechanical and Aerospace Engineering & The Institute of Advanced Aerospace Technology, Seoul National University, Seoul, Korea, 151744.*
yechann@gmail.com

The integrations of a global positioning system (GPS) and an inertial navigation system (INS) usually use error state models with linear or non-linear Kalman filters. In high dynamic environments, these systems introduce errors in the system models due to linearization. To overcome this drawback, the unscented Kalman filter (UKF) is applied on the non-linear total state model of the GPS/INS integrated system because the UKF is a nonlinear estimator that is particularly well suited for complex nonlinear systems. The sigma points in UKF are usually sampled symmetrically around the mean value and the random variable to be transformed is assumed to be Gaussian. If the variables depart from Gaussian nature, the performance of the system is degraded. To enhance the UKF performance the non-symmetric sigma points sampling is addressed in this paper. The non-symmetric factors for sigma points are carefully chosen to avoid local and global sampling problems. The simulations are done using real INS and GPS data for symmetric UKF (SUKF) and non-symmetric UKF (NSUKF) algorithms. The navigation performance and robustness of the proposed algorithm are also compared with that of the SUKF. According to the simulation results from the application of NSUKF on a nonlinear total state model, the performance and robustness of the navigation system is significantly improved under the environment with a number of satellites less than four. Hence, NSUKF is better choice for low cost INS/GPS integrated navigation systems and a good alternative for SUKF.

1. Introduction

In a nonlinear GPS/INS navigation system, the system and the measurement models are simply linearized around the current state estimate to apply the Extended Kalman Filter (EKF). EKF techniques suffer from divergence during GPS outages when using low-cost IMUs due to approximations during linearization process and suboptimal modeling. The main reason is that the low-cost sensors have complex error characteristics which are stochastic in nature and difficult to model. To overcome these drawbacks and to enhance the performance and robustness of the tightly coupled integration, instead of an EKF, the UKF is applied on nonlinear model [1].

The UKF belongs to a bigger class of filters called Sigma-Point Kalman Filters or Linear Regression Kalman Filters, which are using the statistical linearization technique. This technique is used to linearize a nonlinear function of a random variable through a linear regression between $\boldsymbol{N}$ points drawn from the prior distribution of the random variables. Since we are considering the spread of the random variables the technique tends to be more accurate than Taylor series linearization. The spreading sigma points cover the mean and covariance of the variables [2].

The set of sigma points is carefully selected around the mean but the sampling problem arises out of the incorrect scaling of these points. To solve both global and local sampling problems the non-symmetric approach was proposed by K. Kim & C.G. Park [3]. The spreading of sigma points from one side of mean is fixed and that for other side is adjusted using the non-symmetric factor. Their algorithm is successfully applied on the in-flight alignment of an aerial vehicle with a large heading error.

Unscented filter also assumes conditional Gaussianity throughout the filter recursions and may lead to misleading results in case the density departs too far from the assumed Gaussian density [2][4]. In this

paper, we propose the UKF with two unequal non-symmetric distribution factors. Therefore, the set of sigma points can be scaled independently. The proposed algorithm is applied on the land integrated navigation system with GPS signal outages and the performance is evaluated in comparison with the symmetric UKF.

Section 2 introduces the principles of unscented transformation and section 3 describes incorporating concepts and method of proposed non-symmetric unscented transformation incorporation the state constraints. Models of tightly coupled GPS/INS navigation system and the computing steps of NSUKF are explained in section 4. Simulation of navigation algorithm with real navigation data and the comparison of performance between SUKF and NSUKF are described in section 5. Conclusions are reported in the last section.

2. Unscented Transformation

In unscented transformation, to calculate the mean and covariance of a random vector, a set of deterministically selected sigma-points which have the same mean and covariance as the original random vector is chosen. Each sigma-point is propagated through the nonlinear models, and the mean and the covariance of the transformed random vector is calculated from the propagated sigma-points. The weights $\boldsymbol{W^i}$ associated with sigma points $\boldsymbol{\chi^i}$ have to satisfy the following condition to provide an unbiased estimate. [3]

$$\sum_{i=0}^{N} \boldsymbol{W^i} = 1$$

The selected sigma points are propagated through the non-linear function $\boldsymbol{f(\_)}$.

$$\boldsymbol{y}^i = f(\boldsymbol{\chi}^i)$$

Their mean and covariant are then calculated by

$$\bar{\boldsymbol{y}} = \sum_{\boldsymbol{i=0}}^{\boldsymbol{N}} \boldsymbol{W^i y^i}, \quad \boldsymbol{P_{yy}} = \sum_{i=0}^{N} \boldsymbol{W^i}\left(\boldsymbol{y^i} - \bar{\boldsymbol{y}}\right)^T$$

In symmetric sampling strategy, 2n+1 sigma points are symmetrically distributed about the mean $\bar{\boldsymbol{x}}_{\boldsymbol{k}}$ and defined as follows.

$$\boldsymbol{\chi}_k^0 = \bar{\boldsymbol{x}}_{\boldsymbol{k}}, \ \boldsymbol{\chi}_k^i = \bar{\boldsymbol{x}}_{\boldsymbol{k}} + \gamma\sqrt{\boldsymbol{P_k}} \quad \text{for } i = 1 \ldots n, \qquad \boldsymbol{\chi}_k^i = \bar{\boldsymbol{x}}_{\boldsymbol{k}} - \gamma\sqrt{\boldsymbol{P_k}} \quad \text{for } i = n+1 \ldots 2n$$

where $\gamma = \sqrt{n+\lambda}$, and $\lambda = \alpha^2(n+\kappa) - n$ and it is a composite scaling parameter. The constant α determines the spread of the sigma points around $\bar{\boldsymbol{x}}_{\boldsymbol{k}}$ and is usually set to a small positive value $(0 \le \alpha \le 1)$. The constant κ is a secondary scaling parameter which is usually set to *0* to *3 – n* and provides an extra degree of freedom for fine tuning of the higher order moments [2].

The weights associated with the sigma points are defined as

$$W_m^0 = \frac{\lambda}{n+\lambda}, \quad W_c^0 = \frac{\lambda}{n+\lambda} + (1 - \alpha^2 + \beta) \text{ and } W_m^i = W_c^i = \frac{\lambda}{2(n+\lambda)} \quad i = 1 \ldots 2n$$

3. Non-symmetric Sigma Point Sampling

The symmetric distribution of sigma points around the mean value is modified into non-symmetric form by introducing non-symmetric factors in sampling process. The 2n+1 sigma points are chosen as follows,

$$\begin{aligned} \boldsymbol{\chi}_k^0 &= \bar{\boldsymbol{x}} \\ \boldsymbol{\chi}_k^i &= \bar{\boldsymbol{x}}_{\boldsymbol{k}} + \mu_1\gamma\sqrt{\boldsymbol{P_k}} \quad \text{for } i = 1 \ldots n \\ \boldsymbol{\chi}_k^i &= \bar{\boldsymbol{x}}_{\boldsymbol{k}} - \mu_2\gamma\sqrt{\boldsymbol{P_k}} \quad \text{for } i = n+1 \ldots 2n \end{aligned} \qquad (1)$$

where μ_1 and μ_2 are non-symmetric factors and $\mu_1 \neq \mu_2$.

The weights corresponding to the sigma points have to match exactly the expected mean and covariance. It must satisfy the following conditions

$\sum_{i=0}^{2n} \boldsymbol{W^i} = W_0 + n(W_1 + W_2) = 1,$
$\overline{\boldsymbol{x}} = \sum_{i=0}^{2n} \boldsymbol{W^i \chi^i}$ and
$\boldsymbol{P_{xx}} = \sum_{i=0}^{2n} \boldsymbol{W^i}.\left(\boldsymbol{\chi^i} - \overline{\boldsymbol{x}}\right)\left(\boldsymbol{\chi^i} - \overline{\boldsymbol{x}}\right)^{\boldsymbol{T}}$
Substituting sigma points (given in Eqn. (1)) into above equations, we have
$W_1\mu_1 = W_2\mu_2$
$(W_1\mu_1^2 + W_2\mu_2^2)\gamma^2 = 1.$
The weights can be deduced as

$$W_1 = \frac{1}{(\mu_1^2+\mu_1\mu_2)\gamma^2}, W_2 = \frac{1}{(\mu_2^2+\mu_1\mu_2)\gamma^2}, \quad W_0 = 1 - n(W_1 + W_2) \qquad (2)$$

The proposed algorithm uses two degrees of freedom (μ_1 and μ_2) for scaling sigma points. These sigma points are propagated through the nonlinear function and mean and covariant are calculated using the scaling weights. Fig.1 shows the non-symmetric sigma points associated with the weights in 1 dimensional case. Dash curve is Gaussian probability density function (pdf) for symmetric unscented transformation and solid curve represents the non-Gaussian pdf for non-symmetric sampling. According to the nature of pdf, the distribution of sigma points is spread around the mean. μ_1 and μ_2 are needed to adjust to cover the stochastic nature.

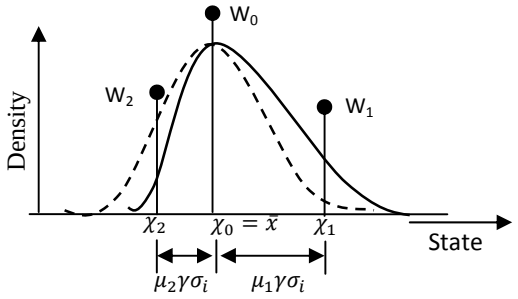

Fig.1 Non-symmetric sigma point sampling in 1 dimensional case
(solid curve for a non-Gaussian pdf and dash curve for a Gaussian pdf)

4. Tightly Coupled GPS/INS Navigation

The proposed NSUKF is applied on the tightly coupled integration scheme. INS data and GPS raw measurements (pseudorange and pseudorange rate) are processed in the data fusion algorithm, and the estimated errors are fed back to the INS to prevent the growth of navigation errors with time exhibited by an unaided INS[5]. The system dynamic models and the pseudorange and pseudorange rate measurement models are the key to the development of GPS/INS data fusion algorithms.

4.1. System Models

The total state INS mechanization model is given by the following differential equations. In this work, navigation frame mechanization was chosen [5][6].

$$\left.\begin{aligned} &\dot{\boldsymbol{L}} = \frac{\boldsymbol{v_N}}{\boldsymbol{R_m+h}}, \ \dot{\boldsymbol{l}} = \frac{\boldsymbol{v_E}}{\boldsymbol{(R_t+h)cosL}}, \ \dot{\boldsymbol{h}} = -\boldsymbol{v_D} \\ &\dot{\boldsymbol{v}}^{\boldsymbol{n}} = \boldsymbol{C_b^n f^b} - (2\,\boldsymbol{\omega_{ie}^n} + \boldsymbol{\omega_{en}^n}) \times \boldsymbol{v^n} + \boldsymbol{g^n} \\ &\text{The attitude quaternion is propagated by} \\ &\dot{\boldsymbol{q}} = \frac{\boldsymbol{1}}{\boldsymbol{2}}\boldsymbol{\Omega}\left(\boldsymbol{\omega_{nb}^b}\right)\boldsymbol{q} \end{aligned}\right\} \qquad (3)$$

where $\boldsymbol{\Omega}(\boldsymbol{\omega}_{\boldsymbol{nb}}^{\boldsymbol{b}}) = \begin{bmatrix} -[\boldsymbol{\omega}_{\boldsymbol{nb}}^{\boldsymbol{b}} \times] & \boldsymbol{\omega}_{\boldsymbol{nb}}^{\boldsymbol{b}} \\ -(\boldsymbol{\omega}_{\boldsymbol{nb}}^{\boldsymbol{b}})^T & 0 \end{bmatrix}$,

$\omega_{nb}^{b}$is angular rate of a body frame relative to navigation frame and $\boldsymbol{q} = [q_0\ q_1\ q_2\ q_3]$ is the attitude quaternion vector.

The state vector is defined as

$$\boldsymbol{x} = \left[L\ l\ h \vdots v_N\ v_E\ v_D \vdots q_0\ \ q_1\ q_2\ q_3 \vdots\ \nabla_x\ \nabla_y\ \nabla_z \vdots\ \ \varepsilon_x\ \varepsilon_y\ \varepsilon_z \vdots cb\ d\right]^T$$

where $\boldsymbol{\nabla} = \left[\nabla_x\ \nabla_y\ \nabla_z\right]^T$ and $\boldsymbol{\varepsilon} = \left[\varepsilon_x\ \varepsilon_y\ \varepsilon_z\right]^T$ are biases in accelerometer and gyro outputs, and $\boldsymbol{v_a}$ and $\boldsymbol{v_g}$ are white Gaussian noise corrupting the measurements. Latitude, longitude and height above the ellipsoid are denoted as $L,\ l$ and h and $v_N,\ v_E$ and v_D are velocities components in navigation frame respectively. The accelerometer bias and gyro bias are modeled as random constants and the clock bias *cb* in meter and clock drift *d* in meter per seconds of GPS receiver are calculated using random walk model [6].

4.2. The Observation Models

The observables in our integration are pseudorange and pseudo-range rate of a GPS receiver. The pseudorange measurement ρ_i to the i[th] satellite can be modeled as follows[6]:

$$\boldsymbol{\rho_i} = \sqrt{\left(\boldsymbol{r_i^n} - \boldsymbol{C_b^n l_b}\right)^T + \left(\boldsymbol{r_i^n} - \boldsymbol{C_b^n l_b}\right)} + cb + \nu_{\rho,i} \qquad (4)$$

The satellite position in n-frame coordinates is denoted with $\boldsymbol{r_i^n}$ while the position of the GPS antenna is $\boldsymbol{C_b^n l_b}$. $\boldsymbol{l_b}$ is the lever arm vector pointing from the origin of the body frame defined by the IMU to the GPS antenna. Additionally, the receiver clock bias *cb* and the measurement noise $\nu_{\rho,i}$ are included. The pseudorange rate can be described by

$$\dot{\boldsymbol{\rho}}_{\boldsymbol{i}} = \boldsymbol{e_i^{nT}}\left(\boldsymbol{v}_i^n - \boldsymbol{v}_{ins}^n - \boldsymbol{C}_b^n \boldsymbol{\omega}_{eb}^b \times \boldsymbol{l}_b\right) + d + \nu_{r,i} \qquad (5)$$

$\boldsymbol{e_i^n}$ is the unit vector pointing from the GPS antenna to the i^{th} satellite and $\boldsymbol{\omega}_{eb}^{b}$the rate of body frame relative to the earth frame. Additionally, measurement noise $\nu_{r,i}$ and the clock error drift *d* enter this observation model.

To apply the proposed NSUKF to the GPS/INS navigation system, the 2n+1 sigma points are generated according to the Eqn(1). They are propagated through the system models (Eqn(3)) and the mean and covariance are calculated using the weights shown in Eqn(2) as follows.

$$\overline{\boldsymbol{x}}_{\boldsymbol{k+1}} = \sum_{\boldsymbol{i=0}}^{\boldsymbol{2n}} \boldsymbol{W}_m^i \boldsymbol{\chi}_{k+1}^i$$

$$P_{k+1}^{xx} = \sum_{i=0}^{2n} \boldsymbol{W}^i \left(\boldsymbol{\chi}_{k+1}^i - \overline{\boldsymbol{x}}_{k+1}\right)\left(\boldsymbol{\chi}_{k+1}^i - \overline{\boldsymbol{x}}_{k+1}\right)^T$$

A set of predicted measurements is computed by propagating sigma points through the nonlinear measurement models given in Eqn(4) and Eqn (5).

$$\boldsymbol{\mathcal{Y}}_{k+1}^i = h(\boldsymbol{\chi}_{k+1}^i)$$

The predicted observation, innovation covariance and cross covariance are determined by

$$\overline{\boldsymbol{y}}_{k+1} = \sum_{i=0}^{2n} \boldsymbol{W}_m^i \boldsymbol{\mathcal{Y}}_{k+1}^i$$

$$\boldsymbol{P_{k+1}^{yy}} = \sum_{i=0}^{2n} \boldsymbol{W}_c^i \left(\boldsymbol{\mathcal{Y}}_{k+1}^i - \overline{\boldsymbol{y}}_{k+1}\right)\left(\boldsymbol{\mathcal{Y}}_{k+1}^i - \overline{\boldsymbol{y}}_{k+1}\right)^T + \boldsymbol{R}_{k+1}$$

$$\boldsymbol{P_{k+1}^{xy}} = \sum_{i=0}^{2n} \boldsymbol{W}_c^i \left(\boldsymbol{\chi}_{k+1}^i - \overline{\boldsymbol{x}}_{k+1}\right)\left(\boldsymbol{\mathcal{Y}}_{k+1}^i - \overline{\boldsymbol{y}}_{k+1}\right)^T + \boldsymbol{R}_{k+1}$$

Finally, the update can be performed by

$$\hat{\boldsymbol{x}}_{\boldsymbol{k+1}}^{+} = \overline{\boldsymbol{x}}_{\boldsymbol{k+1}} + \boldsymbol{K}_{\boldsymbol{k+1}}(\boldsymbol{y}_{\boldsymbol{k+1}} - \overline{\boldsymbol{y}}_{k+1})$$

$$\boldsymbol{P_{k+1}} = \boldsymbol{P_{k+1}^{xx}} - \boldsymbol{K_{k+1}} \boldsymbol{P_{k+1}^{xy}} \boldsymbol{K_{k+1}^T}$$

where $\boldsymbol{K_{k+1}} = \boldsymbol{P_{k+1}^{xy}}\left(\boldsymbol{P_{k+1}^{yy}}\right)^{-1}$

5. Simulation Results

The trajectory data is collected using a low grade IMU and a GPS. The sampling rates are 100 Hz for IMU and 1Hz for GPS respectively. The differential GPS data is used as a reference data in our calculation. The numerical simulations are done in MATLAB using these data. First both SUKF and NSUKF are applied on the navigation system with fully GPS supported situation. There is no significant difference between the results and the trajectories obtained are given in Fig. 2. This is due to the less non-linearity in land navigations and small variation in vehicle dynamics during trajectory data collection.

To test the ability of the NSUKF algorithm on the GPS outages the satellite's data are rejected in data processing and each outage lasts for 60 seconds. The results under complete GPS outages are firstly analyzed and then followed by the results under partial GPS outages. Fig. 3, Fig. 4, Fig. 5 and Fig. 6 illustrate the 3D position errors over the 5 simulated outages in each case (i.e. for number of satellite visible equals 0, 1, 2, and 3). The benefit of more satellite availability can also be seen from these results. The general trend is that having three satellites visible is better than two, which is better than one and zero case. In each case the maximum position errors of NSUKF is less than that of SUKF. SUKF provides a minimum position error for the case of 3 satellites visible and NSUKF cannot reduce the error anymore. The main factor for this is the nonlinear capabilities of both UKFs which enabled the use of nonlinear system model as well as the nonlinear measurement model of the raw measurements without any need for approximations during linearization. Fig.7 shows that the comparison of the average maximum position errors between SUKF and NSUKF. It is found that NSUKF has superior performance than SUKF.

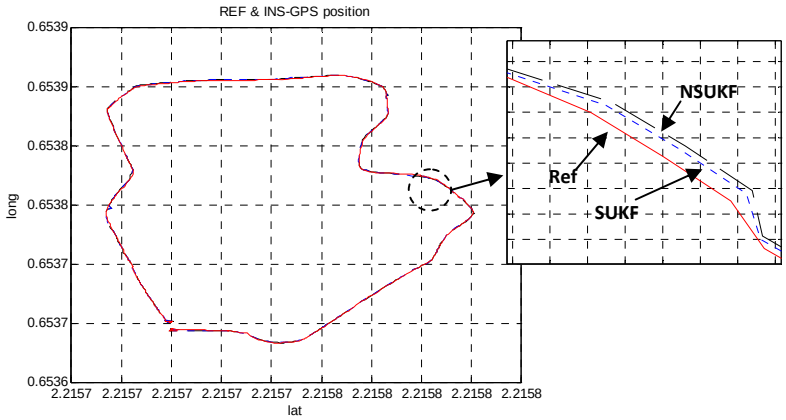

Fig. 2 Trajectories taken by SUKF and NSUKF solutions

6. Conclusion

In this paper, the non-symmetric unscented transformation with two degrees of freedom is proposed. The spreading of sigma points around the mean is adjusted carefully by two independent non-symmetric factors. The proposed algorithm is applied to the tightly coupled INS/GPS integration system and to avoid the linearization error, total state model of INS is used instead of error state model. The performance of the NSUKF is compared with the SUKF for the situations of GPS outages. It can be concluded that applying NSUKF on a nonlinear total state model does not degrade the performance of the navigation system significantly under the environment with less than four satellites. Non-symmetric sampling improves the navigation error and, the performance and robustness of the system is better than the symmetric case.

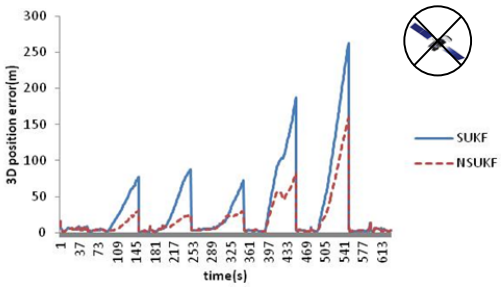

Fig. 3 Comparison of 3D position errors under complete GPS outages

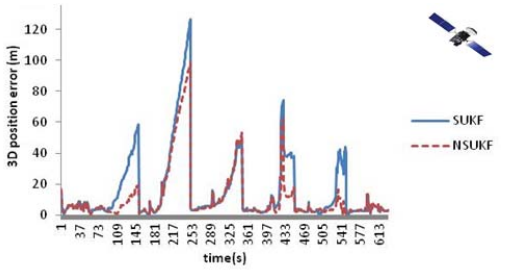

Fig. 4 Comparison of 3D position errors when 1 satellite is visible

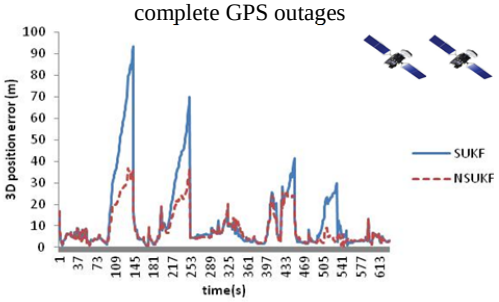

Fig. 5 Comparison of 3D position errors when 2 satellites are visible

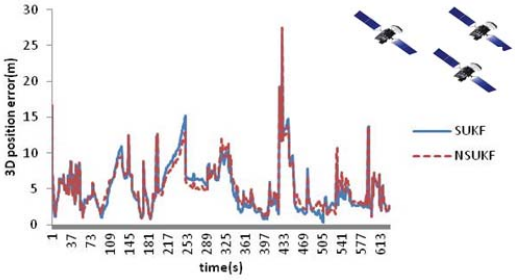

Fig. 6 Comparison of 3D position errors when 3 satellites are visible

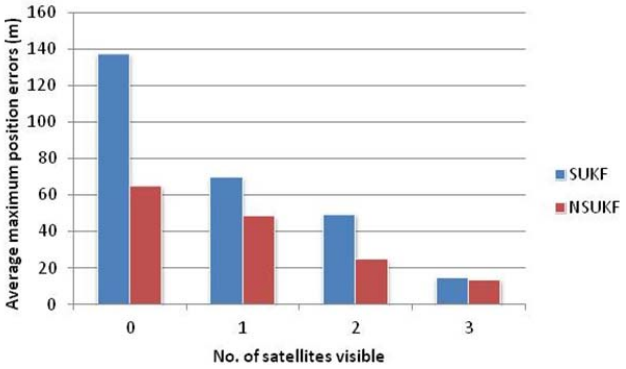

Fig.7 Average maximum position errors over the 5 outages with different numbers of satellites visible.

References

[1] X. Niu, S. Nasser, C. Goodalla1, and N. El-Sheimy, A Universal Approach for Processing any MEMS Inertial Sensor Configuration for Land-Vehicle Navigation. *Journal of Navigation*, 2007, vol. **60**, pp. 233-245.

[2] S. J. Julier, and J. K. Uhlmann, Unscented Filtering and Nonlinear Estimation, *Proceedings of the IEEE*, 2004, Vol . **92**, pp. 401-422.

[3] K.Kim and C.G. Park, Non-Symmetric Unscented Transformation with Application to In-Flight Aligment, *IJCAS*, vol. 8-4, pp. 776-781

[4] S. Sarkka, On Unscented Kalman Filtering for State Estimation of Continuous-Time Nonlinear Systems, *IEEE Tr. on Automatic Control,2007,* vol. **52**, pp. 1631-1641.

[5] D. H. Titteron, and J. L. Weston, *Strapdown Inertial Navigation Techonology*, 2nd Ed., IET and AIAA, 2005.

[6] Z. Syed, , P. Aggarwal, Y. Yang, and N. El-Sheimy, Improved Vehicle Navigation Using Aiding with Tightly Coupled Integration. *Proceedings of Vehicular Technology Conference*, Marina Bay, Singapore, 2008,pp. 3077-3081.

(Received; 23rd December, 2013, Accepted; 2nd August, 2014)

Enhancement of ionic conductivity in CuI-Cu_2MoO_4 superionic conducting glass by nano-structure control

Takao Tsurui*
Faculty of Engineering, Nagaoka University of Technology,
1603-1 Kamitomioka-cho, Nagaoka 940-2188, Japan
**E-mail:tsurui@mst.nagaokaut.ac.jp*

Microstructural changes in CuI-Cu_2MoO_4 superionic conducting glass in the vicinity of glass transition temperature have been studied by thermal analysis and transmission electron microscopy (TEM). In $(CuI)_{0.52}$-$(Cu_2MoO_4)_{0.48}$, nano-crystalline CuI of 2-3 nm in size disperse in amorphous matrix after the heat treatment above the crystallization temperature. Its electrical conductivity significantly increases by about 50 %, due to the nano-crystallization. On the other side, ionic conductivity decreases due to the nano-crystallization of CuI of 3-5 nm in size in $(CuI)_{0.40}$-$(Cu_2MoO_4)_{0.60}$. We can successfully control microstructures at a nanoscopic level by thermal treatment. The correlation between nano-crystalline size of CuI and the ionic conductivity has been discussed.

1. Introduction

The class of solids usually called by superionic conductors exhibits an extraordinarily high ionic conductivity [1-3]. For example, CuI is one of the typical superionic conductors. The value of the electrical conductivity of CuI crystal is 2.5×10^{-5} S/cm at 500 K [4]. On the other side, some kinds of Cu^+-containing glasses are known to show a very high ionic conductivity up to 10^{-3} S/cm at room temperature [3]. The values of Cu^+-containing glasses are much higher than that of CuI crystal. Therefore, superionic conducting glasses have attracted much attention because of the technological needs for solid electrolytes in, for example, high-energy batteries and electrochemical devices. Improvements of devices continue to be made possible by enhanced ionic conductivities. Therefore, development of fast ionic solids has been major concern for the ionics community. Structural properties have been extensively studied by X-ray scattering [5] neutron scattering [6], infrared spectroscopy [2,3,7] and other experimental techniques. The close relationship has been pointed out between the glass structure and the anomalous ionic conductivity.

It has been recognized for a long time that identification of the medium range structure is indispensable for understanding the Cu^+ ionic conduction mechanism of Cu^+-containing superionic conducting glasses. Actually some structural models are proposed based on the existence of "clusters" or "microdomains" of CuI with tetrahedral coordination, which is dispersed in the host matrix constructed with oxyanions in CuI based oxide glasses [2,3,5-7]. Numerous structural studies were performed so far to clarify the medium range structure by various experimental techniques. Among them, it has been reported that small angle scattering appears in a Q range < 1 $Å^{-1}$ by X-ray and/or neutron scattering [8-11]. The characteristic peak is called first sharp diffraction peak (FSDP). The presence of FSDP indicates that some structural ordering exists on a length scale ～7 Å. [12,13].

For the development of future applications, it is indispensable to advance a fundamental understanding of microstructures and overall results of them on the macroscopic properties. Transmission electron microscopy (TEM) is one of the most powerful tools for studying microstructures of materials at a nanoscopic level [14,15]. Figure 1 shows the interactions of electrons with matter. Incident electrons are scattered by specimens, and transmitted electron forms TEM images and electron diffraction patterns. In addition, we can analyze chemical composition and electronic structure by detecting characteristic X-ray and inelastically scattered electrons at a local area. In our previous report [16-18], we have analyzed microstructures of $(CuI)_x$-$(Cu_2MoO_4)_{1-x}$

glasses. In the report, the electrical conductivity increases with finely dispersion of nano-crystalline CuI of 2-3 nm in diameter in the $(CuI)_{0.52}$-$(Cu_2MoO_4)_{0.48}$ anneal at 463 K [16]. In the report, we have also reported that CuI clusters such as $[CuI_4]$-tetrahedra are finely dispersed and connected each other among Cu_2MoO_4 glassy matrix most probably constructed of $[MoO_4]$-tetrahedra and $[MoO_6]$-octahedra [16]. In addition, we have reported that nanoscale phase separation of 5-10 nm in size has been clarified by high-angle annular detector dark field (HAADF) images and energy dispersive X-ray spectroscopy (EDS) experiments, and the size is correspond to the correlation estimated by FSDP wave number [18]. We need further information to clarify the correlation between microstructures and ionic conductivities. In this paper, we have studied structural changes in $(CuI)_x$-$(Cu_2MoO_4)_{1-x}$ in the vicinity of glass transition temperature (Tg) by thermal treatment and TEM, and discussed the relationship between nano-crystalline size of CuI and the ionic conductivity.

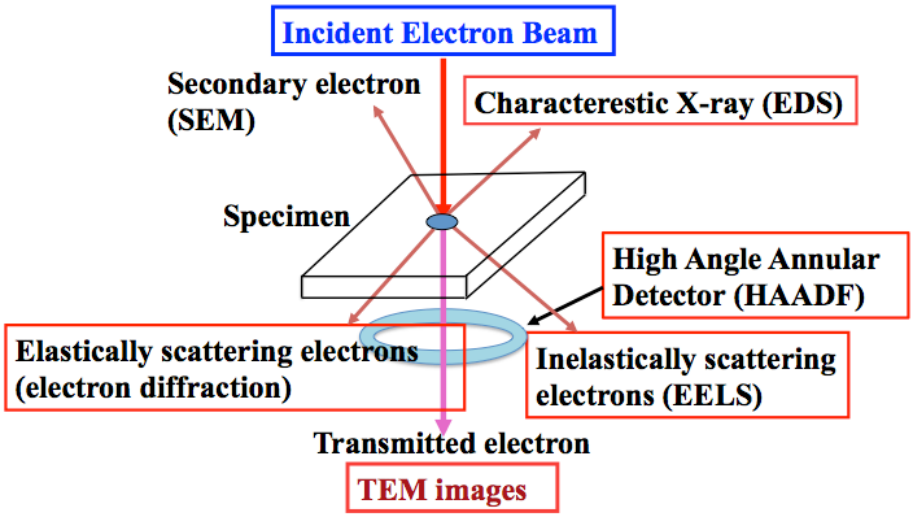

Fig. 1 Interactions of electrons with matter.

2. Experiment

CuI, Cu_2O and MoO_3 powders were capsuled in quartz tubes in purified Ar atmosphere and quenched in ice water from the melt at 973 K. The phase identification and macroscopic homogeneity were examined by conventional powder X-ray diffraction using an X-ray diffractometer (Rigaku) with a CuKα incident beam. Thermal analysis was performed by a differential scanning calorimeter, DSC (Seiko Instrument; DSC220) at a heating rate of 0.333K/sec under an argon gas atmosphere. The electrical conductivities were measured by complex impedance analysis, using a Solartron SI1260 impedance gain/phase analyzer. In the frequency range from 1 Hz to 1 MHz over the temperature range from 300 K to 350 K in N_2 atmosphere, using a furnace. Observation of TEM was performed with JEOL JEM-3000F and JEM-2100F microscopes operating at 300 kV and 200 kV, respectively. In this study, we observed specimens by ion-milling techniques and crushing method. To observe the morphology of specimens at a low magnification, we had to ensure a wide observation area. Thus, specimens were prepared by the standard ion milling techniques using a Fischione Model 1010 at an accelerating voltage of 3.0 kV. In addition, we observed specimens by the crushing method. Because we had to confirm that the specimens are not affected during the ion-milling processes at a local area. Bulk specimens were crushed into fine pieces and put onto microgrids covered with carbon films. In determining the lattice spacings, Si powder (5N) was used as an internal and external standard.

3. Results

In the compositional range of $0.40 \leqq x \leqq 0.52$, X-ray diffraction patterns show that the specimens are fully amorphous phase. However, further increasing in CuI content to 57 at.% results in the formation of crystalline phase, which is identified as cubic CuI [17]. Figure 2 shows DSC curves of $(CuI)_x$-$(Cu_2MoO_4)_{1-x}$ for x=0.40. 0.52 and 0.57 prepared by quenching into water. A DSC curve for

$(CuI)_{0.52}$-$(Cu_2MoO_4)_{0.48}$ annealed at 463 K is also shown for comparison. Tg and Tc denote glass transition and crystallization temperatures, respectively. In the compositional range of $0.40 \leqq x \leqq 0.52$, the DSC traces show an endthermal shift due to the glass transition at about 400 K and two significant exothermic peaks. In $(CuI)_{0.57}$-$(Cu_2MoO_4)_{0.40}$, the DSC trace also shows an endthermal shift due to the glass transition in spite of the existence of CuI crystals. On the other side, $(CuI)_{0.52}$-$(Cu_2MoO_4)_{0.48}$ annealed at 463 K doesn't show an endthermal shift due to the glass transition.

Figure 3 shows the electrical conductivities of $(CuI)_x$-$(Cu_2MoO_4)_{1-x}$ for x=0.40. 0.52 and 0.57 prepared by quenching into water and annealed at various temperatures. Total electrical conductivity values were determined by complex impedance analysis. The bulk impedance is attributed to the semicircles, which are observed at each temperature, and thus the bulk resistance is identified as the intersecting point of the semicircle with the real axis.

In $(CuI)_{0.52}$-$(Cu_2MoO_4)_{0.48}$, the conductivity of the sample annealed at 393 K is slightly higher than that of as-quenched one. Furthermore, the conductivity significantly increases by about 50 % after the heat treatment at 463 K.

In the compositional range of $0.40 \leqq x \leqq 0.52$, electrical conductivity increases with increasing CuI content. However, the electrical conductivity value of $(CuI)_{0.57}$-$(Cu_2MoO_4)_{0.43}$ sample is much lower than that of $(CuI)_{0.52}$-$(Cu_2MoO_4)_{0.48}$ one, in spite of the increase of the CuI content associated with the ionic conduction.

In $(CuI)_{0.40}$-$(Cu_2MoO_4)_{0.60}$, the conductivity of the sample annealed at 393K is slightly higher about 10% than that of as-quenched one. Annealing below Tg causes a slight increase of the conductivity. This result is the same as that of $(CuI)_{0.52}$-$(Cu_2MoO_4)_{0.48}$ one. Further annealing at 443K, the conductivity decreases in the magnitude of about one order compared with that for as-quenched one.

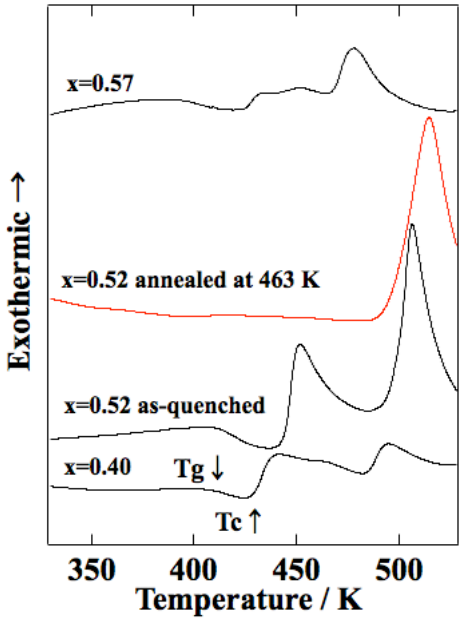

Fig. 2 DSC curves of $(CuI)_x$-$(Cu_2MoO_4)_{1-x}$ for x=0.40. 0.52 and 0.57 prepared by quenching into water and $(CuI)_{0.52}$-$(Cu_2MoO_4)_{0.48}$ annealed at 463 K.

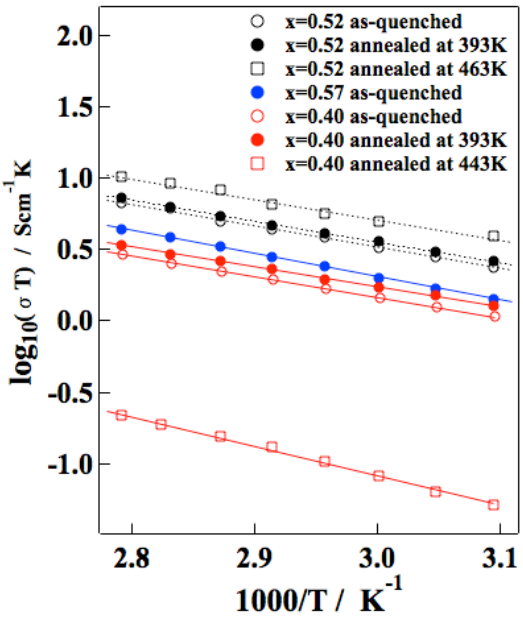

Fig. 3 Electrical conductivities of $(CuI)_x$-$(Cu_2MoO_4)_{1-x}$ for x=0.40. 0.52 and 0.57 prepared by quenching into water and annealed at various temperatures.

Next, we analyze microstructures by TEM in order to clarify the relationship between structural changes and ionic conductivity. Figure 4 shows a bright field (BF) image, a high-resolution electron micrograph (HREM) image and corresponding selected area electron diffraction (SAED) pattern for the sample of $(CuI)_{0.52}$-$(Cu_2MoO_4)_{0.48}$ annealed at 393K. As shown in Fig. 2, this temperature is

below Tg. In Fig. 4(a), the BF image is featureless at relatively low magnification. Furthermore, the HREM image shows a maze pattern that is typical for an amorphous structure. The SAED shows a clear halo-ring contrast that is also typical for an amorphous phase. These results indicate that the sample is a structurally homogeneous glass below Tg.

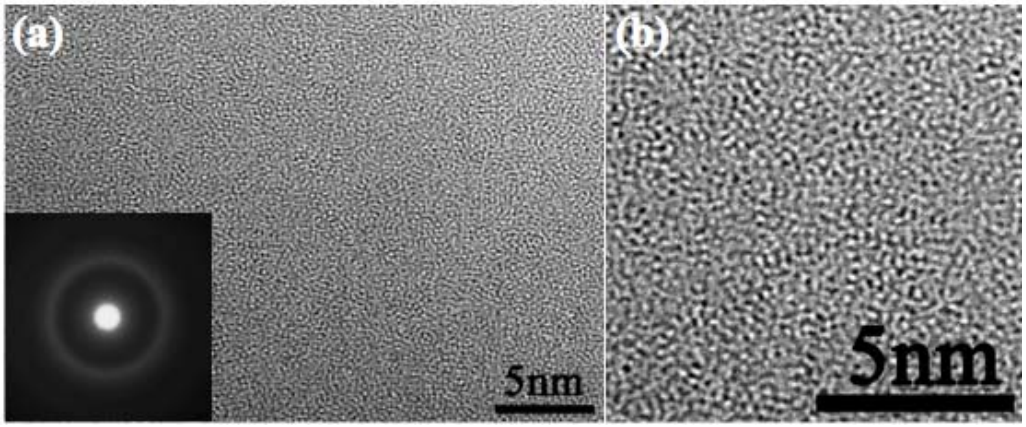

Fig. 4 (a) A bright field TEM image and a corresponding SAED pattern and (b) an HREM image for $(CuI)_{0.52}$-$(Cu_2MoO_4)_{0.48}$ annealed at 393 K.

Figure 5 shows a BF image and corresponding SAED pattern for the as-quenched sample of $(CuI)_{0.57}$-$(Cu_2MoO_4)_{0.43}$. The HREM image shows that nano-scale particles of 3-5 nm in diameter are dispersed uniformly. The SAED shows diffuse rings with a small number of spots and the lattice spacing (d-spacing) corresponding to each ring provides a good match to the known d-spacing for cubic CuI. These results are consistent with those for X-ray diffraction patterns [17]. The spacing of the crossed fringes as indicated in Fig. 5(b) is 0.35 nm, which corresponds to the spacing of the (111) plane of cubic CuI. Structural inhomogeneities of the glass/crystal composites with a length scale of 3-5 nm have been clearly observed from the HREM images.

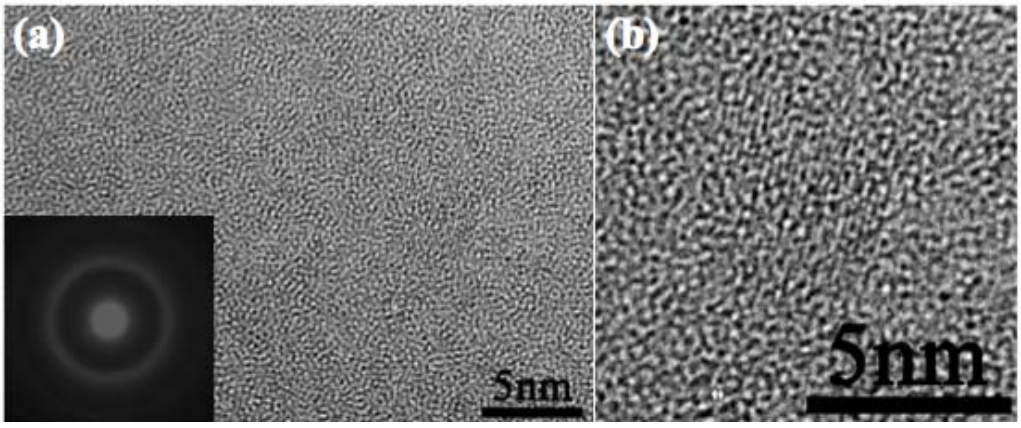

Fig. 5 (a) A bright field TEM image and a corresponding SAED pattern and (b) an HREM image for the as-quenched sample of $(CuI)_{0.57}$-$(Cu_2MoO_4)_{0.43}$.

Figure 6 and Figure 7 show HREM images and corresponding SAED patterns for $(CuI)_{0.40}$-$(Cu_2MoO_4)_{0.60}$ annealed at 393 K and 443 K, respectively. In Fig. 6, the HREM image shows a maze pattern that is typical for an amorphous structure for the annealed sample below Tg. The SAED pattern shows a clear halo-ring contrast that is also typical for an amorphous phase. These result indicate that $(CuI)_{0.40}$-$(Cu_2MoO_4)_{0.60}$ sample is a structurally homogeneous glass below Tg. On the other side, a lattice fringe is observed for the sample annealed at 443 K. The spacing is 0.35 nm, which corresponds to the spacing of the (111) plane of cubic CuI. In addition, a Debye-Scherrer ring pattern of other unidentified phase has been observed in the SAED pattern as

shown by the arrow. At this stage, we cannot identify that phase. This result indicates that crystallization into CuI and other unidentified phase occurs at the first step crystallization. The nano-crystallization process of $(CuI)_{0.40}$-$(Cu_2MoO_4)_{0.60}$ sample is quite different from that of $(CuI)_{0.52}$-$(Cu_2MoO_4)_{0.48}$ one.

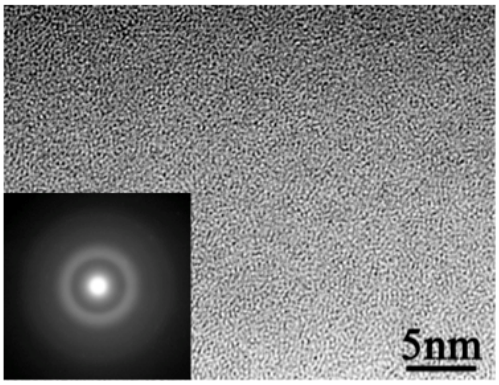

Fig. 6 An HREM image and a corresponding SAED pattern for $(CuI)_{0.40}$-$(Cu_2MoO_4)_{0.60}$ annealed at 393 K.

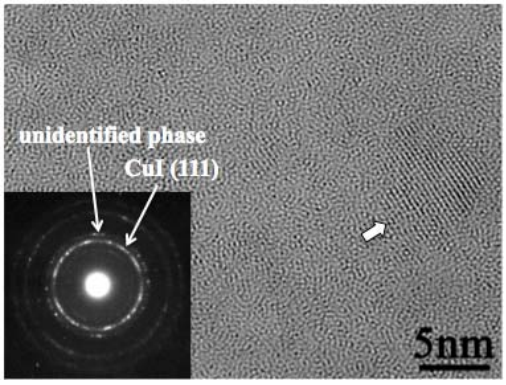

Fig. 7 An HREM image and a corresponding SAED pattern for $(CuI)_{0.40}$-$(Cu_2MoO_4)_{0.60}$ annealed at 443 K.

Table 1 List of formation of phase, crystalline size of CuI, electrical conductivities at 323 K and activation energy for conduction of $(CuI)_x$-$(Cu_2MoO_4)_{1-x}$ prepared quenching into water and annealed sample at various temperatures.

Sample	Formation of phase	CuI size	σ_{323K} (10^{-2}S/cm)	E_a (eV)
x=0.57 as-quenched	CuI + glass	3-5 nm	0.443	0.323
x=0.52 annealed at 393 K	glass single phase	not observed	1.21	0.292
x=0.52 annealed at 463 K [16]	CuI + amorphous	2-3 nm	0.812	0.281
x=0.40 annealed at 393 K	glass single phase	not observed	0.397	0.285
x=0.40 annealed at 443 K	CuI + unidentified phase	3-5 nm	0.0159	0.407

4. Discussion

Here, we discuss the contribution of microstructures to the Cu^+ ionic conductivity. It has been recognized that size control is important factors for the enhancement of the ionic conductivity [19]. Therefore, we now focus on nano-crystalline size of CuI and discuss the relationship between nano-crystalline size of CuI and the ionic conductivity. Formation of phase, crystalline size of CuI, electrical conductivities at 323 K, σ_{323K}, and activation energies for conduction of $(CuI)_x$-$(Cu_2MoO_4)_{1-x}$ as-quenched and annealed sample at various temperatures are summarized in Table 1. Referenced data is also shown for comparison [16]. Nano-crystalline size of CuI is estimated from TEM images in Figs. 4-7. Activation energies for conduction, E_a, were estimated by the Arrhenius-type equation

$$\sigma T = A \exp(-E_a/kT)$$

where σ is the electrical conductivity, A the pre-exponential factor, k the Boltzmann constant and E_a the activation energy for conduction. In x=0.52 sample, after the first step crystallization of precipitating nano-crystalline cubic CuI of 2~3 nm in diameter, its electrical conductivity increases by about 50%. This result indicates that increase in the conductivity of the annealed sample is caused by the nano-crystallization of cubic CuI. On the other side, the electrical conductivity of x=0.57 sample is much lower than that of x=0.52 one, in spite of the existence of nano-crystalline CuI of 3-5 nm in size. In addition, conductivity decrease in x=0.40 sample annealed at 443K, in spite of the existence of nano-crystalline CuI of 3-5 nm in size. In Fig.7, a Debye-Scherrer ring pattern of other unidentified phase has been observed in the SAED pattern. This result shows that the crystallization into CuI and other phase with increasing temperature accelerates a decrease of the conductivity.

These results imply that nano-crystallization is one of the important factors for the enhancement of the ionic conductivity. However, there must be other factors for the enhancement of the ionic conductivity. The first point to be considered is the increase of the volume fraction of nano-crystalline CuI and percolative connection among the nano-crystalline CuI clusters. The second point is interfacial structures between nano-crystalline CuI clusters and matrix phase constructed with oxyanions as proposed by Adams et al. [20]. In this study, we could successfully control microstructures of CuI-Cu_2MoO_4 superionic conducting glass at a nanoscopic level by thermal treatment. However, it is difficult to estimate the amount of nano-crystalline CuI by HREM. Therefore, the contributions have not been quantitatively clarified yet at this stage. Precise analyses are necessary to reveal the detailed local structures on the interface between nano-crystalline CuI clusters and residual oxyanion matrix.

5. Conclusion

Microstructural changes in CuI-Cu_2MoO_4 superionic conducting glass in the vicinity of Tg have been studied by thermal analysis and TEM. In $(CuI)_{0.52}$-$(Cu_2MoO_4)_{0.48}$, nano-crystalline CuI of 2-3 nm in size disperse in amorphous matrix after the heat treatment above Tc. Its electrical conductivity significantly increases by about 50 % due to then nano-crystallization. On the other side, ionic conductivity decreases due to the crystallization of CuI of 3-5 nm in size in $(CuI)_{0.40}$-$(Cu_2MoO_4)_{0.60}$. We can successfully control microstructures at a nanoscopic level by thermal treatment. Nano-crystallization is one of the important factors for the enhancement of the ionic conductivity. However, there must be other factors for the enhancement of the ionic conductivity.

Acknowledgments

This work partly supported by Grants-in Aid for Scientific Research (C) Ministry of Education, Culture, Sports, Science and Technology, Japan (No. 23560827) and by Program for High Reliable Materials Design and Manufacturing in Nagaoka University of Technology.

References

[1] C.A. Angell, Annu. Rev. Phys. Chem **43** (1992) 693.
[2] T. Minami, T. Katsuda and M. Tanaka, J. Non-Cryst. Solids **29** (1978) 389.
[3] N. Machida, M. Chusho and T. Minami, J. Non-Cryst. Solids **101** (1988) 70.
[4] T. Matsui and J.B. Wagner, Jr., J. Electrochem. Soc. **124** (1977) 300.
[5] M. Saito, K. Sugiyama, E. Matsubara, K.T. Jacob and Y. Waseda, Mater. Trans. JIM **36** (1995) 1434.
[6] K. Suzuki, K. Shibata, T. Tsurui and J. Kawamura, J. Non-Cryst. Solids **232-234** (1998) 278.
[7] C.P. Varsamis, E.I. Kamitsos, N. Machida and T. Minami, J. Phys. Chem. **B101** (1997) 3734.
[8] M. Tachez, R. Mercier, J.P. Malugani and P. Chieux, Solid State Ionics **25** (1987) 263.
[9] L. Borjesson, L.M. Torell, U. Dahlborg and W.S. Howells, Phys. Rev. **B39** (1989) 3404.
[10] A.P. Solokov, A. Kisliuk, M. Soltwisch and D. Quitmann, Phys. Rev. Lett. **69** (1992) 1540.
[11] L. Borjesson, A.K. Hassan, J. Swenson and L.M. Torell, A, Fontana, Phys. Rev. Lett. **70** (1993) 1275.
[12] M. Aniya, J. Non-Crystalline. Solids **354** (2008) 365.
[13] M. Aniya and J. Kawamura, Solid State Ionics **154-155** (2002) 343.
[14] T. Tsurui, T. Katsumata and Y. Inaguma, Philosophical Magazine **89** (2009) 843.
[15] T. Tsurui, M. Wataru, M. Watanabe, T. Katsumata and Y. Inaguma, J. Electron Microscopy **58** (2009) 349.
[16] T. Tsurui, J. Kawamura and K. Suzuki, J. Non-Crystalline. Solids **353** (2007) 302.
[17] T. Tsurui, J. Kawamura and K. Suzuki, Solid State Ionics **177** (2006) 2605.
[18] T. Tsurui and J. Kawamura, J. Non-Crystalline. Solids **357** (2011) 132.
[19] N. Sata, K.Eberman, K. Eberl and J. Maier, Nature **408** (2000) 946.
[20] S. Adams, K. Hariharan and J. Maier, Solid State Ionics **75** (1995) 193.

(Received; 23rd December, 2013, Accepted; 5th May, 2014)

Feasibility Study on a Stand-Alone Photovoltaic Hybrid Mini-Grid Power Generation System to Promote the Rural Electrification-Rate in Mandalay Region of Myanmar

Aung Ze Ya[1,*]
[1)] *Associate Professor, Department of Electrical Power Engineering, Mandalay Technological University, Mandalay, Myanmar*
**E-mail: dr.aungzeya010@gmail.com*

It is evident that the major thrust of this comprehensive research is developed to boost the forward prospect of the rural electrification-rate in Mandalay Region of Myanmar. Furthermore, it is intended to implement the Global Strategic reduction of the fossil fuel utilization as well as Green House Gas Emission. There are 102 households in the proposed Ma Gyi Pin (West) village of Towntha township. The total daily primary demand is 95 kWh/day and 14 kW peak. As a consequence, the total daily deferrable demand is estimated as 108 kWh/day and 50 kW peak. Different PV Hybrid Models are simulated by applying reliable and effective software tool, HOMER. Model A is investigated with 14080 simulations on 300 sensitivities. Then, Model B is modified based on the outcomes from Model A and its feasibility is analyzed with 3168 Simulations on 300 Sensitivities. From its result-list of feasible configurations, the most appropriate scenario is selected. Its simulated results are Levelized Cost of Energy (COE) 0.175 $/ kWh (172 Myanmar Kyats/kWh), Net Present Cost 165818 $ (162833276 Myanmar Kyats), Operating Cost 6004 $/yr (5895928 Myanmar Kyats/yr). In the selected scenario, 20 kW PV System and 30 kW Biomass Generator are involved as the Green Generators. Thus, the PV Hybrid Mini-Grid Power Generation Model provided with mixed-coupled AC-DC bus architecture and the maximum RE fraction is addressed to uplift the quality of life of villagers and promotion of Rural Electrification-Rate in Mandalay.

1. Introduction

A. Motivation

About 70 % of total population lives in the rural areas of Myanmar. Then, there are more than 65000 villages and about 66 % of these villages have no access to electricity. Thus, demonstrative research generation project with strategic planning, technology selection and practical effective solution is urgently needed to fulfill the required energy. The stand-alone PV-Biomass Hybrid System is emphazied to harness its rich Solar and Biomass Energy potentials for generation of electrical energy in central dry zone area.

B. Objectives

The objectives of this research are to promote rural electrification-rate by utilizing RE resources and to support National Development Programmes of Clean, Green and Sustainable Society in rural areas. It is also intended to support the implementation of Millennium Development Goals (MDG).

C. Methodology

Demand side analysis covers not only for present loads (Pagoda, 3 Monasteries, 102 households with population of 510 peoples) but also for future loads (primary school, preschool, library, clinic, street lighting system).

The methodology of conceptual bottom-up modeling and analyzing stand-alone PV hybrid micro-grid system is performed by changing the input parameters link with the sensitivity values. After simulation, the most appropriate generation-mix is selected from the sensitivity results as well as from the optimization results.

The supportive tool, HOMER, is developed by the U.S. National Renewable Energy Laboratory (NREL) to assist in the design of micro-power systems and to facilitate the comparison of power generation technologies across a wide range of applications [1].

2. Development of Sustainable Paradigm for Target Site

In this feasibility study, PV hybrid micro-grid system was architecturally modelled and analyzed comprehensively in HOMER based on the mutual elaboration between the experience on site visit, load profiles, availability of RE resources, socio-economic background, technological selections, environmental conservation, financial evaluations and sensitivity analysis of different scenarios.

A. Target Site Location

The target site, Ma Gyi Pin (West) village is situated in the Taungtha Township of Myingyan District in the Mandalay Region, Central Dry Zone Area of Myanmar as mentioned in Fig. 1. It is located at 11.27 km South to Administrative Seat of Taungtha Township, Taungtha Town and 13.27 km South of Myingyan Town. The interest village has 102 households and estimated population is about 510.

Fig. 1 Location of the Taungtha

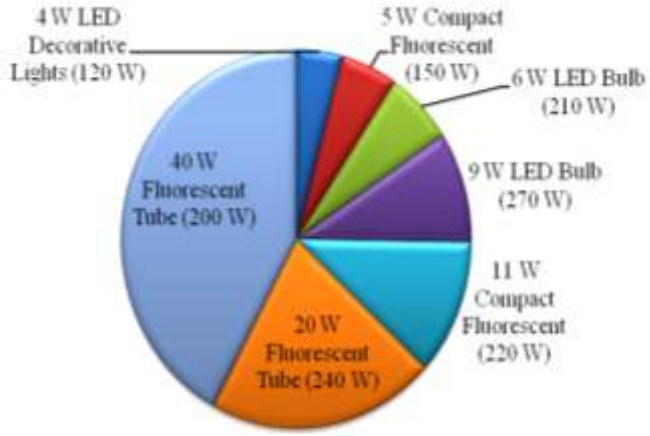

Fig. 2 Demands for Pagoda's Precinct

B. Selection of Suitable RE

Either strong potential or availability of RE is the dominant issue considered before selecting the appropriate RE in order to accomplish the objectives of this research. As mentioned earlier, this village is located at solar plentiful area. Moreover, the large area of its topography is characterized with paddy fields, farmlands, toddy-palms and cowsheds, blessing with enormous biomass energy resources. So, PV and biomass energies are selected as the main energy components to be utilized.

C. Demand Side Analysis

Demand side analysis was performed based on the outcomes from site visit at this village during the April in the Year 2012.

(1) Daily Load Demands for the Pagoda's Precinct

The treasure of religious heritage of this village is the "Thaung Gyi" Pagoda which founded by Bagan King Anawrahta. It is situated on the small eastern mountain, the strategic site and visible from all sides. Images of the Lord Buddha, one Buddhist ordination building, the stairways, the religious buildings on the Pagoda's platform and nine satellite Pagodas are included in this precinct. Fig. 2 mentions the primary loads and the estimated daily demands of it. The mentioned LEDs in Fig.2 is considered to use for 12 hours period (from 6 p.m. to 6 a.m.) and other lamps are used for 4 hours period (from 6 p.m. to 10 p.m.). Then, the total power rating is 1.41 kW and demand is 10.44 kWh.

(2) Daily Load Demands for Three Monasteries

There are three Monasteries in this village, known as Eastern Monastery, Southern Monastery and Northern Monastery due to their respective location. Among them, the first one with religious meditation centre is located near Pagoda. Due to field study, the required energy for the Eastern Monastery is larger than others. After systematic evaluations of primary loads, the combined monthly average for hourly demand scenario of Monasteries is obtained as shown in Fig 3. Similarly, the combined demands of deferrable loads for Monasteries during March to June, July to October and November to February are calculated as 32.80 kWh/day, 33.76 kWh/day and 32.39 kWh/day.

(3) Daily Demands for Ma Gyi Pin (West) Village's Schools, Library and Clinic

There are no schools, library and clinic in this village. But, the daily demands of the Preschool, Primary school, self-reliance library and clinic are evaluated in order to promote rural education care and health care sectors regarding future load growths. The daily time period for schools is from 9:00 (a.m.) to 3:00 (p.m.). Then, the library is opened between 6:00 (p.m.) to 10:00 (p.m.) and clinic is generally considered as 24 hour service. Loads are determined with assuming constant trends and results of hourly demands are expressed as in Fig. 5. Then, the combined demands of deferrable loads for these places are predicted as11.3 kWh/day for the whole year.

(4) Daily Load Demands for Ma Gyi Pin (West) Village's Street Lighting System

Although there is no street lighting system in this village, efficient and reliable street lighting is considered with 25 W high power LED lamps and 25 ft wooden poles. Number of required poles is 30 and daily operating hours are imposed as 12 hours (from 6 p.m. to 6a.m.). Total power rating and daily demand for street lighting system are calculated as 0.75 kW and 9 kWh /day.

(5) Daily Load Demands for Ma Gyi Pin (West) Village's Households

In Ma Gyi Pin (West) village, most of the villagers work the agricultural business. They take raw materials from toddy-palms and agricultural farms. Then, they produce Myanmar traditional snacks and sell at Taungtha market. Figures 4 and 6 are evident photographs that reflected the daily works. Collecting income data of households (HHs) was difficult due to the seasonal variations and general lack of consistency. But, incomes were generally observed that 2500, 3000 and 7000 Myanmar Kyats (MMK). Based on these ranges, it was known that there are 75 Low-Income HHs, 25 Medium-Income HHs and 5 High-Income HHs. Their deferrable loads are predicted as 41.5 kWh/ day; 14.25 kWh/day and 14.25 kWh/day for Low, Medium and High-Income HHs.

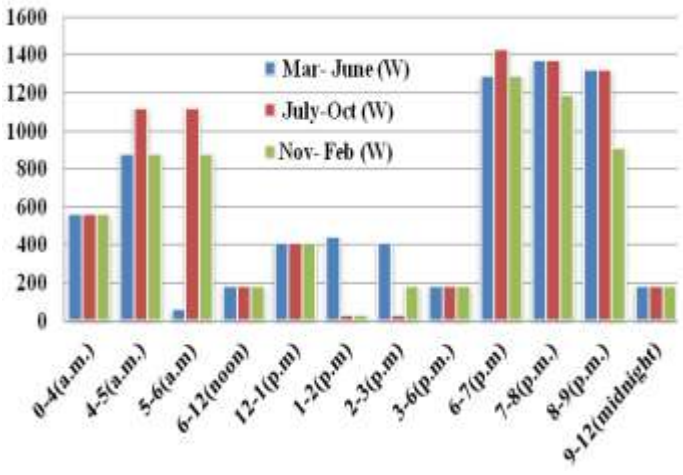

Fig. 3 Demand Scenario for Monasteries

Fig. 4 Climbs on the Toddy-Palm

Fig. 5 Demands for Schools, Library, Clinic

Fig. 6 Preparing Toddy-Palm Sap Pots

D. Stand-Alone PV Hybrid Power Generation Models in HOMER

Two PV Hybrid Mini-Grid Models of this paper are shown in Fig. 7 and Fig. 8. The primary demands and deferrable loads are combined and the total demand scenarios are obtained. These scenarios of primary and deferrable load inputs are depicted in Fig. 9 and Fig. 10. Solar resource data is taken from [2] assuming that this village and Taungtha Township have same solar radiations. Monthly solar radiations and scaled annual average solar radiation (5.54 kWh/m^2/day) are put with 15 sensitivity values as mentioned in Fig.11. Besides, 8 tonnes/day of Biomass is inserted and 4 sensitivity values of Biomass feedstock prices (0, 10, 20, 30, 40) $/t are also inserted. Table 1 obviously expressed the input-matrix that inputted into HOMER.

Table 1 Input-Matrix of PV Hybrid Mini-Grid Models for Ma Gyi Pin (West) Village

Equipment	*Capital Cost* ($)	*Replacement Cost* ($)	*O & M Cost*	*Sizes to Consider*		Sensitivity Values (Cost Multiplier of Capital, Replace, O&M)	
				Model A	*Model B*	Model A	Model B
PV Module (1 kW)	2106	1755	5 ($/yr)	[10,20, 30, …, 90,100] kW	[10,15, 20, …, 40,50] kW	(1,0.99, 0.98, 0.97) Link with Diesel Prices ($/L)	(1,0.99,0.98, 0.97) Link with Maximum Shortage
Battery (Surrette 4KS25P 4V,1900 Ah)	1221	1163	10 ($/yr)	[10,15,20, 25, 30, 35, 40, 45]	[10,15, 20, 25, 30, 35, 40,45]	(1,0.99, 0.98, 0.97) Link with PV Cost Multipliers	(1,0.99, 0.98, 0.97) Link with PV Cost Multipliers
Bio Gen: (1 kW)	1000	833	0.02 ($/hr)	60 kW	[30,…, 60]kW	-	-
Diesel Gen: (10 kW)	9552	6552	0.8 ($/hr)	[10, 20, 50, 70, 80,90, 100] kW	-	(1,0.99, 0.98, 0.97) Link with Diesel Prices ($/L)	-
Converter	2608	2608	40 ($/yr)	[4.4, 5, 6, 8, 10, …, 18] kW	[4.4, 5, 6, 8, 10, …, 18] kW	(1,0.99, 0.98, 0.97) Link with PV Cost Multipliers	(1,0.99, 0.98, 0.97) Link with PV Cost Multipliers

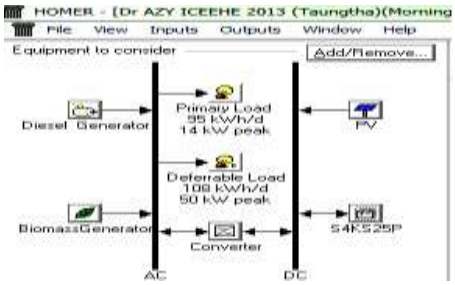

Fig. 7 PV Hybrid Mini-Grid Model A

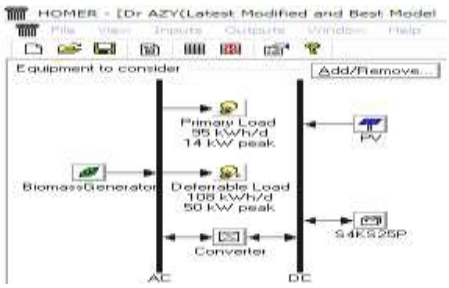

Fig. 8 PV Hybrid Mini-Grid Model B

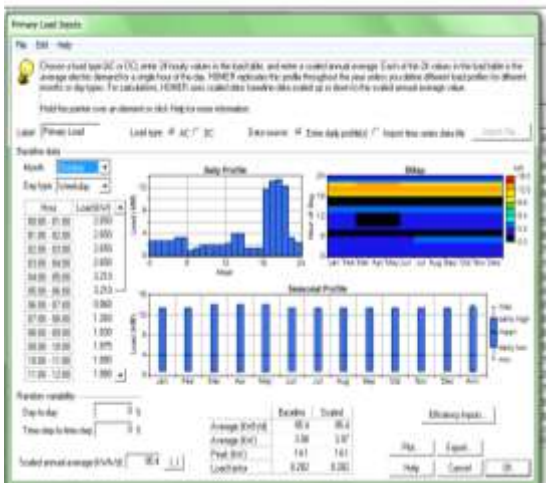

Fig. 9 Scenario of Primary Load Inputs

Fig. 10 Scenario of Deferrable Load Inputs

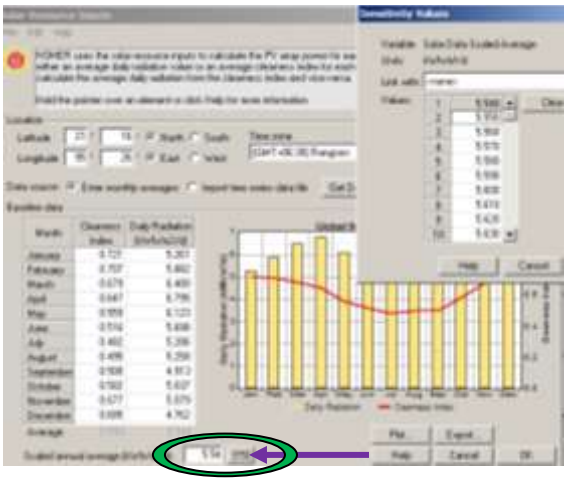

Fig. 11 Radiation Inputs with Sensitivities

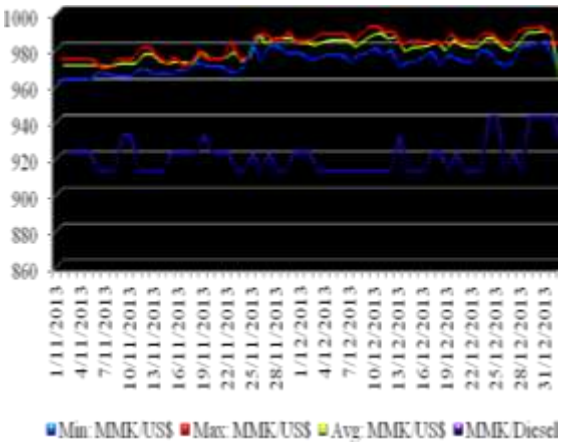

Fig. 12 Money Rates and Fuel Prices

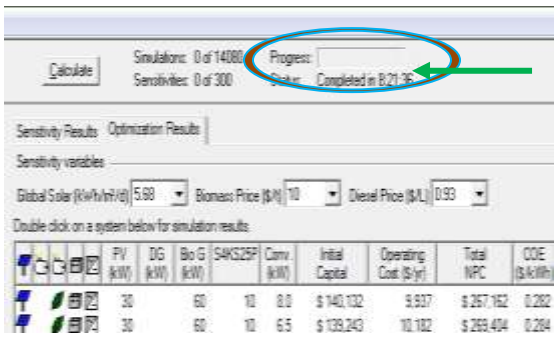

Fig. 13 Completed Model A Simulation

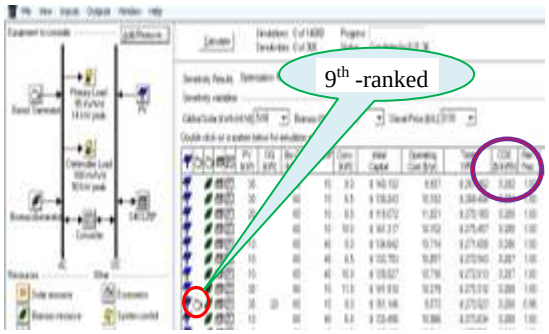

Fig. 14 Simulated Results of Model A

Consequently, the diesel fuel prices are needed to input. Then, dynamics of American currency's exchange rate and diesel oil prices during November and December of the year 2013 from daily newspapers of Myanmar are collected and illustrated as shown in Fig.11. By referring these values, the average value on recent diesel prices and maximum exchange rate are predicted as 0.93 $/L and 982 Myanmar Kyats (MMK)/$. To perform sensitivity analysis on diesel fuel prices for price growth, 0.94 S/L, 0.95 $/L and 1 $/L are also inputted into HOMER software.

3. Simulated Results and Discussion

Based on input-matrix mentioned in Table 1, mixed-coupled PV Hybrid micro-grid systems are simulated in HOMER. Firstly, the scenario of Model A is analyzed with 14080 simulations on 300 sensitivities. Its simulation process took 8 hours 2 minutes and 36 seconds as depicted with the oval ring in Fig. 13. As can be seen from Fig. 14, small circle highlights that Diesel Generator is started to consider at the 9th-ranked scenario and not at the top of overall tabular list. This issue points out that the participating of Diesel Generator in this Model cannot create the high ranked scenario. Furthermore, large circle mentions that even if the first-ranked scenario is chosen in this Model A, its energy cost 0.282 $/kWh (277 Myanmar Kyats/kWh), is expensive tariff range for rural dwellers. So, Diesel Generator is decided to remove and observed to know the impact of this change.

Therefore, the new upgraded version, Model B, is provided with necessary modifications. Sensitivity Variables can be easily changed and analyzed in HOMER software. The significant change is provided for PV sensitivity values that linked with Maximum Annual Capacity Shortage (0, 5, 10 and 15 %). Then, 3168 Simulations on 300 Sensitivities of the Model B is performed in 5 hours 4 minutes and 36 seconds. Thus, Model B takes shorter time with better scenario than Model A.

According to the sensitivity results of Model B expressed in Fig. 20, there are also two scenarios to be analyzed. Comparing the overall electrical production results and others outcomes from two scenarios (the first-ranked and fourth-ranked scenarios), Fig. 17 to Fig. 20, Scenario 1 is better than Scenario 2 due to more excess electricity and more economical at the project life of 25 yr. Thus, Scenario 1 is selected. It is mixed-coupled AC-DC system of 20 kW PV, 30 kW Biomass Generator, 10 Surrette 4KS25P Battery and 8 kW Converter. Its optimization results are Levelized Cost of Energy (COE) 0.175 $/kWh (172 Myanmar Kyats/kWh), Net Present Cost 165818 $ (162833276 Myanmar Kyats), Operating Cost 6004 $/yr (5895928 Myanmar Kyats/yr) and 5410 kWh/yr.

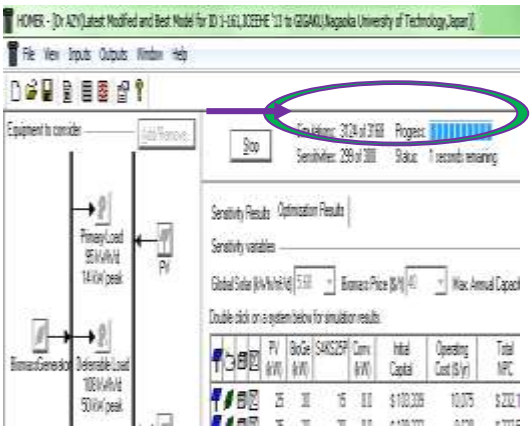

Fig. 15 During Simulation of Model B

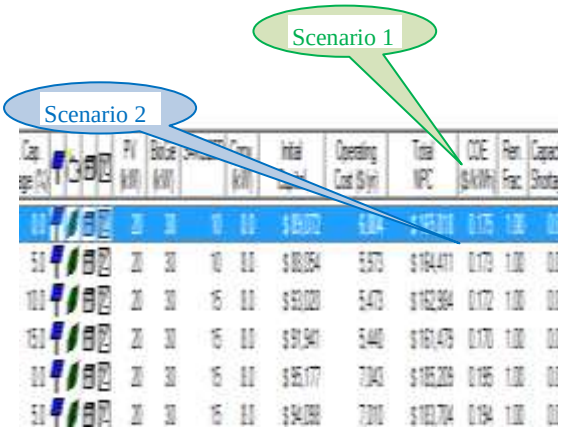

Fig. 16 Sensitivity Results of Model B

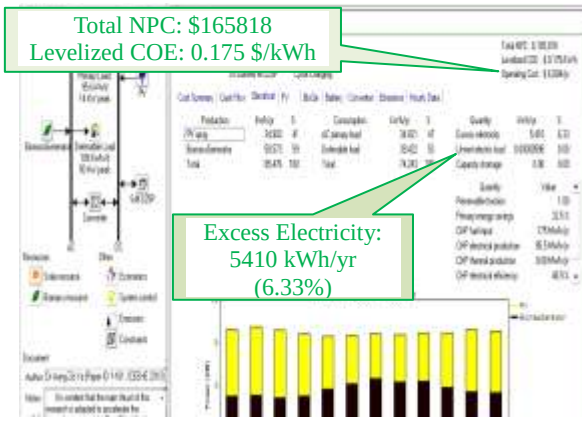

Fig. 17 Electrical Analysis of Scenario 1

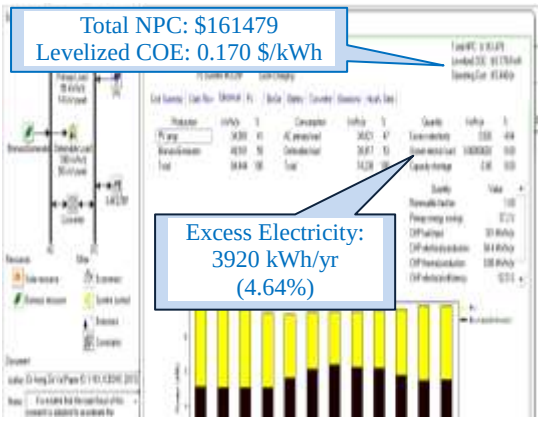

Fig. 18 Electrical Analysis of Scenario 2

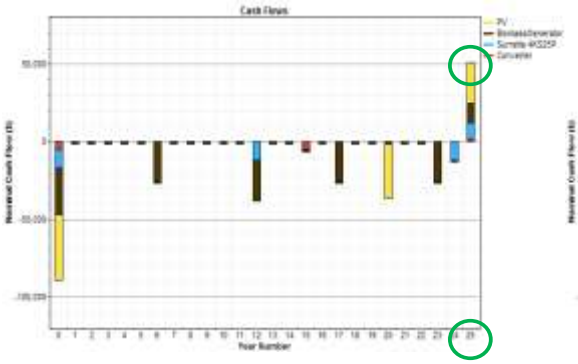

Fig. 19 Cash Flows of Scenario 1

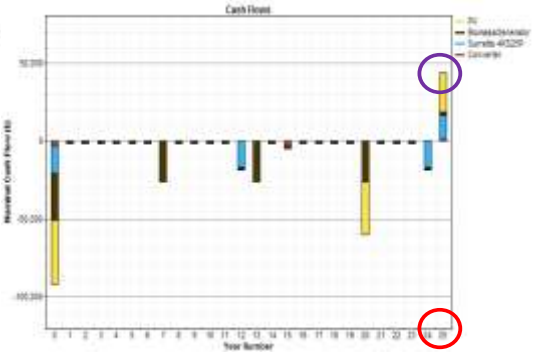

Fig. 20 Cash Flows of Scenario 2

4. Conclusion

The proposed model only relies on Renewable Energies to implement the Environmental Conservation Purpose and Green Energy Evolution. Although there are other Models studied at the beginning stage of this research, only Model A and B are mentioned. Some Models took long simulation times. However, the outcomes from these Models were not optimum from the practical and economical point of views. Therefore, these are not expressed in this paper.

Utilization of electrical loads with high efficiency and saving energy can drive the forward dynamics of Sustainable Paradigm in rural villages. Thus, demand side analysis is systematically emphasized in this comprehensive research. There is no school, library and clinic existing in this village. However, Preschool, Primary school, Self-reliance library and clinic are considered as future load growth. In the rural areas, it can be regarded as rural library can be the University of Knowledge and Clinic may be the Hospital of life-saver. To utilize the benefits of HOMER, the deferrable loads are considered with battery charging, cooking appliances and water pumping systems that are essential loads. Actually, the power ratings of the cooking appliances are large. Thus, these are assumed as deferrable loads considering with the cooking time is not fixed.

Levelized cost of energy (COE) is evaluated as 172 Myanmar Kyats/kWh, which is higher than electricity tariff from conventional grid connected system at present. However, COE from remote supply systems in the country may be higher than that value. Thus, COE form the developed PV-Biomass Hybrid Mini-grid system is cheaper than these systems.

To summarize, the results obtained from 3168 Simulations with 300 Sensitivity Variables highlight that the developed Model B of PV-Biomass hybrid system is obviously feasible. Generally, most of the villages in Mandalay Region have similar culture, profile and life styles. Therefore, this research can enhance the access of electricity and promote the rural electrification rate in this area.

Acknowledgments

First of all, the author wishes to express the deepest gratitude to his parents and uncles for their kind supports and encouragement. Especially, the author is deeply grateful to Dr. Myint Thein, Pro-Rector, Mandalay Technological University, for his noble guidance and support. In addition, the author sincerely appreciates to Dr. Yoshiharu MUTOH, Executive Director, Vice President, Nagaoka University of Technology, for opening and successfully celebrating of ICEEHE 2013 in Yangon. Moreover, the author offers respectful gratitude to Dr. Yuichi Otsuka, Associate Professor, Department of System Safety, Nagaoka University of Technology, for his kind guidance. The author wishes to express his special thanks to New Energy and Industrial Technology Development Organization (NEDO, Japan), ARI, IEEJ, AIST (Japan) and SERT (Naresuan University, Thailand) for their valuable supports during NEDO's capacity building training program in 2011 and 2012.

References

[1] T. Lambert, P. Gilman and P. Lilienthal, Micro-Power System Modelling with HOMER, John Wiley & Sons, Inc. (2006).

[2] Dr. Serm Janijai, Assessment of Solar Energy Potentials for the Union of Myanmar, Solar Energy Research Laboratory, Department of Physics, Silpakorn University, Thailand, (2009).

Hardware In The Loop Integration Design Of Micro Avionics System For AEROMAS UAV

Hline Htet Win[1*], Moe Kyaw Naing[2]
[1)]UAV Research Section, MyanmarAerospace Engineering University,
[2)]UAV Research Section, Myanmar Aerospace Engineering University,
Meikhtila Myo, Mandalay Division,Myanmar
**E-mail: mghlinehtet@gmail.com*

This paper discusses the integration and testing of Hardware-In- the-Loop simulation so called HIL System LAB using a commercial Flight Simulation software package and a custom design Flight Control System. The Flight Control System for AeroMas UAV is developed and validated using HIL System LAB before flight test. The ability and potential of simulation system are increased significantly when the simulation system is linked directly to the actual flight hardware. The aerodynamic model for AeroMas UAV is built with the help of Plane-Maker program bundled with X-Plane Flight Simulator. X-Plane uses actual flow calculations many times per second to figure out how the given aircraft flies in the simulated environment. By accessing X-Plane state variables through plug-in, the real time avionics sensors' data are emulated like an actual way. The X-Plane's plug-in communicate with the Flight Control Computer through RS-232 serial communication which is the GPS port of onboard avionics system. The avionics sensor input data of Flight Control Computer that should be produced by X-Plane are position data of Latitude, Longitude, Altitude, Speed and attitude data of Roll, Pitch, Yaw. The internal design parameters of Flight Control Algorithm can be analyzed and optimized to reduce time and cost effectively during the design phase. Although robust and mature control is not possible, traditional PID control method is used as Flight Control Algorithm to simplify design process and minimize required hardware resource. Monitoring of hardware resource can be possible to observe whether it can response to avionics sensors' data efficiently. Due to the nature of simplicity and fidelity the HIL System LAB can be deployed as a test platform to assist in the studying of flight control systems at Myanmar Aerospace Engineering University. Over all, the results obtain in this paper shown that the effectiveness of HIL System LAB as a Simulated Flight Testing Environment and Educational design tool.

1. Introduction

Hardware-in-the-Loop (HIL) simulation is a kind of real-time simulation that the input and output signals shows the same time dependent values as the real process. It is usually used in a laboratory environment on the ground to test the prototype controller under different working loads and conditions conveniently and safely. HIL simulation has the abilities to simulate UAV flight characteristic, sensor modeling and actuator modeling while communicating in real time with the UAV autopilot hardware. In Myanmar Aerospace Engineering University (MAEU) UAV development, HIL laboratory is an important step in autonomous system design and development. UAV autopilot system is adapted with the HIL simulator to see how the overall system works as a closed loop system.

Development of HIL simulator is based on commercially available simulation software. The chosen simulation software for HIL simulator development is X-Plane because its function is customizable using a plug- in. A plug-in is executable code that runs inside X-Plane, extending what X-Plane does. These are modular, allowing developers to extend the simulator without exciting the

source code to the simulator. It allows to constructs the aircraft model with weight and balance, engine parameter and control surfaces data like real airframe model. The HIL simulator's plug in communicates with the UAV autopilot hardware through HIL bridge like as RS232 serial communication. The reference input data of UAV autopilot hardware that should be produced by HIL simulator are aircraft navigation data (speed, altitude, latitude and longitude) and attitude data (roll, pitch and yaw). Then, telemetry protocol is sent to ground control station (GCS). At the same time, ground station monitors the real-time in-flight data by means of visualization. The requirements of HIL simulation are shown in Fig. 1. HIL simulation can be used to test autonomous hardware reliability, check the closed loop performance of the overall system and tune the controller's parameter. By rigorous testing in the HIL simulator, the risk in the field trail can be minimized.

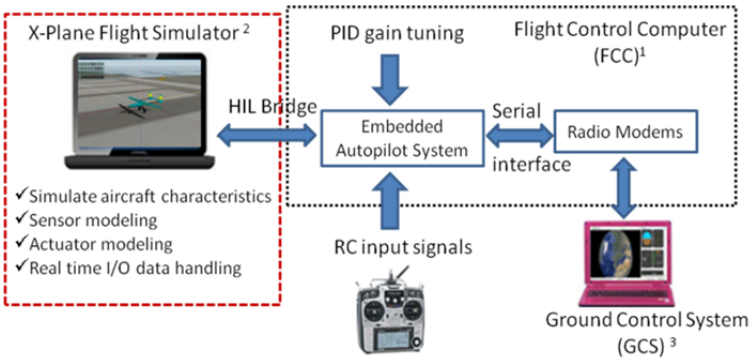

Fig.1 Block diagram of Hardware In the Loop Environment

Aircraft Model Construction

The test UAV that used in the present project is named as AeroMas which is the fifth generation prototype of MAEU UAV research. The AeroMas UAV as shown in Fig. 2 is a high-wing tricycle-gear aircraft. It is made up of carbon and glass composited fiber. It is powered by O.S engine with a shaft horsepower of 3.8 H.P. The wing employs the NACA 4415 airfoil. The level flight speed is about 121 kilo meter per hour. The aircraft was configured with the 3 liters fuel tank, wireless video payload and flight control computer (FCC). The major dimensions of this UAV are described in Table 1.

X-plane supports plane maker program. That can create more realistic flight model. Flight dynamic data for the selected UAV must be entered in detail to plane maker program interface. The Fig. 3 shows the completed wing assemblies in plane maker after all the wing data and controls data are entered.

Fig. 2 AeroMas UAV developed in MAEU

Table 1 Specification of selected aircraft model

Wing Span	3.2m	Maximum speed	121 km/hour
Length	2.4 m	Service ceiling	1000 m
Height	0.355 m	Endurance	1.5 hours
Payload weight	2 kg	Recovery scheme	Return to launch
Takeoff weight	11.5 kg	Payload	Camera

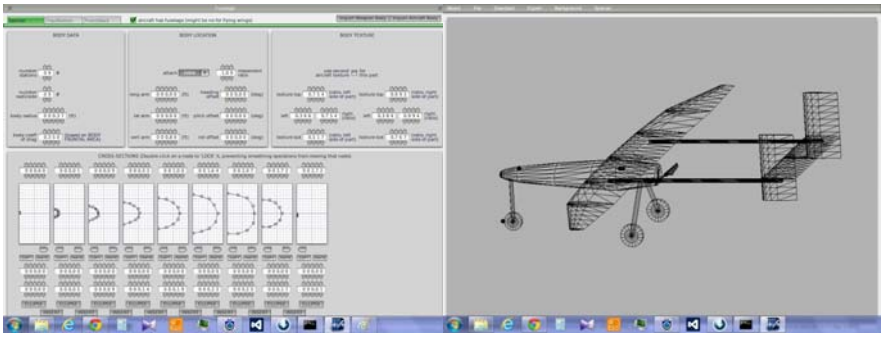

Fig. 3 Building the X-plane flight model

3. THE TEST PLATFORM

The main components of the test platform are as follows:

1. Flight Control Computer containing the autopilot control firmware and HIL interface code,
2. Flight Simulator X-Plane containing the aircraft model to be controlled,
3. X-Plane plug-in for HIL interface,
4. Ground Control Station for in-flight data monitoring.

The test platform configuration is based on the block diagram presented in Fig. 1. The basic principle of the test platform consists of establishing the communication between X-Plane and flight control computer as the following process. The parameters calculated by the autopilot control system are sent to X-Plane in order to command the aircraft's flight control surfaces. The X-Plane calculates the new aircraft attitude according to the inputs that receive from FCC. The X-Plane sends those new aircraft attitude parameters back to FCC as a close loop system. FCC restarts the process by providing updated servo's data to X-Plane aircraft. The input data sending to the aircraft's flight control surfaces from the X-Plane are simultaneously processed at FCC actuator ports which translate these commands into effective servo movement control. The FCC calculates the deflection angle to be imposed to the flight control surfaces and generates a proportional PWM signal to command the servo. The communication between FCC and X-Plane is made through Universal Asynchronous Receiver Transmitter (RS-232) which is GPS port in actual flight. Block diagram shown by Fig. 1 illustrates the platform configuration.

The flight simulator X-Pane provides very accurate aircraft models and has a very important feature: the possibility to exchange data with external systems [4]. Giving its realistic simulations capability, X-Plane is also FAA (Federal Aviation Administration) approved for pilot training. The aircraft models simulated in X-Plane are built based on their real physical dimensions, power and weight among other characteristics. X-Plane is not considered a game, but can be categorized as an engineering tool that can be used to predict the flying qualities of fixed and rotary wing aircraft [4].

Most other flight simulators use the stability derivatives method to compute how an airplane does. This technique involves simply forcing the aircraft nose to return to a centered position along the flight path with certain acceleration for each degree of offset from straight-ahead flight of the airplane. This is too simplistic to be used across the entire flight envelope of the airplane.

Stability derivatives will not normally take into proper account the asymmetric effects of engine failures, the chaotic effects of turbulence, stalls, spins and the myriad of dynamic effects that airplane flight generates. In other words, the commonly used stability derivatives are gross over simplifications of how an airplane flies. In summary, those simulators cannot predict how the airplane will fly. Basically, the airplane designer teaches the simulator how the airplane should fly, and the simulator reproduces that information right back to the user [4].

X-Plane instead, assimilates the geometric shape of any aircraft and then figures out how that aircraft will fly. It does this by an engineering process called "blade element theory", which involves breaking the aircraft down into many small elements and then finding the forces on each little element many times per second. These forces are then converted into accelerations which are then integrated to velocities and positions. This method of computing the forces on the airplane is much more detailed, flexible, and advanced than the flight model that is used by most other flight simulators. By doing this process, X-Plane accurately predicts what will be the performance and handling qualities of an airplane of a given geometry [4].

The FCC represented by block (1) on Fig. 1 symbolizes the Flight Control board dsPIC manufactured by Microchip Technology Inc and shown in Fig. 4.

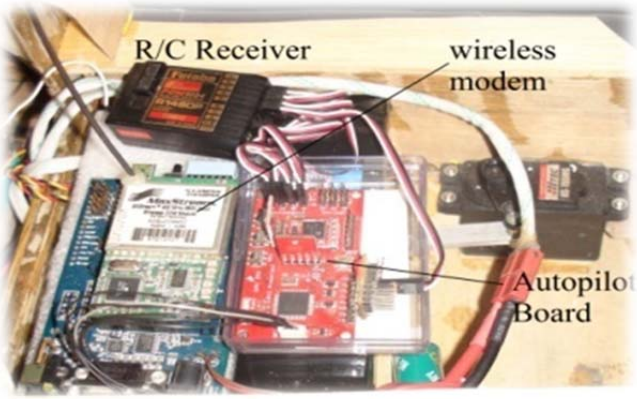

Fig. 4 Installation of onboard autopilot system

The dsPIC is based on 33FJ256GP710A microprocessor family with clock of 16 MHz, low power consumption, featured with a variety of I/O (digital, PWM), besides RAM and flash memory space. The choice for this device is justified by its high processing capability as well as easy integration with digital servos through PWM I/O ports. On block (3) of Fig. 1, it is represented the Ground Control Station that monitor the flight under test. The screen view of GCS is as shown in Fig. 5. It receives telemetry data from the FCC and displays the flight parameters in real time.

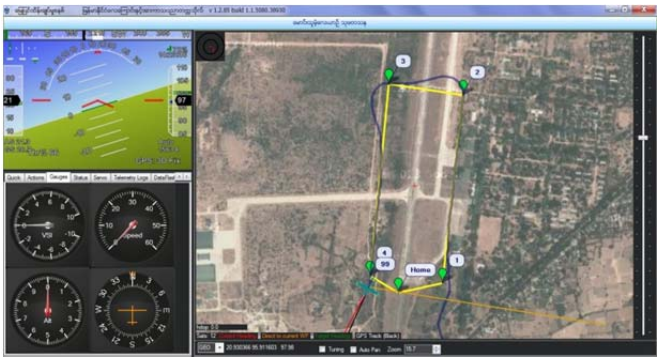

Fig. 5 Ground Control Station

Flight Simulator X-Plane has an important feature that is essential to this test platform development. It is its capacity of sending and receiving data to and from other devices. One way to

implement this communication is by writing plug-in for X-Plane. The plug-in read 'data-refs', which are various variables inside X-Plane and send data over a network or serial port, or anything else the code do.

The X-Plane SDK API gives a generic, flexible, high performance way to read and write data to and from X-Plane and other plug-ins. For example, the API allows reading and setting the navigation parameters, getting the plane location, determining the current effective graphics frame rate, etc. The data access APIs are the way that read and write data from the X-Plane as well as other plug-ins. The API works using opaque data references. A data reference is a source of data; it do not need to know where it comes from, but once it gets, can read the data quickly and possibly write it. Data references are identified by verbose string names (like that, sim/cockpit/radios/nav1_freq_hz). The actual numeric value of the data reference is implementation and defined to change in each time when the simulator is running. The task of looking up a data reference is relatively expensive; look up data references once based on verbose strings, and save the opaque data reference value for the duration of plug-in's operation. Reading and writing data references are relatively fast. This allows data accessing rate to be high performance, while leaving in abstraction; since data references are opaque and are searched for, the underlying data access system can be rebuilt. APIs are provided for reading and writing data in a number of ways.

In the case of roll attitude control, FCC generates the roll angle reference and sends control signal to X-Plane. X-Plane commands the simulated aircraft according to the inputs received. The new aircraft roll angle position is sent from X-Plane back to FCC, restarting the process. Under the FCC processing, the autopilot control system and HIL interface code are responsible for serial data decode and encode process. On the side of simulation computer, X-Plane simulates the aircraft model to be controlled via FCC. Both systems communicate to each other through their COM port using UART stream. The FCC also sends servo PWM output to actuator that commands the model aircraft's flight control surfaces.

4. TEST RESULTS

In order to demonstrate how the test platform could be applied in laboratory classes and also help autopilot systems development, the autopilot system was designed and integrated into the platform. The gains K_p, K_I and K_D of that system were tune base on trial and error basic. The analytical method of PID gains tuning cannot be done, because of the complexity of aircraft dynamics model, in other words, the airframe transfer function. Thus, it's considered the first step to tune the PID gain on trial and error basis since airframe crash is not a problem in HIL simulation.

To initialize the simulation, X-Plane is loaded with AeroMas UAV model with plug-in enable. As soon as the test platform model shown on Fig. 3 runs, the designed autopilot system takes the aircraft control. In principle, for any waypoint data applied as reference into the autopilot system, the aircraft at X-Plane shall respond that references.

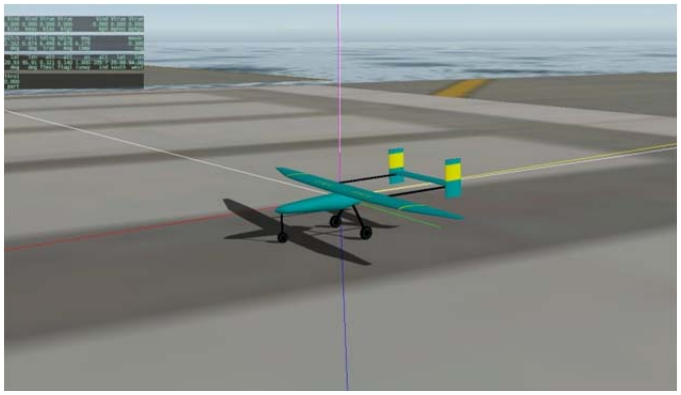

Fig. 6 Testing the AeroMas UAV model in HIL Lab

Table 1 Final gain tuning results of AEROMAS UAV

PID Gains	Roll	Pitch	Yaw
Proportional	0.8	0.58	1.0
Integral	0.01	0.085	0.0
Derivative	0.0	0.2	0.0

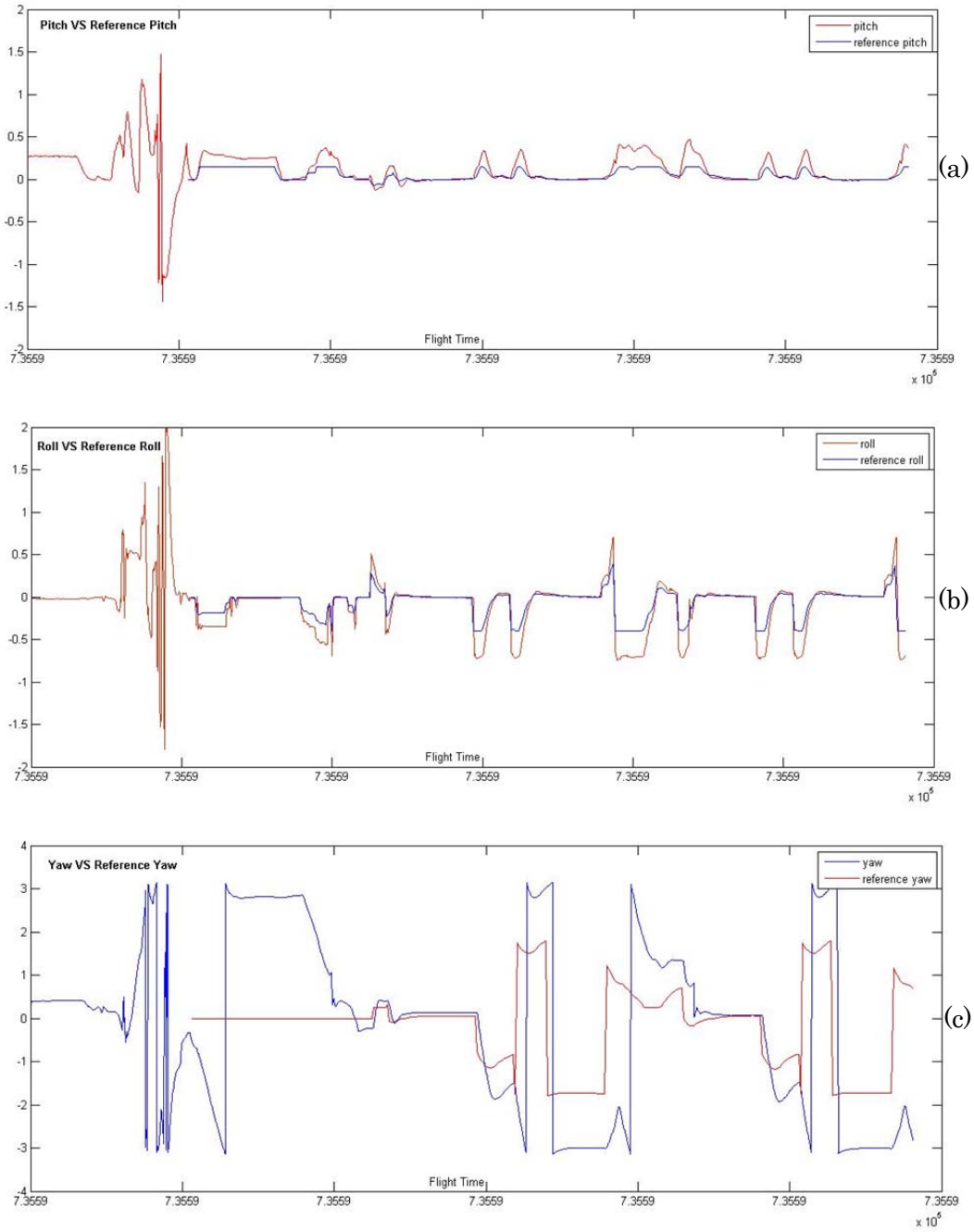

Fig. 7 (a)Pitch reference and response (b)Roll reference and response (c)Yaw reference and response

The reference signals are applied as 3D waypoint (Latitude, Longitudinal, and Altitude) inputs, the system response and also the commands sent to the aircraft flight control surfaces actuators can be monitored through GCS. In the simulated flight, the input is the 3D waypoint, the system response is the new aircraft control command and the commands are the deflections to be imposed to the three control surfaces and Throttle. Fig. 7 shows the results for the proposed attitude autopilot system implemented at the test platform.

5. Conclusion

HIL simulation lab in the UAV development is proved to be valuable without risking the airframe and other devices. It allows finding the problems of control algorithm, refining the firmware of autonomous system, testing the reliability of aircraft models, fine tuning and analyzing the parameters of autopilot system. It also allows monitoring the aircraft responses for a designed autopilot system with high degree of realism.

The test platform also permits the study of longitudinal and lateral directional movement of a specific aircraft which the autopilot system is being designed. Due to the effectiveness of HIL System LAB, it can perform as a Simulated Flight Testing Environment and also an Educational design tool. It is usually used in a laboratory environment on the ground to test the prototype UAV models and autonomous controller under different working loads and conditions conveniently and safely.

Acknowledgments

The author wish to thank his members of UAV project for their work and warmly friendship and also wishes to extend his thanks to Dr. Kyi Thwin, Rector of Myanmar Aerospace Engineering University for his support and guidance. Especially, the author would like to express special thank to the partners for their noble support and encouragement.

References

[1] B. Kada, and Y. Ghazzawi, Robust PID Controller Design for an UAV Flight Control System, vol II, World Congress on Engineering and Computer Science, (2011).

[2] Lucio R. Ribeiro, and neusa Maria F, UAV Autopilot Controllers Test Platform Using Matlab/Simulink and X-Plane, S2H, 40th ASEE/IEEE frontiers in education conference, (2010).

[3] Marco A.A. Sanvido, Vaclav Cechticky and Walter Schaufelberger, Testing Embedded Control Systems Using Hardware In the Loop Simulation and Temporal Logic, 15th Triennial World Congress, (2002).

[4] LAMINAR RESEARCH, X-Plane Description, X-Plane Manual, (2009).

(Received; 23rd December, 2013, Accepted; 2ndh August, 2014)

The Potential of Coconut Oil Biodiesel Utilization in the Delta Regions of Myanmar

Thet Myo[1], Eiji Kinoshita[2]

[1)] United Nations Industrial Development Organization (UNIDO), No. 35(B-15), New University Avenue Road, Yangon, Myanmar

[2)] Department of Mechanical Engineering, Kagoshima University, 1-21-40 Korimoto, Kagoshima 890-0065, Japan

Coconut oil mainly consists of lower carbon number saturated fatty acids such as lauric acid(12:0) and myristic acid(14:0). Research experiments have shown these saturated fatty acids contribute better and cleaner combustion of coconut oil biodiesel. In Myanmar, coconut trees grow naturally and abundantly in the southern part of country where are delta regions with the tropical weather. But there are only very few small scaled traditional farms exist. By developing commercial farming, coconut oil will become one of the major sources for biodiesel production in these delta regions. On the other hand, the development of renewable energy including biodiesel is one of the objectives of ongoing Myanmar's reform. Currently, Myanmar Government is setting up a new department to promote the renewable energy and preparing National Energy Policy including the development of renewable energy sector. Considering renewable energy and environment concerns, biodiesel is one of the best alternative fuels for diesel engines. From our previous research we investigated the utility of coconut oil ethyl ester (CEE) by conducting engine experiments and we have found CEE has favorable fuel properties, better combustion characteristics and less exhaust emissions compared to conventional diesel fuel. Therefore, by promoting the coconut farming in the delta regions of Myanmar, the potential of coconut oil biodiesel utilization is very positive and benefits for these regions especially.

1. Introduction

Agriculture is a backbone of the Myanmar economy and it contributed 36% of GDP in 2010 [1]. Rice is main crop of Myanmar mostly planted in delta regions where are known as rice granary of Myanmar. Currently agricultural mechanization is being implemented and the use of agricultural machineries like farm tractors, harvesters, threshers and water pumps are increasing. These machineries are mainly powered by internal combustion engines. Especially diesel engines are mostly used because of less fuel consumption, more durability and easier maintenance. Considering renewable energy and environmental concern, biodiesel is one of the best alternative fuels for diesel engines.

Generally, biodiesel can be produced form vegetable oils by the transesterification process. Depend on the utilization of alcohol in transesterification process, methyl ester type and ethyl ester type biodiesels can be processed. From our previous research we have investigated the utility of coconut oil ethyl ester (CEE) by conducting engine experiments. The experimental results show CEE has favorable fuel properties, better combustion characteristics and less exhaust emissions compared to conventional diesel fuel. Therefore we recommend ethyl ester type coconut oil biodiesel for agricultural machineries in the delta regions of Myanmar. Furthermore, the alcohol for CEE production, ethanol, has advantages because it is agro product and regionally available.

As mentioned above, although coconut trees grow naturally and abundantly in the delta regions of Myanmar, only very few small scaled traditional farms exist. The production of coconut in Myanmar and neighboring ASEAN countries (2008-2012) [2] is as shown in Table. 1. Comparing between neighboring ASEAN countries, Myanmar has only one third of the production of Thailand and less than 3% of the productions of Indonesia and Philippines. In these countries, coconut oil biodiesel is commercially available in the biodiesel market and widely use. Therefore, by promoting coconut tree plantation in Myanmar, coconut oil is one of the resources for biodiesel production.

Table 1 Production of Coconut in Myanmar and neighboring ASEAN countries (2008-2012) [2]

Country	2008	2009	2010	2011	2012
Myanmar	505,014	420,393	428,075	420,000	430,000
Thailand	1,483,927	1,380,980	1,298,147	1,055,318	1,100,000
Indonesia	17,937,000	19,000,000	18,000,000	17,500,000	18,000000
Philippines	15,319,500	15,667,565	15,510,283	15,244,609	15,862,386

(Unit- tonnes)

2. Research on Coconut Oil Ethyl Ester (CEE)

Test fuels

In our previous research coconut oil ethyl ester (CEE), palm oil ethyl ester (PEE), rapeseed oil ethyl ester (REE) and JIS No.2 diesel fuel were used as test fuels. CEE, PEE and REE were prepared by transesterification reaction of coconut oil, palm oil and rapeseed oil respectively. In the transesterification reaction, 6:1 molar ratio of alcohol (ethanol) to oil and 1 mass% of potassium hydroxide (KOH) to oil were used for PEE and REE. For CEE, 8:1 molar ratio of ethanol to oil and 1 mass% of potassium hydroxide (KOH) to oil were used due to the lower ester conversion rate of CEE in transesterification reaction. The reactions were carried out at 60 ^{o}C for 2 hours. At the end of the reaction, the mixtures were kept at ambient temperature of 20-25 ^{o}C for 8 hours and then the glycerin was drained off. The residual alcohol in the ester was evaporated and the ester was washed with water to remove the residual glycerin and other impurities. The same processes were used in the transesterification reactions of CEE, PEE and REE.

The properties of the test fuels are shown in Table 2. The density, kinematic viscosity, pour point, Carbon, Hydrogen and Oxygen contents, the 50% distillation temperature and the residuals, such as alcohol, and glyceride of the test fuels were carried out by measurements, and the remaining properties were by calculations. The net calorific value of CEE is 35.93 MJ/kg and it is slightly lower than those of PEE and REE, and a gap different with diesel. The density of CEE is 867kg/m^3 and that is slightly lower than those of PEE and REE and higher than diesel. The kinematic viscosity of CEE is 4.5mm^2/s and it is lower than those of PEE and REE, and closer to diesel. The pour point

Table 2 Properties of test fuels

Properties	CEE	PEE	REE	Diesel
Cetane number	-	-	-	56
Net calorific value (MJ/kg)	35.93 *	37.16 *	36.86 *	43.12
Density @ 288K (kg/m^3)	867	869	873	832
Kinematic viscosity @ 293K (mm^2/s)	4.5	7.5	7.0	4.7
Pour point (^{o}C)	-7.5	7.5	-10.0	-12.5
C (mass%)	74.0 *	76.0 *	78.0 *	87.3
H (mass %)	12.4 *	13.0 *	12.0 *	12.5
O (mass %)	13.6 *	11.0 *	10.0 *	0
Alcohol (mass %)	0.010	0.001	0.001	-
Free glycerin (mass %)	-	0.028	0.003	-
Monoglyceride (mass %)	3.095	0.213	0.178	-
Diglyceride (mass %)	0.629	0.748	0.407	-
Triglyceride (mass %)	0.032	0.122	0.012	-
50% distillation temp. (^{o}C)	285	329	338	278
Stoichiometric air-fuel ratio	12.15	12.70	12.63	14.2

* Calculated value

of CEE is -7.5 °C, which is lower than PEE and higher than REE and diesel. CEE, PEE, and REE contain oxygen about 13.6, 11.0 and 10.5 mass% respectively. CEE has higher monoglyceride contents compared to PEE and REE and only a few differences in diglyceride and triglyceride. These residual glycerides were traced by gas chromatography.

The fatty acid ester compositions of CEE, PEE and REE shown in Table 3 were measured by gas chromatography. From these compositions, the net calorific values and the Carbon, Hydrogen and Oxygen contents of CEE, PEE and REE were calculated. In Table 3, it can be seen that CEE contains about 90% lower carbon number saturated fatty acid, such as laurate and myristate in its fatty acid ester compositions. But in PEE and REE, the amounts of saturated fatty acid are about 50% and 5% respectively.

Table 3 Fatty acid ester composition

Fatty	C:N *	CEE	PEE	REE
Caprylic	8:0	5.4	-	-
Capric	10:0	4.4	-	-
Lauric	12:0	52.0	0.3	-
Myristic	14:0	17.3	1.1	-
Palmtic	16:0	8.8	49.5	4.5
Stearic	18:0	1.8	0.9	-
Oleic	18:1	6.9	38.3	64.1
Linoleic	18:2	1.3	9.1	19.5
Linolenic	18:3	0.5	0.6	10.1
Others	-	2.5	0.2	1.8

* carbon double bond

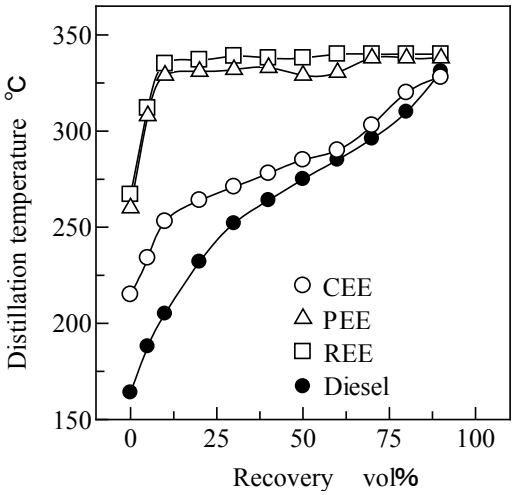

Fig. 1 Distillation temperature of test fuels

The distillation temperatures of the test fuels are plotted in Figure 1. From Figure 1 it can be seen that CEE has lower distillation temperature than that of PEE and REE and the temperature trend is closer to diesel.

Experimental apparatus and procedure

A single cylinder DI diesel engine was used for the experiments. It is a naturally aspirated, water-cooled, four stroke diesel engine. The specifications of the test engine are shown in Table 4. The standard fuel injection system recommended by the engine manufacturer was used for all fuels. The experiments were started after the engine warmed up. When test engine reached a stable condition, the load was applied and the measurements were started. The engine speed was fixed at 2000 rpm and the loads were applied from 0% to 25, 50, 75, 100% using an electronic dynamometer.

Table 4 Specifications of test engine

Engine	DI diesel engine
Engine type	Single cylinder, Four stroke
Bore x Stroke	110mm x106mm
Stroke volume	1007cm^3
Compression ratio	16.3
Rated power	11.77kW@2200rpm
Nozzle opening pressure	19.6 MPa
Injection nozzle type	hole (ϕ0.33mm´4)
Injection timing	18 deg. BTDC

At 100% load condition the brake mean effective pressure (BMEP) of the test engine was 0.67 MPa. The exhaust gases were taken from the exhaust system of the test engine and measured by standard procedure. From the exhaust gases, the CO emission was measured by a non-dispersive infrared detector (NDIR), the HC emission was measured by a flame ionization detector (FID), the NOx emission was measured by a chemiluminescent detector (CLD), and the smoke emission was measured by a light transmitting type smoke meter (Opacimeter). Also the cylinder pressure and the needle lift of the fuel injector were recorded with a digital scope recorder at all load conditions.

Results and discussion

The fuel injection timing, the ignition delay and the ignition timing of the test fuels at BMEP=0.67MPa are as shown in Figure 2. These values were carried out from the needle lift of the fuel injector and the heat release rate of test engine combustion chamber. The fuel injection timing of CEE is almost the same as that of the diesel fuel and those of PEE and REE are faster. The fuel injection timing is mainly influenced by its bulk modulus and viscosity, and the higher bulk modulus and viscosity have the faster injection timings [3]. As it was reported in reference [4], the bulk modulus of saturated fatty acid is lower than that of unsaturated fatty acid. Therefore, it can be considered that CEE with higher saturated fatty acid has later injection timing compared to PEE and REE.

In combustion, the ignitability of biodiesel depends not only on the fatty acid composition, but also on the residual impurities in the fuel [5]. These impurities, such as residual glycerides, methanol and water in biodiesel, may cause negative effects on combustion process. From Figure 2, it can be seen that the ignition delay of CEE is shorter than those of REE and diesel fuel and slightly longer than that of PEE. So CEE has better ignition ability and combustion than those of REE and diesel fuel.

The heat release rate and the needle lift of the fuel injector of CEE, PEE, REE and diesel fuel at BMEP=0.67MPa are shown in Figure 3. By comparing the needle lift intervals of the fuel injector, the fuel injection duration of CEE, PEE and REE are longer than that of the diesel fuel. Due to the lower net calorific values of CEE, PEE and REE, more fuel quantity is necessary to take place combustion process and thus it caused the longer fuel injection duration. The peak heat release rates of CEE, PEE and REE are lower than that of the diesel fuel. The higher initial heat release rate, rapidly emitted after ignition, is probably because of the greater amount of combustible fuel air mixture which formed in the longer ignition delay. Therefore, from Figure 2 and 3, it can be found that the peak of heat release rates is directly proportional to ignition delay time. The combustion end timings of all ester test fuels are almost the same.

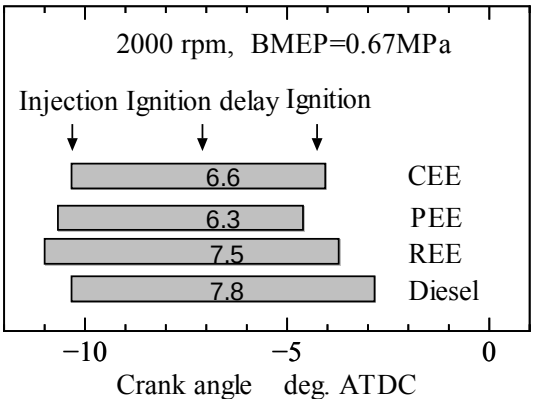

Fig. 2 Injection, ignition delay and ignition

The brake specific fuel consumption (BSFC) and the brake thermal efficiency of (BTE) of the test fuels are shown in Figure 4. BSFC of CEE, PEE and REE are higher than diesel fuel. The increase in BSFC is due to the lower net calorific value of CEE, PEE and REE. BTE of the CEE, PEE and REE are almost the same as that of diesel fuel. This indicates that CEE, PEE and REE have comparable energy conversion rates as diesel fuel.

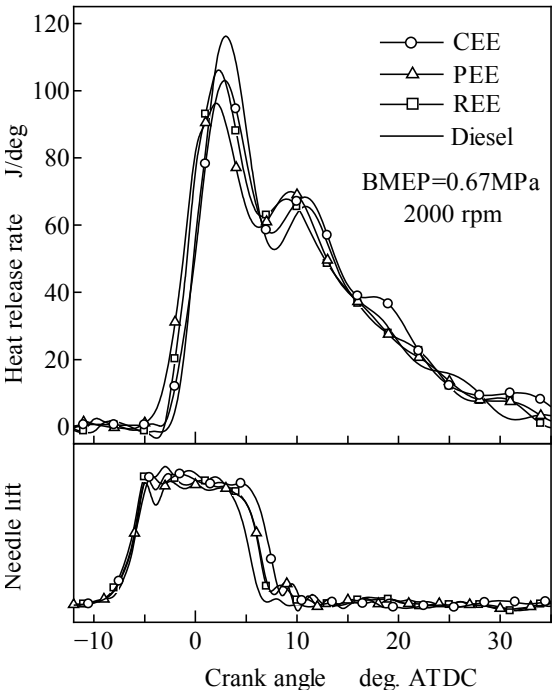

Fig. 3 Heat release rate and needle lift

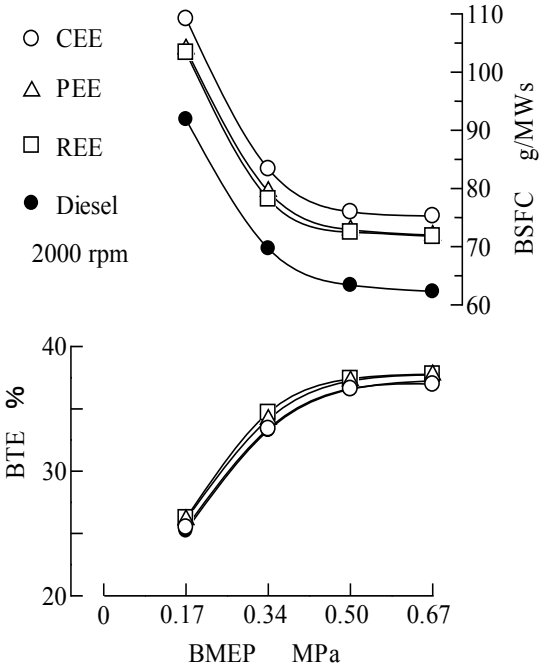

Fig. 4 BFSC and BTE

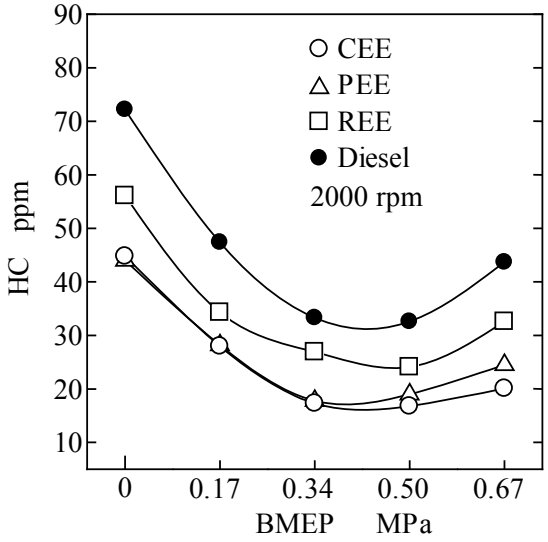

Fig. 5 HC emissions

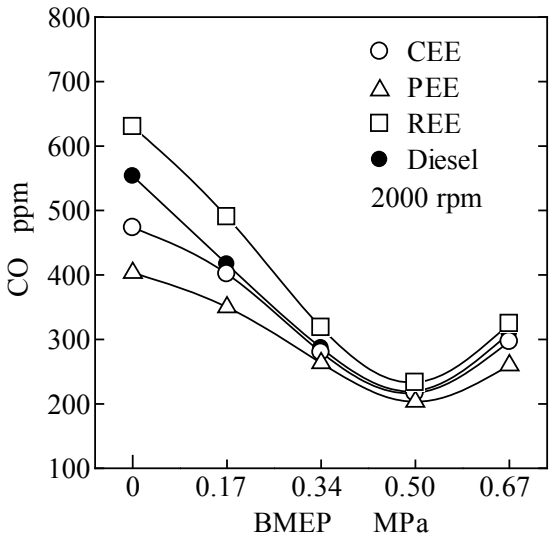

Fig. 6 CO emissions

Figure 5 shows the HC emissions of the test fuels. The HC emissions of CEE, PEE and REE are lower than that of diesel fuel. This is probably due to the oxygen contents in CEE, PEE and REE support better combustion process and reduces incomplete combustion. Therefore, the higher oxygen content CEE has lowest HC emissions compared to PEE, REE and diesel fuel. Moreover, the shorter ignition delay of CEE may also effect on the reduction of HC emission. The CO emissions of the test fuels are shown in Figure 6. The CO emission of CEE is slightly higher than those of PEE and lower than those of REE and diesel fuel. The emission of CO is related with the oxygen content of biodiesel [6].

Figure 7 shows the NOx emissions of the test fuels. CEE and PEE have lower and REE has higher compared to diesel fuel. Especially, in the higher load level, CEE has the lowest NOx emissions. One of the causes of higher NOx emission is higher combustion temperature. Figure8

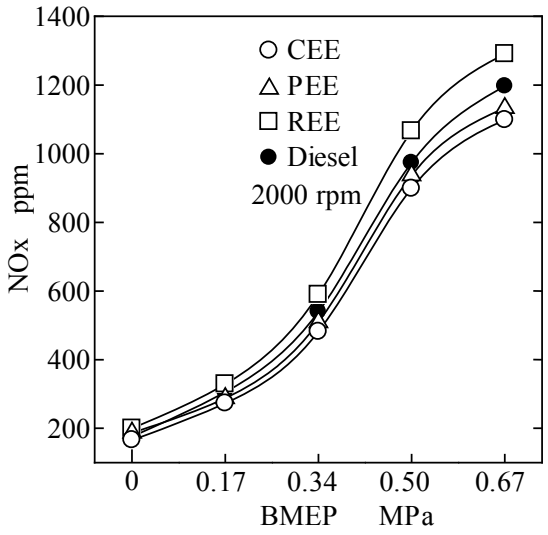

Fig. 7 NOx emissions

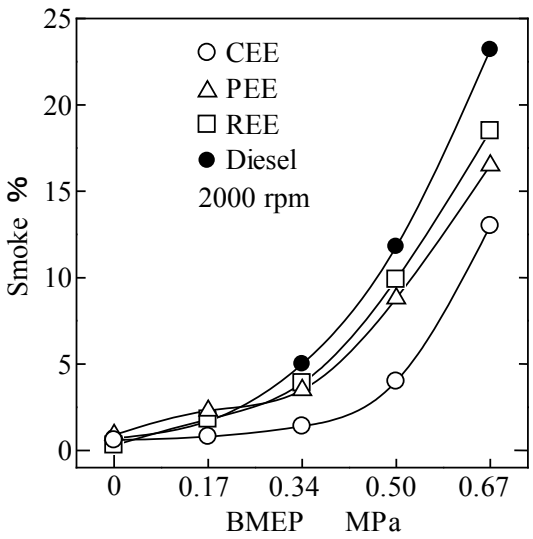

Fig. 8 Smoke emissions

shows smoke emissions the test fuels. The smoke emissions of CEE, PEE and REE are lower than that of diesel fuel. CEE shows the lowest and the significant reductions can be seen. This is the higher oxygen content in CEE increases the oxygen present in fuel rich regions of the fuel spray, which results in a reduction of soot formation and smoke emission compared to PEE and REE.

3. Conclusion

CEE can be processed from coconut oil, ethanol and potassium hydroxide (KOH) by trans-esterification reaction. The process is not so complicated and even farmers can produce fuel for their machineries themselves at home. From the experimental results, we found that CEE has favorable fuel properties, better combustion characteristics and less exhaust emissions compared to diesel fuel. So we confirmed CEE can be utilized for diesel engines and can be considered as an alternative and renewable fuel for agricultural machineries in the delta regions of Myanmar. By implementing so, we can achieve many advantages in environment, renewable energy sector and integrated farming system. Therefore, interest, initiative and both financially and technically encouragement from the local and foreign government organizations, UN originations and NGOs are needed and very important to develop the commercial coconut farming and to establish home industries to large scaled biodiesel industries. Finally, we conclude that the potential of coconut oil biodiesel utilization in the delta regions of Myanmar is very positive.

Acknowledgments

The authors would like to thank the students from Heat Engine Laboratory, Kagoshima University and colleagues from UNIDO Regional Office in Thailand and Yangon Office for their cooperation.

References

[1] Toshihiro Kudo, Satoru Kumagai and Hikari Ishido “Agriculture Plus Plus: Growth Strategy for Myanmar Agriculture”, Institute of Developing Economics (IDE) Paper No. 421, June 2013.

[2] Food and Agriculture Organization, United Nations, Statistical Databases, “Crop Production” available at http://faostat.fao.org.

[3] Heywood. J.B., “Internal Combustion Engine Fundamentals”, McGraw-Hill: New York (1988)

[4] M.E. Tat and J.H. Van Garpen, “Measurement of Biodiesel Speed of Sound and Its Impact on Injection Timing”, NREL/SR-510-31462, 2003.

[5] Thet Myo, Eiji Kinoshita, Hidenori Tsuru, Kazunori Hamasaki, “Combustion Characteristics of a DI Diesel Engine with Palm Kernel Oil Biodiesel and Its Blend(B20)” SAE Technical Paper No. 2007-32-0068; SAE International: Warrendale, PA, USA October 2007.

[6] Eiji Kinoshita, Thet Myo, Kazunori Hamasaki, Hiroshi Tajima and Zhang Ru Kun, “Diesel Combustion Characteristics of Coconut Oil and Palm Oil Methyl Ester” , SAE Technical Paper No. 2006-01-3251; SAE International: Warrendale, PA, USA, October 2006.

(Received; 23rd December, 2013, Accepted;15th July, 2014)

Measuring and Estimating Quality of Server Side Scripts: PHP

Cho Thet Mon[1], Khin Mar Myo[2]

1)University of Computer Studies ,Mandalay, Myanmar

2) University of Computer Studies, Mandalay, Myanmar

**E-mail:chothetmonucsm@gmail.com, kmmyo@gmail.com*

The importance of software measurement is increasing leading to development of new measurement techniques. As the development of object-oriented software is rising, more and more metrics are being defined for object-oriented languages. Many metrics have been proposed related to various object-oriented constructs like class, coupling, cohesion, inheritance, information hiding and polymorphism. Even though the traditional software metrics are modified to assess object-oriented software system, they are inadequate to cover all the new and unique aspects of object-oriented languages. Some metrics may not be suitable for some programming or scripting languages. Thus, new metrics which reflect the characteristics of object-oriented paradigm must be defined. This research addresses this need and introduces a new set of metrics for object-oriented PHP code. Since PHP is an object oriented language, the present metrics are capable to evaluate any object-oriented language. This paper proposes two metrics to measure and evaluate reusable and readable qualities of PHP codes. The metrics are analytically evaluated against Weyuker's proposed set of nine axioms. To assess and evaluate the effectiveness and usefulness of proposed metrics, the results of these measures are evaluated and compared with the results of the Self-Organizing Maps (SOM) .

1. Introduction

Software metrics make it possible for software engineers to measure and predict software processes, and necessary resources for a project and work products relevant for a software development effort. A software measure provides software engineers with a means of quantifying the assessment of a software product. A software engineer collects measures and develops metrics so that indicators can be obtained. An indicator is a metric or combination of metrics that provides insight into the software process, a software project or the product itself, and a metric is a quantitative measure of the degree to which a system, component or process possesses a given attribute. A number of metrics have been proposed for computer software, but not all provide practical support to the software designers, developers and managers [1] (William Frakes, and C. Terry, 1996). To be useful in a real world context, software metric must be simple and computable, persuasive, consistent, and objective. It should be independent of programming language and provide effective feedback to the software engineer [2].

Readability of software has something to do with software development and also its quality. As a matter of fact, readability is the judgment of humans with respect to the ease of reading of given source code. Readability can promote software maintainability and the overall software quality can be ensured [3]. The software systems with less readable source code are recognized as more difficult to maintain than those with more readable source code.

This research develops a novel approach called impact of programming features on code readability, to examine the influence of programming features and the effect of these features on code readability.

Achieving a high level of reuse is also an important goal to accomplish in developing a software system. The measurement of reuse will help developers to monitor current levels of reuse and help to provide insight in developing software that is easily reused. The level of reuse must be measured in a way that provides information on a wide range of reuse attributes. Current reuse metrics are generally based on only one attribute namely program size or length. Moreover, reusability decreases the space, cost and time of a project and this research considers measuring reusability quality of PHP files. This paper presents a set of measurable attributes and two metrics which quantify these attributes for PHP object oriented systems.

2. Experiment

Nowadays, most software codes are written by distant teams. It's very important for source codes to be understandable so that it can be easily adapted. Each programmer may want to review code and adapt it according to his/her own need, so readability is needed. Furthermore, the ability of reading and understanding a program written by others is a critical job. Software programming companies depend on team work instead of one programmer, so each one will write a fragment as part of a team effort. In addition, tailoring a ready code would be very difficult to specify tasks than modify them (*e.g.*, some programs may have thousands of lines of code such as network protocols). Moreover, some programmers may use meaningless variable names, or omit comments that can lead to unreadable and complex codes. Using unreadable program codes may lead to code misunderstanding. Therefore, source code's readability quality is the important factors for software quality development.

On the other hand, software reuse is the process of implementing or updating software systems using existing software components. Reusability of object oriented programming is the use of previous classes or functions or methods in the present class is having no problem. [4].

Among the several software measurement techniques, most of those measurements and metrics are developed covering programming languages. With the emergence of the new technologies, new measurement techniques also evolve. There is lack of metrics in literature which specifically measure the quality of PHP script language. In this respect, specific metrics should be developed and we develop two metrics for PHP which are capable to calculate source code readability quality of PHP code ($SCREA_{php}$) and reusability quality of PHP code ($SCREU_{php}$).

The main goal of this paper is to develop a tool that can automatically collect different readability and reusability attributes. We then want to see the value of those attributes and their ability or level of impact on the overall software quality.

2.1 Attribute Selection for Two Metrics

The aim of metric is to predict the quality of the software products.Various attributes which determine the quality of the software, include maintainability, defect density, fault proneness, understandability, usability etc. The main contribution of this paper is to relate the readable and reusable attributes with the metrics and to find how these metrics can determine the readability and reusability of the object oriented PHP code.

2.1.1 Source Code Readability ($SCREA_{php}$)

For measuring qualities of PHP language more accurately, more related attributes for each of qualities are needed to select. These more related attributes are selected according to experts' judgments in many guide lines. To measure the quality of readability, we tried to extract several readability related features from the PHP source codes based on PHP coding guidelines and standards.PHP coding standards are important factors for achieving a high code quality. A common visual style, naming conventions and other technical settings allow us to produce a homogenous code which is easy to read and maintain. These PHP coding guidelines are based largely on Sun's Code Conventions for the Java Programming Language. Deviations from the Sun code conventions are largely a result of the interaction of PHP with other web server applications, primarily databases.

To enhance readability, variable names should be camel-case started with a lower case letter. Readable class names should be descriptive and should be avoided using abbreviations where possible and must be started with upper case letter [6]. Method names should be camel-case started with a lowercase letter. Private and protected attributes have an underscore prefix. Constants should be all uppercase and words are separated by underscore. Moreover, it is needed to detect when a field has a very short name or very long name.

According to the above factors, in this paper, the number of readable variable names and method names are defined as names that are declared with lowerk camel-case letter and the length of variable or method names are greater than 3 letters. The number of readable class names is defined as the class name started with upper camel-case letter and the length of it is greater than 3 letters.

Moreover, it is needed to detect when a field has a very short name or very long name. The rules and usage of line length in source code and documentation is an important aspect of coding standards for many years. A good line length is one that allows the reader's eyes to flow from the end of one

line to the beginning of the next very easily and naturally. A common line length: 80 characters for PHP to maximize readability [7]. The number of blank lines before functions, return, comment or traits can also lead to readable code.

According to these factors, readable code lines are defined as the number of lines length that are less than 80 characters and to obtain readable lines, they are subtracted from total number of lines.

Having blank lines in source code can increase user's readability quality but they are needed to be in the reasonable places. In this respect, in the proposed system, blank lines before functions, blank lines before comment, return and traits are considered as readable blank lines for program source code.

Using program codes that are deviated from the above factors may lead to unreadable code and misunderstanding that can mainly degrade software quality. Therefore, it is important to consider the above factors and the required attributes for readability metrics are described in 2.1.1.

In our contribution, readability attributes are considered based on the above factors and the following is readability metric to measure quality of PHP code and w1, w2, w3, w4 and w5 are corresponding weights using RS method that will explain in the next section.

$$SCREA_{php} = \sum TVN * w1 + \sum TMN * w2 + \sum TCN * w3 + \sum TL * w4 + \sum TBL * w5 \quad (1)$$

Where,

TVN- Typical variable names = number of readable variable names/total number of variable names

TMN- Typical method names = number of readable method names/total number of method names

TCN- Typical class names = number of readable class names/total number of class names

TL- Typical line = (total number of lines-line length greater than 80)/total number of lines

TBL- Typical Blank lines = (blank lines before functions+ blank lines before comment+ blank lines before return+ blank lines before traits)/total blank lines

2.1.2. Source Code Reusability ($SCREU_{php}$)

Various metrics for measuring the reusability of software have conventionally been proposed, mainly for program source code, including the previous researches [8-9]. We qualitatively identified multiple metrics considered to be effective for measuring reusability. In this paper, we proposed a set of metrics for measuring the reusability of PHP language program source code, and evaluated the effectiveness of our metrics using a certain scale of actual metric values. The objective of our study is to provide a validated way for evaluating the ease of reuse of program source code accurately, without any other software materials such as documents and specifications.

$$SCREU_{php} = \sum NDC * w1 + \sum C * w2 + \sum NPF * w3 + \sum PF * w4 + \sum NT * w5 \quad (2)$$

Where,

NDC- Number of Descendent Class: The NDC is total number of descendent class (subclasses) of a class. The greater the number of subclasses, the greater the reuse, since inherence is a form of reuse.

C- Cohesion: Assesses the relatedness of methods and attributes in a class, strong overlap in the method parameters and attributes types in an indication of strong cohesion. High cohesion implies simplicity and high reusability.

NPF-No of public functions: Total number of functions that are declared public. The more the number of functions that are declared public, the greater reusability of code that is because the function name that is declared with public can be accessed and reused anywhere from other classes or the surrounding applications.

PF-Number of functions without parameters: The greater the value, the smaller the amount of (dependent) data required for use, indicating high reusability of the file.

NT-Number of Traits: Total number of traits that are mechanism for code reuse in single inheritance languages such as PHP. A PHP trait is intended to reduce some limitations of single inheritance by enabling a developer to reuse sets of methods freely in several independent classes living in different class hierarchies.

The greater these attribute values, the higher reusability of the source code.

2.1.3 Assigning Weight

Weighting attribute is a necessary step of the measuring process to get more accurate result. There are many alternative methods: the equal weights (EW) method, rank sum (RS) method, rank reciprocal (RR) method, rank-order centroid (ROC) method and rank exponent method [10]. To assign attribute weight, we need to rank attributes for particular quality based on experts' judgments. The important of individual attributes are not the same and their weights are not equal. The following based attributes are ranked according to quality assurance guidelines.

For the SCREA$_{php}$ metric: Ranks of Attributes: (NDC ≥ C ≥ NPF ≥ NT)

For the SCREU$_{php}$ metric: Ranks of Attributes: (TVN ≥ TMN ≥ TCN≥ TL≥ TBL)

In this paper, after ranking attributes with their important, the attributes are assigned with RS method because it can produce more accurate result than other methods. For readable and reusable qualities, metrics' weights are defined as:

$$R_i(u) = \frac{t + 1 - i}{\sum_{l=1}^{t} j} = \frac{2(t + 1 - i)}{t(t + 1)} \qquad (3)$$

l= 1,2,3..,t ;μ = a metric ;t = the total number of attributes for μ metric ; i=1,2,3…,t

3. Results and Discussion

The proposed two metrics are analyzed by using thirty PHP files. Most of them are extracted from the web and these files are not shown details in this paper. The result of two metrics that are calculated from equation 1 and 2 is shown in figure 1.

The usefulness of any new measurement system should be validated by proper validation and testing process. A new metric should be theoretically evaluated based on strong theoretical base and validated empirically to prove its practical usefulness. There are many evaluation criteria for theoretical validation of a metric and most of them are based on principle of measurement theory. The SCREAphp and SCREUphp metrics are validated theoretically and evaluated empirically in the next sections.

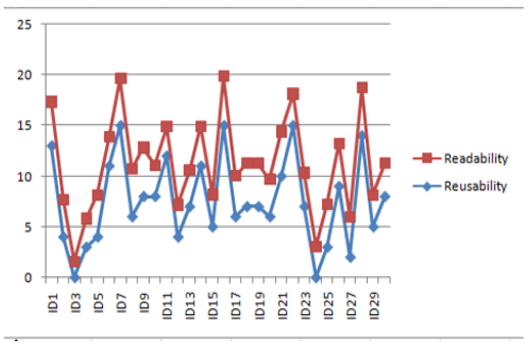

Fig. 1 Related Result of Readability and Reusability

3.1. Theoretical Validation of Proposed Metrics

Amongst available validation criteria, the proposed metrics are proved by using nine Weyuker's properties [5]. This work has been discussed by many authors and is still a point of reference and comparison for anyone investigating the topic of software metrics. Several object oriented metrics are suitable only for the six Weyuker's properties, and other properties are not very useful. The case study, the evaluation of SCREUphp and SCREA$_{php}$ metrics against nine Weyuker's properties are as follows: let P, Q and R be programs.

Property 1: (∃P) (∃Q) (|P| ≠ |Q|)

This property states that the measures should not rank all the programs as equally. There are 30 different values and these different files have different attributes. Therefore, the two metrics satisfy this property.

Property2. Let c be a nonnegative number, and then there are only finitely many programs of reusability and readability for c. This means that there are only a finite number of PHP files of the same quality if quality metric value is non-negative number. Therefore, the two metrics satisfies this property.

Property 3: There are distinct programs P and Q such that |P| = |Q|. The proposed metrics satisfy this property because the same features of different PHP files have the same quality values.

Property 4: (∃P) (∃Q) (P≡Q & |P| ≠ |Q|). If P and Q are different files having the same functionality, their corresponding metrics values can be different because of different implementation. As the proposed metrics are based on the internal structures of codes, they satisfy this property.

Property 5: (∀P) (∀Q) (|P| ≤ |P; Q| and |Q| ≤ |P; Q|). This property states that if the combined program is constructed from P and Q, the value of the combined program is larger than the value of P or Q. The two proposed metrics also satisfy this property.

Property 6: (∃P) (∃Q) (∃R) (|P| = |Q|) & (|P; R| ≠|Q; R|). In the proposed metrics, the numbers of attributes are fixed for any program. Mapping program R with P and Q results the same values. Hence, the proposed metrics cannot satisfy this property.

Property 7: There are program bodies P and Q such that Q is formed by permuting the order of the statement of P and (|P| ≠ |Q|). In this testing, the proposed metrics satisfy this property.

Property 8: If P is renaming of Q, then |P| = |Q|. This property is also satisfied by the two metrics.

Property 9: (∃P)(∃Q)(|P| + |Q|) ≤ (|P;Q|). This property means that when two programs are combined, the metric value of combined program is greater than or equal than the sum of P and Q. If two files have nearly same attribute features, they can satisfy this property. Otherwise, they not satisfy.

In this point of view, satisfying nearly all properties of Weyuker except some case, it can be realized that the proposed metrics are robust measures.

3.2 Empirically Validation of Proposed Metrics

For empirical validation of the proposed metric, the SOM, one of the unsupervised learning methods in Neural Network, is used. SOM is suitable for measuring the validity and usefulness of the proposed metrics that they are difficult to prove their validity and usefulness because they don't have historical data and other comparison metric. One advantage is that they do not require more understanding with input data and they can cluster and estimate incomplete historical data. The SOM learns similarity of input feature vectors and responds groups of similar input vectors [11].

In this paper, only the empirical validation result for reusability metric is shown as an example and the result for readability metrics cannot be presented here due to space limitations but the process is the same. To check validity of proposed metric, the processes are as follow. First, thirty PHP example files are used as input and are calculated metric values for each file. Before clustering, two data files are created for proposed metric, one contains the particular proposed metric's target values of 30 PHP files and another contains its base attributes NDC, C, NPF and NT. In the preprocessing step, base attributes are converted into binary data according to the "hard logic" approach using a threshold t. For example, if $x_i \geq t$ then we assume it as 1 and 0 otherwise [12]. And then, dissimilarity matrix using Jaccard Coefficients is used [12]. Then two files of $SCREU_{php}$ metric are clustered by SOM and the cluster matching result is analyzed. As shown in figures, the first group of figure 1 and the first group of figure 2 are compared and analyzed and the other two second groups are also analyzed. It is clear that the two results are almost equal. Therefore the metric has high accuracy and the proposed metric is suitable for measuring reusable quality of PHP files. The processes of readability metric validation are the same.

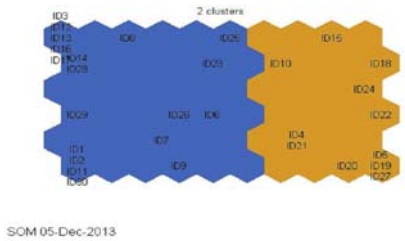

Fig.2 SOM Clustering Result Depending only on Target Values of SCREUphp Metric for 30 PHP Files (ID1-ID30)

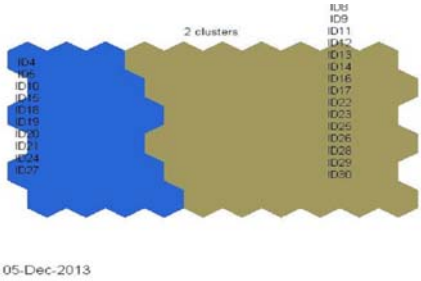

Fig. 3 SOM Clustering Result Depending on Based Attributes of SCREUphp Metric for 30 PHP Files (ID1-ID30)

4. Conclusion

Traditional software metrics may not be inadequate to cover all the new and unique aspects of some programming or scripting languages. In this respect, new metrics which reflect the characteristics of object-oriented paradigm are contributed and defined. The proposed metric measures the quality of PHP programming language with respect to readability and reusability.

The proposed metrics are validated both theoretically and empirically and it will prove usefulness and effectiveness of this proposed system. The two metrics are robust measures because of satisfying measurement properties and the cluster matching results are very high. Therefore, the proposed metrics are suitable for measuring quality of PHP language. In future work, other quality factors such as complexity, maintainability, efficiency and so on can be considered.

Acknowledgments

I would like to express my gratitude and my sincere thanks to Dr. Mie Mie Thet Thwin, Rector of U.C.S.M, allowing me to develop this thesis and giving me more general guidance during the period of study. I would like to express very special thanks to Dr. Khin Mar Myo, Associate Professor, U.C.S.M, for her continuous advice. I would like to express my respectful gratitude to Dr. Khin Thida Lynn, Associate Professor for giving enough consideration to my ideas and views.

References

[1] William Frakes, and C. Terry (1996)"Software Reuse: Metrics and Models," ACM Computing Surveys, vol.28, no.2, Pp.415-435.

[2] Roger S. Pressman, "Software Engineering, A Practitioner's Approach", Pp 438

[3] Rajendar Namani1, Kumar, "A New Metric for Code Readability", IOSR Journal of Compute Engineering (IOSRJCE) ISSN: 2278-0661, ISBN: 2278-8727Volume 6, Issue 6 (Nov. - Dec. 2012), Pp 44-48

[4] Sonia Manhas, Rajeev Vashisht, Reeta Bhardwaj, "Framework for Evaluating Reusability of Procedure Oriented System using Metrics based Approach"

[5] E. J. Weyuker, "Evaluating Software Complexity Measures," IEEE Trans. Software Eng., vol. 14, no. 9, pp. 1357-1365, Sept. 1988.

[6] http://phpmd.org

[7] http://net.tutsplus.com/tutorials/html-css-techniques/top-15 best practices for writing super readable code

[8] Ajay Kumar," Measuring Software Reusability using SVM based Classifier Approach", International Journal of Information Technology and Knowledge Management January-June 2012, Volume 5, No. 1, pp. 205-209 .

[9] Hironori Washizaki, Toshikazu Koike, Rieko Namiki, and Hiroyuki Tanabe, **"**Reusability Metrics for Program Source Code Written in C Language and Their Evaluation"

[10] B. S. Ahn and K. S. Park, "Comparing Methods for Multiattribute Decision Making with Ordinal Weights", Computers & Operations Research 35 (2008) 1660-1670.

[11] Kohonen, T. (2001). "Self-Organizing Maps". Berlin, Springer-Verlag

[12] Fernando Lourenço, Victor Lobo, and Fernando Bação "Binary-based Similarity Measures for Categorical Data and their Application in Self-Organizing Maps"

(Received; 23rd December, 2013, Accepted; 13th September, 2014)

Simultaneous Faults on Medium Voltage Distribution of Myanmar Electric Power System in Mandalay

Thet Tin
Department of Electrical Power Engineering, Mandalay Technological University, Mandalay, Myanmar,
E-mail: thettin.mtu.mdy@gmail.com

In today's technological world, electrical energy is one of the most important forms of energy and is needed directly or indirectly in almost every field. Increase in the demand and consumption of electrical energy leads to increase in the system fault levels. It is not possible to change the rating of the equipment and devices in the system or circuits to accommodate the increasing fault currents. The devices in electronic and electrical circuits are sensitive to disturbance and any disturbance or fault may damage the device permanently so that it must be replaced. The cost of equipment like circuit breakers and transformers in power grids is very expensive. Moreover, replacing damaged equipment is a time and labour consuming process, which also affects the reliability of power systems. Simultaneous faults may be produced on separate circuits, physically close together, by the same lightning disturbance; or a single line to ground fault on one phase may raise the voltage to such an extent as to cause flashovers, or line to line faults, at a second or third point. Though relatively infrequent, simultaneous faults are important because relay systems, operating satisfactorily for single faults, may fail to isolate simultaneous faults. Therefore, it seems worthwhile to have in convenient form a method for calculating and simulation of short-circuit currents and voltages caused by faults occurring at the same time at two or three separate and distinct points of a system. The method for the determination of fault currents and voltages on symmetrical three-phase systems subjected to two simultaneous faults was presented in this paper. The fault analysis was affected by the Method of Symmetrical Components. In order to perform an investigation, the Medium Voltage Myanmar Distribution Network in Mandalay, is used as the building block of Simultaneous fault simulation. Then this network is examined using MATLAB/SIMULINK. The system parameters such as line voltage, line current and reactive power, Q, and real power, P are observed when the simultaneous fault is applied to this system.

1. Introduction

The energy chain contains producing the energy, its transmission, and delivering the energy to the costumer where the distribution feeders are the last nuts of this chain. The importance of the latter part is no less than the former parts in the electrical power system if not higher. Thus, many commercial experts believe that the distribution system should be taken into consideration more seriously as all the efforts to generate electrical power is with the purpose of delivering it to the customer [1].

A fault along that distribution system, that could cause outages and damage, is one of the main problems in the system. It is important that the fault is located in the system so that it can be isolated. If the fault is not isolated, electrical equipment and other parts of the system could be damaged for the long term. An important objective of all the power systems is to maintain a very high level of continuity of service, and when abnormal conditions occur, to minimize the outage times. It is practically impossible to avoid consequences of natural events, physical accidents, equipment failure or misoperation which results in the loss of power, voltage dips on the power system. Natural events can cause short circuits i.e. faults which can either be single phase to ground or phase to phase or phase to phase to ground or a three phase fault. Most faults in an electrical system occur with a network of overhead lines are single-phase to ground faults caused due to lightning induced transient

high voltage and from falling trees. In the overhead distribution lines, tree contact caused by wind is a major cause for faults. The appropriate percentages of occurrences various faults are listed below [2]:

Single line to ground fault	–	70~80%
Line-Line to ground fault	–	10~17%
Line-Line fault	–	8~10%
Three phase	–	2~3%

When faults occur in the power system, they usually provide significant changes in the system quantities like over-current, over or under-power, power factor, impedance, frequency and power or current direction. The most common is the over-current and so over-current protection is widely used. Although, in distribution system the basic approach to calculate the fault location using voltage and current measurement is still the same as in the transmission system case, fault locating in the distribution system is not an easy task because of its high complexity and difficulty caused by the non-homogeneity of lines, fault resistances, load uncertainty, and phase imbalance [3],[4].

2. Simultaneous Faults

The Method of Symmetrical Components embodies the replacement of a system of three vectors (voltages or currents), regardless of their degree of unbalance, by three sets of balanced vectors. These three sets of balanced vectors are known as the positive- sequence, negative-sequence, and zero-sequence systems of vectors. Simultaneous faults occurring at two separate and distinct points on a three-phase system may involve any combination of six conductors and any combination of the short-circuit type faults. Since the current and voltage at each fault depend upon the current and voltage at the other fault, simultaneous faults may not be treated independently. Nevertheless, each fault may be considered separately in determining the relations existing between the symmetrical components of fault current and voltage at each fault point.

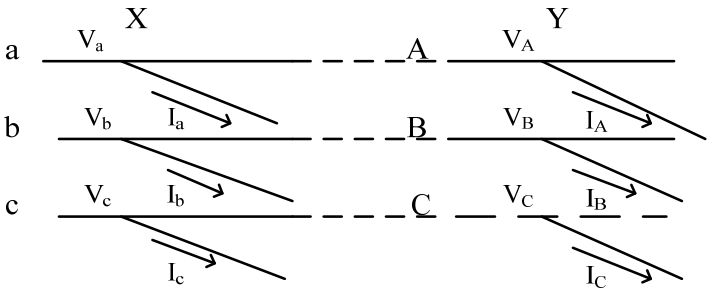

Fig. 1 Simultaneous Faults at Three-phase System. X and Y on a Symmetrical

In Figure 1 let X and Y represent the two short- circuited points with a and A, b and B, and c and C being conductors on the same phase. V_a, V_b, V_c and V_A, V_B, V_C indicate line to ground voltages on phases a, b, c and A, B, C, respectively, and I_a, I_b, I_c and I_A, I_B, I_C, the corresponding fault currents. The six symmetrical components of current and voltage at C are I_{x1}, I_{x2}, I_{x0}, V_{x1}, V_{x2}, and V_{x0} and those at D are I_{y1}, I_{y2}, I_{y0}, V_{y1}, V_{y2} and V_{y0}. Twelve independent equations are necessary for the determination of the twelve unknown components. Two equations may be obtained from a consideration of the positive-sequence network impedances, and the relations between the positive-sequence components of fault current and voltage at each fault location. Similarly, four more equations may be obtained, two from each of the negative- and zero-sequence networks. These six equations may be formed only because the system is assumed to be balanced, with the result that the three sequence-networks are independent of each other. Three more equations, independent of the system impedances, may be developed for each fault point. These equations, which relate the components of voltage and current for the different sequences, depend only on the conditions existing at the fault [5].

Figure 2 shows the equivalent wye replacing the zero-sequence network between the two faults and the zero-potential bus. The branch impedances are X_0, Y_0, and S_0, and they may be either inductive or capacitive. Before the simultaneous faults occur, there are no currents nor voltages in the zero sequence network. The effect of the simultaneous faults is to change the voltages at X and Y

from zero to and from zero to V_{x0}, and from zero to V_{y0}, respectively, and the fault currents from zero to I_{x0} and zero to I_{y0}. Taking the positive direction of current flow as into the faults, the zero-sequence rise in voltage from the zero-potential bus to the points X and Y may be expressed as follows:

$$V_{x0} = -(I_{x0} + I_{y0})S_0 - I_{x0}X_0 = -I_{x0}(X_0 + S_0) - I_{y0}S_0 \quad (1)$$

$$V_{y0} = -(I_{x0} + I_{y0})S_0 - I_{y0}Y_0 = -I_{x0}S_0 - I_{y0}(Y_0 + S_0) \quad (2)$$

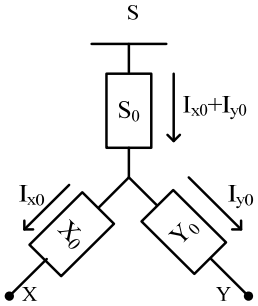

Fig. 2 Equivalent Wye to replace Zero Sequence Network between Fault Points X and Y and Zero-potential Bus S

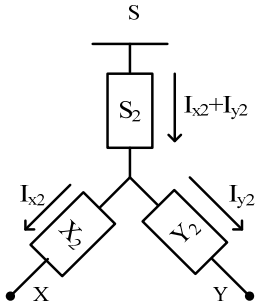

Fig. 3 Equivalent Wye to replace Negative-sequence Network between Fault Points X and Y and Zero-potential Bus

The negative-sequence voltages at the fault points may be obtained in a similar manner from a consideration of Figure 3.

$$V_{x2} = -I_{x2}(X_2 + S_2) - I_{y2}S_2 \quad (3)$$

$$V_{y2} = -I_{x2}S_2 - I_{y2}(Y_2 + S_2) \quad (4)$$

The positive-sequence system will differ from the negative- and zero-sequence systems since it will contain positive-sequence generated Voltages. Let it be assumed that operating conditions existing before the occurrence of the faults are:

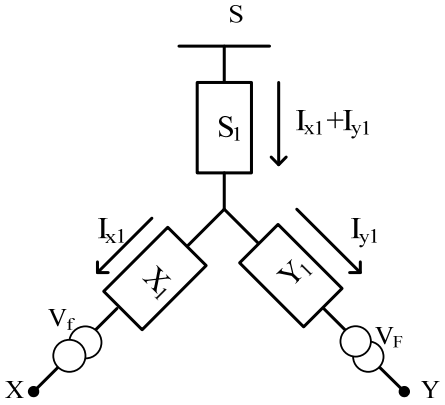

Fig. 4 Equivalent Wye to replace Positive-sequence Network between Fault Points X and Y and Zero-potential Bus

Therefore, the voltage rise from the zero-potential bus to the fault point X is:

$$V_{x1} = V_f - I_{x1}(X_1 + S_1) - I_{y1}S_1 \quad (5)$$

Likewise, the voltage at fault point Y is:

$$V_{y1} = V_F - I_{x1}S_1 - I_{y2}(Y_1 + S_1) \quad (6)$$

The six equations for the two fault points from symmetrical components and equation (1) and (2) from zero sequence network, and equation (3) and (4) from the negative sequence network, the two equations can be put in the form:

$$V_{x1} = k\, I_{x1} + m\, I_{y1} \quad (7)$$

$V_{y1}=n\,I_{x1}+l\,I_{y1}$ (8)

where k, l, m, and n depend upon the branch impedances of the equivalent Y's replacing the negative and zero-sequence networks and the particular combination conductors involved in the simultaneous faults.

Values of k, l, m, and n in terms of the branch impedance networks are tabulated in Table 1 for various combinations of a grounded three-phase system.

Table 1. Values of k, l, m, and n in Terms of the Branch Impedance Networks for Simultaneous Short Circuits at Two Points [6]

Case	Two Faults At		
A. Single Line-to-Ground Faults	(a)Phase a and A $k=Z_{xs}$ $n=S_0+S_2$ $m=S_0+S_2$ $l=Z_{ys}$	(b)Phase b and A $k=Z_{xs}$ $n=a^2S_0+aS_2$ $m=aS_0+a^2S_2$ $l=Z_{ys}$	(c)Phase c and A $k=Z_{xs}$ $n=aS_0+a^2S_2$ $m=a^2S_0+aS_2$ $l=Z_{ys}$
B. Line-to-Line Faults	(a)Phase b, c and B, C $k=X_2+S_2$ $n=S_2$ $m=S_2$ $l=Y_2+S_2$	(b)Phase a, c and B, C $k=X_2+S_2$ $n=aS_2$ $m=a^2S_2$ $l=Y_2+S_2$	(c)Phase a, b and B, C $k=X_2+S_2$ $n=a^2S_2$ $m=aS_2$ $l=Y_2+S_2$
C. Double Line-to-Ground Faults	(a)Phase b, c and B, C $k=\frac{\Delta_2(X_0+S_0)+\Delta_0(X_2+S_2)}{Z_{xys}}$ $n=\frac{\Delta_2S_0+\Delta_0S_2}{Z_{xys}}$ $m=\frac{\Delta_2S_0+\Delta_0S_2}{Z_{xys}}$ $l=\frac{\Delta_2(Y_0+S_0)+\Delta_0(Y_2+S_2)}{Z_{xys}}$	(b)Phase a, c and B, C $k=\frac{\Delta_2(X_0+S_0)+\Delta_0(X_2+S_2)}{Z_{xys}}$ $n=\frac{a^2\Delta_2S_0+a\Delta_0S_2}{Z_{xys}+3S_0S_2}$ $m=\frac{a\Delta_2S_0+a^2\Delta_0S_2}{Z_{xys}+3S_0S_2}$ $l=\frac{\Delta_2(Y_0+S_0)+\Delta_0(Y_2+S_2)}{Z_{xys}+3S_0S_2}$	(c)Phase a, b and B, C Similar to C.(b) with a and a^2 interchanged in n and m.
D. Three-phase Faults	$k=n=m=l=0$		
E. Line-to-Line Fault at X and 1LG Fault at Y	(a)Phase b, c and A $k=X_2+S_2$ $n=-S_2$ $m=-S_2$ $l=Z_{xs}$	(a)Phase a, c and A $k=X_2+S_2$ $n=-aS_2$ $m=-a^2S_2$ $l=Z_{xs}$	(a)Phase a, b and A $k=X_2+S_2$ $n=-a^2S_2$ $m=-aS_2$ $l=Z_{xs}$

where, $Z_{xs}=X_0+S_0+X_2+S_2$; $Z_{ys}=Y_0+S_0+Y_2+S_2$; $\Delta_0=X_0Y_0+X_0S_0+Y_0S_0$; $\Delta_2=X_2Y_2+X_2S_2+Y_2S_2$; $Z_{xys}=(X_0+X_2)(Y_0+Y_2)+(X_0+X_2)(S_0+S_2)+(Y_0+Y_2)(S_0+S_2)$

3. Proposed Medium Voltage Myanmar Distribution Network

To evaluate the performance of the proposed network based simultaneous faults, 11 kV, 4 miles (6.437376km) distribution line from Aung Pin Lae Substation Mandalay, Myanmar as shown in Figure 5 is considered in this study. The 11 kV distribution line is represented by distributed

parameters of the line parameters is taken into account. The line conductor cross-sectional area of 11 kV line is 35 mm^2. There are bamboo tree closely to the 11 kV MTU feeder line as shown in Figure 6 and Figure 7. There are so many bamboo trees and the medium voltage power lines are short circuited when the heavy rain and wind.

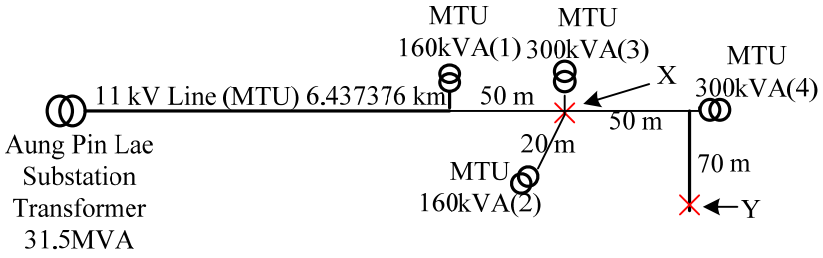

Fig 5. Proposed System for Study

Fig 6. Bamboo Trees at X in Fig 5

Fig 7. Tree Branches over 11 kV MTU Line at Y in Fig 5

4. Simulation Results and Discussion

In the circuit of SIMULINK model, programmable voltage source of amplitude values (p.u) [1 1.06 0.94 1] at time [0 0.2 0.3 0.4] on the 11kV MTU feeder and MTU four transformers with variable Loads are presented as shown in Figure 8.

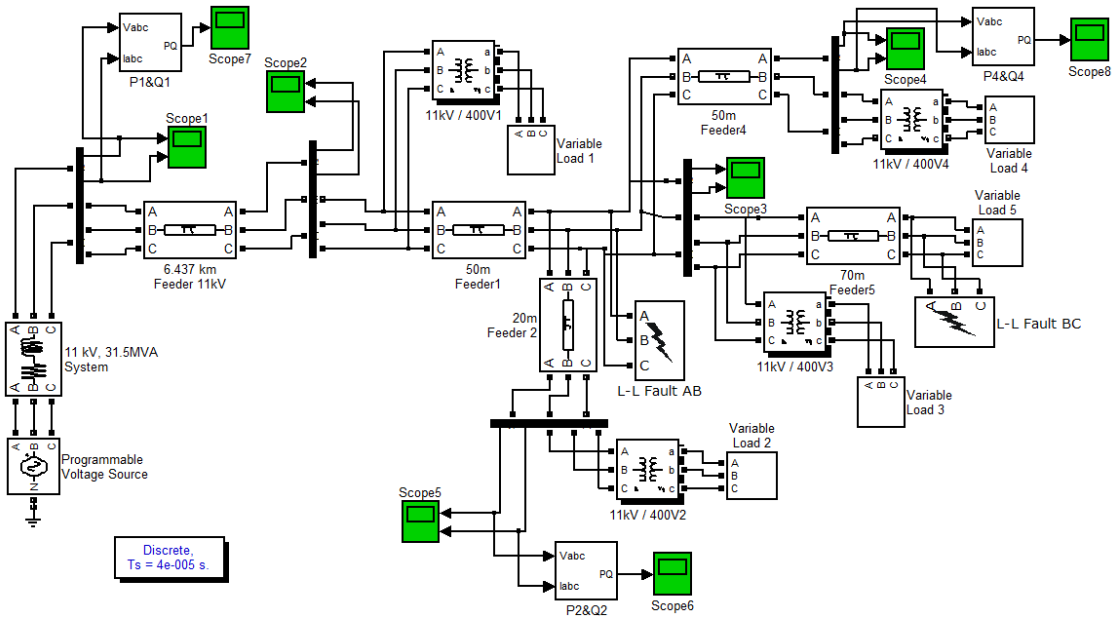

Fig 8. Circuit SIMULINK Model for Simultaneous Faults on MTU 11 kV Feeder

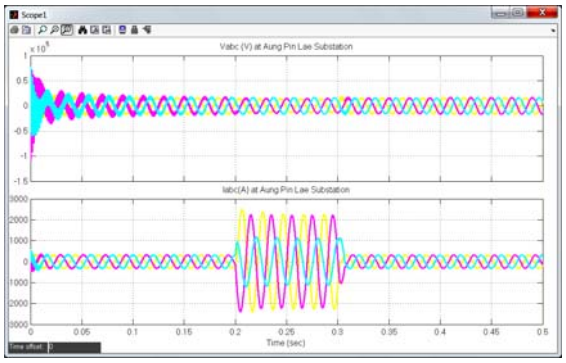

Fig 9. Results of Scope 1 for First Case

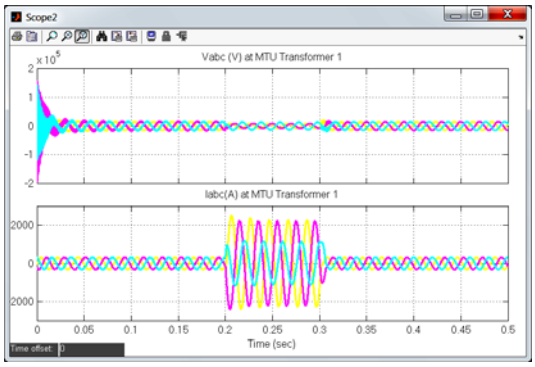

Fig 10. Results of Scope 2 for First Case

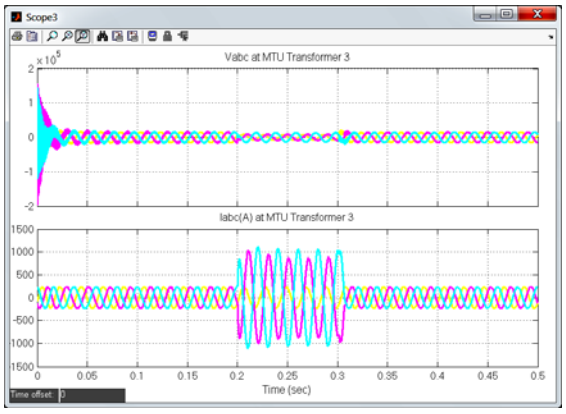

Fig. 11 Results of Scope 3 for First Case

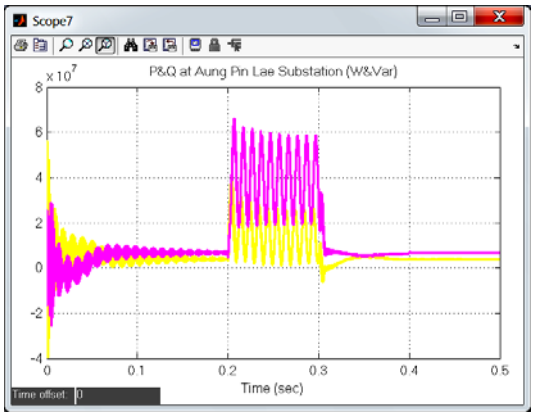

Fig 12. Results of Scope 7 for First Case

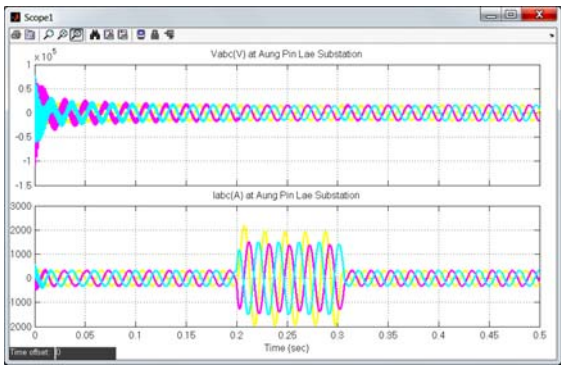

Fig 13. Results of Scope 1 for Second Case

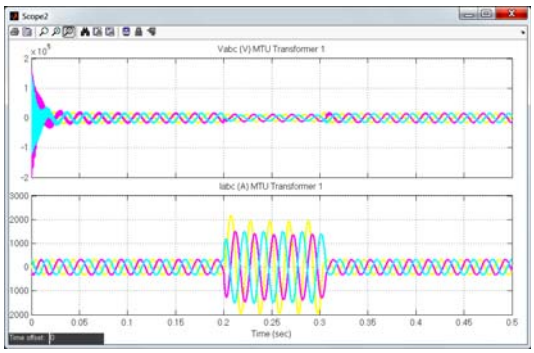

Fig 14. Results of Scope 2 for Second Case

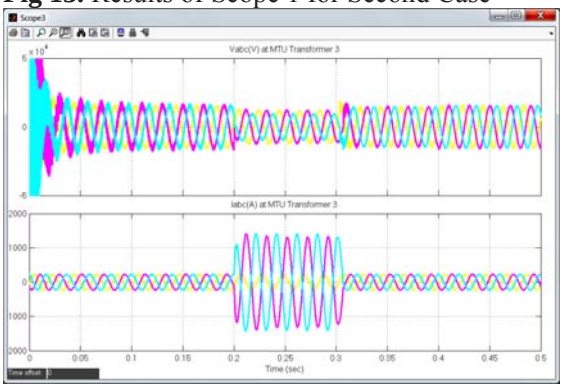

Fig 15. Results of Scope 3 Second Case

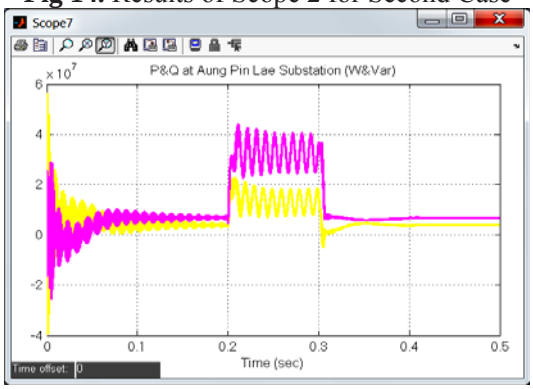

Fig 16. Results of Scope 7 Second Case

In the first case, the simultaneous fault on X with Line-to-Line fault at phase a, b and Y with

Line-to-Line fault at phase B, C were occurred between 0.2 sec and 0.3 sec duration. The simulation results are shown in Fig. 9 to Fig. 12. From these results, MTU transformer 1 and 3, and substation transformer are impacted from the first case simultaneous faults currents. During the fault occur, active and reactive power of the Aung Pin Lae substation transformer is about 6MW and 3Mvar. The fault current at Aung Pin Lae Substation and MTU transformer 1are about 2200 A and at the MTU transformer 3 is about 1000 A.

In the second case, the simultaneous fault on X with single Line-to-Ground fault at phase a and Y with Line-to-Line fault at phase B, C were occurred between 0.2 sec and 0.3 sec. The simulation results are shown in Fig. 13 to Fig. 16. During the fault occur, active and reactive power of the Aung Pin Lae substation is about 4MW and 2Mvar. The fault current at Aung Pin Lae Substation and MTU transformer 1are about 2000 A and at the MTU transformer 3 is about 1200 A. From these results, MTU transformer 3 is more impacted than in the first case from the second case simultaneous fault. But, the Aung Pin Lae substation transformer and MTU transformer 1 are more impacted than in the first case from the second case simultaneous faults. In both case, the simultaneous faults are happened in transient condition. So, the substation circuit breaker will not open or one phase or two phase will open and simultaneous faults at three point may be happened.

5. Conclusion

Reliable protection systems for medium voltage distribution in Myanmar are a prerequisite for development of Myanmar Electric power system reliability. However, due to lack of operational experience, this is a relatively new area to research this field in Myanmar. In this paper, the simultaneous faults on medium voltage distribution line are proposed for fault conditions in Mandalay 11kV distribution feeder. Two types of short-circuit faults (line-to-ground and line-to-line) and combinations thereof were considered in this paper. Simulation results from this paper show for the effectiveness of the protection system giving better responses for Mandalay 11kV distribution feeder. According to this paper results, so many faults are occurred and so many of power distribution transformers are impacted of fault current and reduce of transformers lifetime in Myanmar. Nowadays, power system engineers in Myanmar are neglected this fault impact and they are solved with this problem as cut out the power when heavy rains and wind, and so many consumers are unsatisfied. This can be solved with cut trees, use good quality circuit breakers and so on. The active and reactive powers are about four times for active power and six times for reactive power during the fault time. Therefore so many power losses in medium voltage distribution system of Myanmar and must be solved with convenient solutions.

Acknowledgments

The author is deeply gratitude to Dr. Myint Thein, Pro-Rector, Mandalay Technological University, for his permission to present oral presentation this paper in Yangon.

References

[1] M.A. Mirzai, A.A. Afzalian, “A Novel Fault-Locator System; Algorithm, Principle and Practical Implementation,” Power Delivery, IEEE Transactions on , vol.25, no.1, pp.35,46, Jan. (2010).

[2] J. Lewis Blackburn, Protective Relaying Principles and Applications, Second Edition

[3] E.C. Senger, G. Manassero, C. Goldemberg, E.L. Pellini, “Automated fault location system for primary distribution networks,” Power Delivery, IEEE Transactions on , vol.20, no.2, pp.1332,1340, April (2005).

[4] R.H. Salim, M. Resener, A.D. Filomena, K. Rezende Caino de Oliveira, A.S. Bretas, “Extended Fault-Location Formulation for Power Distribution Systems,” Power Delivery, IEEE Transactions on , vol.24, no.2, pp.508,516, April (2009).
[5] Robert M. Montomer, "Analysis of Simultaneous Faults by the Method of Symmetrical Components," Master Thesis University of Missouri, (1948).
[6] Edith Clarke, “Circuit Analysis of AC Power Systems,” Volume I Symmetrical and Related Components, John Wiley &Sons, Inc: (1948).

(Received; 23rd December, 2013, Accepted; 2nd August, 2014)

Optimizing Feature Selection Techniques for Network Intrusion Detection System

Phyu Thi Htun[1], Kyaw Thet Khaing[2]
[1)]Faculty of Information and Communication Technology,University of Technology(Yatanarpon Cyber City), Myanmar
[2)]Department of Hardware Technology, University of Computer Studies, Yangon, Myanmar
**E-mail:ms.phyuthihtun@gmail.com, kyawthetkhaing.ucsy@gmail.com*

Intrusion Detection Systems (IDSs) are applied to detect network intrusions identified from different sources. Anomaly and signature based schemes are used for the intrusion detection process. Signature based intrusion detection schemes uses the predefined signature collection for the detection process. The anomaly-base model detects the intrusions by learning the network transaction patterns. Feature selection schemes are used to reduce the network transaction features. Performance, time, accuracy and reliability are improved. The main approach is to use a data mining technique for the feature selection process. The Random Forest (RF), the machine learning algorithm which embedded Information gain ratio measure, is used in these feature selection process. The pattern recognition algorithm, K-Nearest Neighbors (KNN), have been used for detection and classification of the intrusions. Scalability and high training error rate problems can be solved by using these feature selection techniques. So, the proposed system is designed to perform the feature reduction and intrusion detection process on Network by using RF and KNN respectively. The central idea is to utilize auditing programs to select an extensive set of features that can get the effective for training error rate, and apply to be used for misuse detection and anomaly detection. Detection models for new intrusions or specific components of a network system are incorporated into an existing IDS through a meta-learning (or co-operative learning) process, which produces a Meta detection model that combines evidence from multiple models. We discuss the strengths of our data mining programs, namely, classification, meta-learning. We report our results of applying these programs to the (extensively gathered) network audit data from the DARPA Intrusion Detection Evaluation Program. Experimental results prove that the proposed method can get the high accuracy in detection those known and unknown attacks by using WEKA tool.

1. Introduction

Intrusions are the result of flaws in the design and implementation of computer systems, operating systems, applications, and communication protocols. Statistics [14] show that the number of identified vulnerabilities is growing. Exploitation of these vulnerabilities is becoming easier because the knowledge and tools to launch attacks are readily available and usable. It has become easy for a novice to find attack programs on the Internet that he/she can use without knowing how they were designed by security specialists.

Indeed, the absence of physical boundaries in the network to monitor, meaning that an attack can be perpetrated from anywhere, is a major threat that can be exploited to undermine the integrity and security of the network. It is, therefore, essential to take into account these considerations when designing and deploying an intrusion detection system. To detect intrusions, classifiers are built to distinguish between normal and anomalous traffic. It has been proved that optimizing the feature set has a major impact on the performance, speed of learning, accuracy, and reliability of the intrusion detection system

2. Related Works

Many researchers tried to increase the performance of detection attacks by using many machine learning algorithms. Reference [3] have presented a comparative study between five data mining algorithms (ID3, C4.5, Random Forest, Multilayer Perceptron, Naive Bayes, k-Nearest Neighbor) applied to the classification of network intrusions. The Algorithms that have shown the highest prediction rate are the Random Forest and Naive Bayes Algorithms. ID3 is a supervised algorithm developed by [4] whose purpose is to build decision trees from a data set. Decision trees are very efficient as they classify new cases from the training data and test data to properly assess the quality of the tree constructed. The decision tree is built recursively. The ID3 calculates, among the remaining attributes, the ones which will generate the most information (information gain), which will classify examples of any level of the decision tree.

The literature suggests that hybrid or assembling multiple classifiers can improve the accuracy of a detection [5][6]. According to [5], an important advantage for combining redundant and complementary classifiers is to increase robustness, accuracy and better overall generalization. Reference [8] demonstrated the use of ensemble classifiers gave the best accuracy for each category of attack patterns. Ensemble methods aim at improving the predictive performance of a given statistical learning technique.

The most related work is done by [5]. They use Random Forests Algorithm [7] over rule-based NIDSs. They applied Random Forests Algorithm for only misuse detection. Misuse detection discovers attacks based on the patterns extracted from known intrusions.

Thus, novel attacks can't be detected in this network intrusion detection system. Surveys of the various data mining techniques have been proposed towards the enhancement of IDSs. Reference [9] shown the ways in which data mining has been known to aid the process of Intrusion Detection and the ways in which the various techniques have been applied and evaluated by researchers.

3. Datasets Descriptions

Since 1999, KDD'99 [13] has been the most widely used data set for the evaluation of anomaly detection methods. This data set is built based on the data captured in DARPA'98 IDS evaluation program. DARPA'98 is about 4 gigabytes of compressed raw (binary) tcpdump data of 7 weeks of network traffic. The two weeks of test data have around 2 million connection records. KDD training dataset consists of approximately 4,900,000 single connection vectors each of which contains 41 features and is labeled as either normal or an attack, with exactly one specific attack type. The simulated attacks fall in one of the following four categories: (1) Denial of Service Attack (DoS), (2) User to Root Attack (U2R), (3) Remote to Local Attack (R2L) and (4) Probing Attack.

Table 1 showed the four categories and their corresponding attacks on each category. It is important to note that the test data is not from the same probability distribution as the training data, and it includes specific attack types not in the training data which make the task more realistic.

Some intrusion experts believe that most novel attacks are variants of known attacks and the signature of known attacks can be sufficient to catch novel variants.

This testing datasets contains more examples of attacks than normal connections and the attack types are not represented equally. In this table described the attacks types in two, known and unknown. In the testing datasets, it will contains the attack which are not included in training datasets are called unknown attacks and described as the bold letters.(such as . apache2 in DoS attack type).

Table 1 Classifying attacks on KDD Datasets

Type	Attack Name
Probing	Port-sweep, IP-sweep, Nmap, Satan , **Saint, Mscan**
Denial of Service (DoS)	Neptune, Smurf, Pod, Teardrop, Land, Back, **Apache2, Udpstorm, Processtable, Mailbomb**
User to Root (U2R)	Buffer-overflow, Load-module, Perl, Rootkit, spy, **Xterm, Ps, Http-tunnel, Sqlattack, Worm, Snmp-guess**
Remote to Local (R2L)	Guess_password, Ftp_write, Imap, Phf, Multihop, Warezmaster,Warezclient, **Snmp-getattack, Named,Xlock, Xsnoop, Send-mail**

For the relevant and redundant of KDD datasets, the NSL-KDD datasets modified those data sets and shared 4 dataset file, Train+, Train+_20Percent,Test+ and Test-21. The first two files represent for training datasets and contain the general attacks. The rest two files represent for testing datasets and contain not only general attacks but also the unknown (novel) attacks which are described with bold in Table 1. The connection for each attack type is shown in Table 2.

Table 2 Number of connections in each attack type

Datasets	Normal	DoS	U2R	R2L	Probe	Total
Train+	67343	45927	993	54	11656	125973
Train+20 Percent	13449	9234	206	12	2289	25190
Test+	9711	7458	2421	533	2421	22544
Test-21	2152	4342	2421	533	2402	11850

4. Experimental Results

Since 1999, KDD'99 [13] has been the most Complex relationships exist between the features, which are practically impossible for humans to discover. IDS must therefore reduce the amount of data to be processed. This is extremely important if real-time detection is desired. Reduction can occur in one of several ways.

Finally, some data sources can be eliminated using feature selection.

A. Data Filtering

The purpose of data filtering is to reduce the amount of data directly processed by the IDS. Some data may not be useful to the IDS and thus can be eliminated before processing. This has the advantage of decreasing storage requirements, reducing processing time and improving the detection rate (as data irrelevant to intrusion detection are discarded). However, filtering may throw out useful data, and so must be done carefully [10].

B. Features Selection

The purpose Feature selection (also known as subset selection or variable selection) is a process commonly employed in machine learning to solve the high dimensionality problem. It selects a subset of important features and removes irrelevant, redundant and noisy features for simpler and more concise data representation.

The benefits of feature selection are multi-fold. First, feature selection greatly saves the running time of a learning process by removing irrelevant and redundant features. Second, without the interference of irrelevant, redundant and noisy features, learning algorithms can focus on most important aspects of data and build simpler but more accurate data models. Therefore, the classification performance is improved. Third, feature selection can help us build a simpler and more general model and get a better insight into the underlying concept of the task [11],[12].

C. Information Gain

In this method, the important features are calculated over multiple RDF iterations, the least important features being removed after each. The objective of using Random Forest is to reduce the impurity or uncertainty in data as much as possible .A subset of data is pure if all instances belong to the same class. The heuristic is to choose the attribute with the maximum Information Gain or Gain Ratio based on information theory.

Entropy is a measure of the uncertainty associated with a random variable. Given a set of examples D is possible to compute the original entropy of the dataset such as:

$$H[D] = -\sum_{j=1}^{|C|} P(c_j) \log_2 P(c_j)$$

where C is the set of desired class.

If we make attribute Ai, with v values, the root of the current tree, this will partition D into v subsets D_1,D_2….D_j . The expected entropy if A_i is used as the current root.

$$H_{A_i}[D] = -\sum_{j=1}^{v} \frac{|D_j|}{|D|} H[D_j]$$

Information gained by selecting attribute A_i to branch or to partition the data is given by the difference of prior entropy and the entropy of selected branch.

$$gain(D, A_i) = H[D] - H_{A_i}[D]$$

We can choose the attribute with the highest gain to branch/split the current tree numbered.

D. Enhanced Classification System

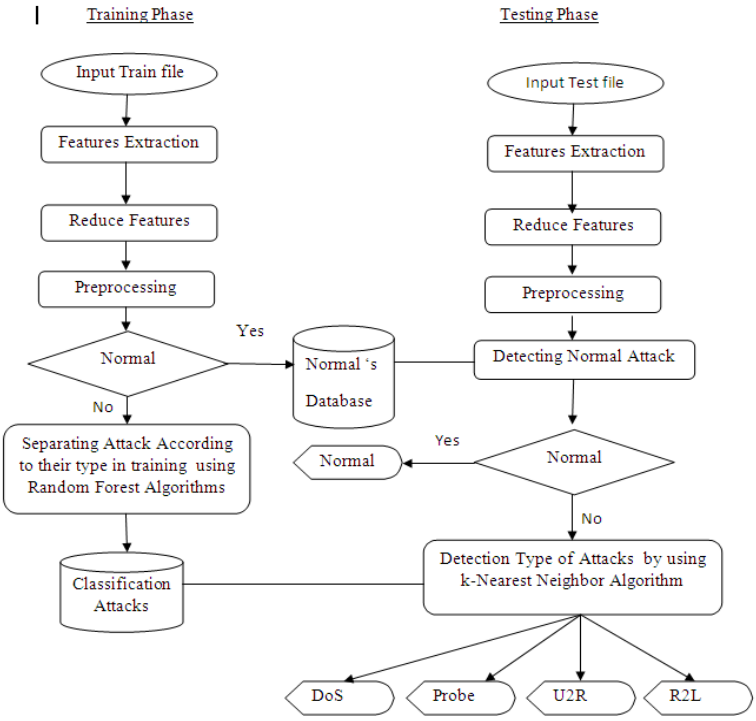

Fig. 1 Proposed System

There are two phase in my proposed Model. This system is process of identifying the abnormal and normal instances in first and then identifying again to classify attacks types of those abnormal instances. The first phase is the training phase and intends to reduce the irrelevant features. After loading the training dataset, features are reduced by Random Forest Algorithm with information Gain. Using those features, the system will classify the normal and abnormal data in first step.
If normal, system keeps that connection in normal database. And then continuing classifies the abnormal connections in four types of attacks and keeps in attack database.
Next phase is detection phase. It will input the testing data set and mapping the data sets as the remaining features of the training data set. As the training phase, will detect normal and four attacks type and display an alert if a connection is a one of the attacks. This system is shown in Fig. 1.

E. Using WEKA Tool

WEKA Tool is a popular suite of Machine Learning software witten in Java, developed at the University of Waikato, New Zealand. The WEKA workbench contains a collection of visualization tools and algorithms for data analysis and predictive modeling together with graphical user interface for easy access to this functionality Weka support several standard data mining tasks, more specifically, data preprocessing, clustering, classification, regression, visutalization, and feature selection(selected attributes).

We summarize the experimental results to detect attacks for intrusion detection with over the NSL-KDD datasets by using WEKA tools. Experimental results are presented in terms of the classes that achieved good level of discrimination from others in the training set.

Firstly, our proposed system will load the training dataset which contain the connection of the normal and attacks class in preprocessing. This dataset also contained the 42 features which important to decide the normal and attacks classes for each connection. We will reduced some features in training dataset by using Random Forest algorithm to each connection at filtering state after loading a training file was loaded in the preprocessing state. The system will use information Gain Algorithm and Ranker to rank and eliminate the amount of features. The amount of eliminated features was getting by using LOOCV(Leave One Out Cross Validation) to eliminate as Fig. 2 .

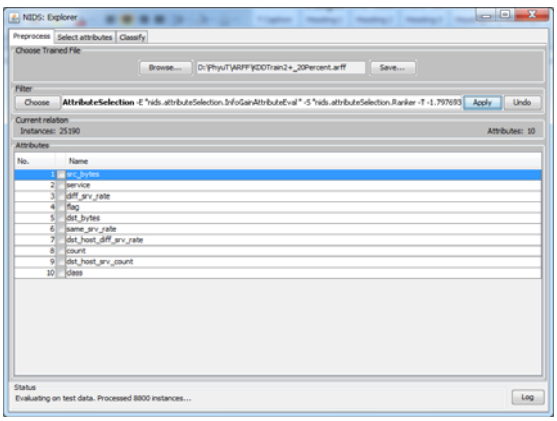

(a)

Fig. 1 Filtering with Information Gain method of Random Forest for feature selection in proposed system

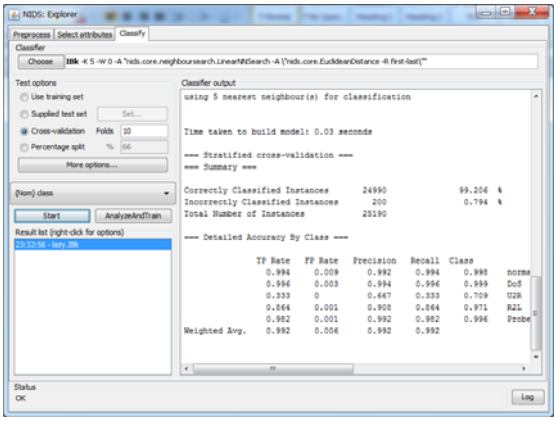

(b)

Fig. 3 Classification step using with KNN in proposed system

So, system will try to detect various anomaly attacks using KDD dataset with KNN classification algorithm in the classification process as shown in fig (3). The proposed system will reduced in training time and will increase the accuracy of the system's classification. It will also solve the imbalance intrusions problem by increasing the accuracy on minority attacks.
For the improvement of detection rate on our proposed system, we examined the number of features to use by ranking and reducing features and getting the best experimental results as shown in fig (4), getting the best number of features is 9.

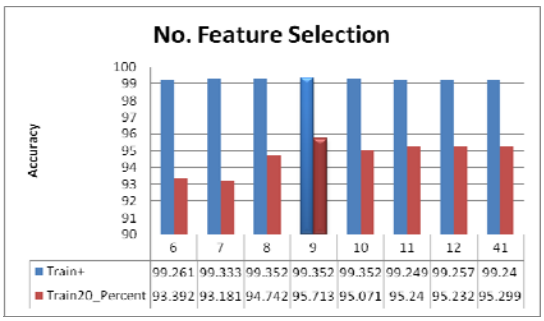

Fig. 4 The comparison results for number of selection to be used in proposed system

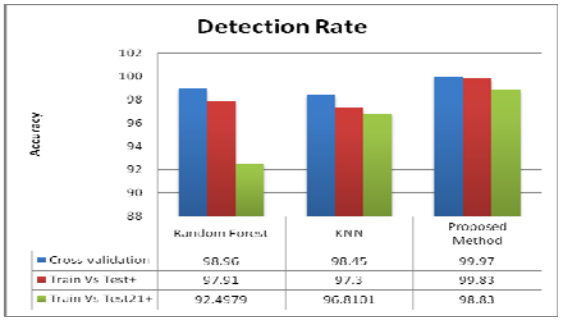

Fig. 5 The comparison between proposed method, RF and KNN in overall attacks type

In the experiments process, the system use 10 trees and reduced 9 features in my proposed method to classify. The accuracy of the system will be increased other systems in overall and the detection rate using proposed method on each minority attack types.
The experiment result in fig. 5 is the comparison between Random Forest, KNN and the proposed method by classifying with training dataset in cross-validation mode and testing with test datasets. The results will shown that the proposed method can detect in more precisely than others.

5. Conclusion

The classification algorithm, Random Forest and KNN are the most useful classification tools and many researchers are presented as a classical tool for Intrusion Detection System as separated algorithm. But in each algorithm has the weakness and draw backs in timing and performance. So, we intend to solve this by combining the advantages of feature selection of Random Forest and the pattern classification of KNN. The experiments prove that the proposed method can stand as a classical tool for IDSs..

Acknowledgments

I would like to express my respectful gratitude to our Rector of University of Technology (Yatanarpon Cyber City),Dr. Aung Win and Department head, Faculty of Information and Communication Technology, Dr. Soe Soe Khaing, for allowing me to develop my research and giving me general guidance during period of my study.

References

[1] F. Anjum, D. Subhadrabandhu and S. Sarkar, “Signature Intrusion Detectio for Wireless Ad Hoc Networks: A Comparative study of various routing protocols”, in 2003.

[2] P C Kishore Raja, Dr.Suganthi.M, R.Sunder, “wireless node behavior based intrusion detection using genetic algorithm”, Ubiquitous Computing and Communication Journal, 2006.

[3] Y. Chihab, A. A. Ouhman, M. Erritali and B. E. Ouahidi, “Detection & Classification of Internet Intrusion Based on the Combination of Random Forest and Naïve Bayes,” Internal Journal of Engineering and Technology, IJET, Vol 5 No 3 Jun-Jul 2013. ISSN : 0975-4024 p. 2116-2126

[4] J. Ross Quinlan, Machine Leaming, 1986, “Induction of decision trees,” p. 81-106.

[5] J. Zhang and M. Zulkernine,” Network Intrusion Detection using Random Forests,” School of Computing Queen’s University, Kingston Ontario, Canada.

[6] D. J. Hand, H. Mannila and P. Smyth, Principles of Data Mining, The MIT Press,

[7] L. Breiman, “Random Forests”, Machine Learning 45(1):5–32, 2001.

[8] J. Zhang and M. Zulkernine, ”Anomaly Based Network Intrusion Detection with Unsupervised Outlier Detection”, Symposium on Network Security and Information Assurance Proc. of the IEEE International Conference on Communications (ICC), 6 pages, Istanbul,Turkey, June 2006.

[9] T. Lappas and K. Pelechrinis, “Data mining Techniques for(Network)Intrusion Detection System,”, UC Riverside, Riverside CA92521.

[10] WEKA software, Machine Learning, http://www.cs.waikato.ac.nz/ml/weka/, The University of Waikato, Hamilton, New Zealand.

[11] M. Dash and H. Liu, “Feature selection for classification,”International Journal of Intelligent Data Analysis, 1(3), 1997.

[12] F. Tan, "Improving Feature Selection Techniques for Machine Learning" (2007). Computer Science Dissertations. Paper 27.
http://digitalarchive.gsu.edu/cs_diss/27

[13] M. Tavallaee, E. Bagheri, W. Lu, and A. Ghorbani, “A Detailed Analysis of the KDD CUP 99 Data Set,” Submitted to Second IEEE Symposium on Computational Intelligence for Security and Defense Applications (CISDA), 2009.

[14] CERT, http://www.cert.org/stats/, 2010.

[15] Khalil El-Khatib “Impact of Feature Reduction on the Efficiency of Wireless Intrusion Detection Systems” IEEE Transactions on Parallel and Distributed Systems, Vol. 21, no. 8, August 2010.

(Received; 23rd December, 2013, Accepted; 5th May, 2014)

Robust Interactive Image Segmentation Integration of Region and Boundary Information

May Thu Win[1], Kay Thi Win[2]
1)University of Computer Studies, Mandalay, Myanmar
2)University of Computer Studies, Mandalay, Myanmar
**E-mail:maythu.ycc@gmail.com, kthiwin11@gmail.com*

Interactive image segmentation has many applications in image processing, computer vision, and computer graphics. In many editing tasks, the aim is to separate a foreground object from its background. Since the color and texture features in a natural image are very complex, the fully automatic segmentation of the object from the background is a big challenge. Due to the difficulty of fully automatic segmentation on a wide range of different images, semi-automatic segmentation algorithms are becoming more and more popular. A wide range of applications motivate the development of efficient interaction methods for image segmentation. Therefore, the proposed system presents a new region merging method based on the color and texture features for interactive image segmentation. The proposed system solves the problem of the purely region-based method and purely boundary-based method.Firstly, the user marks the interest of object and background in the input image.An initial segmentation is required to partition the image into homogeneous regions for merging.Mean shift algorithm is used for initial segmentation.After finishing the initial segmentation, it is necessary to represent initial segmented regions by means of some descriptors such as color and texture to guide the region merging process. And then, detect possible erroneous low-contrast object boundaries to solve the minor inaccuracies and edge misalignments. Finally, refine those boundary regions by using active contour to achieve the accurate object boundary. Therefore, the proposed method is effective and can quickly and accurately segment a wide variety of natural images with ease.

1. Introduction

Interactive image segmentation involves minimal user interaction to incorporate user intention into the segmentation process and is an active research area in recent years because it can achieve satisfactory segmentation results that are unattainable by the state-of-the-art automatic image segmentation algorithms. Interactive image segmentation, which incorporates small amount of user interaction to define the desired content to be extracted, has received much attention in the recent years [11]. Many interactive image segmentation algorithms have been proposed in the literature. In general, interactive image segmentation algorithms can be classified into two categories: boundary-based approaches and region-based approaches. In boundary-based approaches, the user is often asked to specify an initial area that is close to the desirable boundary. This approaches require great care to specify the boundary area or the boundary points, especially for complex shapes, most recent interactive image segmentation algorithms take the regional information as the input. In particular, in region-based approaches, the user is often asked to draw two types of strokes to label some pixels as foreground or background, after which the algorithm completes the labeling of all other pixels. Early interactive image segmentation algorithms utilize either regional properties such as Adobe's magic wand or boundary properties such as active contour [8] and intelligent scissors [5],[3].

Due to the increasing proliferation of digital photos and photo management/editing tools such as Picasa and Adobe Photoshop CS5, image editing is now commonly used in desktop application. Interactive segmentation is a fundamental part of such image editing tools. Extracting the object of interest from the non-trivial background is a crucial step in many interactive multimedia applications. So, these applications motivate the development of effective method for interactive image segmentation. Moreover, the issue of the region based approach is that the distribution in color space of foreground and background pixels have a considerable overlap, thus a satisfactory segmentation result is not achieved. The issue of the boundary based approach is that the shortest path may "shortcut" the desired boundary in the cases of low contrast or noisy boundaries. Another problem is that there exist many alternative "minimal" paths, which require a large

number of user interactions for highly textured regions in order to obtain a satisfactory result. Therefore, the issues of the region and boundary based approaches motivate the proposed method for interactive image segmentation.

Recently, an interactive segmentation based on region merging was proposed by Ning [7]. In [7], the initial image segmentation is firstly used to divide the image into various homogeneous regions and then the color feature is only used for the region merging. So, the satisfactory result is not achieved with this method when segmenting the camouflage images, which are overlapped with its foreground and background colors.

The proposed method in this paper is different from the method by Ning [7]. In the proposed system, the initial segmentation is required to partition the image into the homogeneous regions by Mean shift algorithm. And then, we use both the color and texture features for region merging to segment the foreground from its background because the objective of the proposed method is to achieve the segmentation for different natural scene images, even though the camouflage images. Moreover, if the results obtained by the first segmentation are not satisfactory, the user can refine the selection in the boundary part of the object. So, the proposed method considered the integration of region and boundary information in order to get the accurate result.

The contributions of this paper are (i) a method is proposed by using the color and texture features in region merging, (ii) the integration of the region and boundary information is used in the proposed method; (iii) the hybrid system is designed and implemented using the color, texture and boundary of the interest of object.

2. Experiment

There are two major parts in the proposed system: the proposed region merging and the boundary refinement. For the region merging process, the initial image segmentation is firstly used to divide the image into various homogeneous regions. Mean shift segmentation algorithm [4] is used for initial segmentation. The users need to specify the object and background conceptually. Similar to the users can input interactive information by drawing markers, which could be lines, curves and strokes on the image. The regions that have pixels inside the object markers are thus called object marker regions, while the regions that have pixels inside the background markers are called background marker regions. The green markers to mark the object while using blue markers to represent the background are used.

After marking the user input, it is necessary to represent initial segmented regions by means of some descriptors such as color, texture features to guide the region merging process. Therefore, the color histogram to represent each region is used. The color histogram is an effective descriptor to represent the object color feature statistics and it is widely used in pattern recognition and object tracking, etc. The RGB color space is used to compute the color histogram in this work. For the texture descriptor, Gabor filter is used for discriminating different texture regions. Oriented filter banks have proven to be an effective method to characterize textures [1], [10]. This paper primarily uses local statistics of oriented filter responses to differentiate textures. A two-dimensional Gabor function consists of a sinusoidal plane wave of some frequency and orientation, modulated by a two-dimensional Gaussian. The Gabor filter in the spatial domain is given by

$$g_{\lambda\theta\psi\sigma\gamma}(x,y) = \exp(-\frac{x'^2+\gamma^2y'^2}{2\sigma^2})\cos(2\pi\frac{x'}{\lambda}+\psi) \quad (1)$$

where $x' = xcos(\theta) + ysin(\theta)$, $y' = ycos(\theta) - xsin(\theta)$

In [1], λ representsthe wavelength of the cosine factor, θrepresents the orientation of the normal to the parallel stripes of a Gabor function in degrees, ψ is the phase offset in degrees, and γ is thespatial aspect ratio and specifies the elliptically of the support of the Gabor function, and σ is the standard deviation of the Gaussian determines the size of the receptive field [9].

The parameter λ, is the wavelength and f = 1/λ is the spatial frequency of the cosine factor. The ratio σ/λ determines the spatial frequency bandwidth of simple cells and thus the number of parallel excitatory and inhibitory stripe zones which can be observed in their receptive fields. The half-response spatial frequency bandwidth b (in octaves) and the ratio σ/λ are related as follows:

$$b = \log\frac{\frac{\sigma}{\lambda}\pi+\sqrt{\frac{\ln 2}{2}}}{\frac{\sigma}{\lambda}\pi-\sqrt{\frac{\ln 2}{2}}}, \quad \frac{\sigma}{\lambda} = \frac{1}{\pi}\sqrt{\frac{\ln 2}{2}}\frac{2^b+1}{2^b-1} \quad (2)$$

$\psi = 0^{\circ}$ and $\psi = 90^{\circ}$ return the real part and the imaginary part of Gabor filter respectively.

In this paper, a total of 24 Gabor filters is used at six orientations (0°, 30°, 60°, 90°, 120°, 150°) and four scales (eg. $4\sqrt{2}$, $8\sqrt{2}$, $16\sqrt{2}$, $32\sqrt{2}$) at every pixel. The selection of parameters for Gabor filters is very important because the texture segmentation result from the Gabor filters is very good but computationally expensive. Therefore, we choose the restriction of orientations is six because it is made for computation saving.

A 2-D Gabor function is an oriented complex sinusoidal grating modulated by a 2-D Gaussian function. The parameters of the Gabor function are specified by the frequency, the orientation of the sinusoid (or represented by the center frequency), and the scale of the Gaussian function. Therefore, local orientations and spatial frequencies explicit in Gabor filters are used as the key features for texture processing. The input image is generally filtered by a family of Gabor filters tuned to several resolutions and orientations. The texture features are extracted by filtering the given image using the family of Gabor filters.

Object and background markers provide some key features of object and background, respectively. The proposed region merging method also starts from the initial marker regions and all the non-marker regions will be gradually labeled as either object region or background region. In this work, an adaptive maximal similarity based merging mechanism to identify all the non-marker regions under the guidance of object and background markers is presented. Let Q be an adjacent region of R and denote $S_Q = \{S_i^Q\}$ i= 1, 2, q the set of Q's adjacent regions. The similarity between R and Q is the maximal one among all the similarities $\rho(Q, S_i^Q)$, then R and Q will be merged. The following merging rule is defined: Merge R and Q

$$\rho(R, Q) = \max_{i=1,2,\ldots\ldots q} \rho\left(Q, S_i^Q\right) \quad (3)$$

The merging rule (3) is very simple but it establishes the basis of the proposed region merging process. One important advantage of (3) is that it avoids the presetting of similarity threshold for merging control.

The whole maximal similarity based region merging process can be divided into two stages, which are repeatedly executed until no new merging occurs. Firstly, the marked object regions are merged unmarked object regions until no similar object region left. Secondly, the left unmarked regions are then merged together, and thus the object can be successfully extracted from the complex background.

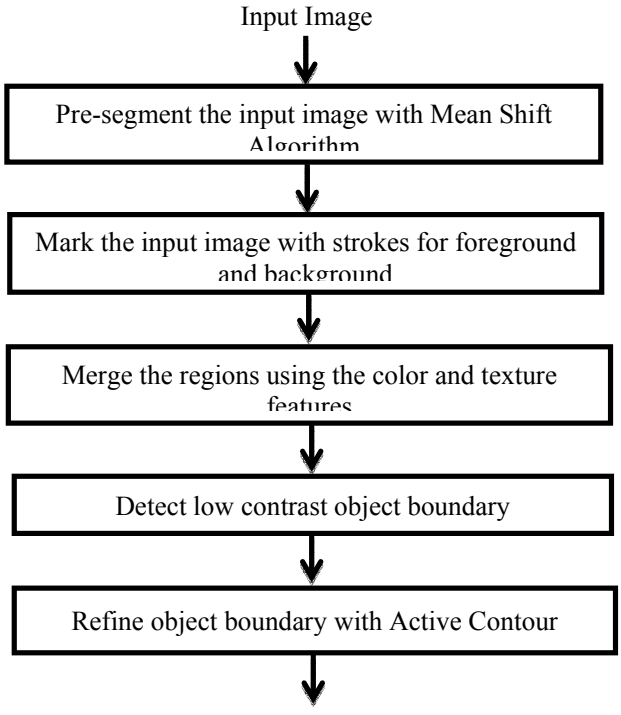

Fig 1. Flowchartof Proposed System

The segmentation from the aforementioned process may still have minor inaccuracies and edge misalignments. It is still a challenging problem to extract accurately the object contour from the background.

Therefore, the boundary refinement stage is necessary to resolve them. Firstly, it is necessary to detect the low contrast object boundary by using the Weighted Canny Edge detection method. Traditional Canny edge detection [6] works on gray scale images and produces binary edge detection results. For color images, weighted canny edge is used in each color channel independently [13].

Finally, this study exploits the active contour for boundary refinement. Snakes, or active contours, are used extensively in computer vision and image processing applications, particularly to extract object boundaries. Snakes use the technique of matching a deformable model to an image by means of energy minimization. A snake initialized near the target gets refined iteratively and is attracted towards the salient contour [5]. Therefore, the satisfying result is achieved using the active contour for boundary refinement. Fig 1 shows the flowchart of the proposed system.

The proposed method is adaptively region merging method based on the color and texture features for interactive image segmentation. With the markers input by the user, it will automatically merge regions and label the non-marker regions as object or background. Therefore, the marker input by the user is important to segmentation. The proposed method is evaluated with many examples. Experiments are conducted to evaluate the effectiveness of the proposed framework. The test images come from the Berkeley segmentation dataset [14].

3. Results and Discussion

The objective of the proposed system is to achieve robust and accurate segmentation in different natural scene images. Table 1 shows the result of initial segmentation with different images by using mean shift. Fig 2 shows the straightforward examples for segmenting the target object from the background with the user input markers. Since the proposed method is mainly based on color and texture features for region merging to extract the desired object, it is very convenient for these examples to get the accurate result.

Table 1 Initial segmentation result of different images

Image	Flower	Fruit	Starfish-2	Starfish-1
Size of image	229*216	259*329	448*368	444*417
Number of regions after initial segmentation	236	218	1572	2353

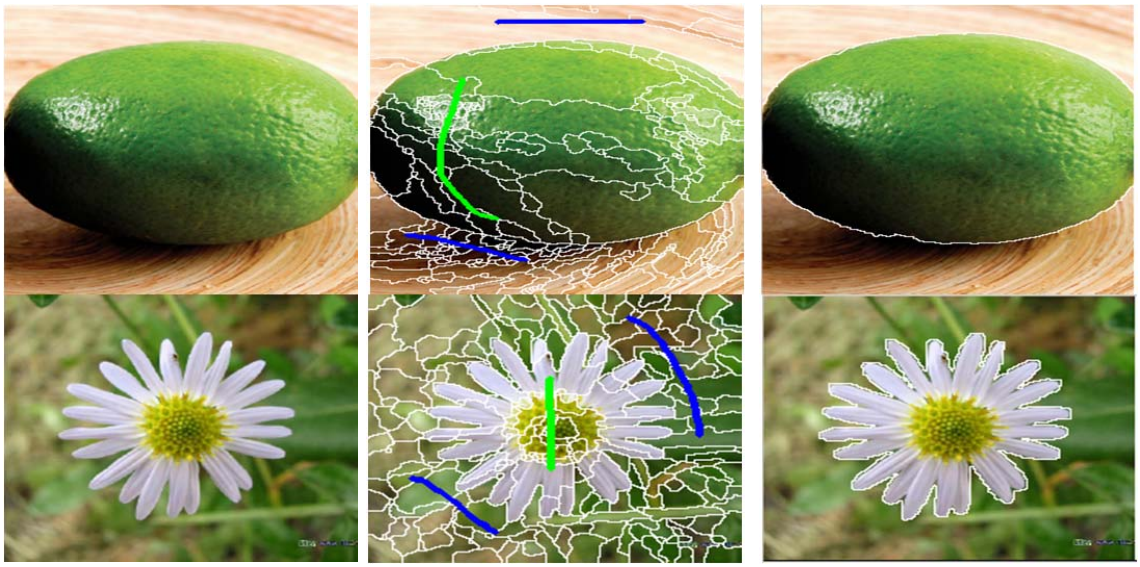

Fig. 2 (a) Original Input Image (b) The source images with user input stokes, where blue strokes are used to mark the background regions, and green strokes are used to mark the foreground regions (c) Result obtained by the proposed method

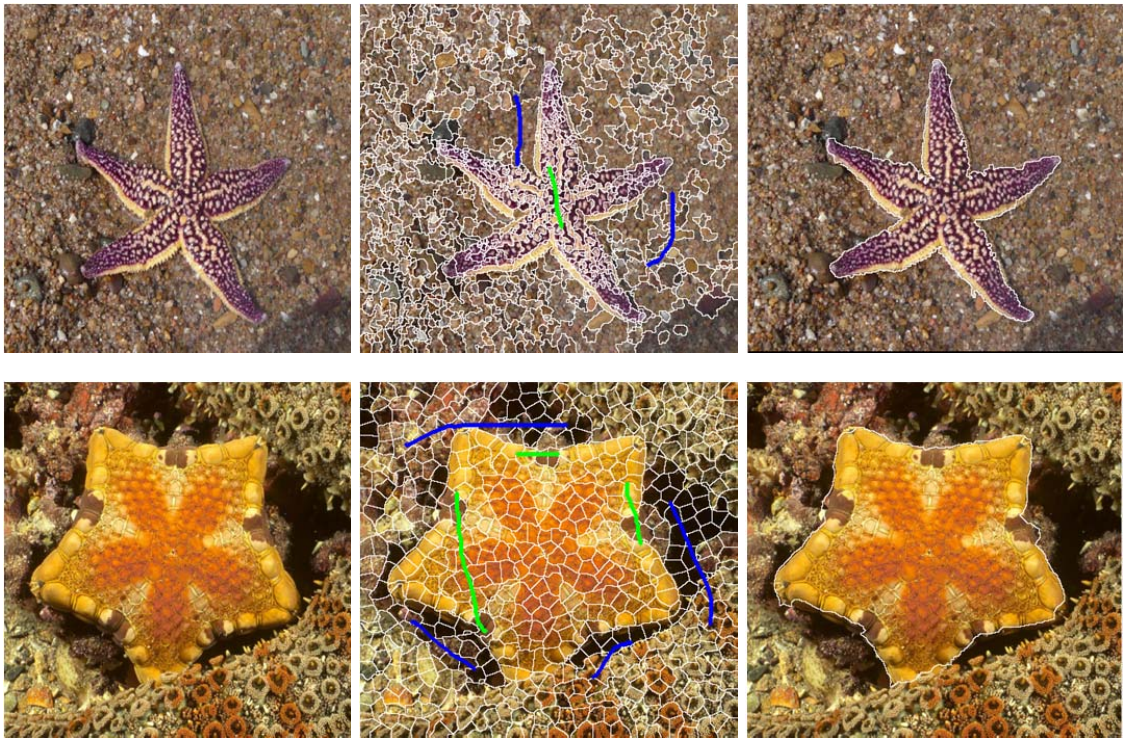

Fig. 3(a) Original Input Image (b) The source images with user input stokes, where blue strokes are used to mark the background regions, and green strokes are used to mark the foreground regions(c) Result obtained by the proposed method

However, for some natural scene images such as complex background, it may require more user input markers to achieve the satisfying result. Therefore, in the proposed method, the color and texture features are used for region merging for the complex images. Fig 3 shows the result of segmenting the foreground from the complex background with less user inputs because of the advantages of the proposed method.

In this paper, not only region information but also boundary information is used to extract the target object from the corresponding background. For some images, if the user's input markers don't cover to indicate the desired object and background region, the segmentation result may be poor. If so, the boundary refinement is necessary for segmenting the target object. In the boundary refinement stage, the user needs to draw the short boundary strokes on the desired object. Therefore, Fig 4 shows the boundary refinement examples. This result shows the accurate result with the proposed method for interactive image segmentation.

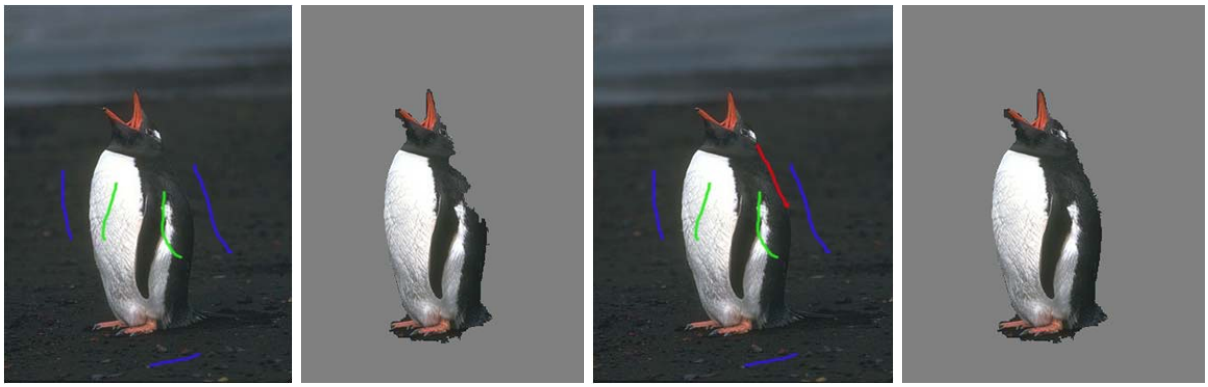

Fig. 4(a) input image with strokes (green for foreground and blue for background); (b) corresponding result; (c) with an additional stroke for refinement (in red); (d) corresponding new result

4. Conclusion

Interactive image segmentation is still a challenging problem. Therefore, a robust interactive image segmentation method is proposed in this paper. The user input strokes are very important for the foreground and background to get a desired object accurately. This paper consists of two components: proposed region merging and boundary refinement. The color and texture features are mainly used in the region merging process. So, it is very convenient for segmenting the object from the complex background in interactive scheme. Sometimes, if the region merging cannot get the satisfying result because of the user's inputs or complex scene images, the additional stage is included in this paper to get the desired object. Therefore, the refining boundary step is used to achieve the accurate result. Moreover, this paper solves the problem of the purely region based method and purely boundary based method. By integrating the region and boundary information for the interactive scheme, the accurate result may be achieved. However, the boundary refinement process is an ongoing research in our proposed system. Therefore, we will continue the second part of the proposed system.

References

[1] B. Manjunath and W. Ma, "Texture Features for Browsing and Retrieval of Image Data," IEEE Trans. Pattern Analysis and Machine Intelligence, vol. 18, no. 8, pp. 837-842, Aug. 1996.
[2] Blake, C. Rother, M. Brown, P. Perez, and P. Torr, "Interactive image segmentation using an adaptive GMMRF model," Lecture Notes in Computer Science, 2004.
[3] C. Rother, V. Kolmogorov, and A. Blake, "Grabcut: Interactive foreground extraction using iterated graph cuts," in ACM SIGGRAPH, 2004.
[4] D. Comaniciu and P. Meer, "Mean shift: A robust approach toward feature space analysis," IEEE Transactions on Pattern Analysis and Machine Intelligence, 2002.
[5] E. N. Mortensen and W. A. Barrett, "Interactive segmentation with intelligent scissors," Graphical Models in Image Processing, 1998.
[6] J.F. Canny, "A Computational Approach to Edge Detection," IEEE Trans. Pattern Analysis and Machine Intelligence, Nov. 1986
[7] J. Ning, L. Zhang, D. Zhang, and C. Wu, "Interactive image segmentation by maximal similarity based region merging" ,Pattern Recognition, 2009.
[8] M. Kass, A. Witkin, and D. Terzopoulos, "Snakes: Active contour models," IJCV, vol. 1, no. 4, pp. 321–331, 1988.
[9] NaotoshiSeo, "Texture Segmentation using Gabor Filters",ENEE731 Project, Nov8, 2006.
[10] T. Leung and J. Malik, "Representing and Recognizing the Visual Appearance of Materials Using Three-Dimensional Textons," Int'l J. Computer Vision, vol. 43, no. 1, pp. 29-44, 2001.
[11] W. Yang, J. Cai, J. Zheng, and J. Luo, "User-friendly interactive image segmentation through unified combinatorial user inputs," IEEE Transactions on Image Processing, 2010.
[12] Y. Boykov and M.-P. Jolly, "Interactive graph cuts for optimal boundary and region segmentation of objects in N-D images," in ICCV, 2001.
[13] Yugang Liu and Yizhou Yu, "Interactive Image Segmentation Based on Level Sets of Probabilities", IEEE Trans. on Visualization and Computer Graphics, vol. 18, 2012.
[14] http://www.eecs.berkeley.edu/Research/Projects/CS/vision/grouping/segbench/.

(Received; 23rd December, 2013, Accepted; 2nd August, 2014)

Edge embedded Marker based Watershed Method for image segmentation

Khin Lay Mon[1], Mie Mie Thaw[2]
[1)]*Hardware Department, University of Computer Studies, Mandalay, Myanmar*
[2)]*Hardware Department, University of Computer Studies, Mandalay, Myanmar*
**E-mail: khinlaymon.tk@gmail.com, miemiethaw@gmail.com*

Image segmentation has been a significant and difficult task digital image processing. Conflict between generality and objectivity becomes an important issue in image segmentation. Segmentation accuracy determines the success or failure of computerized analysis procedure. Therefore, we propose an automatic segmentation method that is useful for computer vision. The Proposed system are combined the modified Laplacian of Gaussian (LoG) edge detection filter which is used to produce accurate gradient magnitude and Marker Controlled Watershed Transformation. In this paper, firstly, watershed algorithm with Laplacian of Gaussian (LoG) edge detector is used to detect the clear edge map of the input image and produce the image which is less sensitive to noise. Marker-controlled watershed segmentation provides to get the beter segmented image with less over segmentation. Therefore, our proposed method can detect a detailed, accurate and satisfactory segmentation image without any broken edges while overcoming over segmentation problem due to conventional watershed segmentation.

1. Introduction

Image segmentation separates the objects and components of the image [4-6]. Segmentation algorithms are classified on the basis of the segmentation techniques like edge and contour based techniques, region based techniques, threshold selection based image segmentation techniques, etc. All these methods have their own limitations and advantages in terms of suitability, applicability, computer's memory space, transmission time of image data, computational cost and overall performance. The main aim of segmentation is to find certain interested objects which may be depicted in the image. But it is encountered with noise. That means if image contains noisy signals, this result makes an unwanted segmentation and cannot detect the detailed image. Noise is the random variation of brightness or color information which is either due to technology limitation or environmental factor. It produces unpredictable results. Therefore, before performing segmentation on images, it is necessary to remove noise from it. Although various spatial and frequency domain filtering techniques exist, in this paper, Laplacian of Gaussian (LoG) edge detector are used. LoG edge detector is combined with the watershed segmentation to yield good results.

A good number of works has already been carried out on watershed segmentation and applied to solve the problem related to digital image segmentation. These are available in the published or online literature [7-12]. Pinaki Pratim Acharjya, Santanu Santra, Dibyendu Ghoshal presented an improved scheme on morphological image segmentation using the gradients. They introduced the concept of edge detection with gradient and used the system to produce an effective watershed technique for natural images[1].

Pinaki Pratim Acharjya, Dibyendu Ghoshal [12] discussed an improved scheme on morphological image segmentation that is suitable for human visual system. They had shown that watershed segmented image obtained by extended LoG mask appears to be much more clear with sharp and prominent watershed ridges and the number of segmented have been found to much less than conventional filter. Bieniek and Moga [8] present an efficient watershed algorithm based on connected components.

Vincent et al. [11] proposed a famous watershed algorithm called 'immersion algorithm,' which provides an effective and efficient implementation for watershed transform. In order to avoid over segmentation, generally marker controlled watershed technique [7] is followed but the whole process has been found to be a comparatively lengthy process in terms of computation. Therefore, many researchers had to try an efficient technique which may yield larger segmented regions and it can be expected that it would solve for the suppression of over segmentation and it will be also easier for handling by the machine. Other researchers also proposed different methods to avoid the problem of watershed. Therefore, in this paper, this research work is expected and motivated to overcome the over segmentation problem and produce the meaningful result.

In the present study, LoG edge detection operator is used with the watershed algorithm to generate the better segmentation results with less over segmentation. Although the 5x5 LOG filtering kernal proposed by Marr-Hildreth [10] is a default mask, the mask can be extended dimensionally on the basis of the need of the image processing situation. A modified scheme of LoG operator with 7x7 mask is proposed to find an initial edge map and contour of a digital image and produces greater accuracy and lesser over segmentation in edge detection. It has been found from the segmented image that in this case the over segmentation is appreciably less than those obtained by using other edge detecting techniques. It has been already found that the watershed segments are very prominent and the watershed boundaries are also very sharp and this lower scale of over segmentation will enable the computers to process the segmented images more easily and with lower cost.

The structure of this work is the following: Section 2 introduces our proposed scheme of the modified Laplacian of Gaussian detector with 7x7 kernel, the conventional Laplacian of Gaussian and describes the brief procedure of the proposed system. Section 3 presents a brief description of experiment. The results are discussed in section 4 and the detailed steps of the proposed system are also described in this section together. We finish this paper with some concluding remarks with section 5.

2. Proposed Scheme

The Laplacian of Gaussian filter (LoG) plays a very important role in image segmentation. This detector finds edges by looking for zero crossings after filtering f(x, y) with a Laplacian of Gaussian filter. It is a convolution filter that is used to highlight edges of different objects.

In this method, the Gaussian filtering is combined with Laplacian to break down the image where the intensity varies to detect the edges effectively.

0	0	-1	0	0
0	-1	-2	-1	0
-1	-2	16	-2	-1
0	-1	-2	-1	0
0	0	-1	0	0

Fig. 1 A conventional 5x5 mask LoG filter

0	1	4	6	4	1	0
1	8	17	18	17	8	1
4	17	-3	-46	-3	17	4
6	18	-46	-137	-46	18	6
4	17	-3	-46	-3	17	4
1	8	17	18	17	8	1
0	1	4	6	4	1	0

Fig. 2 A modified 7x7 mask LoG filter

The proposed system can be divided into two parts: preprocessing step and segmentation step. In the preprocessing part, 7x7LoG mask has been proposed as shown in figure (2). It has been studied that conventional5x5LoG mask with default standard deviation 0.5 in figure (1) needs to be extended in any arbitrary size for more accurate detection of objects. Therefore, we have tried a new approach for modifying conventional LoG mask. To construct the modified 7x7LoG mask, the LoG function centered zero and approximated with the profile of standard deviation 1.4 in equation (1).

$$LoG(x, y) = \frac{-1}{\pi\sigma^4}\left(1 - \frac{x^2+y^2}{2\sigma^2}\right)e^{-\frac{x^2+y^2}{2\sigma^2}} \quad (1)$$

In this mask, there are two annular regions with positive and negative weights which surround the central pixel. The negative weights are assigned for inner one and the positive weights are

assigned for outer one. The weights are depended on the distance from the center pixel and the approximation of Gaussian standard deviation. The size of optimal mask was found in 7x7 dimensions after calculating the larger number of trails. We have also found that there is no loss of generality if the weights of individual pixel in the mask are changed slightly because of keeping in mind the basic requirement of being isotopic for the construction of mask. The better approximation of gradient magnitudes of gray level image is subsequently computed by using this modified 7x7LoG filter. Therefore, the better approximation of gradient image can avoid extremely over segmented regions. The flowchart of the proposed algorithm is depicted in figure (3).

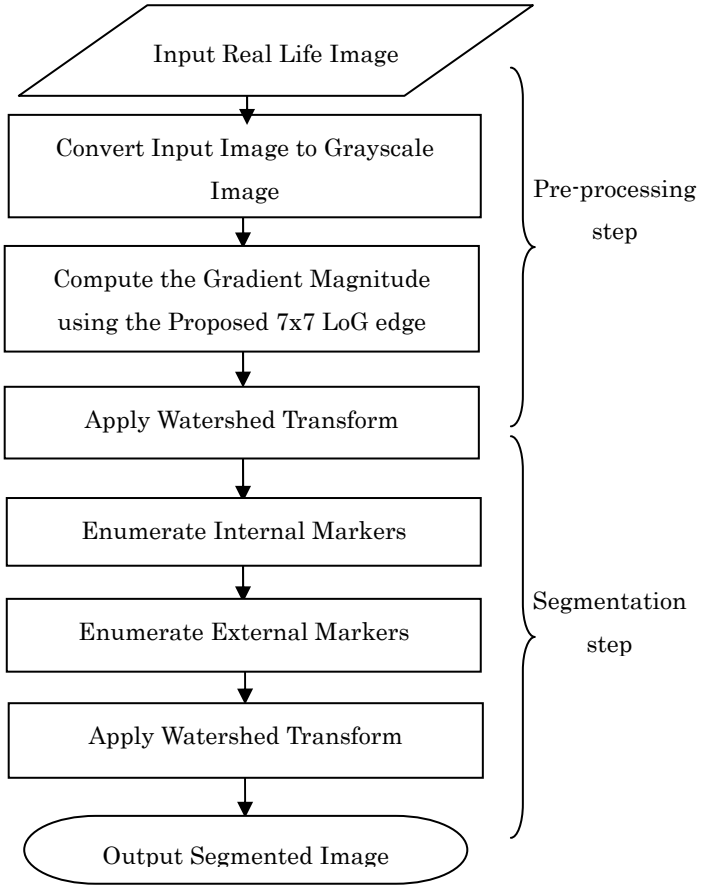

3. Fig. 3 The flowchart of the Proposed Scheme

4. Experiment

The present study performs mainly two processes: preprocessing step and segmentation step. In preprocessing step, the images which obtained from the real life have been tested to find the gradient image with the proposed LoG filter and subsequently applied watershed as a segmentation function. As the initial stage, a color image from the real life is chosen and read with MATLAB editor using 'imread' function. The next step is converting the color image into grayscale or black and white image by using 'rgb2gray'. Then, the gradient image is resulted from the gray level image with the help of proposed modified mask of LoG. The gradient image can directly apply to watershed segmentation. In segmentation step, watershed algorithm is applied for finding initial segmentation map and the image is analyzed the result (over-segmentation). We can easily see many over-segmented regions that are not suitable in subsequent tasks. To reduce over segmented region, a solution can be achieved by using Marker controlled watershed segmentation. External markers are computed by using opening and reconstruction procedure. As the final step, the internal markers are computed and applied the watershed transform as the final segmentation function and visual the

result. The segmented output is more pleasing without over-segmentation and is also less time complex than other conventional algorithms.

5. Results and Discussion

The focus on this experiment is both for getting better image segmentation result and solving over segmentation problem by using marker controlled watershed segmentation and modified LoG edge detector. The experiments are carried out color images from real life. Figure 5(a) and 6(a) display the original colorful images.

The image is converted to gray level image for processing the subsequent algorithms. In watershed segmentation, a gray level image can be interpreted as the topographic image of landscape. Then, the gray level image has been processed to get the corresponding gradient image by using modified 7x7 LoG mask. The gradient image can be directly applied to watershed segmentation. Figure 5(b) and 6(b) displays the corresponding gradient image that has been observed with the proposed system. After that, the gradient image which obtained by using 5x5 LoG filter mask is segmented with conventional watershed transform .There has found over segmented regions as shown in figure 5(c) and 6(c) respectively. It results an unsuitable final segmented image as shown in figure 5(e) and 6(e). In order to get better result, these over segmented regions are processed with marker-controlled watershed transform. The gradient image by applying 7x7 LoG filter is shown in figure 5(d) and 6(d). The image is passed with marker controlled watershed to get the final segmented image. Figure 5(f) and Figure 6(f) display the acceptable segmented image by using the proposed approach.

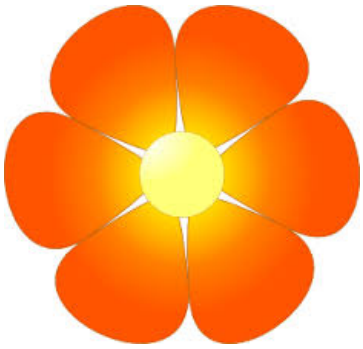

Fig. 5(a) Original color Image

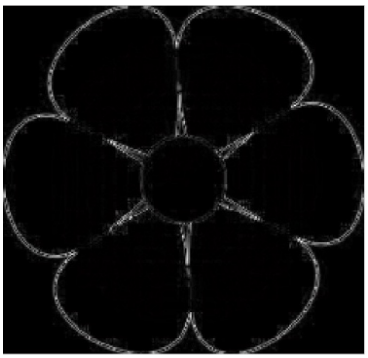

Fig. 5(b) Gradient image using 7x7 LoG filter

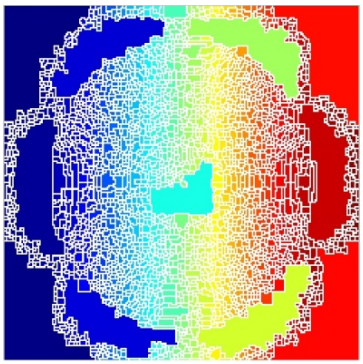

Fig. 5(c) Over segmented image by applying watershed and 5x5 LoG filter

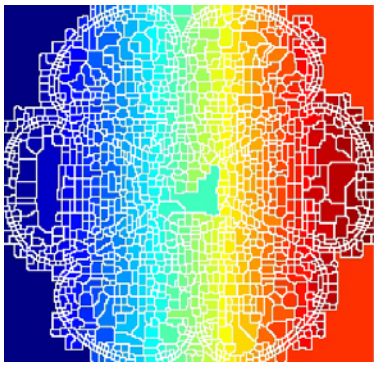

Fig. 5(d) Over segmented image by applying watershed and 7x7 LoG filter

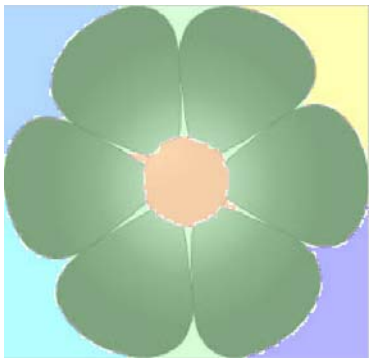

Fig. 5(e) **S**egmented image by applying Marker Controlled watershed and 5x5

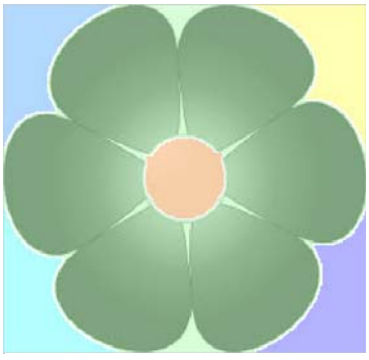

Fig. 5(f) **S**egmented image by applying Marker Controlled watershed and 7x7 LoG filter

We can easily seen by comparing with the segmented images of modified 7x7 LoG mask that

conventional 5x5 Log edge detector have produced pale edges (i.e, the edges in image are not very sharp). Therefore, in practice, these gradient images can affect the segmented images in the next step. On the other hand, we have been found that modified LoG filter can give more enhance gradient images than conventional LoG filter. Thus, it results less over segmented image and gets better final segmented image.

In this case, it has been observed that the edges and boundaries of the images are also seen to be more prominent and clear with better contrast and less over segmented regions. Over segmentation is a very difficult problem in watershed segmentation. However, the proposed filter can be optimized the segmented image by following marker-controlled watershed segmentation.

Fig. 6(a) Original Color Image

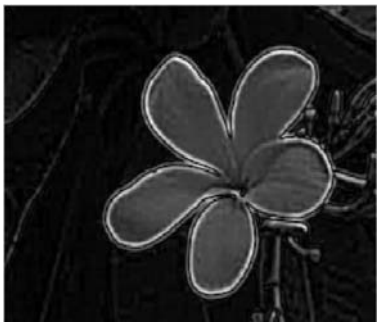

Fig. 6(b) Gradient Image by applying 7x7 LoG filter

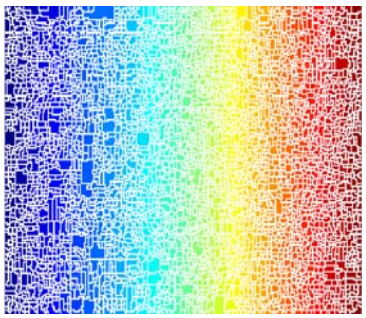

Fig. 6(c) Over Segmented Image by applying watershed and 5x5 LoG filter

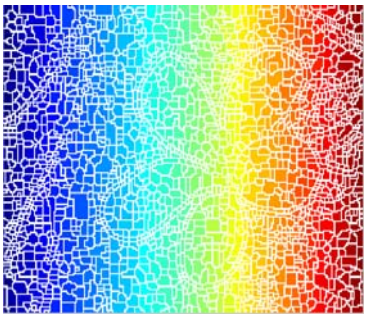

Fig. 6(d) Over Segmented Image by applying watershed and 7x7 LoG filter

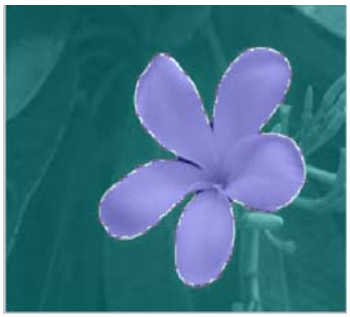

Fig. 6(e) Segmented image by applying Marker Controlled watershed and 5x5 LoG filter

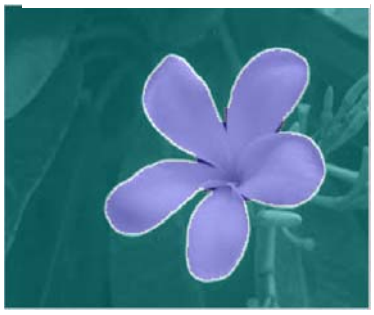

Fig. 6(f) Segmented image by applying Marker Controlled watershed and 7x7 LoG filter

Table1. Entropy of Final Segmented Image

Figure	Entropy of the final segmented Image(5x5 LoG and Marker Controlled Watershed)	Entropy of the final segmented Image(7x7) LoG and Marker Controlled Watershed)
Figure 5(f)	1.3813	1.3567
Figure 6(f)	0.9762	0.9737

The entropies of the final segmented images using marker controlled watershed segmentation through 5x5 LoG filter and the proposed 7x7 LoG filter have been calculated and the values have been shown in the table 1. Experimental results presented in this paper are obtained by using

MATLAB R2010a.

6. Conclusion

Image Segmentation is one of the important fields of image processing and computer vision. The role of image segmentation is to decompose an image into parts that are meaningful with respect to a particular application such as image analysis, image understanding activities, image description and recognition, image visualization and object-based image compression etc. These subsequence steps are highly depend on the segmentation results obtained from previous image segmentation stage. The goal of image segmentation process is to identify the segments of the image according to the characteristics of objects e.g. object shape, image color etc. We have proposed a very simple methodology to control over segmentation for the natural images with marker controlled watershed algorithm. In order to solve the over segmentation problem of traditional watershed technique an improved technique is proposed that uses pre processing methods to reduce the noise of image and adjust the image intensity. The proposed method with LOG filter can make to be better localization when the edges are not very sharp. The presented method has been found to yield better output in term of image quality, clarity and sharpness. The proposed system can perform the input image with the less number of segments and can give the meaningful and acceptable results of image segmentation. The proposed method with marker controlled watershed overcomes over segmentation problem more than conventional watershed transform. This system can be very helpful for image segmentation to detect an accurate image clearer. Experimental results presented in this paper are obtained by using MATLAB R2010a.

References

[1] Pinaki Pratim Acharjya, Santanu Santra, Dibyendu Ghoshal "Improved Scheme on Morphological Image Segmentation Using the Gradients" IJACSA International Journal of Advanced Computer Science and Applications, vol 4, No.2, 2013.

[2] Usha Mittal, Sanyam Anand, "Effect of Morphological Filters on Medical Image Segmentation using Improved Watershed Segmentation" ISSN.Vol 4, No.6 Jun,2013.

[3] Ms.K.Kavi Niranjana, Ms.M.Kalpana Devi, Ms.L.Mary, International Journal of Engineering Research & Technology (IJERT),Vol. 1 Issue 7, September,2012" Image Segmentation Using MCWS Algorithm".

[4] A.K.Jain, Fundamentals of digital image processing, Second Edition, Prentice Hall, 2002.

[5] S. Beucher, "Watersheds of functions and picture segmentation," in Proc.IEEE Int.Conf. Acoustic, Speech, Signal processing pp.182-931, 1982.

[6] Gonzalez & Woods, Digital Image Processing 3rd edition, Prentice Hall India, 2008.

[7] K. Parvati, B. S. Prakasa Rao and M. Mariya Das, "Image Segmentation Using Gray-Scale Morphology and Marker-ControlledWatershed Transformation", Discrete Dynamics in Nature and Society,vol. 2008, pp. 1-8, 2008.

[8] Bieniek, A., & Moga, A., "An efficient watershed algorithm based on connected components", Pattern Recognition, 33, 907-916, 2000

[9] Jie Chen, Meng Lei, Yao Fan, Yi gao, "Research on an improved Watershed algorithm to Image segmentation", The 7th International Conference on Computer Science & Education (ICCSE 2012), 2012

[10] D Marr and E Hildreth, "Theory of edge detection", in proceedings of the Royal Society, vol. 207, pp. 187-217, London, 1980.

[11] Vincent, P.Soille,"Watersheds in Digital Space: "an Efficient Algorithms Based on Immersion Simulation," [J]-IEEE Transactions on Pattern Analysis and Machine Intelligence, 13, No.6, pp.583-598, 1991.

[12] Pinaki Pratim Acharjya ,Dibyendu Goshal, "A Gradient Based Morphological Watershed Segmentation Approach Suitable For Human Visual System" International Journal of Computer Science and Engineering(IJCSE) ISSN 2278-99960, vol.2, Issue 1, Feb 2013, 59-68.

(Received; 23rd December, 2013, Accepted; 11th August, 2014)

Quantifying and Evaluating of Evolvability Software Quality for Aspect-Oriented Software

Khine Zar Ne Win
Ministry of Science and Technology, Myanmar,
University of Computer Studies, Mandalay,
**E-mail: khinezarnewinn1@gmail.com*

Today, real-world software needs evolution after a certain period of time to meet the current trends, technology, changes in user requirement and operational environment. During system evolution, software change is an essential operation. After the evolution of system, we must find out that how much new evolved system is extensible when the software functionalities are added or removed during maintenance, or when the existing programs are modified to reuse. Moreover, we also find that how much design pattern is stable for new environment and how much new evolved system is sustainable. Therefore, we need to have measurement mechanisms for evaluating software quality. In the process of developing software and fulfilling to the present time, every modularized concern needs Stability, Sustainability, Changeability and Extensibility. These qualities are focused as the sub-characteristics of Evolvability in this research. So, we propose metrics to measure these qualities of aspect-oriented software. In this study, we aim to measure the sub characteristics of aspect-oriented (AO) software implemented in AspectJ. The analysis of these sub characteristics is based on MobileMedia, AspectJ project, by using Self-Organizing Map (SOM).

1. Introduction

Aspect-oriented programming (AOP) defines a new program construct, called an aspect, which is used to capture cross-cutting aspects of a software application in separate program entities. It comes into picture because of some limitations of Object-Oriented Programming. In Object-Oriented Programming, there are parts of a system that cannot be viewed as being the responsibility of only one class, they cross-cut the complete system and affect parts of many classes. This problem can be solved by using Aspect-Oriented Approach of Software Development [1].

Separation of concern is vital to quantitatively assess the quality of software produced using Aspect-Oriented Software Development (AOSD). In this view, software metrics are needed to do such assessment. The external quality attributes of aspect-oriented software are usually measured, using modeling techniques, as a function of metrics that quantify the internal structural properties of the aspect-oriented software. However, there are few empirical studies [2,3,4,5] that have been conducted to relate software metrics with external quality attributes of aspect-oriented software in general, and metrics have not been evaluated as indicators of aspect extensible, changeable, design stable and sustainable qualities by using Self-Organizing Map (SOM) in particular.

Motivated by afore mentioned issues, we attempt to prove the presented metrics empirically MobileMedia, AspectJ projects. MobileMedia is a Software Product Line (SPL) that manipulates photo, music, and video on mobile devices. This is a joint project coordinated by Lancaster University and developed on top of MobilePhoto. The availability of adequate metrics for these assessments provides software managers early insight into trends in software evolution, and thus assists them in managing and controlling long-lived software systems. To measure the internal attributes of the proposed metrics, we use the AspectJ Assessment Tool (AJATO) [6] and WinMerge Tool [7].

2. Experiment

2.1 *Proposed Quality Measurement Process*

To demonstrate the four metrics, the aspect-oriented software is analyzed and measured. The

quality measuring process is presented in Fig.1 and the quality model is illustrated in Fig.2.

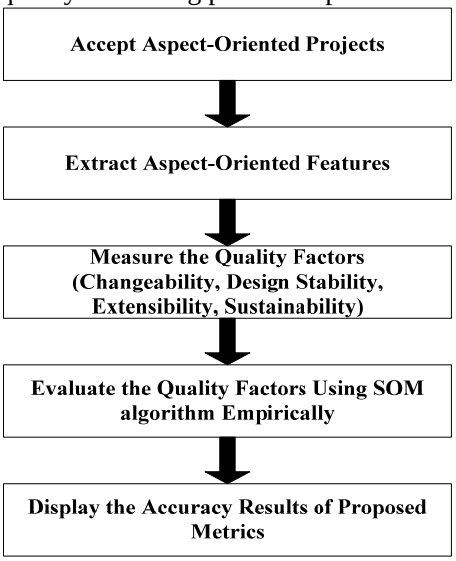

Fig.1 Proposed Quality Measuring System

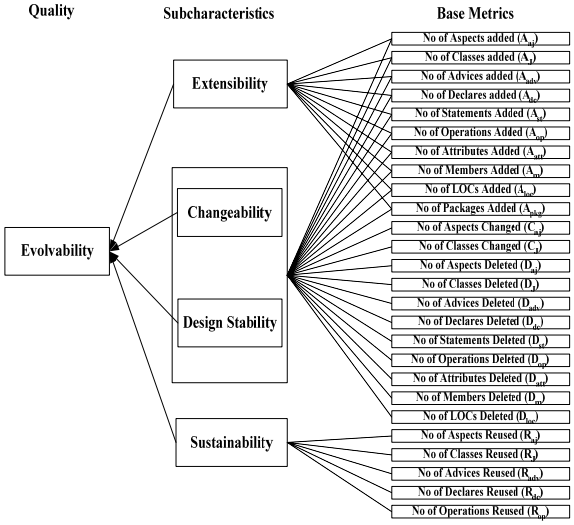

Fig.2 The Quality Model

2.2 Attribute Selections

To evaluate the qualities of the aspect-oriented software more accurately, the related attributes for each of qualities are needed to select. These attributes are selected according to many guide lines and aspect-oriented features. The proposed metrics are formulated based on the rank weighting method to measure the quality of extensibility, changeability, design stability and sustainability. According to guidelines [8], [9], [10] and [11] the selected attributes are identified as having more positively impact on the sub characteristics to measure the evolvable AspectJ projects. In this study, the following attributes are selected for proposed metrics.

Table 1 Selected Attributes for Proposed Metrics

No of Aspects added (A_{aj})	No of Classes Deleted (D_J)
No of Classes added (A_J)	No of Advices Deleted (D_{adv})
No of Advices added (A_{adv})	No of Declares Deleted (D_{dc})
No of Declares added (A_{dc})	No of Statements Deleted (D_{st})
No of Statements Added (A_{st})	No of Operations Deleted (D_{op})
No of Operations Added (A_{op})	No of Attributes Deleted (D_{att})
No of Attributes Added (A_{att})	No of Members Deleted (D_m)
No of Members Added (A_m)	No of LOCs Deleted (D_{loc})
No of LOCs Added (A_{loc})	No of Aspects Reused (R_{aj})
No of Packages Added (A_{pkg})	No of Classes Reused (R_J)
No of Aspects Changed (C_{aj})	No of Advices Reused (R_{adv})
No of Classes Changed (C_J)	No of Declares Reused (R_{dc})
No of Aspects Deleted (D_{aj})	No of Operations Reused (R_{op})

2.3 Weight Assignments

The based attributes in MobileMedia project are counted and used by the proposed metrics for measuring the quality of this project as the input based metrics. To quantify the proposed metrics, the weights of based metrics is needed to assign. Because the important of individual attributes are not the same, their weights are not equal. There are a variety of situations where it is reasonable to

use ranked weights, and there have been various techniques developed to deal with ranked weights and arrive at a choice or rank alternatives under consideration. Therefore, rank-order weighting methods are used to assign weights of attributes.Among these methods,Rank-Order Centroid (ROC) method is suggested the best method in many literatures [12] and is defined as:

$$\mathrm{ROC_i}(\mu) = \frac{1}{t}\sum_{l=i}^{t}\frac{1}{p_l}, \quad i = 1,2,\ldots t \tag{1}$$

where μ is a metric, p_l is the position of i^{th} attribute for μ metric and t is the total number of attributes. After calculating the weight value by using equation 1, it is assigned to each selected attribute and then we can measure the quality factors by using the proposed metrics.

2.4 Changeability Quality Measurement (CQM)

As changeability grows in importance as a consideration in the engineering of systems, there is a critical need to have a more rigorous and quantified definition. Change can be defined as the transition over time of a system to an altered state. A change applies to a class, to a variable or to a method [13]. In this study, the formula for CQM metric is:

$$\begin{aligned}\mathrm{CQM} = {} & \frac{1}{T_{aj}}\left(A_{aj} + C_{aj} + D_{aj}\right) + \frac{1}{T_J}\left(A_J + C_J + D_J\right) + \frac{1}{T_{adv}}\left(A_{adv} + D_{adv}\right) + \frac{1}{T_{dc}}\left(A_{dc} + D_{dc}\right) + \frac{1}{T_{st}}\left(A_{st} + D_{st}\right) \\ & + \frac{1}{T_{op}}\left(A_{op} + D_{op}\right) + \frac{1}{T_{att}}\left(A_{att} + D_{att}\right) + \frac{1}{T_m}\left(A_m + D_m\right) + \frac{1}{T_{loc}}\left(A_{loc} + D_{loc}\right) \\ & + \frac{1}{T_{pkg}}\left(A_{pkg}\right)\end{aligned} \tag{2}$$

2.5 *Extensibility Quality Measurement (EQM)*

Aspect-oriented software development (AOSD) is likely to have positive effect on performance, modularity and evolution. So, it becomes important to reuse components. We focus on a specific kind of reusing of component called extensibility, i.e. the extension of software without accessing existing code to edit or copy it. Extensibility is a systemic measure of the ability to extend a software design principle where the implementation takes into consideration future growth [13]. So, the formula for EQM is:

$$\begin{aligned}\mathrm{EQM} = {} & \frac{1}{T_{aj}}\left(A_{aj}\right) + \frac{1}{T_J}\left(A_J\right) + \frac{1}{T_{adv}}\left(A_{adv}\right) + \frac{1}{T_{dc}}\left(A_{dc}\right) + \frac{1}{T_{st}}\left(A_{st}\right) + \frac{1}{T_{op}}\left(A_{op}\right) + \frac{1}{T_{att}}\left(A_{att}\right) + \frac{1}{T_m}\left(A_m\right) \\ & + \frac{1}{T_{loc}}\left(A_{loc}\right) + \frac{1}{T_{pkg}}\left(A_{pkg}\right)\end{aligned} \tag{3}$$

2.6 Design Stability Quality Measurement (DSQM)

Design Stability covers the sustenance of system modularity characteristics and the absence of ripple-effects in the presence of change [14]. Designs cannot be completely static. Some volatility is necessary if the design is to be maintained. Modules that are more difficult to change are going to be less volatile. For design stability, the harder the module is to change, i.e. the more stable it is, the less volatile it will be. Therefore, we propose that the removing of changeable elements are the measurements of design stability metrics. In this study, the formula for DSQM metric is:

$$\begin{aligned}\mathrm{DSQM} = 1 - \Bigg(& \frac{1}{T_{aj}}\left(A_{aj} + C_{aj} + D_{aj}\right) + \frac{1}{T_J}\left(A_J + C_J + D_J\right) + \frac{1}{T_{adv}}\left(A_{adv} + D_{adv}\right) + \frac{1}{T_{dc}}\left(A_{dc} + D_{dc}\right) \\ & + \frac{1}{T_{st}}\left(A_{st} + D_{st}\right) + \frac{1}{T_{op}}\left(A_{op} + D_{op}\right) + \frac{1}{T_{att}}\left(A_{att} + D_{att}\right) + \frac{1}{T_m}\left(A_m + D_m\right) \\ & + \frac{1}{T_{loc}}\left(A_{loc} + D_{loc}\right) + \frac{1}{T_{pkg}}\left(A_{pkg}\right)\Bigg)\end{aligned} \tag{4}$$

2.7 Sustainability Quality Measurement (SQM)

The Software Sustainability Institute define sustainability as “software we use today will be available and continue to be improved and supported in the future” which implicitly suggests that sustainability is concerned with concepts of availability, extensibility, and the maintainability of the software[5]. As a basis for proposed metric, we consider that software architectures and architectural evaluation methods provide a mechanism for reasoning about software sustainability at an

architectural level [15]. So, we propose that sustainability will be considered in a similar manner to the concept of reusability [16] by using architectural metrics. So, the formula for SQM is:

$$SQM = \frac{1}{T_{aj}}(R_{aj}) + \frac{1}{T_J}(R_J) + \frac{1}{T_{adv}}(R_{adv}) + \frac{1}{T_{dc}}(R_{dc}) + \frac{1}{T_{op}}(R_{op}) \quad (5)$$

2.8 Evolvability Quality Measurement

Software evolvability is a multifaceted quality attribute. It is characterized by inevitable changes of software and increasing software complexities, which in turn may lead to huge costs unless rigorously taking into account change accommodations. This is in particular true for long-lived systems in which changes go beyond maintainability[17]. In this paper, we have identified the subcharacteristics that are primary importance for an evolvable software system. These subcharacteristics serve as the proposed metrics in above mentions and each metric is validated by using the self-organizing map (SOM) in result and discussion session. Finally, we can measure the evolvability of software system by using the following formula:

Evolvability = (EQM * 0.25) + (CQM * 0.25) + (DSQM *0.25) + (SQM * 0.25) (6)

3. Results and Discussion

In this paper, we use the MobileMedia (version 1 to 7) as a case study project [18]. All of the attributes used in quantifying the result are normalizing by total number of each attribute of each version. Fig.3 shows the progress of extensibility quality, changeable quality, design stability and sustainable quality of MobileMedia projects' versions paired from version 1 to 7. These figure shows that the results of how much new evolved system is extensible and sustainable, how much design model is stable and then how many changes are there.

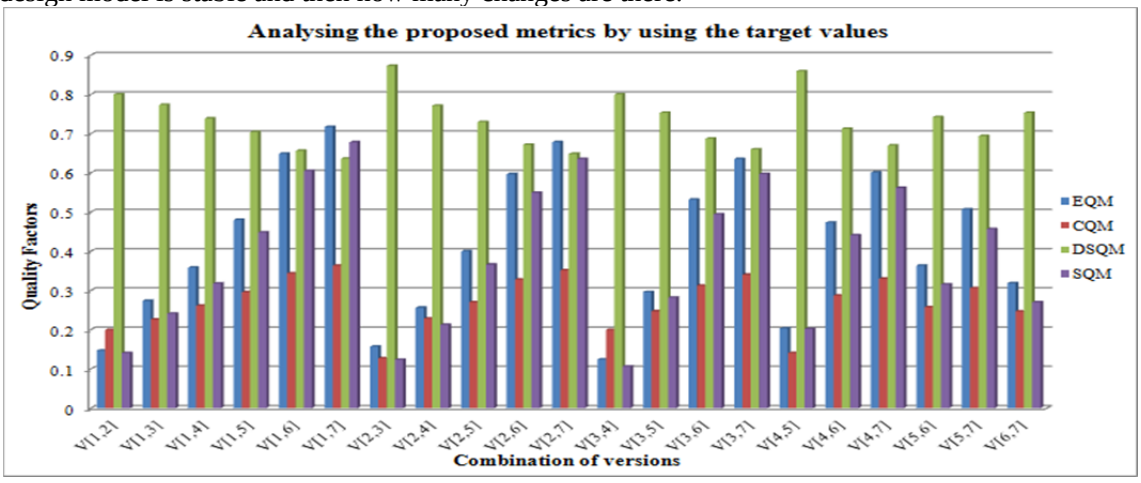

Fig. 3 Comparison of Target Values for Proposed Quality Metrics

Empirical Validation Using Self-Organizing Map (SOM)

The unsupervised learning method, SOM is suitable for measuring the validity and utility of the proposed metrics that they are difficult to prove their robustness and usefulness because they don't have historical data and other comparison metrics. One advantage is that they do not require more understanding with input data and they can cluster and estimate incomplete historical data. The SOM learns similarity of input feature vectors and responds groups of similar input vectors [12].

Before clustering MobileMedia projects, two data files are created for each of proposed metrics, one contains the particular proposed metric values of the combination of number of versions ${}^{n}C_{r} = {}^{7}C_{2} = 21$ pairs and another contains its based attributes of these versions' comparisons. In preprocessing step, file attributes are converted into binary data according to equation 7:

$$f(x) = \begin{cases} 1, & x < \frac{f(y)}{2} \\ 0, & otherwise \end{cases} \quad (7)$$

where f(x) is the binary conversion function that converts the x based metric value into binary data and f(y) is the total number of each attributes of the latest version of MobileMedia, AspectJ project.

After converting binary data, the contingency tables are created for each of versions' pairs. To create the contingency table, dissimilarities are calculated by Jaccard coefficient [12]:

$$d(x,y) = \frac{p}{p+q+r} \quad (8)$$

p=number of times x_i=1 and y_i=1
q=number of times x_i=1 and y_i=0
r=number of times x_i=0 and y_i=1

These dissimilarity matrixes of versions are trained with the SOM and each version are clustered in terms of dissimilarity matrixes. For instance, the internal attributes of EQM, CQM, DSQM and SQM metrics are clustered by SOM and the cluster matching result is analyzed. According to our experiment, most of the clustering results are matched. Therefore, it is obvious that the proposed metrics are validated and useful. The clustering results for all proposed metrics are shown in the following table.

Table 2 Analytical Results for Proposed Metrics Using SOM

Self –Organizing Map (SOM)						
	Quality Factors		Based Metrics		Matched Records	Matching Results (%)
Proposed Metrics	No of Cluster	No of Records	No of Cluster	No of Records		
EQM	2	20	2	18	18	91%
		1		3	1	
CQM	2	20	2	20	19	91%
		1		1	0	
DSQM	2	19	2	17	17	91%
		2		4	2	
SQM	2	20	2	19	18	91%
		1		2	1	

In Fig. 4, SOM clusters MobileMedia project' versions into two groups depending on only EQM values. The first group contains version: V[1,7] and the second group contains other versions. The version contained in first group are the highest value of EQM. So, the other group contains the versions that have the average value of extensibility. In Fig. 5, SOM also clusters two groups depending on its based attributes. The first group contains version: V[1,7], V[2,7] and V[3,7] and the other group contains other versions' pairs. The first groups' members of two types are then compared and analyzed. It is clear that 1 are matched. Moreover, the second groups' members of two types are also compared and analyzed. The result shows that 18 are matched. Therefore the total cluster matching result is 19(91%) for proposed metric EQM.

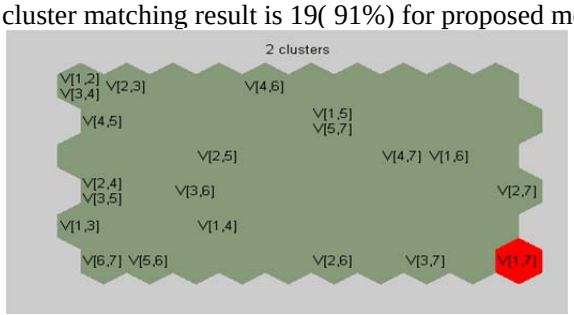

Fig.4 Proposed Metric clustering for Extensibility Metrics

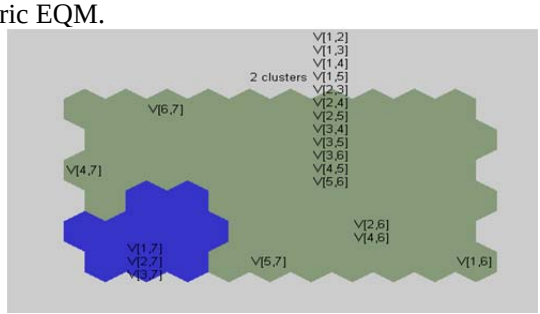

Fig.5 Based Metrics clustering for Extensibility Metrics

After validating the proposed metrics, we can measure the evolvability of MobileMedia, AspectJ projects by using equation 6.We have also tested the AspectJ projects such as HealthWatcher and AJHOTDRAW. According to the accuracy of experiment by using the Self-Organizing Map

Algorithm, we can see that the proposed metrics are validated and useful for software development processes.

4. Conclusion

For improving aspect-oriented software applications, the extensible, changeable, design stable and sustainable quality metrics help software developers to measure these qualities of aspect-oriented software as a self-assessment tool and to save time and money of software development process. To check the validity of the proposed metrics empirically, the self-organizing feature map (SOM) and well-known AspectJ projects are used. Further extension for this research is to create configurability metric as a sub characteristic to measure the evolvability of aspect-oriented software. Therefore, aspect-oriented applications will be robust and widely used for business applications and other web-based information systems.

Acknowledgments

I would like to express my deep gratitude to my supervisor Dr. Khin Mar Myo, Associate Professor, of University of Computer Studies, Mandalay. I greatly appreciate the help I have received from her. Her excellent help and creative ideas have assisted me in broadening my research skills. I am extremely fortunate to work under her supervision of my research.

References

[1] "Aspect oriented Programming in Java",http://www.voelter.de/data/articles/aop/aop.html
[2] C .S. Anna, A. Garcia, C. Chavez, C. Lucena, and A. Staa, "On the Reuse and Maintenance of Aspect-Oriented Software: An Assessment Framework," in Brazilian Symposium on Software Engineering, Agosto, 2003
[3] R. Burrows, F. Ferrari, A. Garcia, and F. Taïani, "An Empirical Evaluation of Coupling Metrics on Aspect Oriented Programs," ICSE, pp. 53-58, 2010
[4] H.Shen, S. Zhang, and J.Zhao, "An Empirical Study of Maintainability in Aspect-Oriented System Evolution Using Coupling Metrics," in 2nd IFIP/IEEE, pp. 233-236, 2008.
[5] P.Tonella and M. Ceccato, "Refactoring the aspectizable interfaces: an empirical assessment," IEEE Transactions on Software Engineering, vol. 31, pp. 819-832, 2005
[6] "AJATO : An AspectJ Assessment Tool", http://homepages.dcc.ufmg.br/~figueiredo/ajato/
[7] "WinMerge Tool", http://tour.winmerge.org/
[8] K. Mguni, Y.Ayalew, "An Assessment of Maintainability of an Aspect-Oriented System", ISRN Software Engineering Volume 2013, http://dx.doi.org/10.1155/2013/121692
[9] A. Przybylek, "Analysis of the impact of aspect-oriented programming on source code quality", GDANSK UNIVERSITY OF TECHNOLOGY, Faculty of Electronics, Telecommunications and Informatics,2011
[10] H.Koziolek, "Sustainability Evaluation of Software Architectures: A Systematic Review", from ACM Digital library
[11] Z. Durdik, B. Klatt, H.Koziolek, K. Krogmann, J. Stammel, R. Weiss, "Sustainability Guidelines for Long-Living Software Systems"
[12] T.Z.Thaw, "Measuring and Evaluation of Reusable Quality and Extensible Quality for XML Schema Documents", IEEE,2011, Cyberjaya, Selangor, Malaysia.
[13] K.Z.N.Winn, "Quantifying and Validation of Changeability and Extensibility for Aspect-Oriented Software", ICAET'2014, Singapore
[14] P.Kumar, "Aspect-oriented Software Quality Model: The AOSQ Model", Advanced Computing: An International Journal (ACIJ), Vol.3, No.2, March 2012
[15] F. Albertao, J. Xiao, C. Tian, Y. Lu, K. Q. Zhang, C. Liu, "Measuring the Sustainability Performance of Software Projects", IEEE, 2010
[16] F. Amin, A. K. Mahmood, A. Oxley, "Reusability Assessment of Open Source Components for Software Product Lines", IJNCAA, 2011 (ISSN: 2220-9085)
[17] H. P. Breivold, I. Crnkovic, P. J. Eriksson, "Analyzing Software Evolvability", Computer Software and Applications, 2008. COMPSAC '08. 32nd Annual IEEE International Conference
[18] "MobileMedia",http://mobilemedia.cvs.sourceforge.net/viewvc/mobilemedia/

(Received; 23rd December, 2013, Accepted; 13th September, 2014)

Mission Control over Multi UAVs in the Real-time Distributed Hardware-In-the-Loop Environment

Soe Linn Htet[1,*], Tin Naing Lat[2], Ye Chan[3], Soe Mya Mya Aye[1] and Pho Kaung[3]
[1]*Department of Computer Studies, University of Yangon*
[2]*Department of Physics, Loikaw University*
[3]*Universities' Research Centre, University of Yangon*
**E-mail: fulcrum.slh@gmail.com*

Mission control has been designed for Multiple Unmanned Aerial Vehicles (Multi-UAVs) and the overall control performance verified by a real-time distributed Hardware-In-the-Loop (HIL) environment. Four modules - onboard hardware, flight control, ground station and mission control software, have been integrated to form a framework under which the HIL test is realized. This design is successfully utilized for several flight tests including basic flight motions, full-envelope flight and multiple UAV formation flight. Results show that the constructed HIL verification system is highly effective and useful tool for UAV mission operations such as disaster management, civil security applications and military operations.

1. Introduction

Unmanned Aerial Vehicles (UAVs) have been widely used not only in military applications, but also in civilian and commercial applications. These include (but not limited to) environmental monitoring, natural resource assessment, wildlife monitoring, bushfire monitoring, search and rescue,telecommunication, precision agriculture, power line inspection, and pipeline patrol.

UAVs require human guidance to varying degrees and an Unmanned Aerial System (UAS) is essentially defined often through several operators. The challenge in achieving effective management of multiple UAV (multi-UAV) -systems in the future is to determine not only whether automation can be used to improve human and system performance but also how and to what degree across hierarchical control loops, the types of decision support the needs of operators in the high-workload environment. This research addresses when and how increasing levels of automation should be incorporated in multi-UAV systems and discusses the impact on human performance and more importantly system performance. It has developed hierarchical control algorithms and a control architecture for multi-UAV systems and extensively tested in simulations with various fidelities, from low fidelity proof of concept simulations, to high fidelity Hardware-In-the-Loop (HIL) simulations.

2. Architecture of Single UAV Control

The architecture of single UAV control operation is hierarchical as represented in Figure 1. The innermost loop represents the basic guidance and motion control, which is the most critical loop that must obey physical laws of nature such as aerodynamic constraints for UAVs. In this loop, operator actions are focused only on the short term and local control (keeping the aircraft in stable flight), and generally human control in this loop requires skill-based behaviors that rely on automaticity.

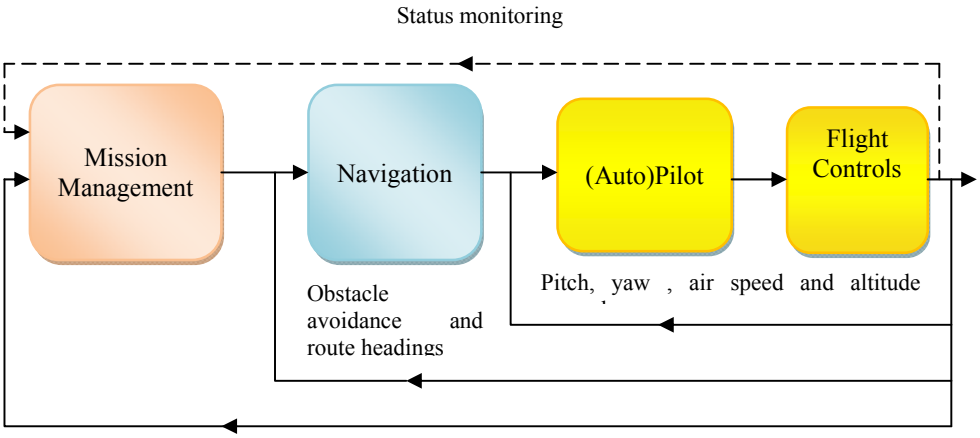

Fig.1 Architecture of UAV Control Operation

The second loop or the navigation loop represents the actions that some agent, whether human or computer-driven, must execute to meet mission constraints such as routes to waypoints, time on targets, and avoidance of threat areas and no-fly zones. The outermost loop represents the highest levels of control, mission and payload management. In this loop, sensors must be monitored and decisions made based on the incoming information to meet overall mission requirements. In this loop, decisions require knowledge-based reasoning that includes judgment, experience, and abstract reasoning that cannot be generally performed by automation.

2.1 Flight Control System

The hardware module consists of the following components: (1) an onboard computer processing system; (2) flight sensors (3) actuators and (3) a wireless modem as shown in Figure 2. Sensors are used to determine the state of the aircraft. Microprocessor analyzes the data attained from the sensors along with commands from ground control radio signals to achieve suitable flight control according to equations of motion. Controls determined by the processor are then used to adjust the flight control surfaces, through the actuators. The control surfaces include ailerons, elevators and a rudder to control the roll, pitch and yaw of the aircraft. The microcontroller does most of the calculations and decision making. In our proposed framework, flight control execution is done by the onboard computer system.

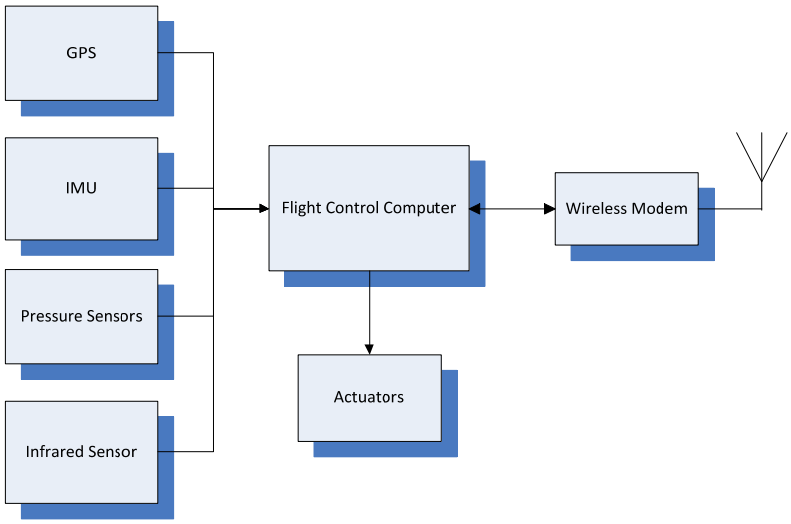

Fig.2 Basic Components of Flight Control System

2.1.1 Controller Design

There are three basic controllers for the UAV flight control which are (a) Attitude controller shown in Figure 3 and Figure 4, (b) Navigation controller in Figure 3 and (c) Altitude and Speed controller in Figure 4 and Figure 5. Attitude controller maintains the aircraft at desired position and altitude and speed controller holds the UAV to fly at a desired altitude and stabilizes the speed in level flight in landing and in take-off. The guidance and navigation controller makes the UAV fly through the desired waypoints.

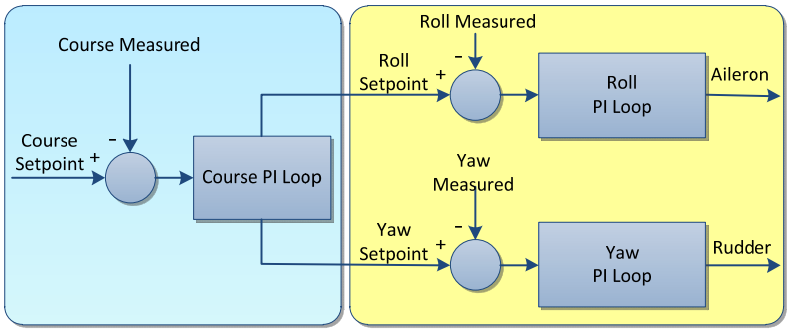

Fig.3 Navigation Control (Outer Loop) and Roll/Yaw Control (Inner Loop)

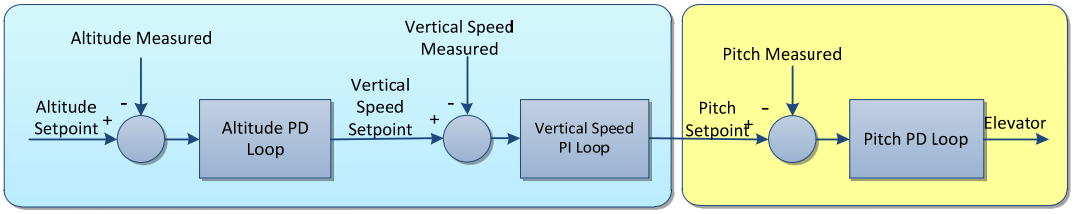

Fig.4 Altitude Control (Outer Loop) and Pitch Control (Inner Loop)

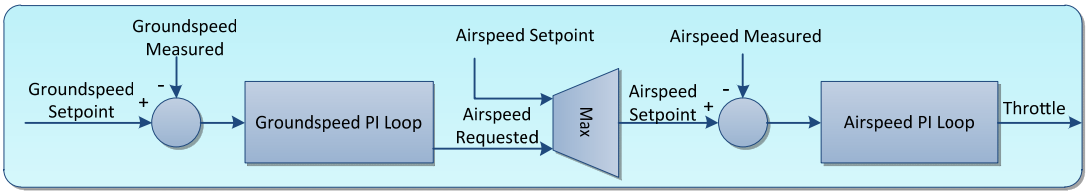

Fig.5 Speed Controller (Outer Loop)

2.1.2 Embedded Firmware

The common methods for embedded application developing environment are super-loop design and thread-oriented design. In this work, the thread-oriented design is used because it has advantages over the super loop design and suitable for more complex applications. With a real time operating system (RTOS), the developer gets not only the tool to create threads, but also tools to communicate between the threads within their real-time constraints.

2.1.3 Thread-Oriented Design of Flight Control System

ChibiOS/RT RTOS is used to develop a flight control system (FCS) on STM32F405RGT6 microcontroller supporting multiple architectures and released under the GPL3 license. It is designed for embedded applications on 8, 16 and 32 bit microcontrollers where size and execution efficiency are their

main requirements. Thread-oriented design of FCS is depicted in Figure 6. It is represented for both typical FCS and simulated FCS for HIL testing. There are five groups of thread in its firmware.

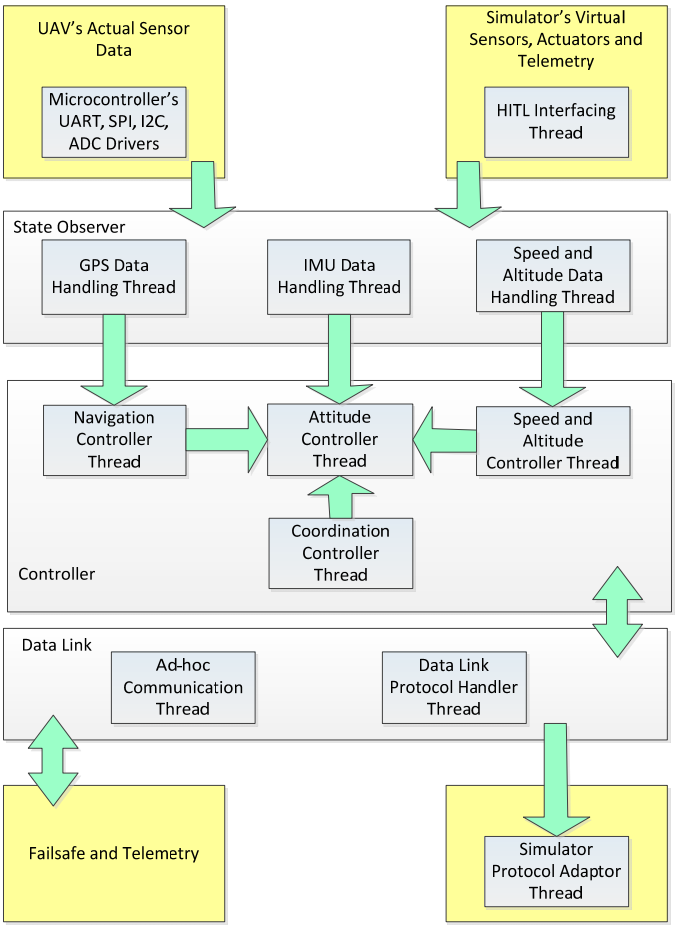

Fig.6 Thread-Oriented Design of Flight Control System

2.2 Ground Control System

Ground control can be divided into three sub systems. They are (1) Flight Instruments, (2) Map and (3) Communication Status. All flight data from FCS via communication system are displayed on the fly on the flight instruments while real time aircraft trajectory and mission status are updated on the localized Map. Task planning and mission control can also be performed on the map system. Communication system, the heart of the entire system, takes responsibility for data transferring between FCS and ground control system (GCS).

In both flight time and pre-flight time, mission controller can plan the missions for all UAVs on the Graphical User Interface (GUI) of the GCS and hence, the communication backbone must be robust. Moreover, weather condition of operation area can also be obtained from the weather server via this link.

2.2.1 Flight Instruments

Flight instruments include Artificial Horizon, Speed Indicator, Altimeter, and Direction Indicator. These instruments can connect to communication system and monitor the flight data of entire flight.

2.2.2 Map System

In GCS, implementation of map system is based on the Google tile map engine. Figure 7 shows the structure of Google tile image.

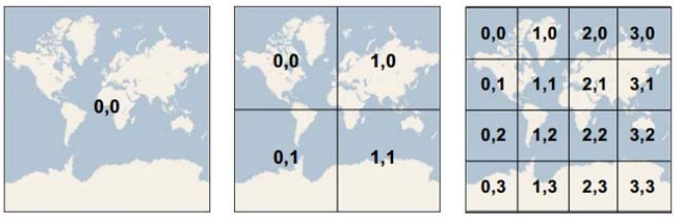

Fig.7 Google Tile Image Structure

Google holds the world in a number of 256*256 pre-rendered images ("tiles") for about 18 zoom stages. The lowest zoom is 0 and the highest 17. At zoom 0, the entire world is kept in one single tile. At zoom 17, the world spreads over giant 17,179,869,184 tiles. The number of tiles needed to cover the entire world for a zoom stage can be calculated with the relation, Number of Tiles = 2 ^ (2*Zoom).

Google uses Mercator projection. There are a couple of algorithms out in order to determine bitmap pixel coordinates for a given geo-coordinate and zoom-stage. The following relations are not only simple but easy to understand the solution of this problem.

$$X = \lambda - \lambda_0$$
$$Y = \frac{1}{2} \ln\left(\frac{1+\sin(\Phi)}{1-\sin(\Phi)}\right)$$

where,

λ = Longitude
λ_0 = Longitude in center of map
Φ = Latitude

There is a simple HTTP request that can be sent to Google Maps servers to obtain these tiles. This is an example of the HTTP request sent to Google:

http://mts0.googleapis.com/vt?lyrs=m&x=48&y=96&z=8

Fig.8 Ground Control System with Customized Map

3. Multi-UAV System Architecture

The hardware architecture of a typical multi-UAV system is illustrated in Figure 9. The main components in the ground station are the Ground Control Stations (GCSs), Mission Controller (MC), weather station and uplink controllers (GBB). During the taxi, takeoff and landing, human pilots control the UAVs with modified hand held Radio Control (R/C) units.It can send the servo control signals to the uplink controllers instead of transmitting them directly to the UAVs. An uplink controller is a unit built around an embedded microcontroller and a spread spectrum radio modem.The GCS for each UAV displays and logs the real-time telemetry data and monitors the data related to mission and cooperative control.

3.1 Mission Controller

Mission controller (MC) is a Ground Control System integrating some authority featuresMission controller has some authority to interact the entire flight and ground system such as task planning, dynamically changing the mission objectives and all other high level decisions. Whereas the low level ground control system can control only its predefined UAV, the mission controller can control all the UAVs and the low level ground control system.

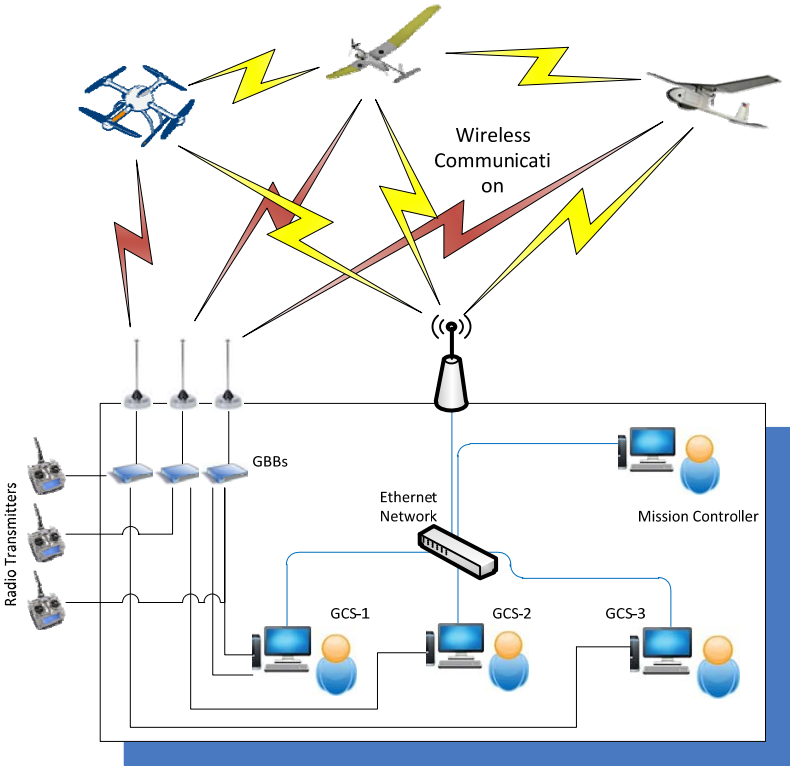

Fig.9 Typical Multiple UAVs Control and Coordination System

3.2 Hardware in the Loop Simulation (HIL)

Figure 10 illustrates the architecture of the distributed real-time HIL test for multi UAVs system. It consists of a number of computers networked with the hardware and software components of the UAVs. In order to reflect the real operational system configuration, the distributed HIL system is designed in such a way that it has almost identical architecture with the system hardware of the real flight missions. Ethernet network (Wi-Fi 801.11b) is used as the communication backbone of HIL system. To perform the HIL test, FlightGear flight simulator is run on each GCS computer of UAVs and it generates the flight data and weather condition of the operation area. These computers also

concurrently run flight vehicle dynamics models to simulate the UAV motions.

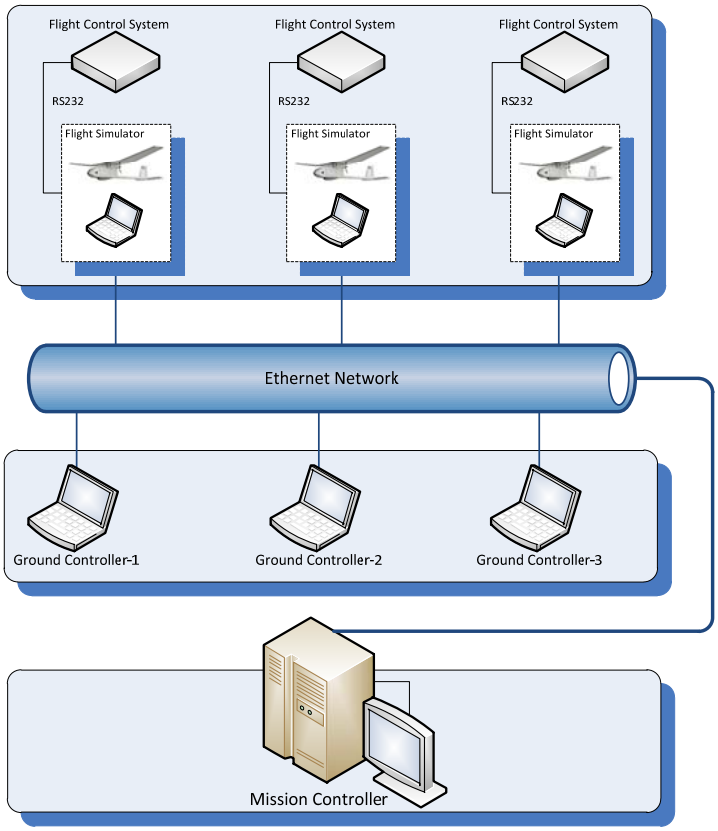

Fig.10 HIL Simulation Network

4. Results and Discussion

In this HIL simulation test, three UAVs are flown in a same flight path at different height levels as shown in Figure 11. They can coordinate each other at specified height levels and be able to avoid the collisions.The results have clearly indicated that the proposed multi-UAV control and coordination system is capable of accurately and efficiently realizing the HIL trial in actual field. Figure 12 shows how accurate each UAV maintained the specific altitude at single flight level.

Fig.12 Coordination Flight of Three UAVs on Single Flight Path

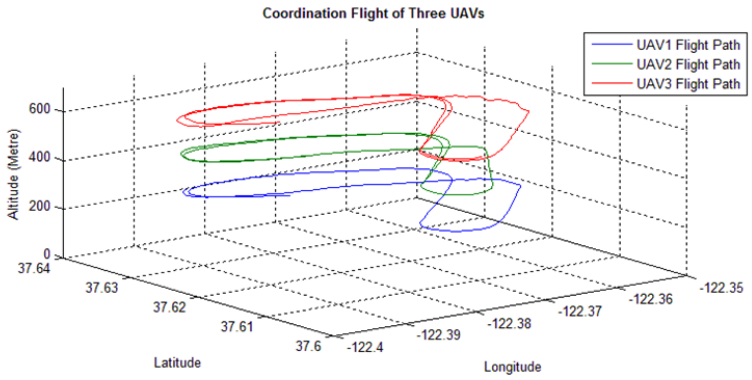

Fig.13 Comparison of Three UAVs' Altitude and Flight Path Coordination

5. Conclusion

The multiple UAV control and coordination system and the complete design of an HIL simulation system have been addressed. The basic motion flight test and the multiple UAV formation test have been carried out at the specific operation area with interactive weather conditions. The results have clearly indicated that the designed HIL system is capable of accurately and efficiently predicting the real flight situations including potential dangers and accidents. The system is certainly an effective and useful tool for UAV mission operations such as disaster management, civil security applications and military operations.

Our system is especially designed for rescue mission in disaster like Cyclone. UAVs are used to assess the situation at first because in rescue situations time is an important factor. Thus, the mission control on the ground station computes initial flight routes for every UAV which can be adopted during mission execution either by sending updated plans from the ground station to the UAVs or by the UAV's on-board drone control. High-resolution images of the affected area will be taken by UAVs within minutes. After the primary danger has been averted, the UAVs will have been used to monitor the progress of securing the operation area by updating the overview image periodically.

References

[1] A HGöktoğan, SSukkarieh, "Simulation of Multi-UAV Missions in a Real-Time Distributed Hardware-In-The-Loop Simulator",Proceeding of the 4th International Symposium on Mechatronics and its Applications (ISMA07), Sharjah, U.A.E. March 26-29, 2007
[2] Caccia Claudio, "ChibiOS-EmbrIO, Embryo Virtual Machines running on Chibi RTOS", September, 16 2012
[3] Darkoman, "GoogleMapsNet - GoogleMaps Control for .NET", http://www.codeproject.com /Articles/463434/GoogleMapsNet-GoogleMaps-Control-for-NET, 21 Sep 2012.
[4] GuoweiCai, Ben M. Chen, Tong H. Lee, Miaobo Dong, "Design and implementation of a hardware-in-the-loop simulation system for small-scale UAV helicopters", Department of Electrical and Computer Engineering, National University of Singapore, Singapore 117576, Singapore, 2009.
[5] Jerry Farmer, "Real-Time Operating System for PICmicro™ Microcontrollers", Microchip Technology Inc, 2002.
[6] Markus Loecher, "Overlays on Google map tiles in R", Berlin School of Economics and Law (BSEL), 2013-08-27.
[7] Mats Pettersson, "Basic Concepts for Real Time Operating Systems", IAR System
[8] Richard E. Kowalski, Frank Huy, "Real-Time Operating Systems", NASA.
[9] Robert L BorettiJr, Breakdown - HTTP Request Headers, WebSphere Application Server L2 Support, IBM Software Group, 2002.
[10] Wikipedia: Chibios/rt. http://en.wikipedia.org/wiki/ChibiOS/RT

(Received; 23rd December, 2013, Accepted; 19th April, 2014)

Web Document Clustering Using Cuckoo Search Clustering Algorithm Based On Gauss Distribution

Moe Moe Zaw[1], Ei Ei Mon[2]
Faculty of Information and Communication Technology
University of Technology (Yatanarpon Cyber City)
**E-mail: moemoezaw@gmail.com*

The World Wide Web continues to grow rapidly a vast resource of information and services. The number of web documents on the internet is growing rapidly day by day. So, the process of finding the relevent information on the web is a major challenge in Information Retrieval. The increasing size and the dramatic content of World Wide Web has created a need for automatic categorization of web pages. One of the techniques that can play an important role towards the achievement of this objective is web document clustering. This paper aims to develop a clustering algorithm and apply in web document clustering area. The novel Cuckoo Search optimization algorithm base on gauss distribution is a recently developed optimization algorithm to increase the convergence rate of the cuckoo search algorithm base on levy flight.In this paper, Cuckoo Search Clustering Algorithm based on gauss distribution is proposed to increase the performance of the Cuckoo Search Algorithm based on levy flight. For testing the performance of the proposed method, this paper will show the experience result by using the benchmark dataset. It can be seen that the Cuckoo Search Clustering algorithm based on gauss distribution outperforms the Cuckoo Search Clustering Algorithm based on levy flight in web document clustering.

1. Introduction

The increasing size and dynamic content of the World Wide Web has created a need for automated organization of web-pages. Document clusters can provide a structure for organizing large bodies of text for efficient browsing and searching. For this purpose, a web-page is typically represented as a vector consisting of the suitably normalized frequency counts of words or terms. Each document contains only a small percentage of all the words ever used in the web. If we consider each document as a multi-dimensional vector and then try to cluster documents based on their word contents, the problem differs from classic clustering scenarios in several ways. Document clustering data is high dimensional, characterized by a highly sparse word-document matrix with positive ordinal attribute values and a significant amount of outliers [1].

Nowadays, the internet has become the largest data repository, facing the problem of information overload. In the same time, more and more people use the World Wide Web as their main source of information. The existence of an abundance of information, in combination with the dynamic and heterogeneous nature of the Web, makes information retrieval a tedious process for the average user. Search engines, meta-search engines and Web Directories have been developed in order to help the users quickly and easily satisfy their information need [3].

Clustering is a technique, in which the data objects are given into a set of disjoint groups called clusters so that objects in each cluster are more analogous to each other than the objects from different clusters. Clustering techniques are used in several application areas such as pattern recognition, data mining, machine learning, and so on.

Text clustering, which has been extensively studied in many scientic disciplines, plays an

important role in organizing large amounts of heterogenous data into a small number of semantically meaningful clusters .In particular, web collection clustering is useful for summarization, organization and navigation of semi-structured Web pages.

One of the best known and most popular clustering algorithms is the k-means algorithm. The algorithm is efficient at clustering large data sets because its computational complexity only grows linearly with the number of data points. However, the algorithm may converge to solutions that are not optimal [6].

PSO is algorithm is presented as document clustering algorithm in [7]. It outperforms K-means clustering algorithm.

In [8], to cluster the web pages, they use the dictionary (standardized) to obtain the context with which a keyword is used and in turn cluster the results based on this context.

A combine approach is proposed to cluster the web pages which first finds the frequent sets and then clusters the documents in [7].

In [10], the Cuckoo Search Clustering Algorithm (CSCA) is proposed. The algorithm is validated on two real time remote sensing satellite- image datasets. In their algorithm, new Cuckoo is calculated by their new equation.In their new Cuckoo solution, the current best solution is considered.

In [4], the Cuckoo Search Clustering Algorithm based on levy flight is proposed. In this algorithm, the new cuckoo solution is generated by levy distribution. The algorithm is applied in web document clustering area and tested with benchmark dataset.The result shows that the algorithm is effective.

The other new Cuckoo equation for CSCA algorithm is proposed in [11].The new Cuckoo solution is calculated by using both current solution and current best solution.

In [2], the KEA-Means algorithm is proposed and it is used for web page clustering. This algorithm combines key phrase extraction algorithm and k-means algorithm.

This paper describes the application of a novel Cuckoo Search optimization algorithm base on Gaussion distribution [1] to find global solutions to the clustering problem in web document clustering area. The optimization algorithm was developed according to the low convergence rate of Cuckoo Search optimization algorithm via levy flight [13] . In this paper, a cuckoo search clustering algorithm based on gauss distribution is proposed and applied in web dosument clustering.

The rest of this paper will present the following. Web document Clustering is explained and Cuckoo Search Clustering Algorithm based on Levy Flight will be discussed. Then, Cuckoo Search Clustering Algorithm based on Gauss Distribution will be proposed. Experimental Setup will be presented and results and discussion will also be presented. Then, we will conclude this paper and suggest future work.

2. Web Document Clustering

Web document clustering is widely applicable in areas such as search engines, web mining, information retrieval and topological analysis. Most document clustering methods perform several pre-processing steps including stop words removal and stemming on the document set. Each document is represented by a vector of frequencies of remaining terms within the document. Some document clustering algorithms employ an extra pre-processing step that divides the actual term frequency by the overall frequency of the term in the entire document set.

The text content of a web document provides a lot of information aiding in the clustering of a page. There are many document clustering approaches proposed in the literature. They differ in many parts, such as the types of attributes they use to characterize the documents, the similarity measure used, the representation of the clusters etc. The different approaches can be categorized into *i.texbased, ii.linkbased and iii.hybrid one*. The text-based web document clustering approaches characterize each document according its content, i.e the words (or sometimes phrases) contained in it. The basic idea is that if two documents contain many common words then it is likely that two documents are very similar.

In most clustering algorithms, the dataset to be clustered is represented as a set of vectors $X=\{x_1, x_2, \ldots, x_n\}$, where the vector xi corresponds to a single object and is called the feature vector. The feature vector should include proper features to represent the object. The web document objects

can be represented using the Vector Space Model (VSM) . In this model, the content of a document is formalized as a dot in the multidimensional space and represented by a vector d, such as d= { w_1 , w_2, w_n..... } , where w_i (i = 1,2,…,n) is the term weight of the term t_i in one document. The term weight value represents the significance of this term in a document. To calculate the term weight, the occurrence frequency of the term within a document and in the entire set of documents must be considered. The most widely used weighting scheme combines the Term Frequency with Inverse Document Frequency (TF-IDF) . The weight of term i in document j is given in Eq (1):

$$w_{j\,i} = tf_{ji} * idf_{ji} = tf_{ji} * \log_2(n/df_{ji}) \quad (1)$$

where tf_{ji} is the number of occurrences of term i in the document j; df_{ji} indicates the term frequency in the collections of documents; and n is the total number of documents in the collection. This weighting scheme discounts the frequent words with little discriminating power.

The similarity between two documents is measured in clustering analysis. This algorithm uses the normalized Euclidean distance as the similarity metric of two documents m_p and m_j in the vector space. Eq-2 is the distance measurement formula.

$$d(m_p, m_j) = \sqrt{\sum_{k=1}^{d_m} (m_{pk} - m_{jk})^2 / d_m} \quad (2)$$

where m_p and m_j are two document vectors; d_m is the dimension number of the vector space; m_{pk} and m_{jk} denote the documents m_p and m_j 's weight values in dimension k. This similarity metric is widely used in the text document clustering.

3. Cuckoo Search Clustering Algprithm based on Levy Flight

Cuckoo Search Clustering Algorithm based on levy flight is designed as a clustering algorithm from Cuckoo Search Optimization algorithm to locate the optimal centroids of the cluster. In web document clustering area, it is possible to view the clustering problem as an optimization problem that locates the optimal centroids of the clusters rather than an optimal partition finding problem. This algorithm aims to group a set of input samples (data points) into clusters with similar features. It will work without the knowledge of the class of the input data during the process. In this algorithm, new cuckoo solutions will be moved by using levy flight.

In this clustering algorithm, the new cuckoo solution is generated by levy distribution as follows:

$$x_i^{(t+1)} = x_i^{(t)} + \alpha * \text{levy}(\lambda) \quad (3)$$

$$x_i^{(t+1)} = x_i^{(t)} + \alpha * S(x_i^{(t)} - x_{best}^{(t)}).r \quad (4)$$

In Mantegna's algorithm, the step Length can be calsulated by [11].

$$S = \mu / |v|^{1/\beta} \quad (5)$$

where β is a parameter between [1,2] and considered to be 1.5. μ and v are drawn from normal distribution as

$$\mu \sim N(0, \delta_\mu^2),\ v \sim N(0, \delta_v^2) \quad (6)$$

$$\delta_\mu = \left\{ \frac{\tau(1+\beta)\sin(\pi\beta/2)}{\tau[(1+\beta)/2]\,\beta\,2^{(\beta-1)/2}} \right\}^{1/\beta},\ \delta_v = 1$$

4. Cuckoo Search Clusering Algorithm based on Gauss Distribution

Levy flight is a random walk whose random steps are drawn from a Levy distribution for large steps. Cuckoo search with levy flight can find the optimal solution but the search relies entirely on random walks. So, a fast convergence and precision cannot be guaranted. So, in this paper, a

cuckoo search clustering algorithm based on gauss distribution is proposed to increase the convergence rate and precision. New cuckoo solutions are generated by gaussian distribution.The algorithm is as shown in fig 1.

1. Begin
   (Parameter Initialization- no of clusters, no of host nests)
2. Consider NH host nests containing 1 egg (solution) each
3. For each solution of host i
4. Initialize x_i to contain k randomly selected cluster centroids (corresponding to k clusters), as $x_i = (m_{i,1},\ldots,m_{i,j},\ldots m_{i,k})$ where $m_{i,k}$ represents the kth cluster centroid vector of ith cluster centroid vector of i^{th} host.
   End for loop
5. For **t** iterations
6. For each solution of host i of the population
7. For each data document z_p
8. Calculate distance $d(z_p,m_{j,k})$ from all cluster centroids $C_{i,k}$ by using Euclidean Distance eq-2
9. Assign z_p to $C_{i,k}$ by
   $d(z_p,m_{j,k}) = \min_{k=1\ldots k}\{ d(z_p,m_{j,k}) \}$
   End for loop in step 7
10. Calculate fitness function $f(x_i)$ for each host nest i by Eq-(9)
11. End for loop in step 6
12. Replace all worse nests by **new Cuckoo eggs produced with gaussian distribution** from their positions
13. A fraction pa of worse nests are abandoned and new ones are built randomly
14. Keep the best solutions (or nests with quality solutions)
15. Find the current best solution
    End for loop in step 5
16. Consider the clustering solution represented by the best solution
17. End

Fig. 1 Cuckoo Search Clustering Algorithm based on Gauss Distribution

$$x_i^{(t+1)} = x_i^{(t)} + \propto \oplus \sigma_s \tag{7}$$

where,

$$\sigma_s = \sigma_0 \exp(-\mu k) \tag{8}$$

σ_0 and μ are constants. k is the current generation.

$$f = \frac{\sum_{i=1}^{N_c}\left\{\frac{\sum_{j=1}^{p_i} d(o_i,m_{i,j})}{p_i}\right\}}{N_c} \tag{9}$$

$m_{i,j}$ = j^{th} document vector which belong to cluster i;
o_i= the centroid vector of i^{th} cluster
$d(o_i,m_{i,j})$= distance between document $m_{i,j}$ and the cluster centroid o_i
p_i = the number of documents which belongs to cluster C_i
N_c= number of clusters

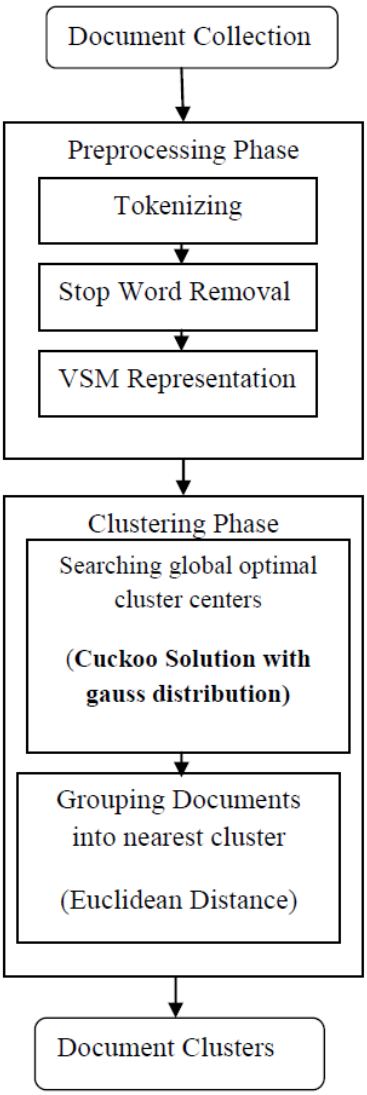

Fig. 2 Proposed Method in Web Document Clustering

In Fig.2, the documents to be clustered must be collected first. The proposed method includes two phases: preprocessing phase and clustering phase. In preprocessing phase, each document will be tokenized and the stop words such as a, an, the etc., will be removed. The remaining words will be represented in Vector Space Model with their TFIDF weight values. In clustering phase, the distance from the center documents to the other documents will be measured by Cosine Similarity measure. The documents to the nearest center will go to this cluster. For next center document selection, the old center will be moved to the new center by Cuckoo Solutions based on gaussian distribution.This clustering process will be performed for a defined number of criteria. The algoithm will finally produce the user-defined number of document clusters.

5. Experimental Setup

Cuckoo Search Clustering Algorithm based on levy flight and the cuckoo search clustering algorithm based on gauss distribution are tested on 7 sector benchmark data set. For our testing process, 600 web pages are randomly selected from the dataset and clustered into 3 classes. The algorithm is tested by using Euclidean distance as similarity measure of the two documents. The algorithm executes for 200 iterations and uses 10 cuckoos.The parameter pa is set as 0.25. μ is 0.0001 and σ_0 is 0.5 in gaussian clustering algorithm. α is 1 in both algorithms.

6. Results and Discussion

The fitness equation is also used for the evaluation of the cluster quality. The smaller the cluster quality value, the more compact the clustering solution. The average fitness comparison of the two algorithms are as shown in Fig 3. The cuckoo search clustering algorithm with gauss distribution achieves its convergence over 120 generations while the other achieves its convergence over 160 generations.

A famous method for evaluating measure in information retrieval (IR) is F-measure. The cluster results of the system are also evaluated using F-measure. It considers the precision (P), recall (R) and is shown in Eq (10). Eq (11) shows F-measure formula. The F-measure values are the average of 100 runs.

$$P = \frac{TP}{TP+FP} \qquad R = \frac{TP}{TP+FN} \tag{10}$$

$$F = \frac{2PR}{(P+R)} \tag{11}$$

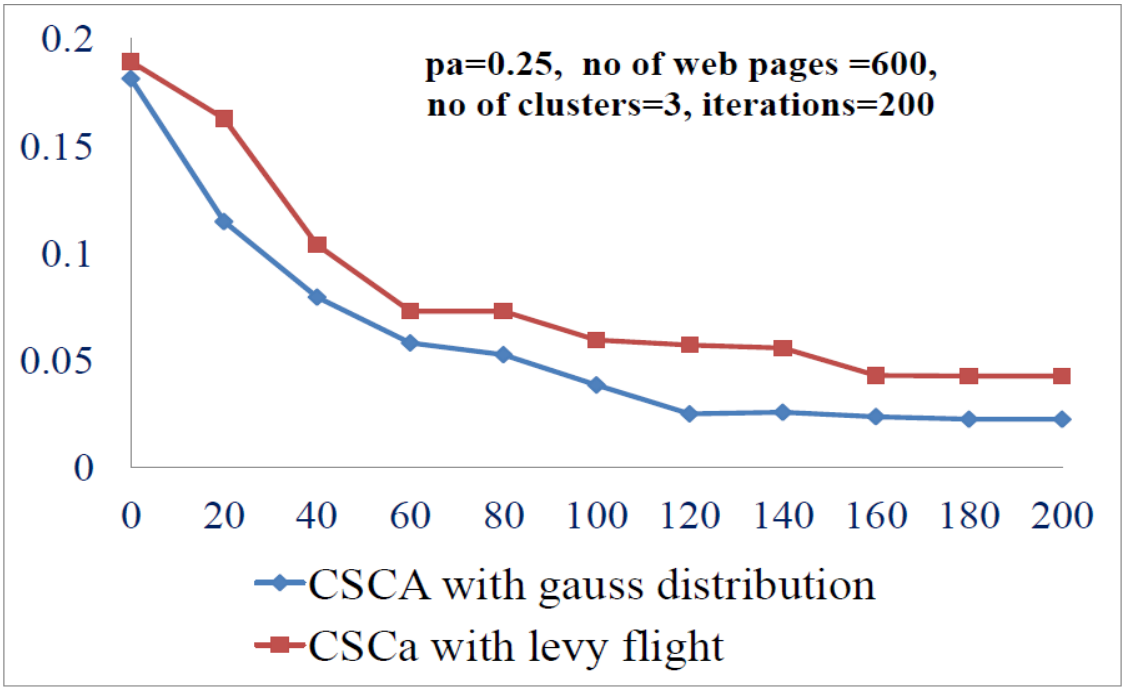

Fig.3 Comparison of Average fitness values of the two algorithms over generation

Table 1 Precision, Recall and F-measure

Methods	Precision	Recall	F-measure
CSCA with gauss distribution	0.635	0.619	0.626
CSCA based on levy flight	0.623	0.615	0.619

Table.1 illustrates the F-measure of the proposed method. High F-measure shows the high accuracy. The proposed method achieves 0.626 of F-measure in clustering 300 web documents into 3 clusters.

7. Conclusion

Cuckoo Search Clustering Algorithm based on gauss distribution is proposed and applied in web document clustering area. The result shows that the cluster quality and the evaluation measure obtained are good. Its performance is compared to the performance of cuckoo search clustering algorithm based on levy flight. The gauss distribution can produce more accurate precision than levy flight in the clustering algorithm. As our future work, the clustering accuracy the Cuckoo Search Clustering Algorithm based on gauss distribution can also be applied to other datasets. And it can also be compared to other swarm intelligence clustering algorithms.

References

[1] Hongqing ZHENG and Yongquan ZHOU, "A Novel Cuckoo Search Optimization Algorithm base on Gauss Distribution",Journal of Computional imfprmation Systems 8: 10(2012), 4193-4200

[2] Swapnali Ware and N.A.Dhawas, "Web Document Clustering Using KEA-Means Algorithm", International Journal of Technologies and Applications, Vol-3(5),1720-1725

[3] N. Oikonomakou and M. Vazirgiannis,"A Review of Web Document Clustering Approaches"

[4] Moe Moe Zaw and Ei Ei Mon, "Web Document Clustering Using Cuckoo Search Clustering Algorithm based on Levy Flight", International Journal of Innovation And Applied Studies, vol. 4, no 1, pp. 182-188 Sep 2013

[5] Jain, A.K. and Dubes, R.C, *Algorithms for Clustering Data, 1988* .Prentice Hall, Englewood Cliffs, New Jersey, USA

[6] Bottou, L. and Bengio, Y. ,"Convergence properties of the k-means algorithm", Advances in Neural Information Processing Systems, 1995, 7, 585-592

[7] Xiaohui Cui, Thomas E. Potok, Paul Palathingal, "Document Clustering Using Particle Swarm Optimization", Swarm Intelligence Symposium, IEEE publication, 8-10 June 2005

[8] Jeevan H E, Prashanth P P , Punith Kumar S N , Vinay Hegde , "Web Pages Clustering: A New Approach", *International Journal Of Innovative Technology & Creative Engineering* (ISSN:2045-8711) vol.1 no.4 April 2011

[9] Rajendra Kumar Roul1, Dr.S.K.Sahay, "An Effictive Web Document Clustering For Information Retrieval", *International Journal of Computer Science and Management Research,* vol. 1, no. 3, p. 481, 2012

[10] Samiksha Goel, Arpita Sharma, Punam Bedi, "Cuckoo Search Clustering Algorithm: A novel strategy of biomimicry", World Congress on Information and Communication Technologies, IEEE publication, 2011

[11] Moe Moe Zaw, Ei Ei Mon, "Improved Cuckoo Search Clustering Algorithm(ICSCA)" , Proceedings of the 11th International Conference on Computer Applications, pp.22-26, 2013

[12] Swapnali Ware, N.A.Dhawas, "Web Document Clustering Using KEA-Means Algorithm", *International Journal Of Computer Technology & Applications*, vol 3 (5), pp.1720 -1725, 2012

[13] Xin-She Yang, Suash Deb, "Cuckoo Search via L´evy Flights", World Congress on Nature and Biologically Inspired Algorithms, IEEE publication, pp.210-214, 2009

[14] X.-S. Yang and S. Deb, "Engineering Optimisation by Cuckoo Search", *International Journal of Mathematical Modelling and Numerical Optimisation", v*ol. 1, no. 4, pp.330-343 ,2010

[15] X.-S. Yang, *Nature-Inspired Metaheuristic Algorithms, 2nd Edition*, Luniver Press, 2010

(Received; 23rd December, 2013, Accepted; 11th August, 2014)